University *of* Exeter

Tipping Points and Early Warning Signals in the Climate-Carbon System

Submitted by

Joseph John Clarke

to the University of Exeter as a thesis for the degree of Doctor of Philosophy in Mathematics,

August 2023

I certify that all material in this thesis which is not my own work has been identified and that any material that has previously been submitted and approved for the award of a degree by this or any other University has been acknowledged.

Abstract

This is a thesis about tipping points and early warning signals. The tipping points investigated are related to various components of the climate-carbon system. In contrast, the work on early warning signals has more generic applications, however in this thesis they are analysed in the context of the climate-carbon system. The thesis begins with an introduction to the climate-carbon system as well as a discussion of tipping points in the Earth system. Then a more mathematical summary of tipping points and early warning signals is given. An investigation into the 'compost bomb' is undertaken, in which the spatial structure of soils is accounted for. It is found that a hot summer could cause a compost bomb. The effect of biogeochemical heating on the stability of the global carbon cycle is investigated and it is found to play only a small role. The potential for instabilities in the climate-carbon cycle is further investigated when the dynamic behaviour of the ocean carbon cycle is accounted for. It is found that some CMIP6 models may be close to having an unstable carbon cycle. Spatial early warning signals are investigated in the context of more rapidly forced systems. It is found that spatial early warning signals perform better when the system is rapidly forced compared with time series based early warning signals. The typical assumptions about white noise made when using early warning signals are also studied. It is found that time correlated noise may mask the early warning signal. It is shown that a spectral analysis can avoid this problem.

He understood for the first time that the world is not dumb at all, but merely waiting for someone to speak to it in a language it understands.

Jonathan Strange & Mr Norrell
Susanna Clarke

Contents

Contents

List of Figures

List of Tables

List of Tables

Associated Papers

Clarke, J., C. Huntingford, P. Ritchie and P. Cox (Apr. 2021). "The compost bomb instability in the continuum limit". In: *The European Physical Journal Special Topics*. ISSN: 1951-6355. DOI: 10.1140/epjs/s11734-021-00013-3.

Ritchie, P. D. L., J. J. Clarke, P. M. Cox and C. Huntingford (Apr. 2021). "Overshooting tipping point thresholds in a changing climate". In: *Nature* 592.7855, pp. 517–523. ISSN: 0028-0836. DOI: 10.1038/s41586-021-03263-2.

Ritchie, P. D. L., I. Parry, J. J. Clarke, C. Huntingford and P. M. Cox (Sept. 2022). "Increases in the temperature seasonal cycle indicate long-term drying trends in Amazonia". In: *Communications Earth & Environment* 3.1, p. 199. ISSN: 2662-4435. DOI: 10.1038/s43247-022-00528-0.

Clarke, J. J., C. Huntingford, P. D. L. Ritchie and P. M. Cox (Feb. 2023). "Seeking more robust early warning signals for climate tipping points: the Ratio of Spectra method (ROSA)". In: *Environmental Research Letters*. ISSN: 1748-9326. DOI: 10.1088/1748-9326/acbc8d.

Huntingford, C., P. M. Cox, M. S. Williamson, J. J. Clarke and P. D. L. Ritchie (Apr. 2023). "Emergent constraints for the climate system as effective parameters of bulk differential equations". In: *Earth System Dynamics* 14.2, pp. 433–442. ISSN: 2190-4987. DOI: 10.5194/esd-14-433-2023.

Acronyms

AC Autocorrelation.

AMOC Atlantic Meridional Overturning Circulation.

BB Boettner and Boers early warning signal.

BP Before Present, defined as 1 January 1950.

CMIP Coupled Model Intercomparison Project.

DGVM Dynamic Global Vegetation Model.

ECS Equilibrium Climate Sensitivity.

ENSO El Niño – Southern Oscillation.

ERA5 ECMWF Reanalysis version 5.

ESM Earth System Model.

EWI Early Warning Indicator.

EWS Early Warning Signal.

GPP Gross Primary Productivity.

IMOGEN Integrated Model Of Global Effects of climatic aNomalies.

IPCC Intergovernmental Panel on Climate Change.

JULES Joint UK Land Environment Simulator.

LC10 Luke and Cox compost bomb model.

Acronyms

NPP Net Primary Productivity.

ROSA Ratio of Spectra Method.

SNR Signal to Noise Ratio.

List of Symbols

A Energy released from respiration.

C_a Atmospheric Carbon.

C_i Carbon in ocean box i.

C_o Ocean Carbon.

C_s^{eq} Equilibrium soil carbon.

C_s Soil carbon.

$C_{1/2}$ Half saturation constant of atmospheric CO_2 for NPP.

C_{a0} Equilibrium C_a.

C_{o0} Equilibrium C_o.

D Diffusion constant.

D Nondimensional soil thermal depth.

F_a Atmosphere-ocean flux.

G_I IMOGEN's Impulse response function.

G Two point correlation function.

G Impulse response function for ocean boxes.

G The stochastic part of a stochastic differential equation.

H Soil carbon e-folding depth.

I Atmosphere-ocean carbon flux calculated by IMOGEN.

J Probability current.

List of Symbols

J Jacobian matrix.

L Domain size.

N Net radiative flux at the top of atmosphere.

Q_{10} The Q_{10} factor.

$Q_{2\times}$ Radiative forcing due to doubling CO_2.

R_h Heterotrophic respiration.

S_0 Solar constant.

S Dimensionless equator to pole salinity difference.

S Climate sensitivity experienced by soils.

T_0 The transition temperature between ice-free and ice-covered states for snowball Earth.

T_a Air temperature.

T_o Ocean temperature.

T_s Soil temperature.

T_{eff} Spatially uniform warming that is equivalent to a spatially varying warming.

T_{ref} Reference temperature for respiration.

T_{a0} Background mean atmospheric temperature.

T Dimensionless equator to pole temperature difference.

T Global mean surface temperature.

T System timescale.

T Period of temperature variations.

U Potential function.

W Lambert W function.

ΔQ Radiative forcing.

$\Delta T(\boldsymbol{r}, t)$ Spatially dependent warming.

ΔT_a Amplitude of temperature variations.

Π_0 NPP in the pre-industrial equilibrium state.

Π_c Critical NPP.

Π_∞ Saturated level of NPP for high atmospheric CO_2.

Π Net Primary Productivity.

Ψ AMOC flow strength.

α_+ The albedo of the Earth in an ice-free state.

α_- The albedo of the Earth in an ice-covered state.

α_1 Lag-1 autocorrelation.

α_s Autocorrelation calculated over space.

α_t Temporal autocorrelation.

α Albedo.

α Sensitivity of respiration to temperature.

$\boldsymbol{F}$ The deterministic part of a stochastic differential equation.

$\boldsymbol{W}$ A multidimensional Wiener process.

$\boldsymbol{\eta}$ White noise.

$\boldsymbol{f}$ The dynamics of a system.

$\boldsymbol{v_i}$ Eigenvectors of J.

$\boldsymbol{x}^*$ System fixed point.

$\boldsymbol{x}$ System state vector.

$\boldsymbol{y}$ Linearised system state vector.

χ_0 Fraction of atmospheric emissions that reside in the ocean.

∂T_a Time dependent change in atmospheric temperature.

$\partial \Sigma CO_2$ Dissolved inorganic carbon.

$\partial\theta$ Nondimensional atmospheric temperature change.

δ_{ij} Kronecker delta.

∂ Dirac delta function.

ε_t Random variable with standard normal distribution.

ε The emissivity of the Earth.

ε Ratio for system timescale to forcing timescale.

ε System timescale.

ε Rate of parameter change.

ε Ratio of two box ocean timescales.

η_1 Thermal forcing.

η_2^* Critical value of η_2.

η_2 Freshwater forcing.

η_3 Timescale ratio of thermal and freshwater forcing.

$\gamma_\pm$ Eigenvalues of the one box ocean model Jacobian.

γ Eigenvalue of J.

κ Global heat transfer coefficient.

κ Soil thermal conductivity.

λ_i Eigenvalues of J.

λ Imaginary part of γ.

λ System recovery rate from perturbations.

λ Climate sensitivity.

λ Heat transfer coefficient.

$\mathcal{C}$ Total Carbon in the atmosphere-ocean-land carbon cycle.

$\mathcal{E}$ Effective Energy.

$\mathcal{H}$ Quadratic approximation to $\mathcal{E}$.

$\mathcal{O}$ Either used formally as big-O notation or informally to mean 'on the order of'.

$\mathcal{W}$ Nondimensional respiration.

ECS Equilibrium Climate Sensitivity.

μ^*_∞ Critical climate-carbon cycle sensitivity ignoring biogeochemical heating.

μ^* Critical value of control parameter.

μ^* Critical climate-carbon cycle sensitivity.

μ_A Areal soil heat capacity.

μ_V Volumetric soil heat capacity.

μ_c Critical value of control parameter.

μ Climate-carbon cycle sensitivity.

μ Control Parameter of a system.

μ Soil areal heat capacity.

ν Ratio of warming over land to warming over ocean.

ω Angular frequency.

σ_t^2 Temporal variance.

σ_s^2 Spatial variance.

σ_y^2 The variance of y.

σ Standard deviation of a white noise process.

σ Stefan-Boltzmann constant.

τ_i Timescale of the ith ocean box.

τ_w Window length.

τ_{crit} Timescale of the system in the direction being destabilised.

τ_{drift} Timescale of the long term drift of the system.

τ_{stab} Timescale of the stable directions of the system.

τ Kendall τ.

τ Nondimensional time.

θ Nondimensional soil temperature.

$\widetilde{\Pi}$ Nondimensional NPP.

ξ Correlation length.

ξ White noise.

ζ White noise.

a_i Coefficients of a cubic polynomial.

c_i Constants determined by initial conditions.

c Global Areal soil heat capacity.

$f(\boldsymbol{r})$ Pattern of warming.

f_i Fraction of the carbon flux into box i.

k Ocean carbon uptake rate.

k Wavenumber.

p Probability density function.

r_0 Specific respiration rate.

r_c Critical system forcing rate.

r Kramers' Escape Rate.

r System forcing rate.

r Noise redness.

r Temperature dependent specific respiration rate.

t^* Critical time.

v Rate of increase of air temperature.

$x_{\pm}^{\mathrm{PB}}$ Pullback attractor and repeller.

$x_{\pm}$ Attractor and repeller.

x Nondimensional depth coordinate.

x State variable.

y System state variable.

y Co-moving coordinate.

z Linearised state variable.

z Vertical coordinate.

List of Symbols

Acknowledgements

Thanks must go first to my primary supervisor, Peter Cox. His willingness to support me and my ideas, combined with his own insight, has been incredibly useful over the years. My second supervisor Peter Ashwin also deserves my thanks, particularly for his ability to help me understand technical topics.

I should also thank my co-authors, Chris Huntingford and Paul Ritchie. The time they took to help me write my papers, from the drafting stage right through to answering reviewer comments was always greatly appreciated. Paul in particular deserves my thanks for his role as (amongst other things) my unofficial supervisor. One day I will beat him at squash.

Jan Sieber (University of Exeter) and Chris Jones (Met Office and University of Bristol) gave very useful feedback on this thesis as my examiners. I would like to thank them for holding my viva and Mark Williamson for having the unenviable job of being the Non-Examining Independent Chair.

I was fortunate to work in the supportive environment of Exeter Climate Systems (XCS). I would like to especially thank all those in Office 901, old and new, who created such a friendly place to work. I started in The Dungeon, but eventually I was allowed my own desk (with a whiteboard!).

Those friends I made along the way, whether through a Laver lunch on the balcony or, more probably, by spending time at Climate and Friends have also earned my thanks. Through trips to the beach, Dartmoor and even further abroad, they have reminded me that there is more to life than bifurcation diagrams.

Ellie and Margaret, who I live with, also have my gratitude. The pandemic meant we saw more of each other than any of us wanted. Thank you for all the cups of tea and trips to the 'pub' which kept me sane over lockdown. I am sorry for all the food I stole.

I would also like to thank my family for all their love and support over the years, not least for taking me in over the first lockdown. It was a strange and disorienting time but being at home made it much more bearable.

Finally, I would like to thank Alice (and Milo), who have made these last few years so happy.

Preface

I arrived in Exeter to start work on my PhD in September 2019, intending to learn something about tipping points. I began by looking at the compost bomb instability — a somewhat esoteric rate-induced tipping point. Just six months later, the government declared a national lockdown and I spent the next year or so working from home. It was then that I became interested in early warning signals, at least in part because they are easy to research from a home office. As a result, my research has two main strands: one that investigates the compost bomb and climate-carbon system instability more broadly and another that looks at early warning signals.

Chapters 1 and 2 serve as an introduction to the thesis. In chapter 1 I outline the climate-carbon system and discuss some potential tipping points in the Earth system. In chapter 2 I develop some of the theory about tipping points and early warning signals. Much of this is quite general but I draw on examples from the Earth system.

Chapter 3 is an investigation into the compost bomb. I did some of that work during the summer of 2020, when Siberia was experiencing a spate of wildfires and stories of 'zombie fires' circulated. This is why the potential for a hot summer to trigger compost bombs was a focus of the chapter.

In chapter 4 I considered the compost bomb feedback at the global scale and its effect on the carbon cycle. The fact that there was the potential for instability combined with the need to update some older research motivated a more thorough investigation of the stability of the climate-carbon system. This was done in chapter 5.

Chapters 6 and 7 contain the work on early warning signals. My desire to draw out the analogies between Earth system tipping points and the established physics of phase transitions led to work on spatial early warning signals, which can be found in chapter 6. I became concerned that many applications of early warning signals were really detecting changes in what drives variability in the system, rather than the stability of the system itself. I investigated this in chapter 7.

In the final chapter, chapter 8 I summarise my work and suggest some future research directions.

So far two of these chapters, chapters 3 and 7, have been published as papers. They appear in this thesis mostly unchanged aside from a few typographical alterations and the inclusion of supplementary material into the main text. The code used in these papers can be found online.

For chapter 3 it is located at www.github.com/josephjclarke/ContinuumCompostBomb and for chapter 7 at www.github.com/josephjclarke/BeyondWhiteNoiseEWS.

For historical reasons Exeter climate scientists are mostly based in the department of mathematics. This has generally been an edifying experience and has influenced the direction of my PhD in all sorts of ways. One of these ways is that I use log to mean the natural logarithm, unless otherwise stated. I am however a physicist at heart and the rest of my notational choices reflect that.

Joe Clarke
Exeter
August 2023

Chapter 1

Tipping Points and the Climate-Carbon System

1.1 Tipping Points

Take a pan of water and heat it up. As its temperature rises, some of the water's properties may change. For example, its thermal conductivity increases. However, the water still remains liquid and these changes will vary continuously with the water temperature. However, if the water is heated beyond a critical temperature of 100 °C something more dramatic happens and the water boils away. The properties of the resulting steam are quite different to the original water — a *qualitative* change has occurred.

It is this type of qualitative transition that this thesis is concerned with. Whilst the boiling of water is a phase transition (Goldenfeld 2018), I shall use the broader terminology of *tipping points* (Lenton et al. 2008) or *critical transitions* (Rahmstorf 1995) or *abrupt changes* (Alley et al. 2003) to describe these phenomena.

1.1.1 Definitions

Although it can be a vague term, the concept of a small perturbation leading to a large change generally forms a part of most formal definitions of tipping points. For example, Lenton et al. 2008 and Armstrong McKay et al. 2022 define the occurrence of a tipping point as when there is a control parameter, ρ, with a critical value ρ_{crit}, above which any significant variation, $\delta\rho > 0$, leads to a qualitative change $\hat{F}$ of a system feature F, after some observation time $T > 0$. They write this mathematically as

$$|F(\rho \geq \rho_{\text{crit}} + \delta\rho|T) - F(\rho_{\text{crit}}|T)| \geq \hat{F} > 0, \tag{1.1}$$

where $F(\rho|T)$ gives the state of F with control parameter ρ at time T. The inclusion of an observation time allows for the fact that changes in the system may not be apparent until

after the critical value has been exceeded. The IPCC (IPCC 2021) defines a tipping point as 'A critical threshold beyond which a system reorganizes, often abruptly and/or irreversibly'. Others, such as Wang et al. 2023 and Kopp et al. 2016, insist that tipping points should occur on fast time scales.

Each of these definitions are deficient in their own way. The IPCC definition views tipping in terms of thresholds which excludes certain types of tipping (see section 2.1). The definition in Lenton et al. 2008 may be too mathematical for widespread understanding and that of Wang et al. 2023 suffers from the problem that many timescales in the Earth system are slow.

The multiple different definitions in the literature reflect the vagueness of the notion of tipping points. In a sense, this is an advantage as it encourages research across a wide variety of phenomena. With this in mind, I will define a tipping point in a way that is closest in style to the IPCC as something that a system undergoes when it experiences a qualitative change in its properties.

1.1.2 Examples of Tipping

Nonlinear changes have long fascinated scientists. Physicists have investigated phase changes not just in terms of the boiling and freezing of substances but also in magnetic materials (Ising 1925; Onsager 1944), superconductivity (Ginzburg and Landau 1965) and percolation theory (Flory 1941). Each of these are different processes, but it is a remarkable fact that near the phase transition different systems can be dynamically very similar, a phenomenon known as universality (Wilson 1983). This idea — that different examples of tipping points across totally different systems can share features — will be a theme commonly returned to.

Tipping points are also important in biology. In medicine, tipping point theory has been used to help understand asthma attacks (Donovan and Brand 2022) and sleeping dynamics (Skeldon, Dijk and Derks 2014). In an influential article, (May 1976), the ecologist Robert May noted that even very simple nonlinear models have rich dynamics and are capable of experiencing tipping points (although he did not use that term). Holling 1973 introduced the idea of resilience which is related to the ability of a system to resist tipping. Tipping points have been found in a range of ecosystems (Scheffer et al. 2001; Dakos et al. 2019). The transition to turbid state in lakes (Scheffer et al. 1993) and the collapse of plant-pollinator communities (Lever et al. 2014) are both examples of ecological tipping points. However other studies (Hillebrand et al. 2020) have challenged how widespread tipping effects are.

Notions of multiple equilibria and the ability to transition between them has been used to explain patterns seen in nature. This was introduced by Turing 1952 to explain patterns found in certain plants and animals. Since then, it has been used to explain patterns in ecosystems (Rietkerk and Koppel 2008).

1.2 The Climate-Carbon System

Whilst some of this thesis is applicable to many systems, the focus of this work has been on applications to the Earth system. Therefore in this section I will give an outline of how the climate-carbon system operates.

The fundamental idea in climate science is that of energy balance (North, Cahalan and Coakley 1981). The Earth receives radiation from the Sun and then re-radiates it to space. In order to reach a steady state, the energy absorbed from the Sun must equal the radiation emitted from the Earth (Peixoto and Oort 1992). It is the need for energy balance, combined with the latitudinally dependent absorption and emission of radiation, that ultimately drives all weather and climate (Lorenz 1967).

The solar constant, $S_0 \approx 1360\ \mathrm{W\ m^{-2}}$ (Johnson 1954) is the amount of radiation received by the Earth per unit area. A fraction of this, called the albedo, $\alpha \approx 0.3$, is reflected back to space (Goode et al. 2021). The rest is absorbed, mostly by the Earth's surface (Trenberth, Fasullo and Kiehl 2009).

Let the amount of radiation the Earth emits per unit area be F. The Earth, with radius R, absorbs energy over a disk, and re-radiates over its entire surface. By energy balance this leads to

$$\pi R^2 S_0 (1 - \alpha) = 4\pi R^2 F \tag{1.2}$$

or

$$F = \frac{1}{4} S_0 \left(1 - \alpha\right). \tag{1.3}$$

Assuming the Earth radiates as a black body with temperature T, then $F = \sigma T^4$ where σ is the Stefan-Boltzmann constant so that $T = 255$ K. This is not far from the true temperature of about 287 K (Jones et al. 1999). This black body temperature is however the effective emission temperature the Earth has to radiate at to maintain energy balance. Due to the presence of atmospheric greenhouse gases, which absorb infrared radiation, principally CO_2 and H_2O, the radiation that escapes to space is emitted from higher in the atmosphere that it would be in their absence. An effective emission height can be defined which radiates with the effective emission temperature and then because the atmospheric temperature increases towards the Earth's surface in the troposphere this makes the surface warmer than it would otherwise be. This is known as the Greenhouse Effect (Pierrehumbert 2010).

1.2.1 Climate Response to Radiative Forcing

When greenhouse gases are emitted into the atmosphere they raise the effective emission height to colder regions of the atmosphere which decreases the amount of outgoing radiation. As less radiation is now emitted to space the Earth's climate responds. It does this by increasing the Earth's surface temperature until it reaches a new equilibrium (Manabe and Wetherald 1967; Pierrehumbert 2010).

The amount that a greenhouse gas decreases the outgoing radiation to space by is known as its radiative forcing. Let T be the global mean temperature and assume that N, the net radiation received by the Earth, depends on T. After emitting a greenhouse gas the change in the top of atmosphere energy flux can be split (Gregory 2004) into a forcing term, ΔQ, and feedback term, $\lambda \Delta T$

$$\Delta N = \Delta Q - \lambda \Delta T. \tag{1.4}$$

The climate responds to the forcing by changing its temperature so that ΔN is zero at equilibrium. Hence the change in global mean temperatures is

$$\Delta T = \frac{\Delta Q}{\lambda}. \tag{1.5}$$

The quantity

$$\lambda = -\frac{\partial N}{\partial T} \tag{1.6}$$

known as the *climate feedback* determines the amount of warming experienced for a given radiative forcing. This quantity is measured in units of W m^{-2} K^{-1} but it has become common to discuss λ in terms of a given radiative forcing, $Q_{2\times}$, the radiative forcing due to doubling the concentration of CO_2 in the atmosphere, giving rise to

$$\text{ECS} = \frac{Q_{2\times}}{\lambda} \tag{1.7}$$

known as *Equilibrium Climate Sensitivity* which is measured in units of temperature (Charney et al. 1979).

Implicit in this definition is the idea that $Q_{2\times}$ is well defined. It is an empirical fact that over a range of concentrations the radiative forcing of CO_2 varies to a good approximation with the logarithm of its concentration (Pierrehumbert 2010), and so the notion of a radiative forcing due to doubling is well defined. It is also usually assumed that ECS is a constant independent of background climate state. Whilst this appears to be a good approximation, some scientists have investigated its state dependence (Caballero and Huber 2013; Ashwin and Heydt 2019; Bloch-Johnson et al. 2021).

The value of ECS is uncertain. State of the art climate models (CMIP6) do not agree on its value, and give a range of 1.8 K to 5.6 K (Zelinka et al. 2020), which represents an increase in uncertainty from CMIP5, although some researchers have suggested that ECS could be even larger (Stainforth et al. 2005). However, these estimates should be combined with other observational estimates, such as Cox, Huntingford and Williamson 2018, as well as paleoclimate records, like Hargreaves et al. 2012, as done by Sherwood et al. 2020. This analysis of multiple lines of evidence lead the IPCC to conclude that the best estimate of ECS is 3.0 K with a likely range of 2.5 K to 4.0 K (IPCC 2021).

1.2.2 Carbon Cycle

Of all the CO_2 emitted by humans by burning fossil fuels, only around half remains in the atmosphere (Friedlingstein et al. 2022). This is because of the terrestrial and oceanic sinks of carbon. The response of the carbon cycle can be partitioned into a carbon-concentration feedback and a carbon-climate feedback (Friedlingstein et al. 2006). The carbon-concentration feedback gives the change in the carbon cycle due to increases in CO_2 before temperature changes are accounted for. The carbon-climate feedback gives the changes in carbon stores due to increases in temperature. In CMIP6 (Arora et al. 2020) the carbon-concentration feedback is 0.97 ± 0.40 Pg C ppm^{-1} for the land and 0.79 ± 0.07 Pg C ppm^{-1} for the ocean. The carbon-climate feedback is -45.1 ± 50.6 Pg C K^{-1} for the land and -17.2 ± 5.0 Pg C K^{-1} for the ocean. This means that increases in CO_2 tend to increase carbon on the land and in the ocean. However increases in global temperature, for example due to elevated CO_2, tend to liberate carbon from the land and oceans. It should be noted that the uncertainties are much higher over land, which reflects the different processes contributing to the land and ocean carbon cycles.

Terrestrial Carbon Cycle

The terrestrial part of the carbon cycle is controlled by the biosphere (IPCC 2021). Carbon enters the biosphere through photosynthesis, the amount of which is known as gross primary productivity or GPP, and leaves via respiration (Jenkinson, Adams and Wild 1991). Respiration can be subdivided into *autotrophic* and *heterotrophic*. These relate to respiration performed by plants (which produce their own food, hence the name *auto*troph) and non-plant organisms respectively. Heterotrophic respiration is primarily performed by soil microbial communities which decompose the organic matter deposited into the soil from plants (Singh and Gupta 1977).

This means that the net carbon flux into the biosphere due to plants called *Net Primary Productivity* (NPP) is given by the difference between photosynthesis and autotrophic respiration. In the absence of other carbon removals, the overall carbon flux between the land and the atmosphere is therefore the difference between NPP and heterotrophic respiration, known as Net Ecosystem Production (NEP). Accounting for these removals such as fire and deforestation leads to Net Biome Productivity (NBP) which is the total flux of carbon into the land (Lovett, Cole and Pace 2006; Fernández-Martínez et al. 2023).

This carbon is stored in vegetation and in soils. There is around 1500 Pg C in the soil, with about 560 Pg C in vegetation (Crowther et al. 2019). There are uncertainties associated with these numbers, with typical estimates for the soil carbon ranging from 1400 Pg C to 1600 Pg C (Batjes 2016) and estimates of vegetation carbon ranging from 450 Pg C to 650 Pg C (Ciais et al. 2014).

The significant stores of vegetation carbon are the tropical rainforests (Malhi et al. 2006), whereas much of the soil carbon can be found at high latitudes (Varney et al. 2020). Permafrost,

soil which is below 0 °C all year round, represents a major store of this carbon (Hugelius et al. 2014). As it is frozen, little decomposition occurs there. However as the Earth warms and the permafrost thaws it could represent a carbon flux of some concern (Schuur et al. 2015).

There are important feedbacks on the land carbon cycle. Increasing the amount of CO_2 in the atmosphere increases the amount of carbon that diffuses through a plant's stomata where it can be used in photosynthesis (Farquhar, Caemmerer and Berry 1980). Furthermore, plants will partially close their stomata at higher CO_2 levels (De Kauwe et al. 2013) which reduces the water lost through transpiration. This can be quantified in terms of the water use efficiency (the ratio of carbon gained to water lost) (Drake, Gonzàlez-Meler and Long 1997). This can increase the growing season in drier ecosystems (Frank et al. 2015). These effects mean that at higher CO_2 levels NPP is expected to increase.

This *CO_2 fertilisation effect* has been detected in models (Friedlingstein et al. 2006; Wenzel et al. 2016; Arora et al. 2020) and observationally (Ainsworth and Alistair Rogers 2007; Kolby Smith et al. 2016). It acts as a negative feedback on global warming as it tends to decrease the amount of CO_2 in the atmosphere by increasing photosynthesis. This feedback is expected to weaken with increased CO_2 as fewer plants become limited by CO_2. There is some observational evidence of this occurring (Wang et al. 2020).

The decomposition of organic matter through heterotrophic respiration is a biochemical process that depends on temperature. In particular, increasing the temperature of the decomposition reaction will increase the rate of this reaction. Hence as CO_2 has a warming effect the amount of respiration will increase (Jenkinson, Adams and Wild 1991). This means there will be a larger flux of carbon to the atmosphere and so this is a positive feedback, which has been termed the Jenkinson effect (Luke and Cox 2010). Many biological reactions are assumed to depend exponentially on temperature, increasing in rate by a factor Q_{10} for every 10 K of warming. It is generally thought that $Q_{10} \approx 2$ (Jones 2001).

Ocean Carbon Cycle

The ocean carbon cycle operates by different mechanisms to the terrestrial carbon cycle. Some carbon enters through run-off from the land but most of the carbon flux to the ocean comes from diffusion from the atmosphere to the ocean (DeVries 2022). This diffusion depends on the solubility of CO_2 in water and the difference in partial pressure of CO_2 between the atmosphere and the ocean (Wanninkhof 1992). The CO_2 reacts with seawater to form two other species of dissolved inorganic carbon, or DIC: HCO_3^- and CO_3^{2-} (Dickson and Millero 1987).

The reaction between CO_2 and seawater is

$$CO2 + H2O \rightleftharpoons H2CO3 \rightleftharpoons H^+ + HCO3^- \rightleftharpoons 2\,H^+ + CO3^{2-}, \tag{1.8}$$

hence adding CO_2 to the ocean will increase the concentration of hydrogen ions, decreasing the pH. This is known as ocean acidification (Doney et al. 2009).

Strong vertical gradients exist in DIC in the ocean, with more DIC at depth due to increased solubility at depth and the biological pump (Volk and Hoffert 2013). Organisms convert DIC into biomass through photosynthesis near the surface where there is enough light. Most of this is respired near the surface but due to sinking, mixing and the migration of organisms some biomass will make its way to the deeper ocean where it is released as DIC into the deep ocean. This transport of DIC away from the surface increases the capacity of the ocean to absorb carbon (Sarmiento and Toggweiler 1984).

The ocean carbon cycle will be affected by climate change. Most of these changes are related to the physical and chemical components of the ocean carbon cycle rather than the biological components (IPCC 2021). As a result there is much less uncertainty about future changes in the ocean carbon cycle relative to the terrestrial carbon cycle (Arora et al. 2020).

The reactions in equation (1.8) can be combined to give

$$CO2 + H2O + CO3^{2-} \rightleftharpoons 2\,HCO3^{-}. \tag{1.9}$$

Therefore as more CO_2 is added to the ocean, the amount of CO_3^{2-} will decrease which leads to more CO_2 remaining in its dissolved form which reduces the uptake of carbon (Archer 2010; Egleston, Sabine and Morel 2010). Furthermore the solubility of CO_2 decreases with temperature so warming thus reduces the strength of the ocean sink (Weiss 1974). Additionally the ocean is expected to become more stratified due to climate change which decreases vertical mixing which again reduces the uptake of CO_2 (DeVries, Holzer and Primeau 2017).

1.3 Tipping Points in the Earth System

In this section I will give some background on Earth system tipping points, including outlining some mechanisms. I will focus on a few key sub subsystems. I will then discuss some of the evidence for tipping behaviour in the Earth's past.

The most recent IPCC report (IPCC 2021) finds it 'unequivocal that human influence has warmed the atmosphere, ocean and land'. Humans have done this through the release of greenhouse gases, most importantly carbon dioxide (CO_2), and also through land use change. This has led to observable changes in the Earth's climate. Most obvious is the changes in global mean surface temperature, with a most likely temperature increase of 1.07 K relative to the period 1850 to 1900 (IPCC 2021) in the global mean but with clear regional differences (Morice et al. 2021) such as Arctic amplification as well as more warming over land than over ocean. Other effects include rise of around 0.2 m in sea levels (Frederikse et al. 2020) and increase in heavy precipitation events (Fischer and Knutti 2016).

1.3.1 Tipping at the global scale

This global warming is unprecedented in at least the last 2000 years and has caused global temperature levels not seen in the last 125,000 years (IPCC 2021). This naturally leads to

speculation about the nature of the change the Earth system is experiencing. It could be a smooth function of increasing CO_2 or tipping dynamics could be possible (Broecker 1987).

A controversial paper, Steffen et al. 2018, considered the possibility that ongoing global warming could make the Earth transition from its current current glacial-interglacial limit cycle state into a new 'hothouse' state. This state would be defined by high temperatures and sea levels, posing challenges both to humanity and the wider biosphere. This state would be reached through biogeochemical feedbacks leading to a cascade of tipping points. They advocate humanity operating within certain 'planetary boundaries' (Rockström et al. 2009) to avoid this possibility.

Part of the reason Steffen et al. 2018 proved so controversial is that there is little evidence of this nonlinear response at the global scale. Global temperature rise is approximately linear in emitted carbon dioxide (Allen et al. 2009; Rogelj et al. 2019) and not expected to continue after emissions cease (MacDougall et al. 2020), which is related to decreasing atmospheric CO_2 levels offsetting the thermal inertia of the climate system. However certain cloud resolving models report that at sufficiently high levels of global warming stratocumulus cloud decks can break up causing 8 K of warming globally (Schneider, Kaul and Pressel 2019).

1.3.2 Tipping Elements

Nevertheless there is still the possibility of more regional tipping point behaviour. Lenton et al. 2008, introduced the notion of *tipping elements* which are components of the Earth system that are 'at least subcontinental in scale' ($\mathcal{O}(1000\,\mathrm{km})$) which can undergo tipping behaviour as a result of anthropogenic influence. Lenton led an expert elicitation of potential tipping elements in the Earth system to estimate how much warming would be needed to trigger the tipping element and what the key uncertainties were. More recently, Armstrong McKay et al. 2022 updated this study by reviewing the literature published since. Following this, I will discuss some key tipping elements.

Atlantic Meridional Overturning Circulation

The Atlantic Meridional Overturning Circulation, known as the AMOC, is a large-scale current in the ocean. The AMOC transports warm water polewards. This heat transport plays an important role in the climate of, for example, northern Europe where it keeps temperatures warmer than they would be otherwise. The AMOC is driven by the salt-advection feedback, whereby warm saline water is transported northwards where it cools and becomes more dense. It then sinks and can make the return journey to the equator completing the circulation (Dijkstra 2011). If the water freshens, then its density decreases and the sinking decreases, which leads to a weaker flow and therefore less polewards salt transport.

The potential for the AMOC to exhibit bistability was postulated by Stommel in a pioneering paper (Stommel 1961). He showed in a simple two box model that if the North Atlantic was freshened then the salt-advection feedback means that meridional transport could shift to

a different state. Later work (Bryan 1986; Manabe and Stouffer 1988; Rahmstorf 1995; Hawkins et al. 2011) found multistability in complex ocean models, when the north Atlantic was subject to a 'hosing' experiment in which fresh water was added to the oceans. Other research has shown the AMOC is sensitive to the rate of hosing (Alkhayuon et al. 2019) in a complex way (Lohmann and Ditlevsen 2021). By this it is meant that there is no well defined critical hosing rate but that increasing the rate will switch the rate from a dangerous to a safe one and back again. Should the AMOC tip, this would have serious impacts on British agriculture (Ritchie et al. 2020), global climate (Jackson et al. 2015) and the carbon cycle (Bozbiyik et al. 2011).

Increased Arctic precipitation, melting of the Greenland ice sheet and increases in surface temperatures all act to weaken the AMOC (Armstrong McKay et al. 2022). Over the past half century, there is evidence that the AMOC has weakened by around 15% (Caesar et al. 2018) and might be the weakest in a millennium (Caesar et al. 2021). There is observational evidence of decreasing AMOC stability (Boers 2021; Michel et al. 2022; Ditlevsen and Ditlevsen 2023). Some CMIP5 models show AMOC tipping at low levels of global warming (Drijfhout et al. 2015), although most models show only a gradual decline in the AMOC, which helps explain why the IPCC view AMOC shut-down as being unlikely, although they view the modelled AMOCs as being unrealistically stable (IPCC 2021). Armstrong McKay et al. 2022 estimate the AMOC's threshold to be at 4 °C, with a range of 1.4 °C to 8 °C.

Ice Sheets

Ice sheets, found in Greenland and Antarctica are believed to be able to tip due to many feedback processes. The melt elevation feedback, which is when an ice sheet melts and therefore loses height, exposing its surface to warmer air, increasing the melt rate, is an important feedback (Levermann and Winkelmann 2016). Another relevant feedback is the marine ice sheet instability, which occurs when the grounding line of an ice sheet meets a reverse slope (Schoof 2007).

Complex ice sheet models of Antarctica (Garbe et al. 2020) show hysteresis when global temperatures are reduced. Tipping behaviour has also been observed in complex models of Greenland (Robinson, Calov and Ganopolski 2012; Van Breedam, Goelzer and Huybrechts 2020; Noël et al. 2021). There is evidence of destabilisation in Greenland (Boers and Rypdal 2021) and Armstrong McKay et al. 2022 estimate the critical threshold to be between 0.8 K and 3.0 K with a best estimate of 1.5 K. For Antarctica they estimate a similar threshold for the West Antarctic Ice Sheet but a higher threshold of around 8.5 °C for the East Antarctic Ice Sheet. In all these cases, the tipping dynamics are very slow, taking $\mathcal{O}(1000\ \mathrm{yr})$ to materialise.

Amazon Rainforest

The Amazon Rainforest is a significant store of carbon, containing around 123 Pg C (Malhi et al. 2006), and has for many years been a sink, albeit a weakening one, of anthropogenic carbon (Brienen et al. 2015). The forest affects climate by changing the albedo and aerodynamic

roughness of the surface, and through evapotranspiration, influencing both the global climate and its own conditions (Baker and Spracklen 2019). Furthermore, the forest recycles its own rainfall, which acts to increase the precipitation it experiences (Spracklen, Arnold and Taylor 2012). It is these feedback processes that give the potential for tipping.

Early coupled climate-carbon models (Cox et al. 2000) showed strong decreases in carbon stored in the Amazon. This dieback (Cox et al. 2004) from a forested to a savannah state was caused by drying in the Amazon, where 25% of precipitation reductions over the Amazon under elevated CO_2 was caused by forest feedbacks (Betts et al. 2004). However, Amazon dieback was found to be sensitive to the parametrisation of land surface interactions and the control climate (Huntingford et al. 2004). Since then, some CMIP5 models (Drijfhout et al. 2015) showed signs of Amazon dieback and CMIP6 models show examples of regional Amazon dieback (Parry, Ritchie and Cox 2022).

Other anthropogenic factors can cause abrupt shifts in the Amazon. An example is shifting fire regimes. Fire in the Amazon is driven by humans (Cochrane 2002). Furthermore, fires occur generally below a tree cover threshold (Wuyts, Champneys and House 2017) and fires tend to decrease the tree cover so that as fires become more common in the Amazon due to global warming (Cochchrane and Barber 2009) there could be a shift to a low tree cover and high fire frequency regime (Wuyts and Sieber 2022), behaviour which has been seen in Dynamic Global Vegetation Models (DGVMs) (Lasslop et al. 2016). This result can be understood as resulting from a percolation process (Schertzer, Staver and Levin 2015; Cardoso et al. 2022), in which if the probability of a location having low tree cover is above a critical threshold then large (formally infinite) clusters of fire prone regions will appear.

Percolation theory (Stauffer and Aharony 1994) has also been used to understand the increasing fragmentation of tropical forests (Taubert et al. 2018). It has been argued that as deforestation reduces forest area, this causes an increase in the number of forest fragments. Based on results from percolation theory they found tropical forests were near to the critical point. Other work (Boers et al. 2017) has also found that deforestation in the Amazon can cause tipping as reduced transpiration of water weakens the feedbacks on the South American Monsoon system.

There is observational evidence to believe that the Amazon is bistable, and that it is heading towards a tipping point. There exists a range of mean annual precipitation such that Amazon tree cover can either be high or low, which is evidence of bistability (Hirota et al. 2011; Staver, Archibald and Levin 2011). Furthermore, states with lower mean annual precipitation appear to be less stable (Ciemer et al. 2019). There is evidence of drying in Amazonia (Ritchie et al. 2022), which is a driver of dieback. There is now reason to believe the Amazon is a source of carbon to the atmosphere (Gatti et al. 2021). There are also indications of a loss of resilience in the Amazon (Boulton, Lenton and Boers 2022) which is consistent with an approaching tipping point.

Armstrong McKay et al. 2022 estimate Amazon dieback to occur at global warming levels of 2 K to 6 K with a best estimate of 3.5 K but could be lower when the impact of deforestation is

included. Furthermore, timescales involved in this tipping point ($\mathcal{O}(100\,\mathrm{yr})$) are the timescales of a human life, and so make understanding this tipping point important for environmental policy.

Other Tipping Elements

The Atlantic Meridional Overturning Circulation, ice sheets in Greenland and Antarctica and the Amazon Rainforest are three of the most important tipping elements in the Earth system. However there are other proposed tipping elements. For example, high latitude permafrost may be at risk (Lenton 2012), however there is debate about whether this is a true threshold or a more continuous change (Armstrong McKay et al. 2022). Climate model simulations have suggested the possibility of hydrological tipping points (Teufel and Sushama 2019) which could imply an increased risk of fire.

Coral reefs can have tipping behaviour, as coral death occurs at certain temperature thresholds (Frieler et al. 2013). The tipping point occurs at around $1.5 \pm 0.5\,\mathrm{K}$ of global warming (Armstrong McKay et al. 2022). As a result coral reefs are at high risk of tipping.

1.3.3 Tipping Cascades

In recent years, a number of scientists have investigated the possibility of tipping cascades (Kriegler et al. 2009; Lenton and Williams 2013; Rocha et al. 2018; Steffen et al. 2018; Klose et al. 2021; Wunderling et al. 2021, 2023). A tipping cascade refers to situation where one tipping element tips, causing another tipping element to tip. For example, loss of Greenland ice sheets could increase the probability of the AMOC tipping (Rahmstorf et al. 2015; Caesar et al. 2018). However, other interactions between tipping elements might have a stabilising effect, For example, loss of the west Antarctic ice sheet could stabilise the AMOC (Sinet, Heydt and Dijkstra 2023) due an increased melt water flux.

Whilst many of the findings about tipping points are uncertain, this is particularly acute in the case of research into tipping cascades where much of the research involves the use of conceptual models with highly stylised interactions between elements. However, although many researchers would regard these tipping elements and tipping cascades as unlikely to be triggered, they are often considered 'too risky to bet against' (Lenton et al. 2019). The concept of being too risky to bet against relates to the fact that high impact-low likelihood (HILL) events (Wood et al. 2023) dominate the costs in a cost benefit analysis (Weitzman 2009) as long as they have a non-negligible probability of occurring. To demonstrate that these events can occur, I will give some examples of abrupt shifts from the Earth's past.

1.3.4 Evidence of Tipping Points from Paleoclimate

The Earth is about four and a half billion years old (Dalrymple 2001), and over that time the Earth has experienced many different climates (Alley et al. 2003). Evidence about these past

climates can be obtained through reconstructions based on proxy data. For example, CO_2 concentrations found in Antarctic ice cores can be used to estimate atmospheric CO_2 levels for the last 800, 000 years (Bereiter et al. 2015). Other methods, for example using isotopic data, can be used to reconstruct even older climates (Tierney et al. 2020).

When examining the time series these reconstructions generate, some abrupt shifts can be seen (Brovkin et al. 2021; Boers, Ghil and Stocker 2022). Although it is challenging to work out if these shifts represent tipping points or continuous change (Brovkin and Claussen 2008), there is evidence that some of these shifts are examples of tipping (Dakos et al. 2008). Three example abrupt shifts are considered here. The Snowball Earth is considered as an example of a global shift, Dansgaard-Oeschger events as an example of a rapid abrupt shift and the Green Sahara as an example of an abrupt shift in the biosphere.

Snowball Earth

Budyko and Sellers (Budyko 1969; Sellers 1969) both investigated the role albedo feedbacks on the Earth's energy balance. This feedback is caused when the Earth cools leading to more ice formation which increases the albedo of the Earth, reflecting more energy to space leading to more cooling. This means that the Earth could potentially exist in two states, its current warmer state, and a much colder state known as 'Snowball Earth' where much of the Earth is covered in ice (Held and Suarez 1974; Ghil 1976).

Equation (1.3) is specialised to have a temperature dependent albedo and $F = \varepsilon\sigma T^4$ giving

$$\frac{1}{4}S_0\left(1-\alpha\left(T\right)\right) = \varepsilon\sigma T^4, \tag{1.10}$$

where T is the Earth's mean temperature and ε is the Earth's emissivity. Suppose that the albedo has the following temperature dependence

$$\alpha(T) = \begin{cases} \alpha_-, & T < 273\,\mathrm{K} \\ \alpha_+ + \frac{\alpha_+ - \alpha_-}{T_0 - 273}\left(T - T_0\right) & 273\,\mathrm{K} \leq T \leq T_0 \\ \alpha_+, & T > T_0 \end{cases} \tag{1.11}$$

This form means that the Earth's albedo transitions between the values of α_- to α_+ as the temperature increases and the parameter T_0 controls this location of this transition. Equation (1.10) can be solved, revealing two possible stable states as shown in figure 1.1.

This snowball state was predicted without empirical evidence, however decades after it was postulated evidence arose for its existence (Kirschvink 1992; Hoffman and Schrag 2002). This state appears to have existed in the Neoproterozoic around 650 Myr BP. There is evidence for glaciers near the equator during this time. It is not clear if the Earth was totally covered in ice, or if there was a thin equatorial ocean, leading to a 'slushball' Earth, rather than a 'Hard Snowball' (Pierrehumbert 2005; Pierrehumbert et al. 2011).

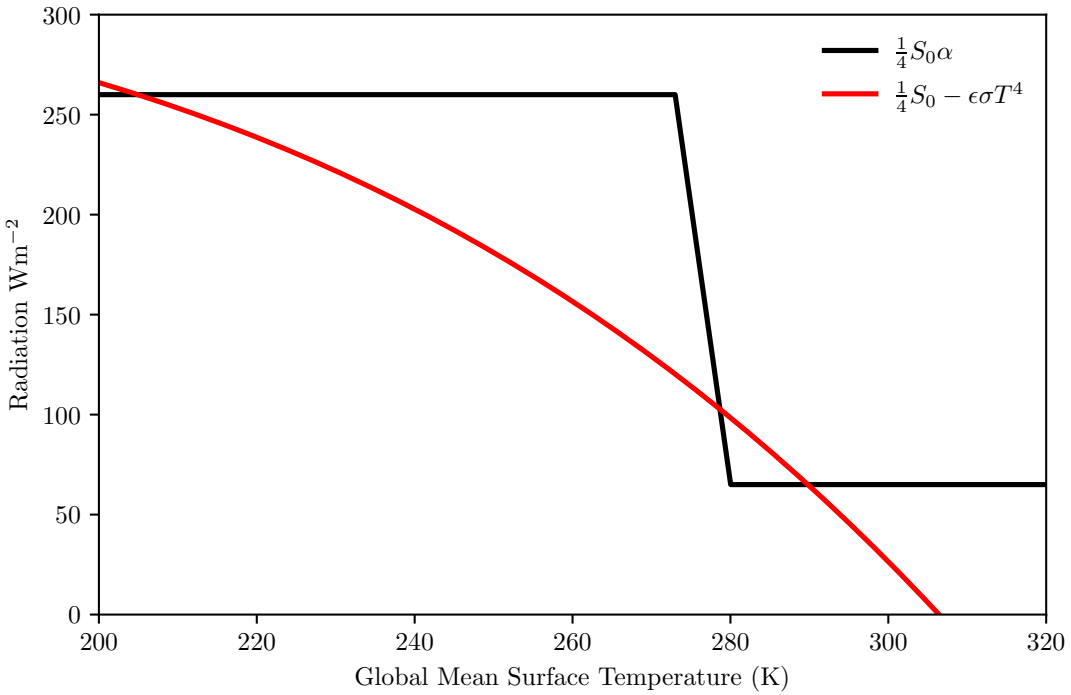

Figure 1.1: The solutions to equations (1.10) and (1.11) are given by the intersections of these curves. The solution at $T \approx 210$ K is the snowball state and the solution at $T \approx 290$ K is the present day state. The intermediate state can be shown to be unstable and as such is not physically observable. The parameters were chosen somewhat arbitrarily, but give a good approximation to the present day state. The parameters are $\alpha_+ = 0.8$, $\alpha_- = 0.2$, $\varepsilon = 0.65$, $T_0 = 280$ K, $S_0 = 1300$ W m^{-2} and $\sigma = 5.67 \times 10^{-8}$ W m^{-2} K^{-4}.

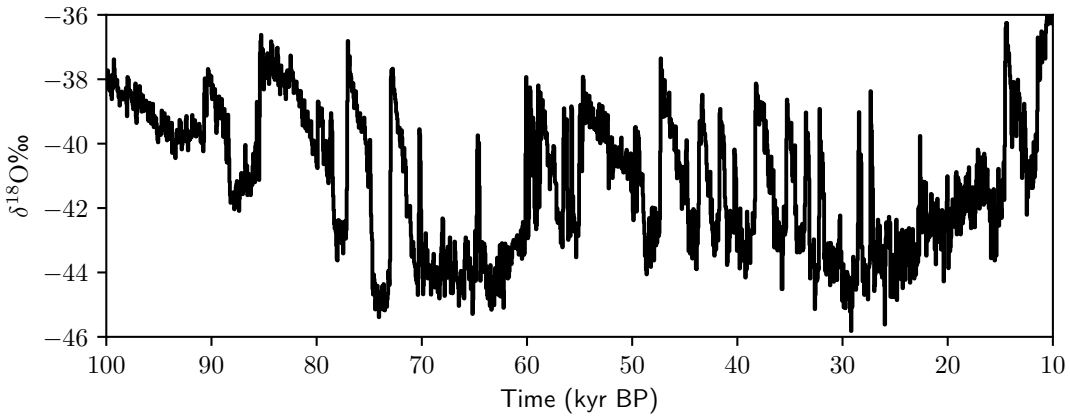

Figure 1.2: A record of δ^{18}O from the NGRIP ice core from Greenland (North Greenland Ice Core Project members 2004) over the last 100,000 years. Higher values correspond to warmer temperatures. The clear spikes in this record are Dansgaard-Oeschger events. Note the rapid warming and slower cooling.

Dansgaard-Oeschger Events

Less dramatic warm/cold transitions exist within the Earth system. During the Quaternary period, which is the current geological period, the Earth has existed in interglacial and glacial states (Lisiecki and Raymo 2005). Within the last glacial period, around 100 kyr BP to 10 kyr BP, there were rapid transitions between cool stadial and warmer interstadial states (Oeschger et al. 1984; Dansgaard et al. 1993). These transitions were discovered in ice cores from Greenland, and represent rapid (on the timescale of 10 years) warming, some of which are up to 16.5 K (Kindler et al. 2014). However the relaxation period back to the stadial state is longer, occurring on centennial timescales. A record of the Dansgaard-Oeschger events is plotted in figure 1.2. There is evidence that these Dansgaard-Oeschger events had a global impact as ice core records show synchronous changes in Antarctica (Buizert et al. 2015).

There is no consensus on the mechanisms of the Dansgaard-Oeschger events, but they are generally believed to be caused by the subtle interplay of atmospheric, sea ice and AMOC dynamics (Boers, Ghil and Rousseau 2018; Vettoretti et al. 2022; Riechers, Gottwald and Boers 2023). There is ongoing debate about the nature of the transition observed in Dansgaard Oeschger events, with different researchers arguing that Dansgaard Oeschger events are driven stochastically (Ditlevsen 1999; Ditlevsen and Johnsen 2010) or deterministically (Boers 2018).

Green Sahara

In the more recent past, a different sort of abrupt shift happened involving the biosphere. During the early part of the Holocene there was a northward expansion of shrub and savannah

ecosystems into what was the Sahara desert, as revealed in the pollen record (Hoelzmann et al. 1998; Hély, Lézine and Contributors 2014). This is therefore a 'greening' of the Sahara. It was a time of enhanced rainfall (Tierney, Pausata and DeMenocal 2017) and is termed the African Humid Period.

The African Humid Period came to an end between 6000 yr BP to 4000 yr BP. Different reconstructions (Kröpelin et al. 2008; Shanahan et al. 2015) disagree on how abrupt the transition was, which may relate to the different regions involved in the reconstruction. An explanation for this involves a biogeophysical feedback proposed by Jule Charney (Charney 1975; Charney, Stone and Quirk 1975). The mechanism is that vegetated ground has a lower albedo than non-vegetated ground, so decreasing the vegetation increases the albedo, leading to decrease in net incoming radiation and a radiative cooling of the atmosphere, and so the air sinks by adiabatic compression which inhibits convection and thus rainfall. This decrease in rainfall would then cause a further vegetation decrease.

Some climate models (Renssen et al. 2006) found that the transition was not abrupt. However, more recent work (Hopcroft and Valdes 2021) using a model that was tuned with mid-Holocene data was able to simulate an abrupt transition.

1.4 Summary

This chapter has given an introduction to climate tipping points as well as the coupled climate-carbon system. I have described some of the main processes at work which govern the climate-carbon system and examined some climate tipping points. In the next chapter, the mathematical theory that underlies tipping points will be explored. In addition, I will provide an introduction to early warning signals for tipping points.

Chapter 2

Mathematical Theory of Tipping Points and Early Warning Signals

Having explained, in chapter 1, the relevance of tipping elements to the Earth system, I will now review the theory behind tipping points in this chapter. To do this I will categorise the ways in which a system can tip. I will also give an example of a system undergoing each of these types of tipping. In part due to the difficulties in accurately representing tipping points in Earth System Models (ESMs), it has become popular to look for generic 'early warning signals' of tipping points. I give a summary of these techniques and how they have been applied to Earth system tipping elements at the end of the chapter.

2.1 A Typology of Tipping Points

It is helpful to classify tipping according to a typology developed by Ashwin et al. 2012. They identified three types of tipping:

B-tipping which refers to a tipping caused by a system crossing a bifurcation due to a change in a parameter of the system.

N-tipping which refers to a tipping caused by noisy fluctuations driving the system from one attractor to another.

R-tipping which refers to a tipping caused by a system failing to track its continuously changing attractor. The 'R' is for 'rate' because the attractor is changing too fast for the system to adapt to it.

Since then, other researchers have found it useful to consider additional types of tipping. For example, Halekotte and Feudel 2020 introduced the concept of shock or S-tipping which is when a single large perturbation can push the system into a new state. When the system's

attractor is not a steady state but is instead a limit cycle, the tipping can depend on the phase of the cycle, a phenomenon which has been dubbed P-tipping (Alkhayuon, Tyson and Wieczorek 2021). More generally, if the tipping depends on the system's location on its attractor then it is known as partial tipping (Alkhayuon and Ashwin 2018). In spatial systems, fragmented tipping is possible (Bastiaansen, Dijkstra and Heydt 2022) in which only part of the domain experiences tipping.

A more detailed examination of B,N,R and S tipping will now be given.

2.1.1 B-Tipping

Theory

Consider a system with a state variable $\boldsymbol{x} \in \mathbb{R}^n$ described by the system of ordinary differential equations

$$\frac{\mathrm{d}\boldsymbol{x}}{\mathrm{d}t} = \boldsymbol{f}(\boldsymbol{x}). \tag{2.1}$$

Suppose the system has a fixed point at $\boldsymbol{x}^*$, such that $\boldsymbol{f}(\boldsymbol{x}^*) = 0$ then the linear stability of the system (Strogatz 2015) is characterised by the behaviour of a small perturbation $\boldsymbol{y}$ about this fixed point, where $\boldsymbol{y} = \boldsymbol{x} - \boldsymbol{x}^*$. Then the dynamics of $\boldsymbol{y}$ are governed by

$$\frac{\mathrm{d}\boldsymbol{y}}{\mathrm{d}t} = J\boldsymbol{y} \tag{2.2}$$

where terms of order $\mathcal{O}\left(|\boldsymbol{y}|^2\right)$ or higher have been neglected and J is a matrix called the Jacobian defined by

$$J_{ij} = \left.\frac{\partial \boldsymbol{f}_i}{\partial \boldsymbol{x}_j}\right|_{\boldsymbol{x}=\boldsymbol{x}^*}. \tag{2.3}$$

The solution to equation (2.2) is

$$\boldsymbol{y} = e^{tJ}\boldsymbol{y}(0). \tag{2.4}$$

Suppose J has n linearly independent eigenvectors (although similar conclusions will hold if it does not (Guckenheimer and Holmes 1983)). Let the set of eigenvectors be $\{\boldsymbol{v}_i\}$ and the set of eigenvalues $\{\lambda_i\}$ then equation (2.4) can be written as

$$\boldsymbol{y} = \sum_i c_i e^{t\lambda_i}\boldsymbol{v}_i \tag{2.5}$$

where $\{c_i\}$ are a set of constants chosen to match the initial conditions. It can be seen then that the long-time behaviour of $\boldsymbol{y}$ is $\boldsymbol{y} \sim c_1 e^{t\lambda_1}\boldsymbol{v}_1$ where λ_1 is the eigenvalue with largest real part. If this is positive, then $\boldsymbol{y}$ will leave the vicinity of $\boldsymbol{x}^*$, whereas if it is negative $\boldsymbol{y}$ will approach $\boldsymbol{x}^*$. Suppose $\boldsymbol{x}^*$ is a hyperbolic fixed point, which means that J has no eigenvalues with zero real part. Then the Hartman-Grobman Theorem (Grobman 1959; Hartman 1960, 1963) guarantees

that the trajectories of $\boldsymbol{y}$ will be topologically conjugate — that is to say qualitatively the same — in some neighbourhood of $\boldsymbol{x}^*$ to the trajectories of $\boldsymbol{x}$. This means that $\boldsymbol{x}^*$ is linearly stable only when J has eigenvalues with only negative real parts. The directions $\boldsymbol{v}_k$ with $\operatorname{Re}\lambda_k < 0$ are known as stable directions (as the flow is attracted to the fixed point along these directions), those with $\operatorname{Re}\lambda_k > 0$ are unstable directions (Strogatz 2015).

B- or Bifurcation-tipping refers to tipping which is driven by changes to the stability, or the loss altogether, of these fixed points. A bifurcation is a concept from the mathematical theory of dynamical systems, introduced by Poincaré 1885. It is used to describe a situation where the fixed points of a system qualitatively change as a control parameter is varied.

Consider a modification to equation (2.1) where a control parameter $\mu \in \mathbb{R}$ (which could, for example, be atmospheric CO_2) has been introduced

$$\frac{\mathrm{d}\boldsymbol{x}}{\mathrm{d}t} = \boldsymbol{f}_\mu(\boldsymbol{x}). \tag{2.6}$$

The fixed points are described by $\boldsymbol{f}_\mu(\boldsymbol{x}^*) = 0$. By the Implicit Function Theorem (Spivak 1965), $\boldsymbol{x}^*$ is a smooth function of μ except at points where J has a zero eigenvalue, these points in $(\boldsymbol{x}, \mu)$ space are known as bifurcation points. Other bifurcation points can occur when a stable fixed point becomes unstable (or vice versa). In both cases an eigenvalue of J must cross the imaginary axis, i.e. have zero real part (Guckenheimer and Holmes 1983). As a result of this, the Hartman-Grobman Theorem is not applicable and so a non-linear analysis must be undertaken.

Fortunately, there are techniques to deal with this, using the Centre Manifold Theorem (Hirsch, Pugh and Shub 1977), which can be stated loosely as

Theorem 1 (Centre Manifold Theorem)**.** *Let the eigenvalues, $\{\lambda_i\}$, of J be divided into three sets such that* $\operatorname{spec} J = \sigma_s \cup \sigma_u \cup \sigma_c$*, where $\sigma_s = \{\lambda_i : \operatorname{Re}\lambda_i < 0\}$, $\sigma_u = \{\lambda_i : \operatorname{Re}\lambda_i > 0\}$ and $\sigma_c = \{\lambda_i : \operatorname{Re}\lambda_i = 0\}$. Let their respective eigenspaces be E_s, E_u and E_c. Then there are stable and unstable invariant manifolds W_s and W_u tangent to E_s and E_u at $\boldsymbol{x}^*$, and a centre manifold W_c tangent to E_c at $\boldsymbol{x}^*$.*

The upshot of this theorem is that the dynamics are now controlled by the centre manifold. Suppose that the unstable manifold is empty (the most relevant case for tipping point research) then theorem 1 implies that the dynamics are topologically conjugate to

$$\frac{\mathrm{d}\boldsymbol{u}}{\mathrm{d}t} = g(\boldsymbol{u}) \tag{2.7a}$$

$$\frac{\mathrm{d}\boldsymbol{v}}{\mathrm{d}t} = -\boldsymbol{v} \tag{2.7b}$$

with $(\boldsymbol{u}, \boldsymbol{v}) \in W_c \times W_s$. At long times $\boldsymbol{v} \to \boldsymbol{0}$ so at long times the dynamics are given by $\boldsymbol{u}$ on the centre manifold (Guckenheimer and Holmes 1983). In order to calculate g, suppose

that $\boldsymbol{x} = (\boldsymbol{u}, \boldsymbol{z}) \in \mathbb{R}^n$ so that

$$\frac{\mathrm{d}\boldsymbol{u}}{\mathrm{d}t} = A\boldsymbol{u} + p(\boldsymbol{u}, \boldsymbol{z}) \tag{2.8a}$$

$$\frac{\mathrm{d}\boldsymbol{z}}{\mathrm{d}t} = B\boldsymbol{z} + q(\boldsymbol{u}, \boldsymbol{z}) \tag{2.8b}$$

where A, B have eigenvalues with zero and negative real parts respectively and p, q are nonlinear functions without any linear terms. Then the centre manifold can be written as a graph $W_c = (\boldsymbol{u}, h(\boldsymbol{u}))$ with $\boldsymbol{z} = h(\boldsymbol{u})$, so that on the centre manifold

$$\frac{\mathrm{d}\boldsymbol{u}}{\mathrm{d}t} = A\boldsymbol{u} + p\left(\boldsymbol{u}, h\left(\boldsymbol{u}\right)\right). \tag{2.9}$$

The next step is to make equation (2.9) as simple as possible. By the Hartman-Grobman Theorem, equation (2.9) cannot be linearised. However the next most simplest approach is to use normal forms, which describe the different sorts of possible bifurcations (Dijkstra 2011).

Consider again equation (2.6), but now enlarge the state space to $\mathbb{R}^{n+1}$ by viewing μ as a dynamic variable with $\dot{\mu} = 0$. Suppose further, without loss of generality, that there is a bifurcation point at $(\boldsymbol{x}, \mu) = (\boldsymbol{0}, 0)$ where J has a simple zero eigenvalue. Then using theorem 1 a centre manifold passing through $(\boldsymbol{0}, 0)$ can be found. If the trajectories are restricted to the centre manifold and certain transversality conditions are met ($\partial_\mu f \neq 0$, $\partial_{xx} f \neq 0$ at the bifurcation point) the trajectories will be topologically equivalent (Guckenheimer and Holmes 1983) to

$$\frac{\mathrm{d}x}{\mathrm{d}t} = \mu + x^2. \tag{2.10}$$

This type of bifurcation is known as a saddle-node or a fold bifurcation. This remarkable fact has simplified a high dimensional dynamical system to a generic one-dimensional system near the bifurcation point (Glendinning 1994).

The saddle-node bifurcation is very important as other bifurcation problems can be perturbed into a saddle-node bifurcation problem (as it is unusual for the transversality conditions not to be met). In this sense, saddle-nodes are the type of bifurcations to be expected in nature. However if the transversality conditions are not met other types of bifurcations can arise.

If $\partial_\mu f = 0$, then the system is equivalent to

$$\frac{\mathrm{d}x}{\mathrm{d}t} = \mu x - x^2, \tag{2.11}$$

which is the normal form for a transcritical bifurcation. If $\partial_\mu f = 0$ and $\partial_{xx} f = 0$ with $\partial_{xxx} f \neq 0$ the bifurcation is known as a pitchfork bifurcation with normal form

$$\frac{\mathrm{d}x}{\mathrm{d}t} = \mu x - x^3. \tag{2.12}$$

Another important sort of bifurcation is a Hopf bifurcation (Hopf 1942). For this bifurcation, a complex conjugate eigenvalue pair become purely imaginary, $\lambda = \pm i\omega$. As there are no zero eigenvalues the Implicit Function Theorem implies no new equilibria will be created. However it will lead to a change in the dimensions of the stable and unstable manifolds, leading to a qualitative change in the behaviour of the system. It can be shown that there is a centre manifold on which a limit cycle can exist (Guckenheimer and Holmes 1983). In other words, these bifurcations lead to the creation of periodic oscillatory behaviour. These bifurcations can occur only in systems of dimension two or higher. The normal form of this bifurcation (Kuznetsov 2004) can be expressed as a differential equation involving the complex variable $z = x + iy$

$$\frac{\mathrm{d}z}{\mathrm{d}t} = (\mu + i)z - z|z|^2. \tag{2.13}$$

Stommel's AMOC Model

As an example of B-tipping, consider Stommel's AMOC model (Stommel 1961), which after a rescaling (Dijkstra 2011) can be written as:

$$\frac{\mathrm{d}T}{\mathrm{d}t} = \eta_1 - T\,(1 - |\Psi|) \tag{2.14a}$$

$$\frac{\mathrm{d}S}{\mathrm{d}t} = \eta_2 - S\,\big(\eta_3 + |\Psi|\big) \tag{2.14b}$$

$$\Psi = T - S \tag{2.14c}$$

where T and S are (dimensionless) equator to pole temperature and salinity differences respectively. The flux $\Psi = T - S$ is the strength of the AMOC. The parameters η_1, η_2, η_3 represent thermal forcing, freshwater forcing and the ratio of their timescales respectively.

Figure 2.1 shows the equilibria of equation (2.14) as well the solution to equation (2.14) for the case where η_2 slowly increases to a maximum and then slowly decreases again following a parabolic trajectory. As η_2 is increased the strength of the AMOC decreases until it reaches a saddle-node bifurcation point at $\eta_2^* \approx 1.2$ where the AMOC abruptly transitions to a weaker state with flow in the opposite direction. Near the bifurcation point, the flux behaves like $\Psi \sim \sqrt{\eta_2^* - \eta_2}$, which reflects the normal form equation (2.10). Note that when η_2 is decreased, it must be brought down to the lower value of 0.9 to transition back into its original state. This is known as hysteresis.

2.1.2 N-tipping

If a system with multiple stable states is subject to stochastic forcing, then it will perform transitions between these states if observed for long enough. This phenomenon is called N- or noise-tipping. This has an important difference to B-tipping. In B-tipping an external driver

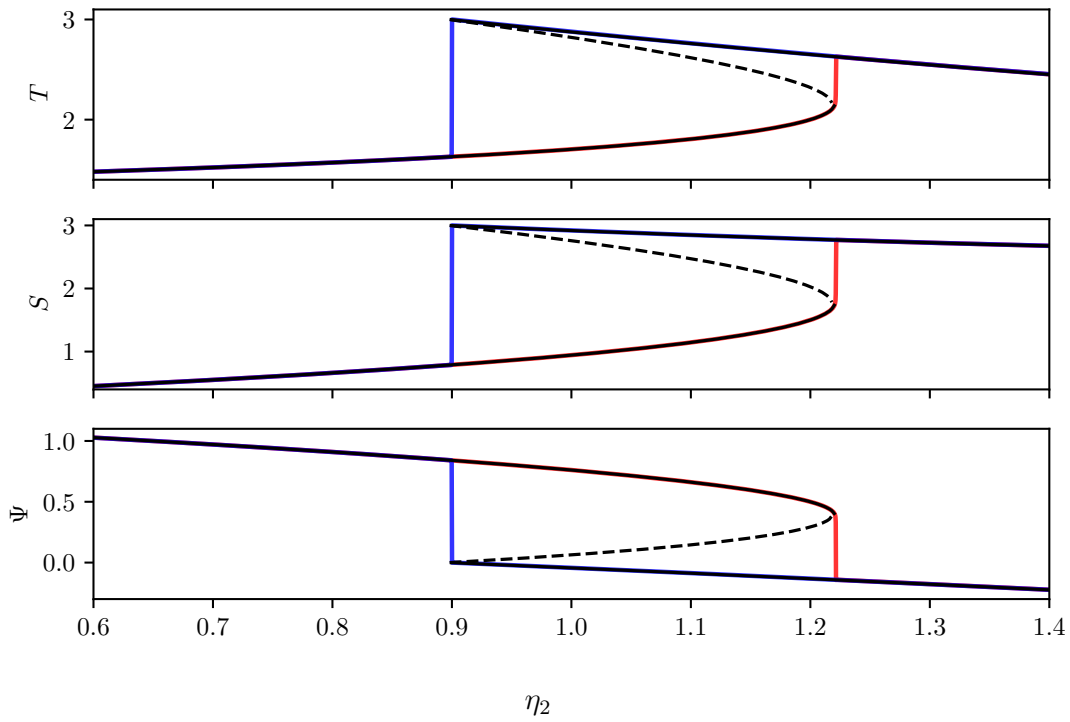

Figure 2.1: This shows the state of the Stommel model, equation (2.14), as a function of the parameter η_2. The stable equilibrium states are given by solid black lines and the unstable states are given by the black dashed line. The red line shows the instantaneous state of the AMOC for η_2 slowly increasing from 0.6 to 1.4. The blue line shows the instantaneous state for η_2 decreasing from 1.4 to 0.6. As η_2 is increased, the AMOC transitions from a strong poleward flow to a weaker equatorward state. Note that near the bifurcation point around $\eta_2 \approx 1.2$ the stable states seem to behave like the square root of the control parameter. This reflects the normal form of the bifurcation. Note that when η_2 is decreased the transition back to the poleward flow state happens at a lower value of η_2 — this is an example of hysteresis. The other parameters were set to $\eta_1 = 3$, $\eta_3 = 0.3$.

changes a control parameter, causing a system to tip but in N-tipping the natural variability of the system causes it to tip.

The role of noise in the climate system was identified by Hasselmann 1976. He viewed the 'slow' components of the Earth system (the ocean, the vegetation and the ice sheets) as being deterministic and the 'fast' components (the atmosphere) as being essentially stochastic. This stochasticity may be viewed as an effective model for chaotic systems (Lorenz 1963) or resulting from unresolved processes (Palmer et al. 2009). Certain paleoclimate abrupt shifts, such as the Dansgaard-Oeschger events, have been viewed as N-tipping (Ditlevsen 1999).

Stochastic differential equations can be written (Jacobs 2010) as

$$\frac{\mathrm{d}\boldsymbol{x}}{\mathrm{d}t} = \boldsymbol{F}(\boldsymbol{x}) + G(\boldsymbol{x})\boldsymbol{\eta}(t). \tag{2.15}$$

The vector function $\boldsymbol{F}$ represents the deterministic evolution and the matrix function G represents the stochastic evolution. The function $\boldsymbol{\eta}(t) = \mathrm{d}\boldsymbol{W}/\mathrm{d}t$ is known as white noise and is the derivative of a Wiener process. It is the source of the stochasticity. It has mean zero and is 'delta correlated' in time, by which is meant

$$\mathbb{E}\left(\boldsymbol{\eta}_i(t)\boldsymbol{\eta}_j(t')\right) = \delta_{ij}\delta(t-t') \tag{2.16}$$

where δ_{ij} is the Kronecker delta and $\delta(t-t')$ is the Dirac delta function. This notation is somewhat misleading as it suggests that all the functions involved are differentiable, however realisations of the Wiener process are almost surely not differentiable (McKean, Birnbaum and Lukacs 2014). More rigorously, equation (2.15) should be written as

$$\mathrm{d}\boldsymbol{x}_t = \boldsymbol{F}(\boldsymbol{x}_t)\,\mathrm{d}t + G(\boldsymbol{x}_t)\,\mathrm{d}\boldsymbol{W}_t \tag{2.17}$$

where the differentials are understood to imply integration. The notation of equation (2.15) tends to be favoured by physicists and that of equation (2.17) by mathematicians.

Viewing individual solutions of equation (2.15), or sample paths, is one approach to analysing stochastic systems. Another useful approach is to calculate the probability density function (pdf), $p(\boldsymbol{x}, t)$ of $\boldsymbol{x}$ and how it evolves in time. The tool to do this is the Fokker-Planck equation (Fokker 1914; Planck 1917), given by

$$\frac{\partial p}{\partial t} = -\sum_i \partial_i\left(\boldsymbol{F}_i p\right) + \sum_i\sum_j \partial_i\partial_j\left(D_{ij}p\right) \tag{2.18}$$

where $D = GG^T/2$.

Kramers' Escape Rate

Often a very simple one-dimensional model is used in studies of N-tipping

$$\frac{\mathrm{d}x}{\mathrm{d}t} = -\frac{\mathrm{d}U}{\mathrm{d}x} + \sigma\eta(t). \tag{2.19}$$

This is an example of a potential system because the deterministic dynamics are given by the gradient of a potential function, $U(x)$. Any one dimensional system can be put in this form but that is not always the case for higher dimensional systems. Furthermore, the noise is assumed to be 'white', with constant variance σ^2. It is known as white noise because in the frequency domain, all frequencies are excited with equal amplitude. This is a questionable assumption for the Earth system, where the spectrum is not white (Mitchell 1976; Heydt et al. 2021) and may change due to climate change (Huntingford et al. 2013).

Equation (2.19) has an associated Fokker-Planck equation

$$\frac{\partial p}{\partial t} = \frac{\partial}{\partial x}\left(\frac{\mathrm{d}U}{\mathrm{d}x}p\right) + \frac{1}{2}\sigma^2\frac{\partial^2 p}{\partial x^2}, \tag{2.20}$$

which can also be written in the form of a continuity equation

$$\frac{\partial p}{\partial t} + \frac{\partial J}{\partial x} = 0 \tag{2.21}$$

where J is the probability current given by

$$J(x) = -\frac{\mathrm{d}U}{\mathrm{d}x}p - \frac{1}{2}\sigma^2\frac{\partial p}{\partial x}. \tag{2.22}$$

If equation (2.19) has multiple stable states, then an estimate of the transition rate between these states can be made. This estimate is known as the Kramers' Rate (Kramers 1940). This derivation follows Risken 1984.

Suppose that U has the form given by figure 2.2, which has a stable state at x_{min}, an unstable state at x_{max}. The rate at which the system transitions from near x_{min}, in the region between x_1 and x_2, to the other side of the maximum, near x_3, is to be determined. Assuming the system is in a near steady state, equation (2.21) implies that J is approximately constant. By multiplying equation (2.22) by the integrating factor $\exp\frac{2U(x)}{\sigma^2}$, J can be put into the form

$$J = -\frac{1}{2}\sigma^2 e^{-\frac{2U(x)}{\sigma^2}}\frac{\partial}{\partial x}\left(p(x)e^{\frac{2U(x)}{\sigma^2}}\right). \tag{2.23}$$

This can then be integrated from x_{min} to x_3 to give

$$J = \frac{\sigma^2}{2}\left(p(x_{min})e^{\frac{2U(x_{min})}{\sigma^2}} - p(x_3)e^{\frac{2U(x_3)}{\sigma^2}}\right)\left(\int_{x_{min}}^{x_3} e^{\frac{2U(x)}{\sigma^2}}\,\mathrm{d}x\right)^{-1}. \tag{2.24}$$

As it will be rare to find the system at x_3, as the noise is weak enough to make the transitions rare, $p(x_3)$ is negligible. To estimate $p(x_{min})$, assume this is given by the equilibrium distribution which can be found by setting J to a constant. This constant can be chosen to be the value of J at x_{min}, giving the following expression for the equilibrium pdf, p_{eq},

$$p_{eq}(x) = p(x_{min})e^{\frac{2U(x_{min})}{\sigma^2}}e^{-\frac{2U(x)}{\sigma^2}}. \tag{2.25}$$

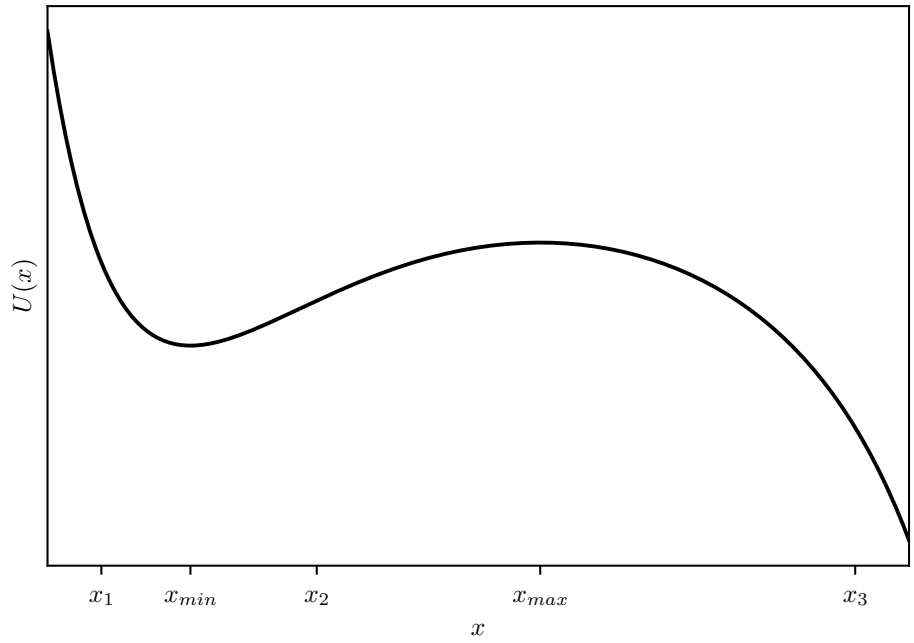

Figure 2.2: An example of a potential with a stable state at x_{min} from which a system can escape over the potential barrier at x_{max} to a new state near x_3. The precise locations of x_1, x_2, x_3 do not matter at the level of approximation Kramers' escape rate formula works at.

The probability of finding the system near x_{min} is therefore

$$P = \int_{x_1}^{x_2} p_{eq}(x)\,\mathrm{d}x = p(x_{min})e^{\frac{2U(x_{min})}{\sigma^2}} \int_{x_1}^{x_2} e^{-\frac{2U(x)}{\sigma^2}}\,\mathrm{d}x. \tag{2.26}$$

The escape rate is $r = J/P$ which becomes

$$r^{-1} = \frac{2}{\sigma^2} \int_{x_1}^{x_2} e^{-\frac{2U(x)}{\sigma^2}}\,\mathrm{d}x \int_{x_{min}}^{x_3} e^{-\frac{2U(x)}{\sigma^2}}\,\mathrm{d}x. \tag{2.27}$$

Each integral can be asymptotically evaluated using Laplace's Method (Bender and Orszag 1978) to give Kramers' escape rate

$$r^{-1} \sim \frac{2\pi}{\sqrt{U''(x_{min})\left|U''(x_{max})\right|}} e^{\frac{2}{\sigma^2}(U(x_{max})-U(x_{min}))}, \tag{2.28}$$

for $\sigma \to 0$.

Example

As an example consider the potential

$$U(x) = -\frac{1}{2}x^2 + \frac{1}{12}x^4 \tag{2.29}$$

which has symmetric stable states at $x = \pm\sqrt{3}$. There is a potential barrier at $x = 0$. Assuming that $\sigma = 0.75$, Kramers' rate predicts a transition timescale of $r^{-1} \approx 65$ time units. Figure 2.3 shows transitions happening on this timescale.

2.1.3 R-tipping

A relatively recently discovered type of tipping is R-tipping. First discovered by Luke and Cox 2010 in a simple model of soil temperatures, R-tipping or rate-induced tipping refers to a situation where the rate of change of a control parameter, rather than the magnitude of the parameter itself controls whether a system tips or not (Wieczorek et al. 2011). This type of tipping occurs in nonautonomous dynamical systems, which is a system with explicit time dependence (Ashwin, Perryman and Wieczorek 2017).

This sort of tipping is best explained through an example, taken from Ashwin et al. 2012. The system is

$$\frac{\mathrm{d}x}{\mathrm{d}t} = \left(x+\mu\right)^2 - 4 \tag{2.30a}$$

$$\frac{\mathrm{d}\mu}{\mathrm{d}t} = r. \tag{2.30b}$$

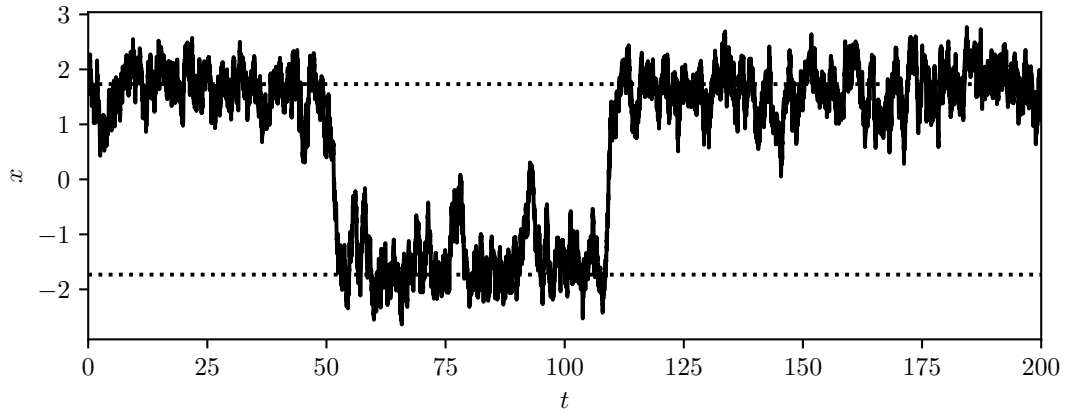

Figure 2.3: A time series showing transitions between two stable states (indicated by a dotted line). Kramers' formula, equation (2.28) predicts a transition timescale of about 65 time units. The time series shows transitions happening on this timescale.

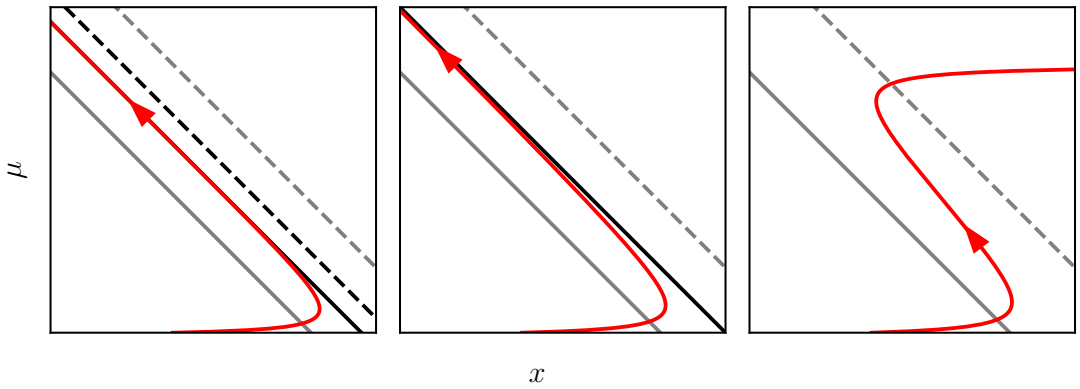

Figure 2.4: Panels showing the state space of a system, equation (2.30), undergoing R-tipping. From left to right, the figures show the system below the critical rate, at the critical rate and above the critical rate. In the left panel, with $r = 3.2$ the lines $x_{\pm}^{\mathrm{PB}}$ exist and are separated. In the centre panel with $r = r_c = 4$, $x_{\pm}^{\mathrm{PB}}$ exist and have collided into one line. In the right panel, $r = 4.8$ and therefore $x_{\pm}^{\mathrm{PB}}$ do not exist. As a result trajectories diverge as the system has undergone R-tipping. Note that for all values of r, the quasi-static equilibria exist.

These equations can be interpreted as a system with state x in a changing environment represented by parameter μ that changes at some finite rate, r.

Consider the 'frozen system' (Wieczorek, Xie and Ashwin 2023), which is equation (2.30a) with μ constant — this describes the dynamics in the case where the environment is unchanging. It has equilibria at $x^*_\pm = \pm 2 - \mu$. The stability of these equilibria can be found in the manner described in section 2.1.1, which in this case amounts to evaluating the derivative of equation (2.30a) with respect to x at $x^*_\pm$. These quasi-static equilibria are shown as grey lines in figure 2.4, where the stable quasi-static equilibria are shown in solid grey and the unstable quasi-static equilibria are shown as a dashed line. It can be shown that x_- is stable for all μ values, and x_+ is unstable for all μ values. As a result a naïve B-tipping analysis would suggest this system cannot tip. However, as will be shown, this system can undergo R-tipping.

To see this, make a change of coordinates into a co-moving frame by setting $y = x + \mu$. Then the system becomes

$$\frac{\mathrm{d}y}{\mathrm{d}t} = y^2 + r - 4. \tag{2.31}$$

This equation has a stable fixed point at $-\sqrt{4-r}$ and an unstable fixed point at $\sqrt{4-r}$. Returning to the x coordinates these solutions correspond to the pullback attractor and repeller of the system, $x^{\mathrm{PB}}_\pm = \pm\sqrt{4-r} - \mu$. These pullback objects are the appropriate generalisation of attractors and repellers to the nonautonomous case (Ghil and Lucarini 2020). They are plotted in black in figure 2.4 where the solid line is the stable state and the dashed line is unstable. It is to x^{PB}_- rather than x_- that the solutions of equation (2.30) are attracted to, plotted in red in figure 2.4.

If $r < 4$, then x^{PB}_- exists and so solutions evolve towards it. However if $r > 4$ then x^{PB}_- does not exist and so solutions diverge to infinity. As a result there is a critical rate, $r_c = 4$, above which R-tipping occurs.

The Compost Bomb

The paradigmatic example of R-tipping is the Compost Bomb instability (Luke and Cox 2010; Wieczorek et al. 2011; Clarke et al. 2021; O'Sullivan, Mulchrone and Wieczorek 2023), which is a thermal instability in the soil. This phenomenon is caused by microbial respiration warming the soil, which in turn increases the soil temperature. However, this respiration decreases the supply of soil carbon and thus decreases the amount of respiration and thus heating in the soil. Due to the differences between the (rapid) timescale of heating and the (slow) timescale of soil carbon decrease there is the possibility for a dramatic increase in soil temperature. Luke and Cox 2010 found that if the air temperature raised faster than a critical rate then the compost

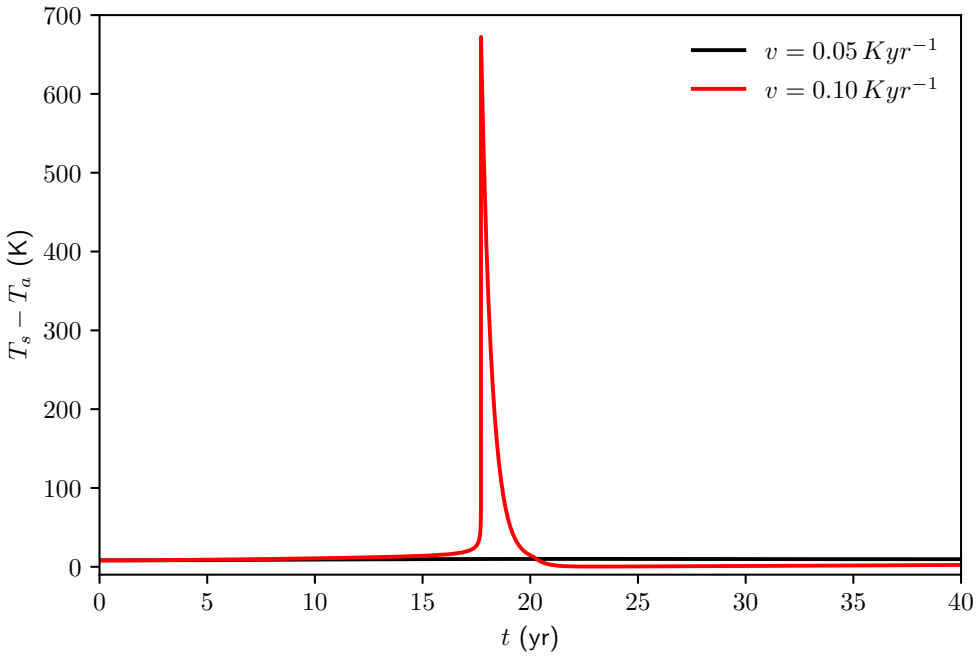

Figure 2.5: A plot of soil temperature relative to air temperature with two different rates of warming, calculated from equation (2.32). Note the spike in temperatures for high enough rates of warming—an example of R-tipping.

bomb instability would be caused. Their model was

$$\mu \frac{\mathrm{d}T_s}{\mathrm{d}t} = -\lambda\,(T_s - T_a) + A r_0 C_s e^{\alpha T_s} \tag{2.32a}$$

$$\frac{\mathrm{d}C_s}{\mathrm{d}t} = \Pi - r_0 C_s e^{\alpha T_s} \tag{2.32b}$$

$$\frac{\mathrm{d}T_a}{\mathrm{d}t} = v \tag{2.32c}$$

where T_s is the soil temperature, T_a is the air temperature and C_s is the soil carbon. The parameters, taken from Wieczorek et al. 2011, are a heat capacity $\mu = 2.5 \times 10^6\,\mathrm{J\,m^{-2}\,K^{-1}}$, a thermal coupling $\lambda = 5.049 \times 10^6\,\mathrm{J\,yr^{-1}\,m^{-2}\,K^{-1}}$, a heat of respiration $A = 3.9 \times 10^7\,\mathrm{J\,kg^{-1}\,C}$, a specific respiration $r_0 = 0.01\,\mathrm{yr^{-1}}$, a temperature dependence of respiration $\alpha = 0.09\,\mathrm{K^{-1}}$ and a net primary productivity $\Pi = 1.055\,\mathrm{kg\,C\,m^{-2}\,yr^{-1}}$. When the rate of increase in temperature is increased above a critical rate, $v \approx 0.08\,\mathrm{K\,yr^{-1}}$ the instability is triggered.

Figure 2.5 shows two time series of equation (2.32) with $v = 0.05\,\mathrm{K\,yr^{-1}}$ and $v = 0.1\,\mathrm{K\,yr^{-1}}$. For the larger rate of warming there is a clear spike in the soil temperatures.

2.1.4 S-tipping

A more recent addition to the tipping points typology is that of S- or shock-tipping. This refers to a situation where a single large perturbation can push a system from one state to another (Halekotte and Feudel 2020; Feudel 2023), such as an extreme weather event on an ecosystem. In this sense it is closely related to ideas of resilience introduced by Holling 1973.

It is related to N-tipping but should be differentiated from it in the following sense. If $\boldsymbol{x}^*$ is a fixed point, with a basin of attraction $\mathcal{B}$ then the smallest perturbation required to push the system into a new state is given by

$$\boldsymbol{\Delta} = \arg\min\{|\boldsymbol{x}'|\colon \boldsymbol{x}^* + \boldsymbol{x}' \notin \mathcal{B}\}. \tag{2.33}$$

If the system is the potential system equation (2.19), then this is equal in magnitude to the distance to the nearest maximum, $|x_{max} - x_{min}|$. This should be compared to Kramers' formula, equation (2.28), which is a function of the difference in potential $U(x_{max}) - U(x_{min})$. In other words, S-tipping depends on the distance to the potential barrier, but N-tipping depends on the height of that barrier.

Allee Effect

Consider a population growing via logistic growth with carrying capacity k that is subject to the Allee Effect (Allee and Bowen 1932; Stephens, Sutherland and Freckleton 1999), which is an effect that reduces growth rates at low population densities. A simple model of this is

$$\frac{\mathrm{d}x}{\mathrm{d}t} = x\,(x-1)\left(1 - \frac{x}{k}\right), \tag{2.34}$$

where $k > 1$ and x is a population density. This has equilibria at $x_1 = 0, x_2 = 1$ and $x_3 = k$. The equilibria at x_1 and x_3 are stable. x_1 corresponds to an extinct state and x_3 to a populated state.

If the system is initially in equilibrium at x_3, the distance to the basin boundary is $\Delta = |x_3 - x_2| = k - 1$. Hence if the system receives a kick of this magnitude or greater then the system will transition to the extinction state. Figure 2.6, shows the evolution of x as equation (2.34) is integrated with $k = 2.0$ and given perturbations of magnitude 0.99 and 1.01 at times 25.0 and 50.0. The first perturbation is not large enough to push the system across the boundary of the basin of attraction, yet the second one is, which is why the population undergoes S-tipping after the second perturbation.

2.1.5 Tipping in Reality

This typology has given the impression that individual tipping phenomena can be easily assigned to the categories of B,N,R or S-tipping. However this is not the case as any real tipping point will have aspects of many of the different tipping types. For example, if a control parameter is changing such that the system is approaching a B-tipping point, then

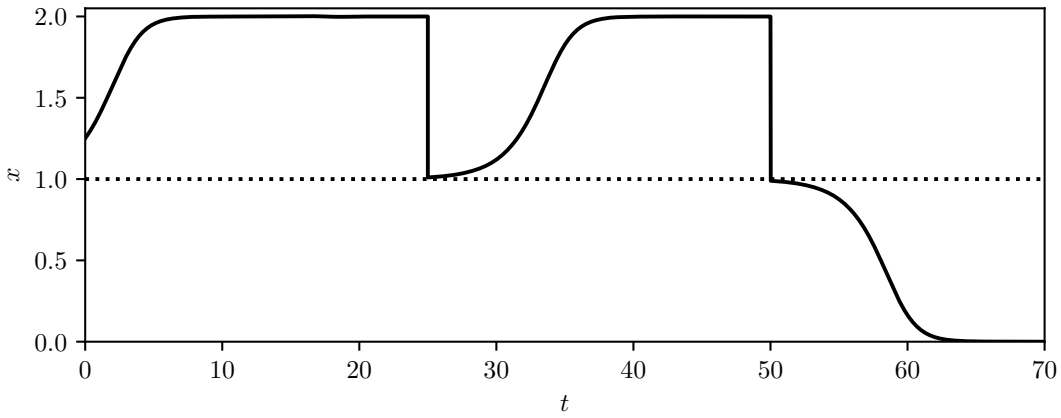

Figure 2.6: An example of shock-tipping. The system given by equation (2.34) receives a perturbation of 0.99 at time 25.0. This is not large enough to make it cross the basin boundary (given by the dotted line) and so the system recovers. However at time 50.0 a perturbation of 1.01 is given which is enough to make it cross the basin boundary and thus to make the population go extinct.

Kramers' formula equation (2.28) implies that the system is more likely to undergo N-tipping. Furthermore, a system nearing a tipping point will be more likely to undergo S-tipping as Δ, defined by equation (2.33), is smaller as the basin of attraction shrinks. If a system is experiencing a shock, it is also likely that its parameters will be changing quickly as well so this tipping will have an R-tipping character too.

Although real tipping points may have multiple characteristics it is still often possible and, more importantly, still useful to categorise the tipping into one of the above categories.

2.2 Early Warning Signals

Given the large impact a climate tipping point would have (Lenton et al. 2019), it would be useful to know at what level of climate forcing they would be triggered. However models show little agreement about the level of forcing required to cause them (Drijfhout et al. 2015). The processes of interest are by their nature nonlinear and often involve interactions between the physical climate and the biosphere, where the 'correct' equations are inherently uncertain. Furthermore, some tipping behaviour may depend on subgrid scale processes, such as in the case of fire (Mangeon et al. 2016). As a result a precise determination of the dangerous level of climate forcing is challenging.

Instead, a theory of *early warning signals* (EWS), sometimes known as *early warning indicators* (EWI), has emerged (Dakos et al. 2008; Scheffer et al. 2009; Lenton 2011; Williamson and Lenton 2015). These techniques attempt to use certain generic statistical features of tipping points to provide an indication as to whether a system is moving towards a tipping point. This

is closely related to ideas about normal forms developed in section 2.1.1.

However not all types of tipping will give good early warning signals. Noise and shock tipping are not driven by a continuously changing external factor and so early warning signals (in the conventional sense) will not be useful in these cases. For the case of rate tipping, there has been some work on early warning signals (Ritchie and Sieber 2016). However most of the work has been done for bifurcation tipping where statistics can be calculated as a function of a slowly evolving parameter.

2.2.1 Critical Slowing Down

The basic idea of early warning signals is that of *critical slowing down* (Dakos et al. 2008). Suppose there is a system

$$\frac{\mathrm{d}x}{\mathrm{d}t} = f(x, \mu) \tag{2.35}$$

which has a stable state for $\mu < \mu_c$ at x^* and undergoes a bifurcation when $\mu = \mu_c$. Then before the bifurcation, the system can be linearised about this steady state to give

$$\frac{\mathrm{d}y}{\mathrm{d}t} = -\lambda y \tag{2.36}$$

where $y = x - x^*$ and $\lambda = -f'(x^*, \mu)$. As the bifurcation is approached, $\lambda \to 0$ so any method that detects changes in λ can act as an early warning signal, in a quite generic way, for B-tipping.

Solving equation (2.36) gives

$$y = e^{\lambda t} y(0) \tag{2.37}$$

and so λ^{-1} gives the timescale for perturbations to relax to equilibrium. This means that as $\lambda \to 0$, this timescale approaches infinity, hence the name critical slowing down.

2.2.2 Variance and Autocorrelation

A very common way to approach early warning signals is to assume that the system of interest can be modelled as a one dimensional system subject to additive Gaussian white noise. The first of these assumptions is defensible on the grounds that near a bifurcation point, generic systems behave qualitatively like equation (2.10). The second assumption is more suspect as systems are generally subject to time correlated noise, such as red noise. However in the case of red noise, as long as the dynamics are considered over long enough timescales, then the noise can be approximated as white. This assumption amounts to analysing the Langevin equation (Langevin 1908)

$$\frac{\mathrm{d}x}{\mathrm{d}t} = f(x) + \sigma\eta(t) \tag{2.38}$$

where η is delta correlated noise and σ^2 is the variance of the noise. This system can then be linearised to give

$$\frac{\mathrm{d}y}{\mathrm{d}t} = -\lambda y + \sigma\eta(t) \tag{2.39}$$

where y and λ are defined as in equation (2.36). This is the equation that defines an Ornstein-Uhlenbeck process (Uhlenbeck and Ornstein 1930) and its statistical properties are well known. The Fluctuation-Dissipation Theorem (Einstein 1905; Kubo 1966; Leith 1975; Marconi et al. 2008) provides a link between the variability of a system and its response to forcing, i.e. λ.

In this case the important statistics are

$$\sigma_y^2 = \frac{\sigma^2}{2\lambda} \tag{2.40}$$

$$\alpha_1 = e^{-\lambda} \tag{2.41}$$

where σ_y^2 is the variance of y and α_1 is the autocorrelation of y at lag 1. As $\lambda \to 0$

$$\sigma_y^2 \to \infty \tag{2.42}$$

$$\alpha_1 \to 1. \tag{2.43}$$

This means that as a system with state x approaches a B-tipping point, then its fluctuations about equilibrium, given by y, should have their variance diverge and their autocorrelation tend to unity.

The question remains how to extract y from a time series of x. If x^*, the equilibrium, was known then this could be directly subtracted from x to give y. However if the equilibrium was known then there would be no need for early warning signals as the bifurcation point could be calculated explicitly. Instead it is usually assumed that by subtracting a (possibly nonlinear) trend off of x what remains will approximate y.

This leads to the following method to generate early warning signals from a time series:

1. Split the time series of x into rolling windows of length τ_w. Let x_i refer to the x values in window i.

2. Detrend the time series x_i to get y_i.

3. Calculate the variance $\sigma_{y_i}^2$ and autocorrelation α_1 of y_i.

4. Perform statistical tests to detect if $\sigma_{y_i}^2$ and α_1 are increasing. Statistical tests, such as the Mann-Kendall test (Wilks 2019) or a phase surrogate approach (Boettner and Boers 2022) are commonly used.

5. If they are increasing, then this can be taken as an early warning of an approaching B-tipping.

In order for this technique to work, a particular assumption about timescales must be satisfied (Thompson and Sieber 2011). This is that

$$\tau_{\text{drift}} \gg \tau_{\text{crit}} \gg \tau_{\text{stab}}, \tag{2.44}$$

which are the timescales of the long term drift of the system, the timescale of the critical direction of the system (which is the one being destabilised) and the other timescales of the stable directions respectively. The first inequality is needed so that μ can be assumed to be constant in each sliding window. The second is needed so that the timescale being detected is the timescale corresponding to the critical direction. It should be noted that $\tau_{\text{crit}} \to \infty$ as the bifurcation is approached and so inequality 2.44 will be violated eventually. Furthermore anthropogenic climate change is happening on fast timescales so it may be the case that $\tau_{\text{drift}} \approx \tau_{\text{crit}}$ or even $\tau_{\text{drift}} \ll \tau_{\text{crit}}$.

Example

In figure 2.7 early warning signals are calculated for the system

$$\frac{\mathrm{d}x}{\mathrm{d}t} = x - \frac{1}{3}x^3 - \mu + \sigma\eta(t) \tag{2.45}$$

where $\mu = \varepsilon t$, $\sigma = 0.025$ and $\varepsilon = 1 \times 10^{-4}$. The value of ε has been chosen to be small to enable an autonomous analysis. The system has a bifurcation when $\mu = 2/3$. The value of λ can be calculated by taking a derivative:

$$\lambda = (x^*)^2 - 1 \tag{2.46}$$

where x^* is the equilibrium. The variance and autocorrelation are estimated empirically from the detrended time series of x. In addition, the variance and autocorrelation predicted by equations (2.40) and (2.41) are calculated. It can be seen there is a good agreement and a clear early warning signal before the bifurcation.

2.2.3 Other Early Warning Signals

These indicators have been generalised to higher dimensional and periodically forced systems (Williamson and Lenton 2015; Williamson, Bathiany and M Lenton 2016). Attempts have also been made to estimate λ, the inverse timescale directly (Boers 2021; Boettner and Boers 2022). The idea to look at changes in timescale of fluctuations has been investigated using Detrended Fluctuation Analysis (Livina and Lenton 2007), where it was used to anticipate the warming at the end of the Younger Dryas. Changes in these timescales can also lead to spectral reddening (Kleinen, Held and Petschel-Held 2003). Higher order moments have proved useful too, such as the skewness (Guttal and Jayaprakash 2008) and kurtosis (Xie et al. 2019). The phenomenon of flickering (Wang et al. 2012), in which systems 'flicker' back and forth between alternative stable states can also be used to detect upcoming transitions. More

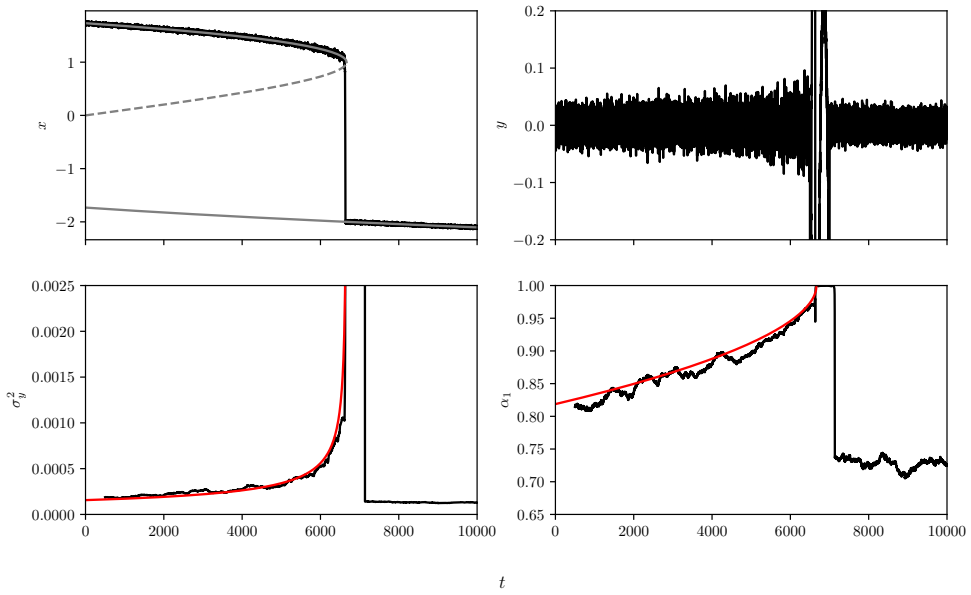

Figure 2.7: An example of using early warning signals to detect an approaching tipping point. In the top left is the original time series in black, obtained from integrating equation (2.45) with a timestep of 0.1. Also shown in grey are the quasi-static equilibria, where the unstable equilibria are shown with a dotted line. The top right shows the time series detrended using a cubic polynomial in windows of length 500 time units. The bottom left shows the variance of the detrended time series with the variance calculated through equation (2.40) in red. The bottom right shows the autocorrelation of the detrended time series with the autocorrelation calculated by equation (2.41) shown in red. There is a clear early warning signal of rising variance and autocorrelation before the bifurcation.

recently, machine learning techniques have had success in giving early warning for modelled transitions (Bury et al. 2021). Any measure of resilience of an ecosystem can function as an early warning indicator, see Krakovská, Kuehn and Longo 2023 for examples of ecological resilience.

Methods which calculate the early warning statistics over space rather than over time have also been used (Guttal and Jayaprakash 2009; Donangelo et al. 2010). Changes in spatial patterns, for example of vegetation, have also been suggested as early warning indicators (Kéfi et al. 2007, 2014) although introducing spatial dynamics can complicate the analysis of tipping points (Rietkerk et al. 2021).

Whilst these indicators generally try to be generic — in that they are applicable to many different systems — there is no reason why early warning indicators cannot be designed for specific systems. Parry, Ritchie and Cox 2022 found that the seasonal cycle in temperature was a potential early warning system for Amazon dieback and Boulton, Good and Lenton 2013 found the sensitivity of net ecosystem productivity to temperature decreases towards the tipping point.

2.2.4 The Use of Early Warning Signals

Early Warning Signals have been applied to the Earth system. For example Dakos et al. 2008 applied them to a variety of abrupt shifts and found that they were preceded by rises in autocorrelation, although some of these trends could have occurred by chance. They have also been used to provide evidence for the subpolar gyre circulation destabilising prior to the Little Ice Age (Arellano-Nava et al. 2022). Furthermore their presence has been used to argue that Dansgaard-Oeschger events are B-tipping (Boers 2018) and their absence has been used to argue that Dansgaard-Oeschger events are N-tipping (Ditlevsen and Johnsen 2010). These contradictory findings are related to differences in the way the ice core data is processed.

Early Warning Signals have been investigated for the Greenland ice sheet (Boers and Rypdal 2021). This study suggested the ice sheet was close to a tipping point. However given the slow response of the ice sheet and the fast change of the climate, inequality 2.44 is likely to be violated with the timescale of the drift to be much faster than the timescale of the dynamics. Furthermore, the analysis is of melt rates rather than a state variable which describes the ice sheet itself. However, the researchers could relate the observed fluctuations to a physically motivated simple nonlinear model of the ice sheet, which would suggest the ice sheet is approaching a tipping point.

Later that year, another paper (Boers 2021), was published suggesting the AMOC was approaching a tipping point due to increases in autocorrelation and variance. Other work (Ditlevsen and Ditlevsen 2023) went as far as to suggest that most likely year for the AMOC to tip is 2057. Although the dynamics of the AMOC are faster than that of the ice sheets (Armstrong McKay et al. 2022), it is still not clear if inequality 2.44 is satisfied but early warning signals have been used in complex models to detect AMOC shut-down (Boulton, Allison and Lenton 2014). Furthermore, the analysis was not based on the AMOC strength directly but

on 'fingerprints' derived from sea surface temperature and salinity data.

Recent work (Boulton, Lenton and Boers 2022) found increases in the autocorrelation in the Vegetation Optical Depth (a satellite measure of vegetation biomass) in the Amazon, which is consistent with a loss of resilience in that ecosystem. The results for changes in variance were more equivocal. Whilst the Amazon is a relatively fast tipping point (Ritchie et al. 2021), some complex models do not show generic early warning signals before the tipping point (Boulton, Good and Lenton 2013). Other work (Fernández-Martínez et al. 2023), which examined global datasets of net biome productivity, did not find increasing autocorrelation over the Amazon. However net biosphere productivity is a flux, not a state variable.

Chapter 3

The Compost Bomb Instability in the Continuum Limit

To begin the research section of this thesis, I will examine a specific example of a tipping point, namely the 'Compost Bomb'. The Compost Bomb instability refers to a proposed uncontrolled increase in soil temperature. This instability is caused when sufficiently rapid atmospheric warming increases soil heterotrophic respiration which, in turn, heats the soil further. This generates a runaway effect in which soil temperatures rise rapidly. I will investigate this process, neglected in Earth System Models, but which has thus far been analysed with a conceptual model using ordinary differential equations. That model is deliberately idealised without any representation of the spatial structure of soils. I confirm using a partial differential equation framework that this runaway effect still occurs when accounting for soil depth. Using this newer representation I investigate the forcing parameters that make soils vulnerable to this instability. In particular, I find that the effect of dangerously large seasonal cycle variations in air temperature can create plausible conditions for a 'compost bomb' thermal instability.

This chapter is based on a published paper, 'The Compost Bomb Instability in the Continuum Limit' (Clarke et al. 2021).

3.1 Introduction

Coupled climate-carbon cycle Earth System Models (ESMs) show that rising temperatures will cause carbon cycle feedbacks that accelerate global warming further (Cox et al. 2000). Although the magnitude of the increase remains uncertain, a major contributing factor is the response of the land carbon cycle to increased temperatures (Friedlingstein et al. 2006; Arora et al. 2020). Over the last decade, there has therefore been a strong focus on improving models

of the expected response of terrestrial carbon to global warming.

The largest uncertainties are associated with the response of soil carbon to warming (Varney et al. 2020). The Jenkinson effect (Jenkinson, Adams and Wild 1991) is a positive carbon cycle feedback related to the soil. Heterotrophic respiration converts organic matter held in soils into CO_2. At higher temperatures the rate of this reaction increases, leading to larger emissions of CO_2 from soils. However, a key aspect of heterotrophic respiration, ignored by ESMs (Arora et al. 2020), is that due to respiration being an exothermic reaction, the released heat must raise the temperature of the soils it occurs in. This biogeochemical heating has been shown to be important in the thawing of permafrosts (Khvorostyanov et al. 2008a,b).

Furthermore, because the rate of respiration increases with temperature, the biogeochemical heating will tend to further increase the rate of respiration. This positive feedback creates the possibility of a tipping point, in which runaway respiration also significantly increases the soil temperature.

This runaway potential was first investigated in Luke and Cox 2010. The Luke and Cox model (hereafter referred to as the LC10 model) showed an instability if the rate of increase of air temperature was large compared to the soil turnover time. They dubbed this instability the 'compost bomb' due to the known capability of compost heaps to self-heat (Browne 1929; Nelson et al. 2007; Sidhu et al. 2007).

A range of climate tipping points have been observed in paleoclimate records (Alley et al. 2003), and both expert opinion (Lenton et al. 2008) and ESMs (Drijfhout et al. 2015) raise the possibility that they may be triggered this century by climate change. These tipping points associated so far with the behaviour of the Earth system are believed to correspond to bifurcations. The mechanisms underpinning the compost bomb instability are more unusual in that this is an example of rate-dependent tipping (Ashwin et al. 2012).

This rate-dependence was analysed mathematically by Wieczorek et al. 2011 where the compost bomb was studied as an 'excitable' system in which critical rates were calculated analytically. They found that when the air temperature was raised sufficiently slowly the system could follow the steady state equilibrium. However, when the air temperature was raised more rapidly, the system was unable to adapt sufficiently quickly to the new equilibrium and thus tipped.

Here a focus is on the compost bomb instability in response to the seasonal cycle. In this case the timescale of the forcing (1 year) is much faster than the response timescale of the soil carbon (decades), and the soil carbon can be treated as a prescribed time-invariant quantity (this is the 'compost bomb limit' of LC10).

Some limitations of the LC10 model are that it neglects important thermal processes and soil structure, and in particular vertical variation. For example, as a 'single box' model, it assumes that the soil is well represented by averaged quantities, such as an average soil temperature, when in fact these quantities can be quite heterogeneous (Gedney and Cox 2003).

By definition, box models neglect processes such as heat diffusion which tend to suppress regions of unusually high temperature. Hence an initial assumption might be that diffusive

damping may make the compost bomb harder to trigger. Additionally, the LC10 model assumes a single pool of carbon, rather than a spatially extended distribution, which might increase the possibility for a compost bomb.

Despite these caveats, the LC10 model captures the essence of the system. The aim is to add realism to the LC10 model by considering the vertical structure and heat conductivity of the soil. The new model will consist of a one dimensional soil column in which heat can diffuse and soil carbon decreases exponentially with depth. Whether or not an instability still exists in this model will be investigated.

The compost bomb has generally been considered in relation to an upward decadal timescale linear ramp in air temperature, which is an idealisation of the change in air temperature due to human caused climate change. However, there is also the possibility of rate-induced tipping by the sinusoidal variations in air temperature caused by the diurnal and seasonal cycles. These possibilities are investigated here, to see if there exist features of these oscillations that may raise the risk of a compost bomb.

3.2 LC10 Single Box Conceptual Model

The compost bomb instability is based on the idea that heterotrophic respiration in the soil is both an exothermic reaction (Thornley 1971) and also a reaction whose rate increases with temperature. Hence this reaction could lead to a scenario of thermal runaway, where respiration warms the soil which increases respiration further. The rate of respiration is often modelled with a Q_{10} form (Kirschbaum 1995) for temperature dependence. In this representation the reaction rate increases by a factor Q_{10} for every 10 °C of temperature increase. Hence the specific rate of respiration, $r(T_s)$ ($\mathrm{m^{-2}\,s^{-1}}$) can be modelled as $r(T_s) = r_0 Q_{10}^{(T_s - T_{\mathrm{ref}})/10}$ where T_s (°C) is the soil temperature and r_0 is the reaction rate at T_{ref}. The rate of reaction also increases in proportion to the available substrate, here soil carbon C_s ($\mathrm{kg\,C\,m^{-2}}$). The Q_{10} form implies an exponential dependence of the specific respiration rate on temperature: $r(T_s) = r_0 \exp(\alpha(T_s - T_{\mathrm{ref}}))$, where $\alpha = \log Q_{10}/10$. The soil carbon is increased by Net Primary Production (NPP) Π ($\mathrm{kg\,C\,m^{-2}\,s^{-1}}$) and decreased by heterotrophic respiration. Introducing the parameters A ($\mathrm{J\,kg^{-1}\,C}$), the specific heat of respiration, μ_A ($\mathrm{J\,m^{-2}\,K^{-1}}$) the areal soil heat capacity and λ ($\mathrm{W\,m^{-2}\,K^{-1}}$) the soil-to-atmosphere heat transfer coefficient leads to the LC10 model:

$$\mu_A \frac{\mathrm{d}T_s}{\mathrm{d}t} = -\lambda(T_s - T_a) + AC_s r_0 e^{\alpha(T_s - T_{\mathrm{ref}})}, \tag{3.1a}$$

$$\frac{\mathrm{d}C_s}{\mathrm{d}t} = \Pi - C_s r_0 e^{\alpha(T_s - T_{\mathrm{ref}})}. \tag{3.1b}$$

The model assumes that in the absence of biogeochemical heating the soil temperature equilibrates to the atmospheric temperature T_a. The amount of soil carbon is set by the equilibrium

balance between Π and heterotrophic respiration. If the decrease in soil carbon is too slow to offset an increase in air temperature, the compost bomb instability is triggered, corresponding mathematically to an instability in which T_s is 'excited' to a very large value, well in excess of 100 °C. This model implies a value for the equilibrium soil carbon

$$C_s^{\mathrm{eq}} = \frac{1}{r_0} e^{-\alpha(T_a - T_{\mathrm{ref}})} \Pi e^{-\Pi/\Pi_c} \tag{3.2}$$

where $\Pi_c = \lambda/\alpha A$. This equilibrium value is obtained by setting the derivatives in equation (3.1) to zero.

3.3 Continuum Model With Vertical Depth

To investigate the effects of the representation of spatial variability in the vertical z (m) direction the soil column is modelled as existing on a semi-infinite line, which extends from the surface at $z = 0$ down to $z = -\infty$. The vertical structure of soil carbon is set, as is sometimes assumed (Burke, Chadburn and Ekici 2017), by the balance of the diffusion and decomposition of soil carbon. It is assumed that these processes are in equilibrium, which yields an exponential decrease of soil carbon with depth over a characteristic distance of H. The soil temperature is modelled by a reaction-diffusion system, in which heat is generated by heterotrophic respiration and diffused vertically. The conductivity of the soil is given by κ (W m^{-1} K^{-1}) (Best, Cox and Warrilow 2005), it has heat capacity μ_V (J m^{-3} K^{-1}) and contains a total amount C_s of soil carbon. Therefore the heat equation for the soil temperature $T_s(z, t)$ becomes:

$$\mu_V \frac{\partial T_s}{\partial t} = \kappa \frac{\partial^2 T_s}{\partial z^2} + \frac{A C_s r_0}{H} e^{\alpha(T_s - T_{\mathrm{ref}})} e^{z/H}. \tag{3.3}$$

At $z = -\infty$ a no flux boundary condition is imposed. At the upper boundary the soil temperature is controlled by the turbulent heat flux from the atmosphere which has temperature $T_{a0} + \delta T_a(t)$, where T_{a0} represents a background mean temperature and $\delta T_a(t)$ a time dependent warming. Mathematically:

$$\frac{\partial T_s}{\partial z} = 0 \quad \text{at} \quad z = -\infty, \tag{3.4a}$$

$$-\kappa \frac{\partial T_s}{\partial z} = \lambda \left(T_s(0, t) - T_{a0} - \delta T_a(t) \right) \quad \text{at} \quad z = 0. \tag{3.4b}$$

Here the parameter λ characterises the turbulent heat transfer from the atmosphere to the top layer of the soil. C_s is set to the equilibrium value using equation (3.2) where the air temperature is taken to be T_{a0}. This approximation is justified provided the system is investigated on timescales short relative to the turnover time of soil carbon, which is on the order of many decades (Varney et al. 2020).

Parameter	Symbol	Equation	Value
Net Primary Productivity	Π	3.1b	$0.5\,\mathrm{kg\,C\,yr^{-1}}$
Temperature response of respiration	Q_{10}	3.3	2.5
Characteristic Soil Depth	H	3.3	0.4 m
Soil Thermal Conductivity	κ	3.3	$0.16\,\mathrm{W\,m^{-1}\,K^{-1}}$
Specific Heat of Respiration	A	3.3	$3.9 \times 10^7\,\mathrm{J\,kg\,C^{-1}}$
Volumetric Heat Capacity	μ_V	3.3	$1.0\,\mathrm{MJ\,m^{-3}\,K^{-1}}$
Heat Transfer Coefficient	λ	3.4b	$10\,\mathrm{W\,m^{-2}\,K^{-1}}$
Average Air temperature	T_{a0}	3.4b	0.0 °C

Table 3.1: Parameter values used to produce the figures in this study.

Throughout this study I undertake the mathematical investigation using nondimensional values. However, to aid understanding I plot certain figures using dimensional units, with standard values given in table 3.1. It should be noted however that these parameters are choices I have made, and different choices will lead to different figures, whereas the nondimensional plots are valid for all parameter choices.

3.3.1 Numerical Investigation

The continuum model was integrated in both space and time, and it was found that it can give rise to a compost bomb instability. The PDE, equation (3.3), was solved using the 'method of lines' technique (Schiesser 1991). It was discretized spatially into 100 equally spaced intervals. The spatial derivatives were approximated using central differences. This was then integrated using the backwards differentiation formula BDF method from the scipy library (Virtanen et al. 2020). The BDF method was chosen as it is well suited to stiff problems. If scipy's solver could not find a solution, then it was assumed that compost bomb had occurred.

This is a first piece of evidence that the results of the LC10 model remain when soil depth is taken into account. Figure 3.1 is a plot of the temperature profile of soil at different times, initialised to be in equilibrium, undergoing the compost bomb thermal runaway after five months. δT_a was set to a a sinusoid of frequency one year. Figure 3.1 shows that the instability remains in the continuous case, and it is not prevented by diffusion.

3.3.2 Consistency of the continuum model with LC10

In this subsection the LC10 model and continuum model are compared numerically. The level of soil carbon is chosen such that the soil temperature is initially in an equilibrium state with $\delta T_a = 0$. The models are then integrate forward in time with δT_a constant and greater than zero. For sufficiently large values of δT_a the system has an instability. The smallest value of δT_a for which this is true is referred to as the 'critical warming level', because if air temperatures were

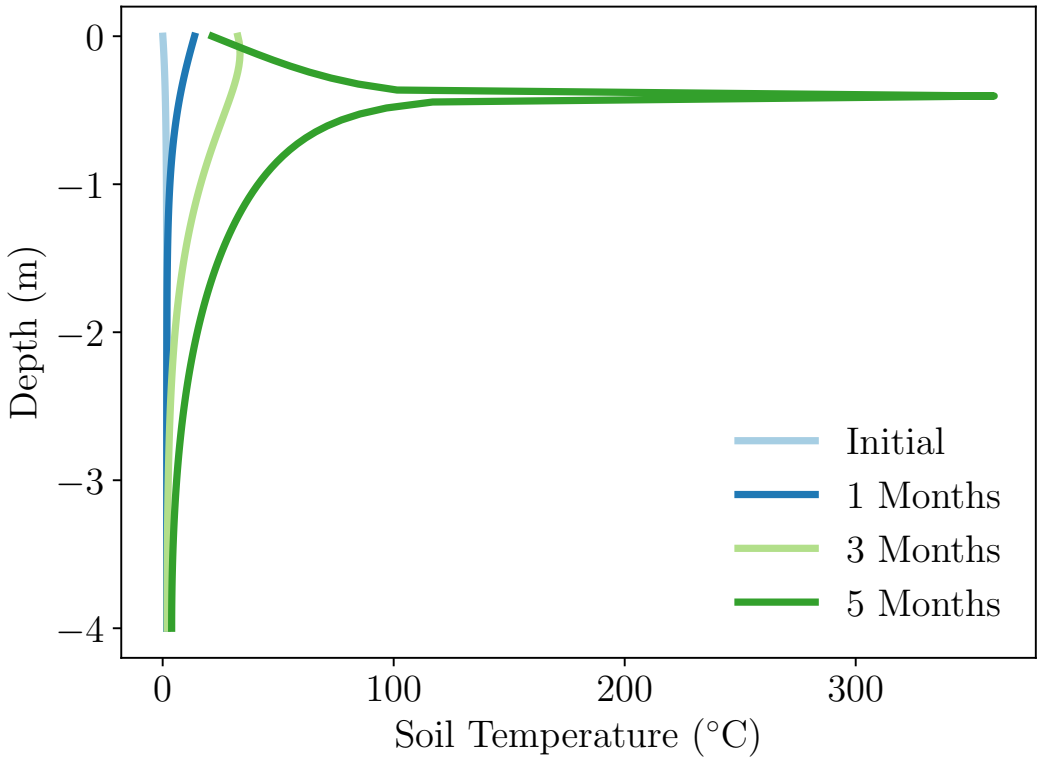

Figure 3.1: Vertical temperature profiles of soil undergoing a compost bomb thermal runaway when subject to a seasonal cycle of temperatures with amplitude 32.5 °C.

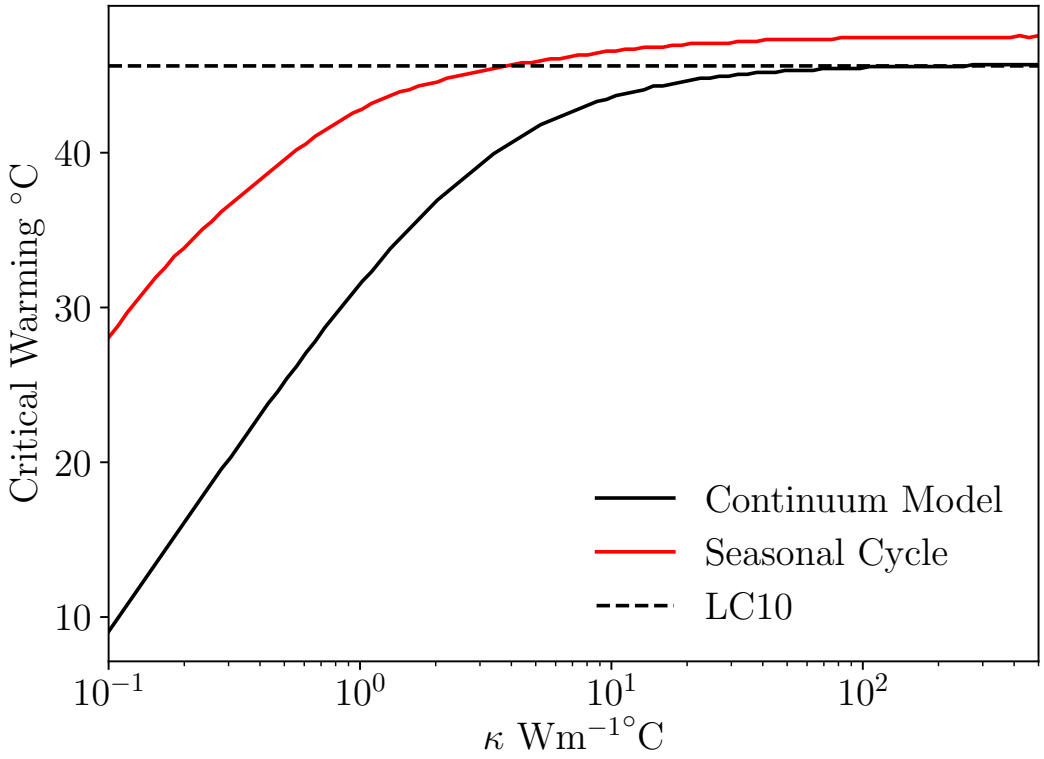

Figure 3.2: The warming required to make the continuum model unstable as a function of κ, compared to the LC10 model. Also plotted on is the seasonal cycle amplitude required for this instability.

increased by this amount quickly with respect to the soil carbon turn over time, an instability would be triggered.

This critical warming is plotted, as a function of κ in figure 3.2. Also overlaid is the warming required to cause a compost bomb in the LC10 model. Also shown is the amplitude of the seasonal cycle needed to cause a compost bomb. It can be observed that as $\kappa \to \infty$ the vertical structure matters less and the continuum result asymptotes to the LC10 case. In addition, the soil is more stable to seasonal cycle oscillations than instantaneous jumps. This 'overshoot' behaviour (Ritchie, Karabacak and Sieber 2019; Ritchie et al. 2021) is due to the fact that soil temperatures do not instantly respond to the seasonal cycle. Surprisingly for smaller values of κ the critical warming is actually lower in the continuum case than the LC10 case, despite the damping effects of diffusion.

To investigate this further, the LC10 model will be derived from the continuum case. This is done by vertically averaging equation (3.3). Vertically averaged quantities are denoted by

$\langle q \rangle = \frac{1}{H}\int_{-\infty}^{0} q \mathrm{d}z$. Begin by integrating equation (3.3) over the vertical domain:

$$\mu_V \frac{\mathrm{d}}{\mathrm{d}t}\int_{-\infty}^{0} T_s \,\mathrm{d}z = \kappa \left.\frac{\partial T_s}{\partial z}\right|_{z=0} - \kappa \left.\frac{\partial T_s}{\partial z}\right|_{z=-\infty} + \frac{AC_s r_0}{H}\int_{-\infty}^{0} e^{\alpha(T_s - T_{\mathrm{ref}})} e^{z/H}\,\mathrm{d}z. \tag{3.5}$$

Applying boundary conditions (equation (3.4)) gives

$$\mu_V H \frac{\mathrm{d}\langle T_s \rangle}{\mathrm{d}t} = -\lambda\left(T_s(0,t) - T_{a0} - \delta T_a(t)\right) + \frac{AC_s r_0}{H}\int_{-\infty}^{0} e^{\alpha(T_s - T_{\mathrm{ref}})} e^{z/H}\,\mathrm{d}z. \tag{3.6}$$

Assuming the vertical distribution of soil carbon does not affect the average value too much and setting $\mu_A = \mu_V H$ gives

$$\mu_A \frac{\mathrm{d}\langle T_s \rangle}{\mathrm{d}t} = -\lambda\left(T_s(0,t) - T_{a0} - \delta T_a(t)\right) + AC_s r_0 \left\langle e^{\alpha(T_s - T_{\mathrm{ref}})} \right\rangle. \tag{3.7}$$

This is equivalent to the LC10 model if $T_s(0,t) \approx \langle T_s \rangle$ and $\langle e^{\alpha T_s} \rangle \approx e^{\alpha \langle T_s \rangle}$. These approximations become exact when T_s is not a function of z, which occurs when $\kappa \to \infty$, as shown in figure 3.2. Note however that because $\langle e^{\alpha T_s} \rangle \geq e^{\langle \alpha T_s \rangle}$ the LC10 model underpredicts the amount of respiration in soils when κ is finite, and so the LC10 model will need a higher amount of warming to trigger a compost bomb.

3.3.3 Existence of the Compost Bomb in the Continuum Case

Now that there is numerical evidence for a compost bomb in the continuum case, this will be investigated analytically. In the approximation where soil carbon is constant, the rate dependent tipping feature of the model is lost, and instead it reverts to a classical bifurcation-induced tipping problem. Consider the case where δT_a is a constant, given by the temperature increase relative to the long term background state, T_{a0}, which is referred to as an atmospheric warming. In this case δT_a is the bifurcation control parameter. To begin the following nondimensionalisations are made:

$$\theta = \alpha\left(T_s - T_{a0}\right) \tag{3.8a}$$

$$\delta\theta_a = \alpha \delta T_a \tag{3.8b}$$

$$x = \frac{\lambda z}{\kappa} \tag{3.8c}$$

$$\tau = \frac{\lambda^2 t}{\kappa \mu_V} \tag{3.8d}$$

$$\widetilde{\Pi} = \Pi / \Pi_c \tag{3.8e}$$

then equations (3.3) and (3.4) become

$$\frac{\partial\theta}{\partial\tau} = \frac{\partial^2\theta}{\partial x^2} + \mathcal{W}e^{\theta}e^{x/D} \tag{3.9a}$$

$$\frac{\partial\theta}{\partial x} = 0 \quad \text{when} \quad x = -\infty \tag{3.9b}$$

$$-\frac{\partial\theta}{\partial x} = \theta(0,t) - \delta\theta_a(t) \quad \text{when} \quad x = 0 \tag{3.9c}$$

The nondimensionalisation process reveals two parameter clusters $D = H\lambda/\kappa$ and $\mathcal{W} = \widetilde{\Pi}e^{-\widetilde{\Pi}}/D$, which correspond to a nondimensional soil thermal depth and a nondimensional respiration strength. In terms of the parameters in table 3.1, these values are $D = 25$ and $\mathcal{W} = 0.0001$. Note that θ and $\delta\theta_a$ should be interpreted as (nondimensional) temperatures relative to the background air temperature, so in particular $\delta\theta_a$ is a temperature anomaly.

It will now be shown that the model defined by equation (3.9) only has an equilibrium state for low levels of atmospheric warming, $\delta\theta_a$. First a change of variables is made to reveal the first integral of the steady-state of equation (3.9a). Then a second integration followed by a change of variables reveals a standard integral with a well-known solution.

Let $\delta\theta_a$ be constant, set $\partial_\tau\theta = 0$, and then let $\psi = \theta + x/D$. Then equation (3.9a) becomes

$$\frac{\mathrm{d}^2\psi}{\mathrm{d}x^2} + \mathcal{W}e^{\psi} = 0. \tag{3.10}$$

Multiplying this by $\mathrm{d}\psi/\mathrm{d}x$ and integrating gives

$$\int \frac{\mathrm{d}\psi}{\mathrm{d}x}\frac{\mathrm{d}^2\psi}{\mathrm{d}x^2}\,\mathrm{d}z + \int \mathcal{W}\frac{\mathrm{d}\psi}{\mathrm{d}x}e^{\psi}\,\mathrm{d}x = 0 \tag{3.11}$$

$$\int \frac{\mathrm{d}}{\mathrm{d}x}\left(\frac{1}{2}\left(\frac{\mathrm{d}\psi}{\mathrm{d}x}\right)^2\right)\mathrm{d}x + \mathcal{W}\int \frac{\mathrm{d}e^{\psi}}{\mathrm{d}x}\,\mathrm{d}x = 0 \tag{3.12}$$

$$\frac{1}{2}\left(\frac{\mathrm{d}\psi}{\mathrm{d}x}\right)^2 + \mathcal{W}e^{\psi} = \frac{1}{2}c_1 \tag{3.13}$$

with c_1 a constant. Rearranging and recognising that this is a separable differential equation gives

$$\int \frac{\mathrm{d}\psi}{\sqrt{1 - 2\mathcal{W}c_1^{-1}e^{\psi}}} = \pm\sqrt{c_1}\int \mathrm{d}x = c_2 \pm \sqrt{c_1}x \tag{3.14}$$

where c_2 is another integration constant. The left hand side is then reduced to a standard integral (Riley, Hobson and Bence 2006) with the substitution $u = \left(1 - \frac{2\mathcal{W}}{c_1}e^{\psi}\right)^{1/2}$, giving

$$\int \frac{\mathrm{d}\psi}{\sqrt{1 - 2\mathcal{W}c_1^{-1}e^{\psi}}} = \int \frac{2}{u^2 - 1}\,\mathrm{d}u = -2\operatorname{artanh} u. \tag{3.15}$$

Inverting this then leads to

$$\sqrt{1 - 2\mathcal{W}c_1^{-1}e^{\psi}} = \tanh\left(c_2 \pm \sqrt{c_1}x\right), \tag{3.16}$$

where c_1 and c_2 have been redefined to absorb the factor of -2. As a result, ψ can be expressed as

$$\psi = \log\frac{c_1}{2\mathcal{W}} + \log\left(1 - \tanh^2\left(c_2 \pm \sqrt{c_1}x\right)\right). \tag{3.17}$$

Using the Pythagorean identity (Riley, Hobson and Bence 2006) this can be reduced to

$$\psi = \log\frac{c_1}{2\mathcal{W}} + 2\log\left(\operatorname{sech}\left(c_2 \pm \sqrt{c_1}x\right)\right). \tag{3.18}$$

In terms of θ, the solution is

$$\theta = \log\frac{c_1}{2\mathcal{W}} + 2\log\operatorname{sech}\left(\frac{c_2 \pm \sqrt{c_1}x}{2}\right) - \frac{x}{D} \tag{3.19}$$

Applying the boundary condition at $x = -\infty$ implies that $c_1 = \frac{1}{D^2}$. The solution becomes:

$$\theta = \log\frac{1}{2\mathcal{W}D^2} + 2\log\operatorname{sech}\left(\frac{1}{2}\left(c_2 \pm \frac{x}{D}\right)\right) - \frac{x}{D}. \tag{3.20}$$

Now applying the boundary condition at $x = 0$ gives

$$\pm\frac{1}{D}\tanh\frac{c_2}{2} - 2\log\operatorname{sech}\frac{c_2}{2} = -\frac{1}{D} - \log 2\mathcal{W}D^2 - \delta\theta_a. \tag{3.21}$$

Denoting the left-hand side of this equation as $F(c_2)$, it can be shown that F has a minimum. To see this note that F is a continuous function which for $|c_2| \to \infty$ behaves like $F(c_2) \sim |c_2|$ so it follows that F has a minimum. Hence for sufficiently large $\delta\theta_a$, the right-hand side will always be less than the left-hand side. This means there is no equilibrium solution, consistent with a compost bomb having been triggered.

To determine the critical level of $\delta\theta_a$ to cause a compost bomb, the c_2 that satisfies $F'(c_2) = 0$ must be found and substituted back into equation (3.21). The derivative of F is

$$F'(c_2) = \pm\frac{1}{2D}\operatorname{sech}^2\frac{c_2}{2} + \tanh\frac{c_2}{2} = \pm\frac{1}{2D}\left(1 - \tanh^2\frac{c_2}{2}\right) + \tanh\frac{c_2}{2} \tag{3.22}$$

so that $F'(c_2) = 0$ can be solved for $\tanh c_2$ and so equation (3.21) becomes

$$\delta\theta_a^{\text{crit}} = \log\left(2D\sqrt{D^2+1} - 2D^2\right) - 1 + \frac{1}{D}\sqrt{D^2+1} - \frac{1}{D} - \log 2\mathcal{W}D^2 \tag{3.23}$$

Note that for sufficiently large values of $\mathcal{W}$, the right-hand side of this equation is negative, which can be interpreted as the soil being inherently unstable without any warming.

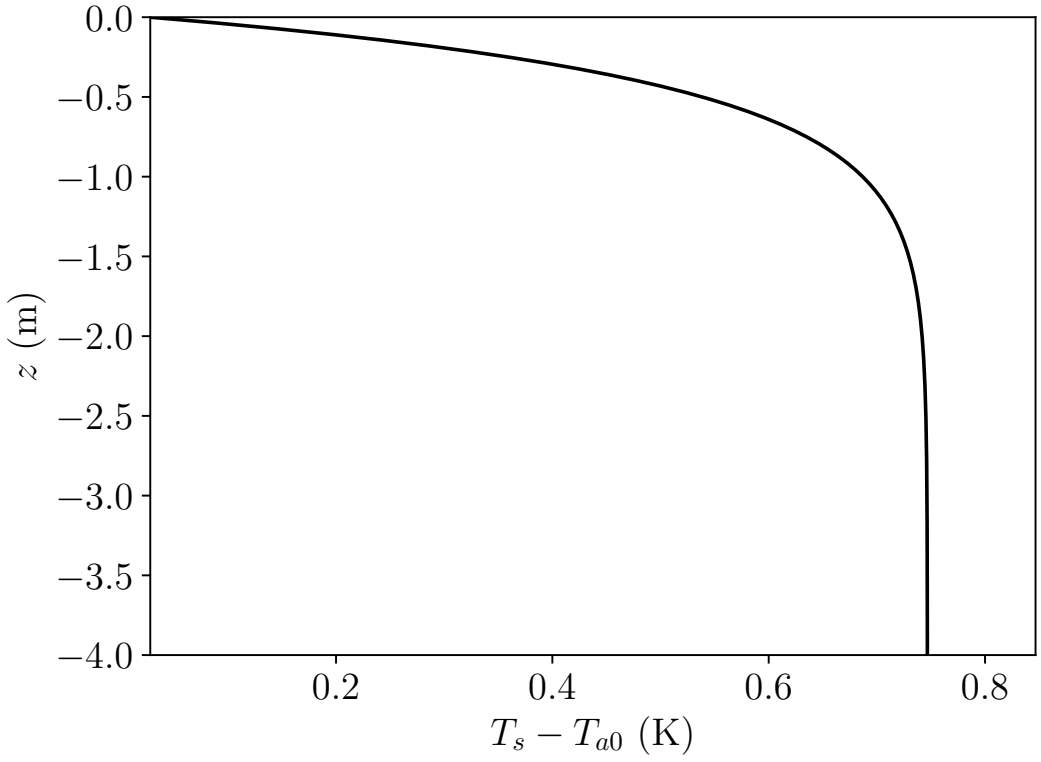

Figure 3.3: The equilibrium soil temperature profile, using the parameters in table 3.1. This is given as an anomaly relative to T_{a0}. The soil was assumed to be 4 m deep and that δT_a was zero.

Using the parameters in table 3.1 and setting $\delta\theta_a = 0$, equation (3.21) was numerically solved for c_2 and thus the equilibrium distribution of θ was found. This was then converted back to dimensional units and plotted in figure 3.3. Much like observations (Ping 1987), the temperature was found to be nearly constant for depths below about 1 m. Near-surface soil is in good thermal contact with the atmosphere, the temperature of which varies over short timescales, and therefore it is unlikely that observed near-surface soil temperatures will have reached their equilibrium value. Nevertheless, the profile here is compatible with soil temperature observations.

As $\mathcal{W}$ is a function of $\widetilde{\Pi}$ and D, specifying $\widetilde{\Pi}$ and D is enough to determine $\delta\theta_a^{\text{crit}}$, through equation (3.23). The critical maximum warming is plotted in figure 3.4 for a range of $\widetilde{\Pi}$ and D values. Figure 3.4 shows the critical warming, above which no equilibrium solutions exist, corresponding to triggering a compost bomb. Increasing the 'fuel', $\widetilde{\Pi}$, decreases the warming required to trigger a compost bomb. Furthermore, the figure shows that in this model, soils with larger D, corresponding to soils that are well insulated and have a soil carbon with a weak dependence on depth, are more unstable.

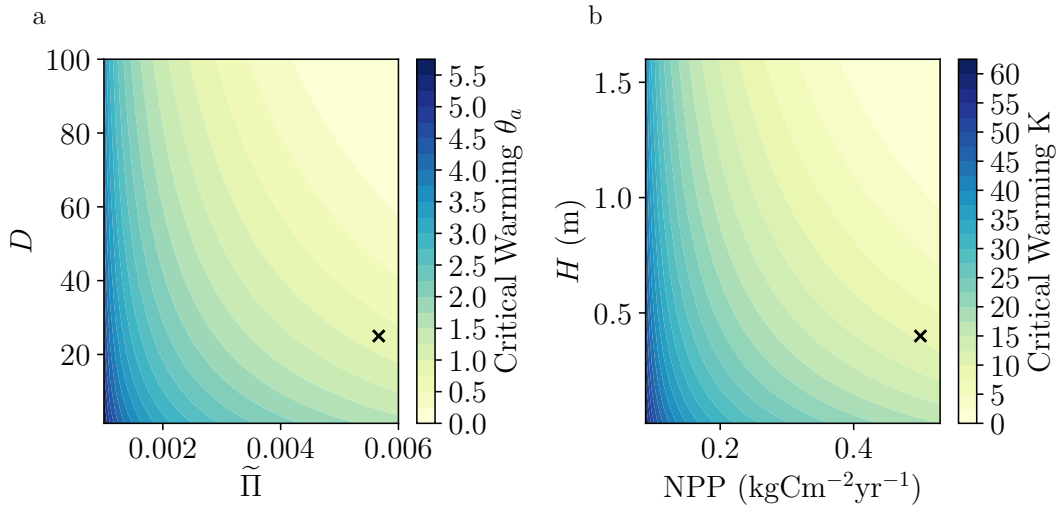

Figure 3.4: Panel a: the relationship between nondimensional soil carbon e-folding depth D, nondimensional NPP $\widetilde{\Pi}$ and the critical warming required to cause a compost bomb $\delta\theta_a$. **Panel b**: Also plotted is a dimensional version using the standard parameters in table 3.1. The black crosses denote the point corresponding to using the NPP and H values from table 3.1.

3.4 Vulnerability To Seasonal Cycle

The compost bomb instability is a rate-induced instability. To trigger the compost bomb instability, the rate of increase in air temperature needs to be fast relative to the rate of decrease of soil carbon. Prior work (Luke and Cox 2010) examined a linear increase in air temperature, corresponding to the increase in mean air temperature being caused by anthropogenic influence.

However, air temperature varies on multiple timescales. Two important modes of rapid air temperature change (relative to the timescale of soil carbon) are the diurnal and seasonal cycles. Suppose δT_a varies sinusoidally,

$$\delta T_a(t) = \Delta T_a \sin \frac{2\pi t}{T} \tag{3.24}$$

and numerically integrate equation (3.9a) for a range of forcing periods, using the standard parameters in table 3.1. Sufficiently large forcing amplitudes will lead to a compost bomb. These are plotted in figure 3.5.

Whilst the rate dependence alone would suggest that higher frequency oscillations are more unstable, high frequency oscillations can be too rapid to affect the soil temperature. Such high frequencies are in effect 'averaged out', as the air cannot heat the soil rapidly enough to have an effect deeper in the soil. Hence diurnally driven compost bombs are unlikely except at very high and unrealistic amplitudes.

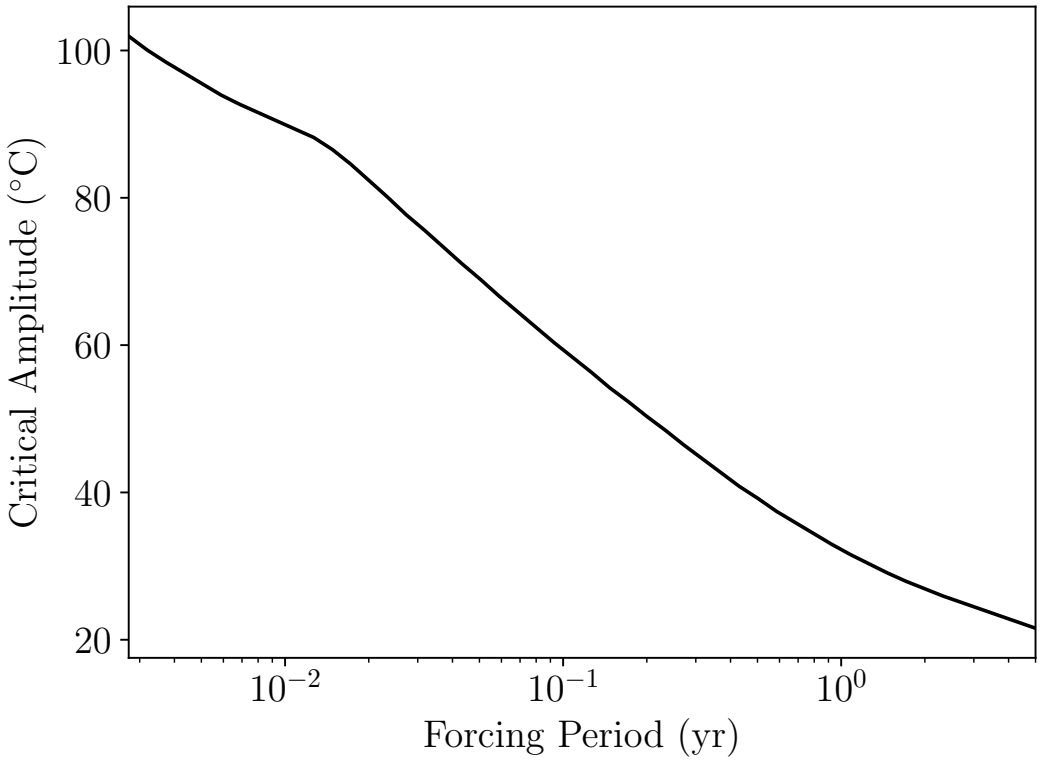

Figure 3.5: The relationship between forcing period T and the amplitude of the minimum near-surface air temperature changes required to trigger a compost bomb.

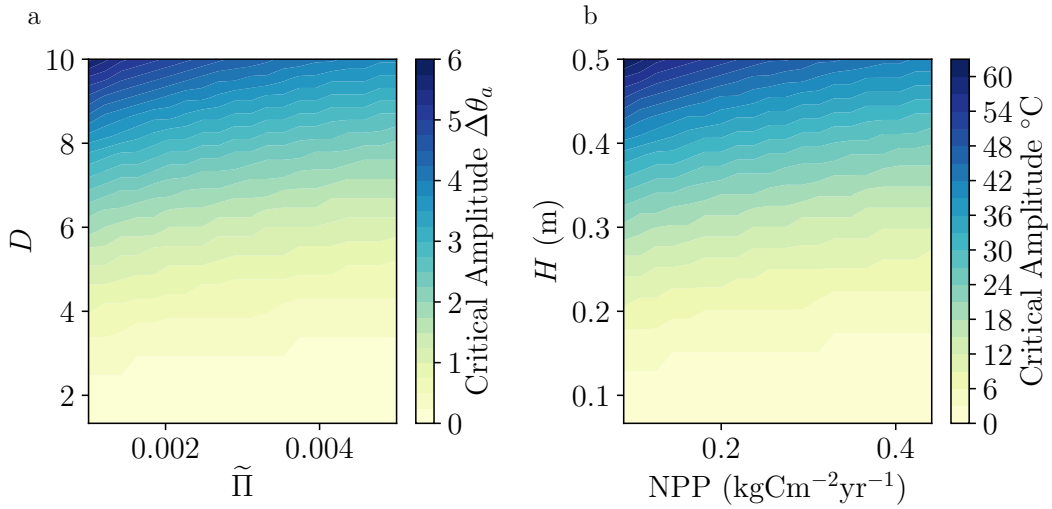

Figure 3.6: Panel a: the relationship between nondimensional respiration, soil depth and the seasonal cycle amplitude required to cause a compost bombs. For typical values of Q_{10}, the seasonal cycle could trigger a compost bomb. **Panel b**: Also plotted is the dimensional version, where the standard value of κ is modified to 0.5 W m^{-1} K^{-1} so make the H values more realistic.

In particular from figure 3.5, the amplitudes required to cause a compost bomb from the very high frequency diurnal cycle are about 100 °C, which is implausibly large. However for oscillations corresponding to timescales of the annual seasonal cycle, the magnitude is around 30 °C. This remains large, but such variations occur in high latitude, soil carbon rich ecosystems, for instance in parts of Siberia (Peixoto and Oort 1992).

The possibility of a seasonal cycle triggered compost bomb was investigated and plotted in figure 3.6, by scanning across the two nondimensional parameters. This shows that for a variety of plausible parameters, a large seasonal cycle could trigger a compost bomb. Soils with larger $\widetilde{\Pi}$ are more susceptible to a seasonal cycle driven compost bomb as they have more 'fuel'. However, in marked contrast to the conditions for the existence of an equilibrium, shallower soils are more susceptible to seasonal cycle driven compost bombs. This susceptibility can be understood as the atmosphere being able to warm larger fractions of shallower soils per unit of time.

3.5 Discussion

The purpose of this research is to determine features of raised near-surface temperature that could trigger thermal runaway in soils, a process called a 'compost bomb'. The compost bomb instability was originally identified in a single box model. The overarching finding of this chapter is that when accounting for vertical heterogeneity, thermal runaway still occurs. For

all finite values of thermal conductivity, I find these temperature thresholds are lower than those in the LC10 model, which I attribute to the strongly nonlinear respiration response to temperature.

The analysis undertaken suggests there are two important nondimensional parameters, D and $\mathcal{W}$ which characterise the 'thermal thickness' and energy output of respiration respectively. However, I have created a deliberately simplified model of the compost bomb. This has the advantage of being analytically tractable, yet ignores certain processes. Most obviously, I assume soil carbon is in equilibrium. This is not an unreasonable assumption however as I consider short enough timescales where this is approximately true. More importantly I neglect the role of soil moisture. Although this is not a thorough analysis, I offer some justification for why this model captures the essential features of the system. The addition of soil moisture has two principal effects.

Firstly, it affects the amount of respiration in the soils. In the framework of our model, weakening respiration corresponds to decreasing $\mathcal{W}$, a nondimensional parameter that encodes the amount of soil carbon, the heat released from respiration and the thermal properties of the soil. Although this affects the precise value for the air temperature warming that leads to a compost bomb, for any $\mathcal{W} > 0$ there is still a critical level of warming that produces a compost bomb.

Secondly soil moisture affects heat transport by setting the conductivity of the soil. However the thermal conductivity can be modelled as varying linearly with soil moisture (Best et al. 2011), whereas respiration has an exponential dependence on temperature. Therefore, temperature variations should play a more important role than moisture variations in the dynamics of the compost bomb.

3.6 Conclusion

In this chapter I present an advance in the realism of compost bomb models, by accounting for the vertical structure of the soils. I have found that even accounting for the diffusive effects of vertical structure, compost bombs can still occur. Furthermore, for realistic levels of heat diffusion, warming levels required to initiate the instability are much smaller than in the LC10 case. For the set of parameters investigated a rapid warming of the order of 10 °C is enough to push soils into an unstable regime. Furthermore, I have also found that for annual temperature cycles of around 30 °C risk triggering compost bombs.

This research adds to the evidence base that fires may self-ignite in high-latitude soils, which would have implications for the carbon cycle in these regions. This should encourage the development of biogeochemical heating in state-of-the-art land surface models to study the situations in which biogeochemical heating is important.

Chapter 4

Biogeochemical Heating and the Terrestrial Carbon Cycle

A vertical dimension was introduced into a model of the compost bomb in chapter 3. It was shown that this doesn't suppress the compost bomb. That analysis was local — the modelling was done at a single point on the Earth's surface. It would be interesting to see what a globally-averaged model that included biogeochemical heating would predict. Work by Cox, Huntingford and Jones 2006 suggested that the terrestrial carbon cycle is stable only for certain parameter ranges. In this chapter, I will explore the impact that biochemical heating has on the stability of the global climate-carbon cycle system

4.1 Compost Bomb Bifurcation Analysis

4.1.1 Dynamical Equations

The compost bomb equations, introduced by Luke and Cox 2010, are

$$c\frac{\mathrm{d}T_s}{\mathrm{d}t} = -\kappa\left(T_s - T_a\right) + Ar_0C_se^{\alpha T_s} \tag{4.1a}$$

$$\frac{\mathrm{d}C_s}{\mathrm{d}t} = \Pi - r_0C_se^{\alpha T_s}, \tag{4.1b}$$

where T_s and C_s are soil temperature and carbon, T_a is the atmospheric temperature, $\alpha = 0.1 \log Q_{10}$ is the sensitivity of temperature to respiration, Π is Net Primary Productivity, A is the heat released by respiration, κ is a heat transfer coefficient, c is a heat capacity and r_0 is the specific rate of respiration.

While the analysis in Luke and Cox 2010 was local, it will be assumed that equation (4.1) hold at the global scale too, where quantities are replaced by their global value. It will also be

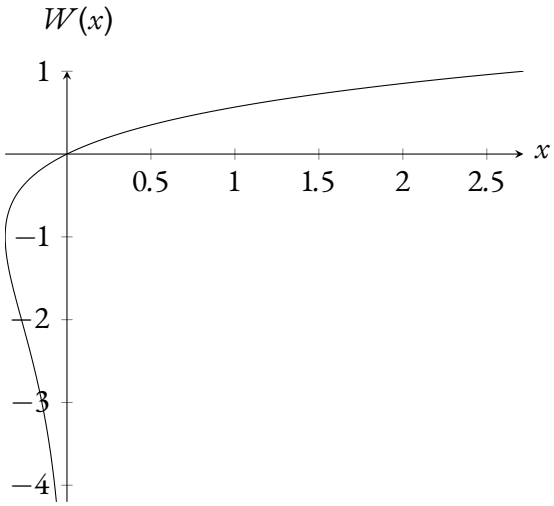

Figure 4.1: The Lambert W function, for $x \in [-1/e, e]$. The minimum value of x for which $W(x)$ is real is $-1/e$. For $x < 0$, $W(x)$ is multivalued.

assumed that Net Primary Productivity, Π, is an increasing function of atmospheric CO_2, as is T_a.

There is a timescale separation in equation (4.1). The dynamic of soil carbon are relatively slow, with a soil turn over time measured in the decades (Varney et al. 2022), whereas the dynamics of soil temperature are much faster, reaching an equilibrium with the air temperature on the time scale of a day (Best, Cox and Warrilow 2005). With this in mind, the soil temperature can be set to equilibrium, as calculated by putting equation (4.1a) equal to zero. This gives

$$0 = -\kappa(T_s - T_a) + Ar_0 C_s e^{\alpha T_s}$$

which can be solved for the soil temperature

$$T_s = T_a - \frac{1}{\alpha} W\left(-\frac{Ar_0 C_s \alpha e^{\alpha T_a}}{\kappa}\right), \tag{4.2}$$

where $W(x)$ is the Lambert W function (Corless et al. 1996). The Lambert W function, plotted in figure 4.1, is defined as the solution to the equation

$$W(x)e^{W(x)} = x. \tag{4.3}$$

This function is multivalued, and the larger (less negative) of the two possible values should be taken, which corresponds to the smaller value of T_s, which is the stable solution.

After noting that the argument of W is dimensionless, and that $r_0 C_s$ has units of Net Primary Productivity, the quantity

$$\Pi_c = \frac{\kappa}{\alpha A} \tag{4.4}$$

can be defined, which measures the influence of biogeochemical heating. No biogeochemical heating occurs for $A = 0$ or, equivalently, for $\Pi_c = \infty$. Similarly biogeochemical heating is strongest for $A \to \infty$ or, again equivalently, for $\Pi_c = 0$.

Equation (4.2) can now be rewritten as

$$T_s = T_a - \frac{1}{\alpha} W\left(-\frac{r_0 C_s e^{\alpha T_a}}{\Pi_c}\right). \tag{4.5}$$

Equation (4.5) was then inserted into equation (4.1b) to give

$$\frac{\mathrm{d}C_s}{\mathrm{d}t} = \Pi + \Pi_c W\left(-\frac{r_0 C_s e^{\alpha T_a}}{\Pi_c}\right). \tag{4.6}$$

which for given Π and T_a determines the evolution of C_s.

The implied equilibrium value for C_s occurs when equation (4.6) is zero. The value of C_s for which this is true is

$$C_s^{\mathrm{eq}} = \frac{\Pi}{r_0} e^{-\alpha T_a} e^{-\Pi/\Pi_c}. \tag{4.7}$$

The no biogeochemical heating case can be recovered by sending $\Pi_c \to \infty$ which gives $C_s^{\mathrm{eq}} = \Pi / r_0$.

4.1.2 Closing the System

It has been stated that T_a and Π are functions of atmospheric carbon, so determining their behaviours requires specifying the behaviour of the rest of the carbon cycle. The total carbon in the carbon cycle is conserved and so

$$C_s + C_a + C_o = C_s^{\mathrm{eq}} + C_{a0} + C_{o0} \tag{4.8}$$

where C_a and C_o are atmospheric and oceanic carbon and the quantities on the right-hand side are the equilibrium values. Following Cox, Huntingford and Jones 2006, it will be assumed that a fixed fraction, χ_0, of atmospheric emissions reach the ocean, meaning

$$C_a = C_{a0} - \frac{1}{1+\chi_0}(C_s - C_s^{\mathrm{eq}}). \tag{4.9}$$

In the rest of this chapter it will be assumed that $\chi_0 = 1/4$, on the grounds that roughly half of atmospheric emissions remain in the atmosphere (Jones and Cox 2005) with the other half split approximately evenly between the land and the ocean (Friedlingstein et al. 2022).

Making the further assumption that atmospheric temperatures scale logarithmically with atmospheric CO_2 (Pierrehumbert 2010) gives

$$T_a = \frac{S}{\log 2} \log \frac{C_a}{C_{a0}} \tag{4.10}$$

where S is the effective climate sensitivity experienced by the soils. Substituting equation (4.10) into equation (4.6) leads to

$$\frac{\mathrm{d}C_s}{\mathrm{d}t} = \Pi(C_a) + \Pi_c W\left(-\frac{r_0 C_s}{\Pi_c}\left(\frac{C_a}{C_{a0}}\right)^{\mu}\right), \tag{4.11}$$

where

$$\mu = \frac{\alpha S}{\log 2} \tag{4.12}$$

and C_a is determined through equation (4.9). By definition, $C_s = C_s^{\mathrm{eq}}$ when the left hand side of equation (4.11) is set equal to zero. This will correspond to a pre-industrial equilibrium when $C_a = C_{a0}$ or equivalently when $T_a = 0$. This requires that

$$r_0 = \frac{\Pi_0}{C_s^{\mathrm{eq}}} e^{-\Pi_0/\Pi_c}, \tag{4.13}$$

where $\Pi_0 = \Pi\left(C_{a0}\right)$ is the NPP during the pre-industrial period.

4.1.3 Computation of Bifurcation Point

The stability of the equilibrium at $C_s = C_s^{\mathrm{eq}}$ is determined by the Jacobian of equation (4.11), which in this case amounts to taking the derivative of the right-hand side of equation (4.11) when $C_s = C_s^{\mathrm{eq}}$. The system will transition from being stable to unstable when

$$\frac{\mathrm{d}\dot{C}_s}{\mathrm{d}C_s} = 0.$$

In order to calculate the derivative the identity

$$W'(x) = \frac{W(x)}{x\left(1 + W\left(x\right)\right)} \tag{4.14}$$

will be useful, which follows from taking the derivative of equation (4.3).

If the derivative of the right hand side of equation (4.11) is taken and set to zero,

$$\frac{\mathrm{d}\Pi}{\mathrm{d}C_a}\frac{\mathrm{d}C_a}{\mathrm{d}C_s} + \frac{\Pi_c}{C_s^{\mathrm{eq}}}\frac{W\left(-\frac{r_0 C_s^{\mathrm{eq}}}{\Pi_c}\right)}{1 + W\left(-\frac{r_0 C_s^{\mathrm{eq}}}{\Pi_c}\right)}\left(1 + \mu\frac{C_s^{\mathrm{eq}}}{C_{a0}}\frac{\mathrm{d}C_a}{\mathrm{d}C_s}\right) = 0 \tag{4.15}$$

is obtained. This can be rearranged for μ to give

$$\mu = -\frac{C_{a0}}{C_s^{\mathrm{eq}}}\frac{\mathrm{d}C_s}{\mathrm{d}C_a}\left(\frac{\mathrm{d}\Pi}{\mathrm{d}C_a}\frac{\mathrm{d}C_a}{\mathrm{d}C_s}\frac{C_s^{\mathrm{eq}}}{\Pi_c}\frac{1 + W\left(-\frac{r_0 C_s^{\mathrm{eq}}}{\Pi_c}\right)}{W\left(-\frac{r_0 C_s^{\mathrm{eq}}}{\Pi_c}\right)} + 1\right) \tag{4.16}$$

which simplifies to

$$\mu = \left(1+\chi_0\right)\frac{C_{a0}}{C_s^{\mathrm{eq}}} - \frac{C_{a0}}{\Pi_c}\frac{1+W\left(-\frac{r_0 C_s^{\mathrm{eq}}}{\Pi_c}\right)}{W\left(-\frac{r_0 C_s^{\mathrm{eq}}}{\Pi_c}\right)}\frac{\mathrm{d}\Pi}{\mathrm{d}C_a}. \tag{4.17}$$

This can be further reduced, by using equation (4.7), to

$$\mu = \left(1+\chi_0\right)\frac{C_{a0}}{C_s^{\mathrm{eq}}} - \frac{C_{a0}}{\Pi_c}\frac{1+W\left(-\frac{\Pi_0}{\Pi_c}\exp\left(-\frac{\Pi_0}{\Pi_c}\right)\right)}{W\left(-\frac{\Pi_0}{\Pi_c}\exp\left(-\frac{\Pi_0}{\Pi_c}\right)\right)}\frac{\mathrm{d}\Pi}{\mathrm{d}C_a}$$

and then by using the definition of the Lambert W function, equation (4.3), to give

$$\mu = \left(1+\chi_0\right)\frac{C_{a0}}{C_s^{\mathrm{eq}}} - \frac{C_{a0}}{\Pi_c}\frac{1-\frac{\Pi_0}{\Pi_c}}{-\frac{\Pi_0}{\Pi_c}}\frac{\mathrm{d}\Pi}{\mathrm{d}C_a}.$$

This can then be cleaned up to give a final form for the critical μ value, notated as μ^*, which separates stable from unstable soil carbon states. μ^* is therefore

$$\mu^* = \left(1+\chi_0\right)\frac{C_{a0}}{C_s^{\mathrm{eq}}} + \frac{C_{a0}}{\Pi_0}\frac{\mathrm{d}\Pi}{\mathrm{d}C_a} - \frac{C_{a0}}{\Pi_c}\frac{\mathrm{d}\Pi}{\mathrm{d}C_a}. \tag{4.18}$$

It is instructive to take the $\Pi_c \to \infty$ limit, which gives the behaviour in the no biogeochemical heating case:

$$\mu^*_\infty = \left(1+\chi_0\right)\frac{C_{a0}}{C_s^{\mathrm{eq}}} + \frac{C_{a0}}{\Pi_0}\frac{\mathrm{d}\Pi}{\mathrm{d}C_a}. \tag{4.19}$$

Therefore the effect of biogeochemical heating is the reduce the critical μ value for which an instability occurs by the amount

$$\frac{C_{a0}}{\Pi_c}\frac{\mathrm{d}\Pi}{\mathrm{d}C_a}. \tag{4.20}$$

When $\Pi_c \to 0$ this reduction becomes infinite and no stable soil carbon state is possible.

Equation (4.18) can be plotted, as has been done in figure 4.2, to divide the (μ, Π_c) parameter plane into stable and unstable regions, for a range of $\mathrm{d}\Pi/\mathrm{d}C_a$ values. For a 33% increase in NPP due to doubling CO_2 (Wenzel et al. 2016), then $\mathrm{d}\Pi/\mathrm{d}C_a \approx 0.05\ \mathrm{yr}^{-1}$.

4.1.4 Numerical Determination of Bifurcation Diagram

To numerically compute the equilibria of equation (4.11), the dependence of Π on C_a must be set. It is chosen to be

$$\Pi(C_a) = \frac{\Pi_\infty C_a}{C_a + C_{1/2}}, \tag{4.21}$$

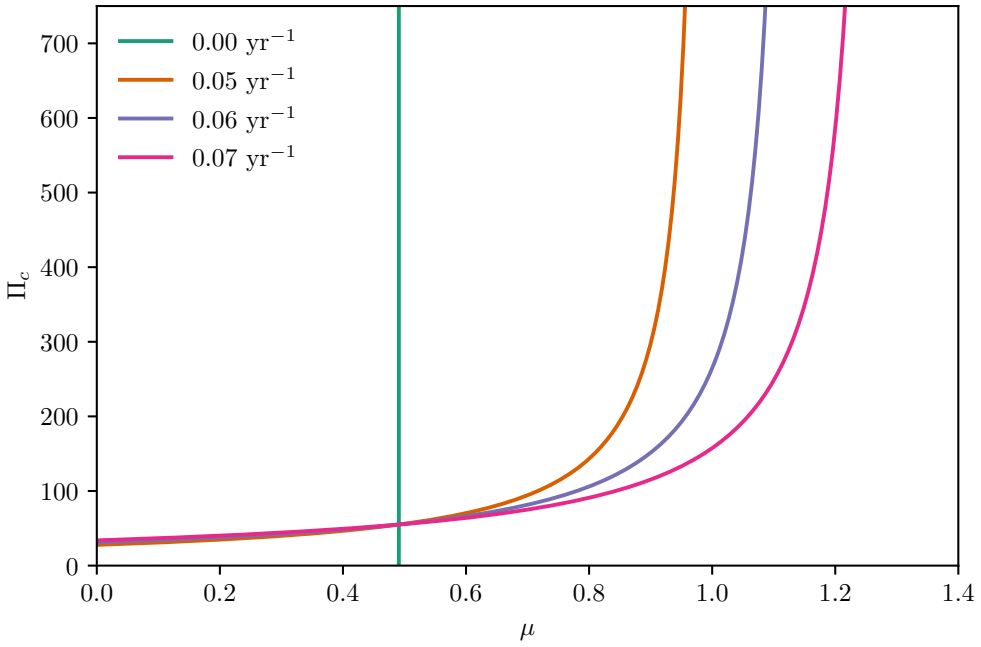

Figure 4.2: A plot of the (μ, Π_c) parameter plane, where the lines are drawn according to equation (4.18) for a range of different $\mathrm{d}\Pi/\mathrm{d}C_a$ values. The lines separate the stable and unstable regions such that stable regions are to the left of the lines. The other parameters are $\chi_0 = 0.25$,$\Pi_0 = 55\,\mathrm{Pg\,C\,yr^{-1}}$, $C_{a0} = 589\,\mathrm{Pg\,C}$ and $C_s^{\mathrm{eq}} = 1500\,\mathrm{Pg\,C}$.

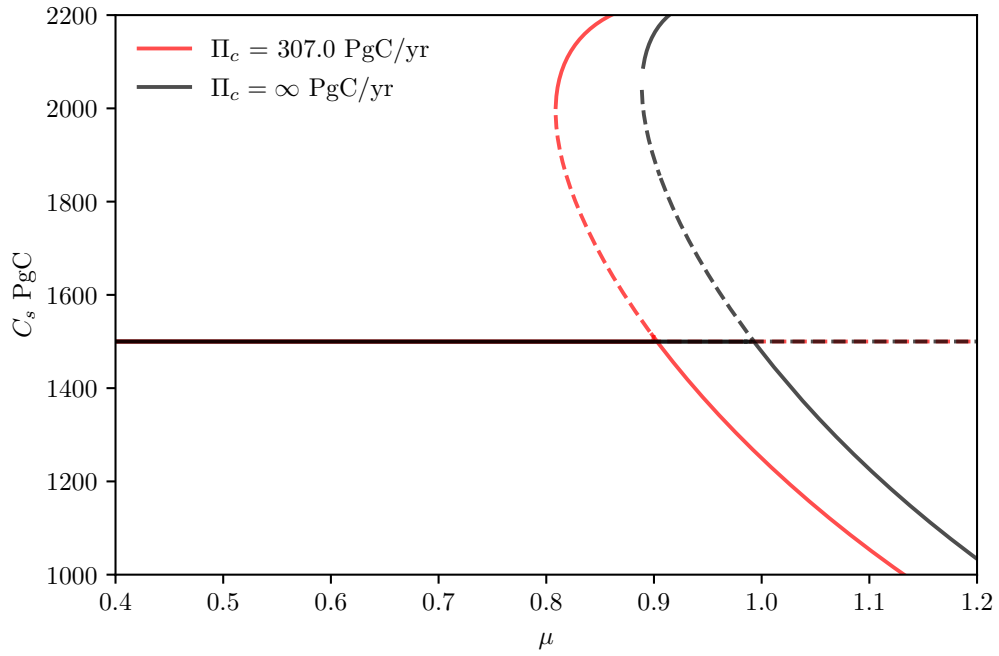

Figure 4.3: The equilibrium state of equation (4.11) for two values of Π_c as a function of μ. The two values of Π_c represent a no biogeochemical heating case ($\Pi_c = \infty$) and a biogeochemical heating case ($\Pi_c = 308\,\mathrm{Pg\,C\,yr^{-1}}$). The other parameters were set to $\chi_0 = 0.25$, $\Pi_0 = 55\,\mathrm{Pg\,C\,yr^{-1}}$, $C_{1/2} = 593.6\,\mathrm{Pg\,C}$, $C_{a0} = 589\,\mathrm{Pg\,C}$, $C_s^{\mathrm{eq}} = 1500\,\mathrm{Pg\,C}$.

which is the same choice as Cox, Huntingford and Jones 2006. The parameter $C_{1/2}$ determines the strength of the CO_2 fertilisation effect. The value of Π_∞ represents the saturation value of NPP at high CO_2 levels. As the pre-industrial NPP, Π_0, is more accurately known than the saturation value, Π_∞ can be determined from Π_0 using the formula

$$\Pi_\infty = \Pi_0 \frac{C_{a0} + C_{1/2}}{C_{a0}}. \tag{4.22}$$

It is now straightforward to compute the bifurcation diagram, which is plotted in figure 4.3. The figure shows the equilibrium soil carbon as a function of μ for different values of Π_c. It can be seen that there is a transcritical bifurcation at a certain value of μ. This value of μ decreases with decreasing Π_c. The numerical calculations also reveal a stable state with large amounts of soil carbon in addition to the pre-industrial state for large enough values of μ. The calculations in section 4.1.3 are performed by linearising about the pre-industrial state and as such apply only to that state, which is most scientifically relevant.

4.2 Determining the Parameters

4.2.1 The Effective Climate Sensitivity, S

A first guess to the value of S may be the Equilibrium Climate Sensitivity, ECS, namely the increase in global mean surface temperatures when atmospheric CO_2 concentrations are doubled (Sherwood et al. 2020). However, the pattern of warming is spatially heterogeneous, with more warming happening over land than over oceans (Morice et al. 2021). As soil carbon is found on land not in the oceans, it may be better to view S as the climate sensitivity over land.

In order to determine what S should be, the soil carbon balance will be considered at every point on the Earth's surface. There will be a spatially varying amount of warming, $\Delta T_a(\boldsymbol{r}, t)$, which will lead to a change in global soil carbon. This will then be compared to what level of spatially uniform warming would be required to give the same change in soil carbon. By setting the spatially varying pattern of warming to the pattern of warming caused by doubling CO_2, the resulting effective warming will be S.

Ignoring the effects of biogeochemical heating, the spatially resolved soil carbon balance can be written as:

$$\frac{\partial C_s(\boldsymbol{r}, t)}{\partial t} = \Pi(\boldsymbol{r}, t) - r_0(\boldsymbol{r}) C_s(\boldsymbol{r}, t) e^{\alpha \Delta T_a(\boldsymbol{r}, t)}, \tag{4.23}$$

where $\boldsymbol{r}$ is the position on the Earth's surface and Π, r_0 and C_s are allowed to vary spatially. It is assumed that α is constant and that there is no horizontal transport of soil carbon.

Equation (4.23) can be averaged over space. Denoting spatial averages with $\langle \bullet \rangle$, this gives

$$\frac{\mathrm{d}\langle C_s \rangle}{\mathrm{d}t} = \langle \Pi \rangle - \left\langle r_0 C_s e^{\alpha \Delta T_a} \right\rangle. \tag{4.24}$$

Assuming the warming (and therefore the soil carbon change) is small, the exponential can be expanded to first order using $e^x \approx 1 + x$. This will not affect the behaviour of the model as long as $\alpha \Delta T_a \ll 1$. Assuming $Q_{10} = 2$, this requires that $\Delta T_a \ll 33\,\mathrm{K}$, which is the case for realistic amounts of climate change. This means that, to first order in ΔT_a and soil carbon change

$$\begin{aligned} \frac{\mathrm{d}\langle C_s \rangle}{\mathrm{d}t} &\approx \langle \Pi_0 + \Delta\Pi \rangle - \left\langle \left(r_0 C_s^{\mathrm{eq}} + r_0 \Delta C_s \right) (1 + \alpha \Delta T_a) \right\rangle \\ &\approx \langle \Pi_0 + \Delta\Pi \rangle - \langle r_0 C_s^{\mathrm{eq}} + \alpha r_0 C_s^{\mathrm{eq}} \Delta T_a + r_0 \Delta C_s \rangle + \mathcal{O}(\Delta T_a \Delta C_s), \end{aligned}$$

where $\Pi_0(\boldsymbol{r})$ is the local NPP when $\Delta T_a(\boldsymbol{r}) = 0$, $\Delta\Pi(\boldsymbol{r})$ is the local change in NPP, $C_s^{\mathrm{eq}}(\boldsymbol{r})$ is the local equilibrium soil carbon when $\Delta T_a(\boldsymbol{r}) = 0$ and $\Delta C_s(\boldsymbol{r})$ is the local change in soil carbon. Respiration must balance NPP in equilibrium when $\Delta T_a(\boldsymbol{r}) = 0$, so $\Pi_0(\boldsymbol{r}) = r_0(\boldsymbol{r}) C_s^{\mathrm{eq}}(\boldsymbol{r})$. As a result, equation (4.24) can be written

$$\frac{\mathrm{d}\langle C_s \rangle}{\mathrm{d}t} \approx \langle \Delta\Pi - r_0 \Delta C_s \rangle - \alpha \langle \Pi_0 \Delta T_a \rangle. \tag{4.25}$$

Introducing an effective temperature change ΔT_{eff}, defined so that

$$-\alpha \left\langle \Pi_0 \Delta T_a \right\rangle = -\alpha \left\langle \Pi_0 \right\rangle \Delta T_{\text{eff}} \tag{4.26}$$

which implies

$$\Delta T_{\text{eff}} = \frac{\left\langle \Pi_0 \Delta T_a \right\rangle}{\left\langle \Pi_0 \right\rangle}. \tag{4.27}$$

After a doubling of CO_2, $\Delta T_{\text{eff}} = S$ and $\left\langle \Delta T_a \right\rangle = \text{ECS}$ which means that

$$\frac{S}{\text{ECS}} = \frac{\left\langle \Pi_0 \Delta T_a \right\rangle}{\left\langle \Pi_0 \right\rangle \left\langle \Delta T_a \right\rangle}. \tag{4.28}$$

In words, this means S is given by an NPP weighted average of global temperatures. A simple estimate of this ratio can be made by noting that Π_0 is zero over ocean. Assuming that over land the correlation between NPP and ΔT_a is weak then

$$\frac{S}{\text{ECS}} = \frac{\left\langle \Pi_0 \right\rangle_{\text{land}} \left\langle \Delta T_a \right\rangle_{\text{land}}}{\left\langle \Pi_0 \right\rangle_{\text{land}} \left\langle \Delta T_a \right\rangle_{\text{global}}} = \frac{\left\langle \Delta T \right\rangle_{\text{land}}}{\left\langle \Delta T \right\rangle_{\text{global}}} \tag{4.29}$$

which means that S is the climate sensitivity over land, as predicted by the rough guess. The IPCC find that there has been about 1.5 times more warming over land than over the globe as a whole (IPCC 2021).

Equation (4.28) can be used with abrupt-4xCO_2 CMIP runs (Eyring et al. 2016) to estimate S. Taking Π_0 to be the initial NPP in these simulations gives an estimate of S of around 1.5, as will be shown in table 5.1.

4.2.2 The influence of biogeochemical heating, Π_c

The quantity Π_c, which measures the role of biogeochemical heating on the global carbon cycle depends on the sensitivity of heterotrophic respiration to temperature, the heat released by respiration and the heat transfer coefficient between the land and the atmosphere.

The first of these, α, is reasonably well known. In terms of Q_{10} it is $\alpha = 0.1 \log Q_{10}$. Q_{10} is usually taken to be about 2 (Jones 2001; Clark et al. 2011). This means that $\alpha \approx 0.07$.

The second quantity, A, can be estimated biochemically. Its value is taken to be $A = 3.9 \times 10^7 \,\text{J kg}^{-1}\,\text{C}$ (Luke and Cox 2010).

The final quantity to estimate is the heat transfer coefficient between the land and the atmosphere. This varies from region to region, depending on the land surface cover (Beringer et al. 2001), the soil hydrology (Dharssi et al. 2009) and the soil type (Best et al. 2011). As such an effective heat transfer coefficient will be required.

The heat transfer coefficient can be estimated from the conductivity via

$$\kappa = \frac{2\lambda}{\Delta z} \tag{4.30}$$

where Δz is a soil thickness and λ is the conductivity. Taking the thickness $\Delta z = 0.1\,\mathrm{m}$ and the conductivity $\lambda = 0.227\,\mathrm{W\,m^{-1}\,K^{-1}}$ (Cox et al. 1999) gives a value of $\kappa = 4.5\,\mathrm{W\,m^{-2}\,K^{-1}}$ and a value of $\Pi_c = 8000\,\mathrm{Pg\,C\,yr^{-1}}$. This value is much larger than typical values of NPP and so this biogeochemical heating effect must be small at the global scale. However, it should be noted that κ can be smaller in, for example, well insulated mossy soils and as such the biogeochemical heating may still be significant regionally.

4.3 Conclusions

In this chapter, I have investigated the role of biogeochemical heating at the global scale. I have shown how the terrestrial carbon cycle is only stable for a certain parameter range, and that biochemical heating reduces the maximum carbon-climate system sensitivity compatible with a stable carbon cycle.

There are a number of deficiencies with this modelling approach. Firstly, the representation of the ocean is very simple and does not capture any dynamic features of the ocean carbon cycle. This is an issue taken up in chapter 5. Furthermore, this chapter only looks at the compost bomb at the global scale, whereas it is more likely to be important regionally where κ and thus Π_c values may be substantially smaller. However there is no reason to believe the dependencies on climate-carbon system sensitivity and the CO_2 fertilisation effect would not hold at the regional as well as the global scale.

Chapter 5

The Stability of Conceptual Models of the Carbon Cycle

In chapter 4, I adapted a result of Cox, Huntingford and Jones 2006 which showed that there were conditions under which the pre-industrial state of the carbon-climate system was unstable. This instability was driven by the terrestrial carbon cycle. That analysis involved representing the effect of the ocean as taking up a fixed fraction, χ_0, of carbon emissions to the atmosphere. This neglects any dynamical role of the ocean, including processes that occur on different timescales. Furthermore that analysis made inconsistent assumptions about the pre-industrial climate. This chapter will update Cox, Huntingford and Jones 2006, by constructing a model of the climate-carbon system with a dynamical ocean component that is consistent about the pre-industrial state.

I will neglect the role of biogeochemical heating as chapter 4 found it a small effect at the global scale.

5.1 Background

5.1.1 Climate Response to Radiative Forcing

As was outlined in chapter 1, the climate system responds to increasing levels of greenhouse gases in the atmosphere by increasing in temperature. The radiative forcing forcing and associated temperature rise caused by doubling the concentration of CO_2 in the atmosphere is generally assumed to be state independent. The amount of warming in the global mean caused by doubling CO_2 is known as the equilibrium climate sensitivity, ECS, and is 3.0 K with a likely range of 2.5 K to 4.0 K (Sherwood et al. 2020; IPCC 2021). However the latest generation CMIP6 climate models have climate sensitivities up to 5.6 K (Zelinka et al. 2020) and some climate models can give sensitivities of over 11 K (Stainforth et al. 2005).

It should also be noted that the warming is not globally uniform, with land warming more than the oceans (Morice et al. 2021) and higher latitudes warming more than the tropics (Serreze and Barry 2011). This enhanced warming in the Arctic is known as 'Arctic amplification'. A common approximation is 'pattern scaling' which related the spatially dependent warming, $\Delta T(\boldsymbol{r}, t)$ to the change in global mean surface temperature $\Delta T(t)$ by a time invariant pattern of warming, $f(\boldsymbol{r})$, through $\Delta T(\boldsymbol{r}, t) = f(\boldsymbol{r})\Delta T(t)$ (Huntingford and Cox 2000).

5.1.2 Terrestrial Carbon Cycle Response to CO_2

Whilst the above discussion of ECS treats the amount of CO_2 in the atmosphere as a given quantity, in reality it is also affected by the climate system, which determines the fluxes of carbon into and out of the atmosphere through biogeochemical cycles (Rothman 2014).

One important feedback is the so-called Jenkinson effect (Jenkinson, Adams and Wild 1991) which is enhanced heterotrophic respiration due to elevated surface temperatures. This tends to increase the amount of CO_2 in the atmosphere and so it is a positive feedback on climate change.

At higher levels of CO_2, the net primary productivity (NPP) of vegetation increases, this effect is called the CO_2 fertilisation effect (Wenzel et al. 2016). This tends to decrease the levels of CO_2 in the atmosphere and is thus a negative feedback on climate change.

The net effect of these two feedbacks is that the terrestrial response to CO_2 is uncertain as the sign of the response depends on the relative magnitude of these effects. Overall it is thought that CO_2 fertilisation dominates at lower CO_2 levels, which is consistent with the observed carbon sink, however at higher CO_2 levels the Jenkinson effect dominates (Cox et al. 2000; Friedlingstein et al. 2006; Arora et al. 2020).

5.1.3 Potential For Instability

Combining these two sensitivities gives the potential for an instability. Consider the following situation. Suppose some carbon is transferred from the land to the atmosphere. Then the Earth will warm. Due to positive feedbacks from the land more carbon will be released into the atmosphere leading to further warming and more carbon released. This cycle could continue until all the carbon from the land has been released into the atmosphere. However, because of the negative feedbacks in the system (principally CO_2 fertilisation) these positive feedbacks would have to be sufficiently strong in order for this to happen.

The fact that there is carbon on land (Crowther et al. 2019) combined with the small variation in atmospheric CO_2 over the pre-industrial Holocene (Marcott et al. 2014; Bauska et al. 2015), therefore indicates something about the magnitudes of the land carbon feedback and the climate sensitivity, namely that they cannot be too large. To make progress analysing this we must include the effect of the other store of carbon: the ocean.

5.2 A Climate-Carbon Cycle model using IMOGEN as the Ocean Component

5.2.1 IMOGEN description

The land surface model JULES is often used in conjunction with IMOGEN (Huntingford et al. 2004, 2010) which is a model that 'closes' the carbon cycle in that it provides an atmospheric and oceanic response to changes in terrestrial carbon. In this chapter, the ocean component of IMOGEN will be isolated. The ocean component is based on the model of Joos et al. 1996 which represents ocean carbon in terms of an impulse response to atmospheric CO_2.

It calculates the changes in dissolved inorganic carbon in the surface water as

$$\delta\Sigma CO2 = \int_0^t F_a(t-s)G_I(s)\,\mathrm{d}s. \tag{5.1}$$

where F_a is the atmosphere to ocean flux of carbon and G_I is IMOGEN's impulse-response function. This function is defined as

$$G_I(t) = \begin{cases} 1 - 2.2617t + 14.002t^2 - 48.770t^3 & t \leq 1\,\mathrm{yr} \\ f_0 + \sum_{i=1}^{5} f_i e^{-t/\tau_i} & t > 1\,\mathrm{yr} \end{cases} \tag{5.2}$$

where $f_0 = 0.014819, f_1 = 0.70367, f_2 = 0.24966, f_3 = 0.066485, f_4 = 0.038344, f_5 = 0.019439$ and $\tau_1 = 0.70177$, $\tau_2 = 2.3488$, $\tau_3 = 15.281$, $\tau_4 = 65.359$, $\tau_5 = 347.55$, the τ_i have units of years. This function is dimensionless and plotted in figure 5.1.

The carbon flux is given by

$$F_a(t) = k\,(\Delta C_a - \Delta C_o) \tag{5.3}$$

where ΔC_a and ΔC_o are the perturbations in atmospheric and ocean carbon. To take into account ocean temperature feedbacks on the ocean carbon cycle ΔC_o and $\delta\Sigma CO2$ are related by

$$\Delta C_o = g(T_o, \delta\Sigma CO2)e^{0.0423\Delta T_o} \tag{5.4}$$

where T_o is the initial ocean temperature, ΔT_o is the change in ocean temperature and g is a quintic polynomial in $\delta\Sigma CO2$ whose coefficients depend on T_o.

5.2.2 Terrestrial Carbon Cycle

The total carbon in the carbon cycle is a constant given by $\mathcal{C} = C_s + C_a + C_o$ where C_s is the soil carbon, C_a is the atmospheric carbon and C_o is the ocean carbon. Therefore to close the system, given the ocean dynamics, only the land carbon dynamics need to be set, with the dynamics of atmospheric carbon being controlled by this conservation law.

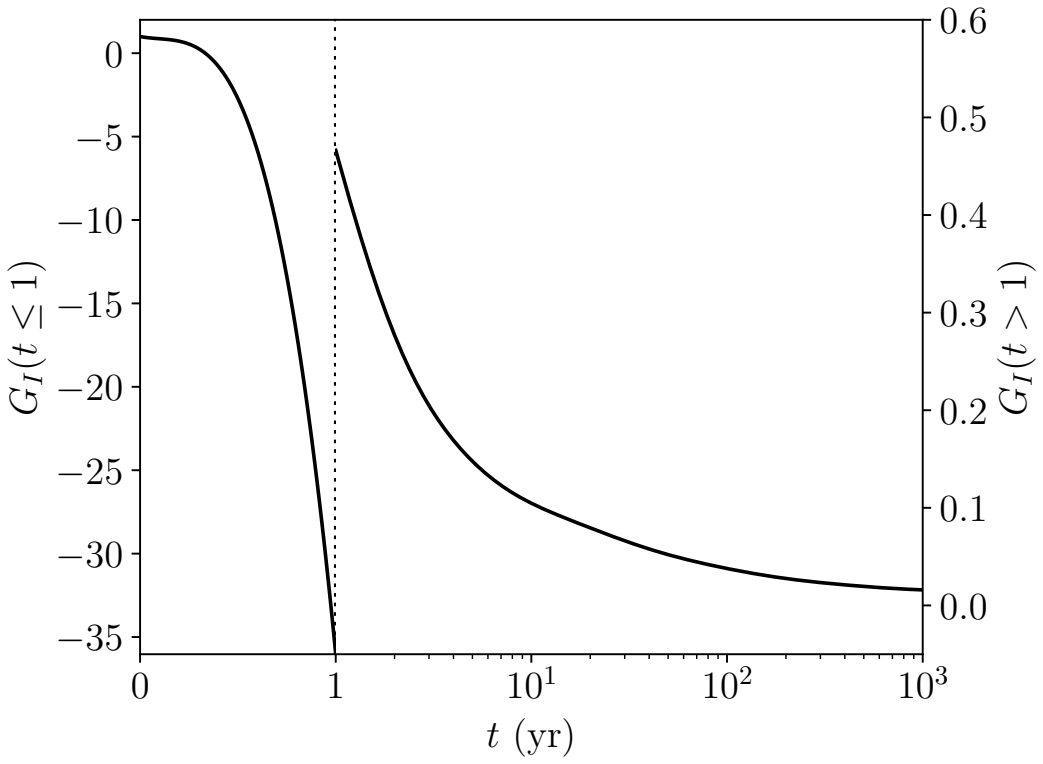

Figure 5.1: The impulse-response function for the ocean carbon uptake in IMOGEN, described by equation (5.2). The function is discontinuous at $t = 1\,\mathrm{yr}$. The dotted line indicates this discontinuity. Note the differences in scales on both the x and y axes either side of this discontinuity. On the left of the discontinuity, the scale is linear, but it is logarithmic to the right.

The change in soil carbon is given by the difference between net primary productivity and heterotrophic respiration. Heterotrophic respiration is assumed to have the following form:

$$R_h = r_0 C_s Q_{10}^{\Delta T_a/10} = r_0 C_s e^{\alpha \Delta T_a} \tag{5.5}$$

where ΔT_a is the change in atmospheric temperature, r_0 is a reference respiration level and $\alpha = 0.1 \log Q_{10}$ is the strength of the temperature feedback.

It is assumed that ΔT_a depends logarithmically on atmospheric carbon

$$\Delta T_a = \frac{S}{\log 2} \log \frac{C_a}{C_{a0}} \tag{5.6}$$

where C_{a0} is a reference CO_2 level, set at 589 Pg C, which is approximately the pre-industrial level of CO_2 (Lade et al. 2018). The parameter S is an NPP weighted climate sensitivity, as shown in chapter 4. This could be larger than ECS by a factor of about 1.5, estimates of S/ECS are given in table 5.1. Equation (5.5) can be combined with equation (5.5) to give

$$R_h = r_0 C_s e^{\frac{\alpha S}{\log 2} \log \frac{C_a}{C_{a0}}} = r_0 C_s \exp\left(\log\left(\left(\frac{C_a}{C_{a0}}\right)^{\frac{\alpha S}{\log 2}}\right)\right) \tag{5.7}$$

or

$$R_h = r_0 C_s \left(\frac{C_a}{C_{a0}}\right)^{\mu} \tag{5.8}$$

where

$$\mu = \frac{1}{\log 2} \alpha S. \tag{5.9}$$

Following Cox, Huntingford and Jones 2006, net primary productivity is modelled as

$$\Pi(C_a) = \Pi_\infty \frac{C_a}{C_a + C_{1/2}}, \tag{5.10}$$

which is an increasing function of CO_2 that saturates for $C_a \gg C_{1/2}$. Unless otherwise stated, $C_{1/2} = 280$ ppm, which is compatible with other estimates (Kolby Smith et al. 2016; Wenzel et al. 2016). This parameter controls the strength of the CO_2 fertilisation feedback. Equation (5.10) assumes that net primary productivity depends only on CO_2. Allowing for other factors like nitrogen limitation would act to reduce the effective $C_{1/2}$ value. Π_∞ is set so that $\Pi_0 = \Pi(C_{a0})$ is the pre-industrial level of net primary productivity 55 Pg C yr^{-1} (Lade et al. 2018).

CMIP5		CMIP6	
Model	*S*/ECS	Model	*S*/ECS
BCC-CSM1-1	1.1	BCC-CSM2-MR	1.4
BCC-CSM1-1-M	1.4	BCC-ESM1	1.2
BNU-ESM	1.4	CanESM5	1.2
CanESM2	1.4	CAS-ESM2-0	1.4
IPSL-CM5A-LR	1.6	CESM2	1.1
IPSL-CM5A-MR	1.7	CESM2-FV2	1.3
IPSL-CM5B-LR	1.7	CESM2-WACCM	1.3
MIROC-ESM	1.6	CESM2-WACCM-FV2	1.2
HadGEM2-ES	1.3	CMCC-CM2-SR5	1.6
MPI-ESM-LR	1.4	CMCC-ESM2	1.6
MPI-ESM-MR	1.5	GFDL-ESM4	1.3
MPI-ESM-P	1.6	NorCPM1	1.2
GISS-E2-H	1.5	GISS-E2-1-G	1.5
GISS-E2-R	1.6	GISS-E2-1-H	1.5
CCSM4	1.3	GISS-E2-2-G	1.4
NorESM1-M	1.3	GISS-E2-2-H	1.5
GFDL-ESM2G	1.6	INM-CM4-8	1.4
GFDL-ESM2M	1.5	INM-CM5-0	1.4
		IPSL-CM5A2-INCA	1.9
		IPSL-CM6A-LR	1.2
		NorESM2-LM	1.2
		NorESM2-MM	1.3
		TaiESM1	1.3
		UKESM1-0-LL	1.3
Ensemble Mean	1.5 ± 0.2	Ensemble Mean	1.4 ± 0.2

Table 5.1: Estimates of the ratio of S to ECS for CMIP5 and CMIP6 models, calculated by the methodology described in chapter 4. The ensemble mean is given plus or minus one standard deviation.

Putting this all together leads to the following set of coupled differential equations:

$$\frac{\mathrm{d}C_s}{\mathrm{d}t} = \Pi(C_a) - C_s r_0 \left(\frac{C_a}{C_{a0}}\right)^{\mu} \tag{5.11a}$$

$$\frac{\mathrm{d}C_o}{\mathrm{d}t} = I(C_a, \Delta T_o, C_o) \tag{5.11b}$$

$$C_a = \mathcal{C} - C_s - C_o \tag{5.11c}$$

$$\Delta T_o = \frac{1}{\nu}\frac{S}{\log 2}\log\frac{C_a}{C_{a0}}. \tag{5.11d}$$

As the dynamics are highly non-trivial, the function I has been used to represent the IMOGEN model. ΔT_o is the change in ocean temperature which is related to the change in land temperature by the factor $\nu = 1.45$. Note that S and Q_{10} (through μ) appear separately in this equation, so both parameters will affect the bifurcation point.

Note that there is an equilibrium at $C_a = C_{a0}$, $C_s = C_s^{\mathrm{eq}} = \Pi(C_{a0})/r_0$, $C_o = 0$, $\Delta T_o = 0$, corresponding to the pre-industrial equilibrium, which has been experienced only small variations over the (pre-industrial) Holocene.

The realism of this model could be challenged. Firstly, atmospheric and ocean temperatures do not adjust instantaneously to changes in atmospheric CO_2. Secondly, I have neglected any temperature dependence on NPP as well as the spatial structure of the land response. Furthermore, IMOGEN's representation of ocean carbon is not 'processed based', but is instead based on fitting an impulse-response function to a GCM. As such, it is hard to give a physical explanation for the precise functional form chosen. However, it has been found that this functional form gives a good representation for ocean carbon uptake (Joos et al. 1996).

5.2.3 Bifurcations in IMOGEN

Equation (5.11) is solved for a range of values of S with $Q_{10} = 2$. The system was initialised close to equilibrium and then allowed to equilibrate over 5000 years. The results for atmospheric carbon are plotted in figure 5.2 and other carbon cycle quantities in figure 5.4. For values of S between 10 K to 11 K there is a transition to oscillatory behaviour. In section 5.5 this will be shown to be caused by a Hopf bifurcation. This represents very pronounced climate change, possibly putting the system in a state far from states the model was designed to handle. As such, the validity of the model for these larger values of S should be questioned.

To scan the parameter space, this IMOGEN model was used to estimate the critical S as a function of Q_{10} and $C_{1/2}$, the parameter that controls the CO_2 fertilisation effect. This is plotted in figure 5.3.

As some CMIP6 models have an $S \approx 9\,\mathrm{K}$ this imposes limits on the strength of their carbon cycle feedbacks. Furthermore, because these models are near this bifurcation point, they will be subject to critical slowing down. This could lead to unrealistic CO_2 variability, even if they are in the non-oscillatory branch of the carbon cycle.

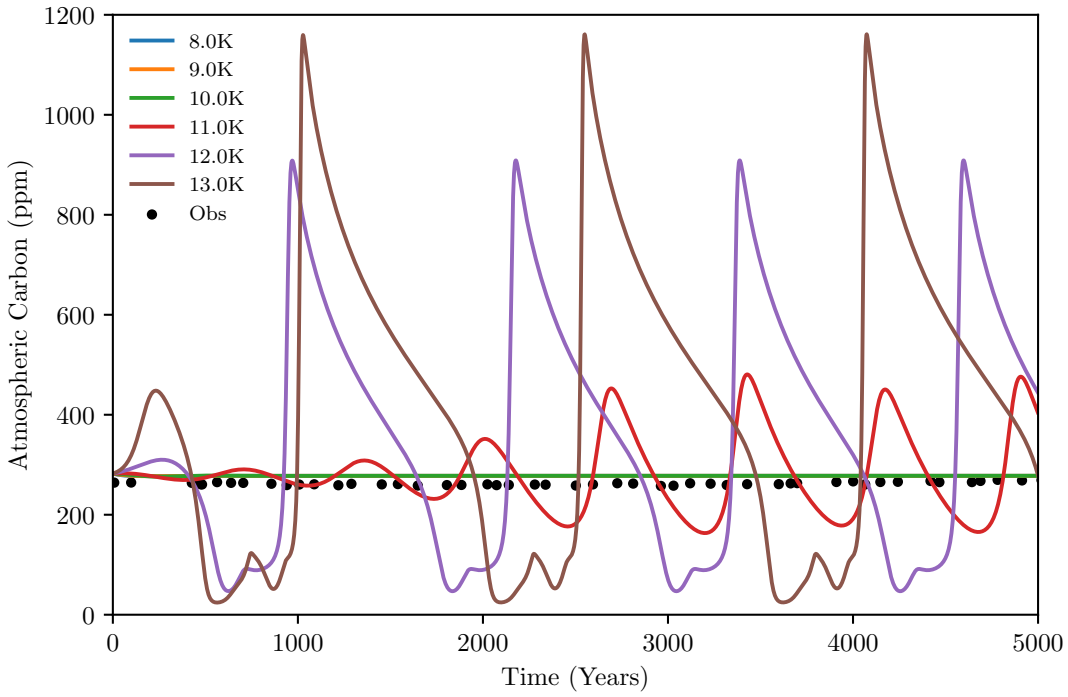

Figure 5.2: Atmospheric carbon calculated with the IMOGEN model given by equation (5.11) for a range of S values, with $Q_{10} = 2$. Overlaid are measurements of early Holocene (10 000 yr BP to 5000 yr BP) CO_2 levels, taken from Bereiter et al. 2015. Note that large S values lead to behaviour incompatible with the observed atmospheric CO_2 record.

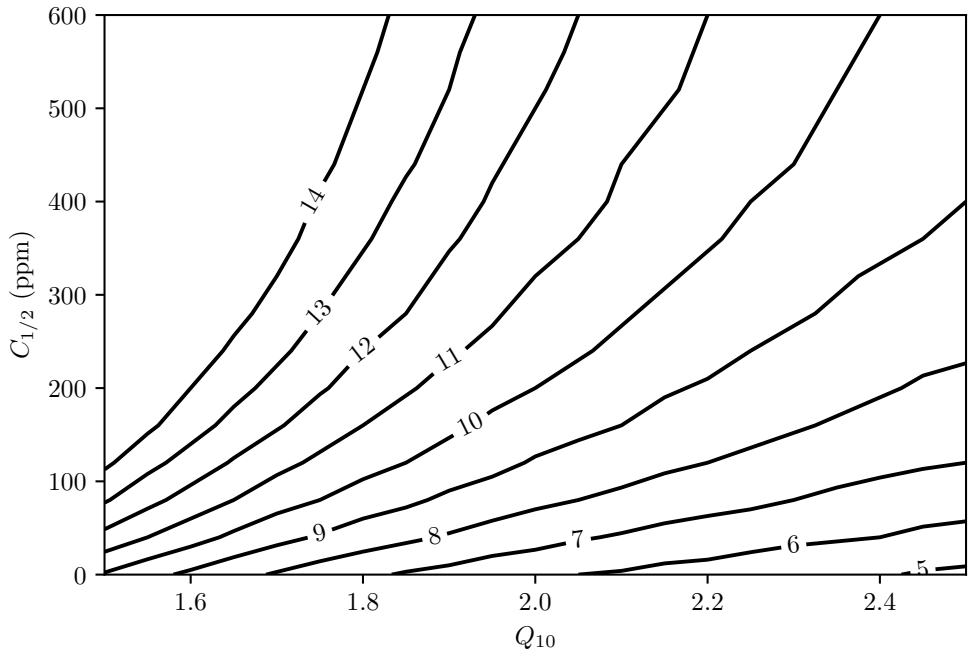

Figure 5.3: A contour plot showing the value of S as a function of Q_{10} (the temperature dependence of respiration) and $C_{1/2}$ (the strength of the CO_2 fertilisation feedback) at which the Hopf bifurcation occurs in equation (5.11). Values of S larger than this are incompatible with the observed behaviour of the carbon cycle.

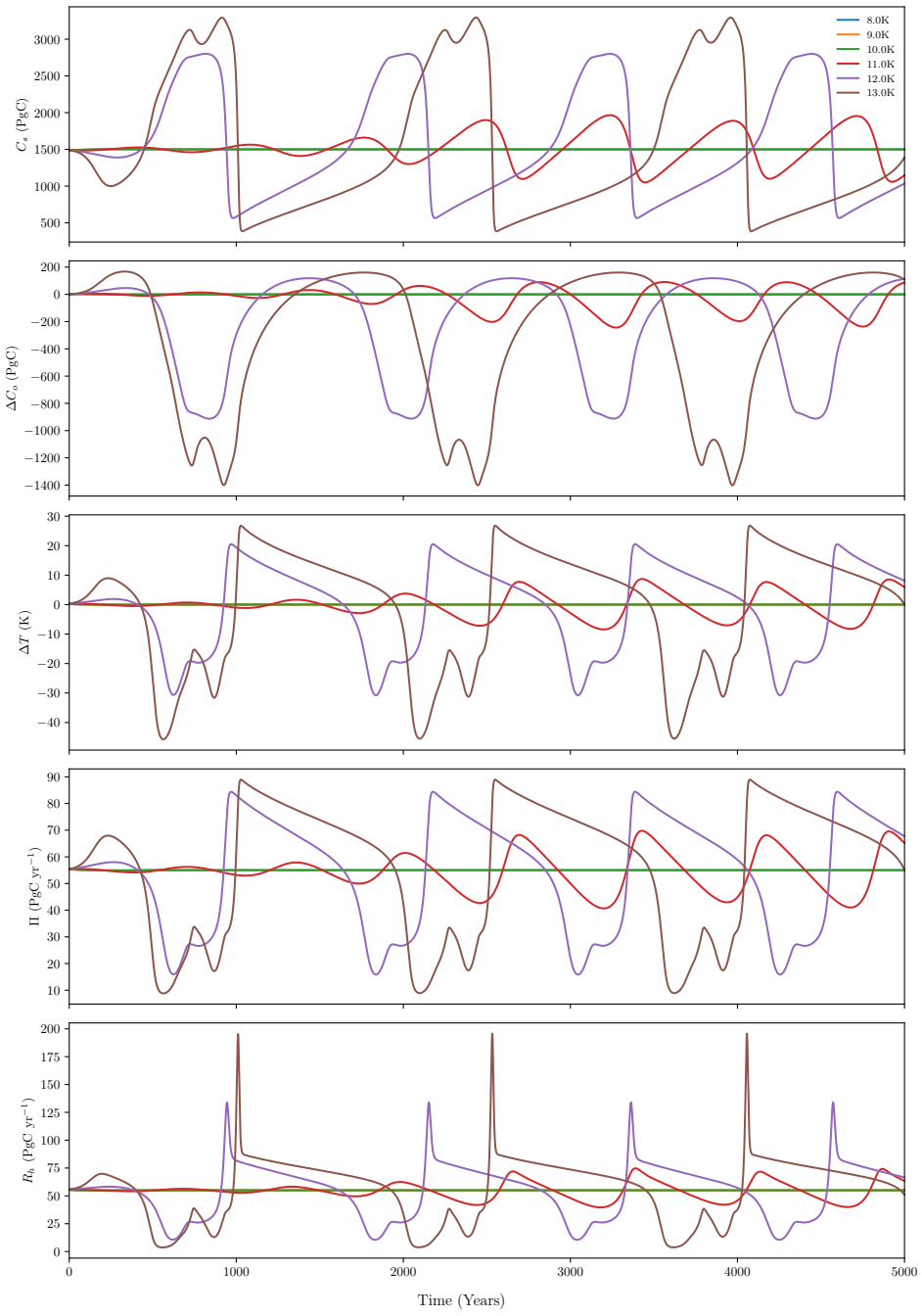

Figure 5.4: Soil carbon, ocean carbon change, global temperature change, NPP and heterotrophic respiration calculated with the IMOGEN model for a range of S values, with $Q_{10} = 2$. Large S values give behaviours incompatible with the observed behaviour of the carbon cycle over the Holocene.

Despite the simplicity of this model, it is still too complex to analyse mathematically. In the next section a simplified model will be developed to enable this bifurcation to be investigated further.

5.3 A Simpler Ocean Model

This simpler model will neglect temperature feedbacks on the ocean response. Further assumed is that the ocean carbon carbon uptake can be viewed as N non-interacting boxes which each respond over a timescale τ_i where i indexes the boxes. A fraction f_i of the total carbon flux will enter the ith box. These assumptions can be justified in that they represent a simplification of the IMOGEN model and can be used to fit the observed ocean carbon uptake, which is done in section 5.6.1.

The model is as follows: the change in carbon stored in the ith box, C_i, is given by

$$\frac{\mathrm{d}C_i}{\mathrm{d}t} = f_i k \Delta C_a(t) - \frac{C_i}{\tau_i}, \tag{5.12}$$

where $k = 0.2\ \mathrm{yr}^{-1}$ gives the timescale of the ocean uptake and ΔC_a is the change in atmospheric carbon from its equilibrium value.

For a given $C_a(t)$ equation (5.12) can be solved in quadratures to give

$$C_i(t) = \int_0^t f_i k e^{-s/\tau_i} \Delta C_a(t-s)\,\mathrm{d}s, \tag{5.13}$$

where $C_i(0) = 0$.

The overall ocean response is therefore

$$\Delta C_o(t) = \sum_{i=1}^{N} \int_0^t f_i k e^{-s/\tau_i} \Delta C_a(t-s)\,\mathrm{d}s. \tag{5.14}$$

or

$$\Delta C_o(t) = \int_0^t G(s) \Delta C_a(t-s)\,\mathrm{d}s \tag{5.15}$$

where

$$G(t) = \sum_{i=1}^{N} f_i k e^{-t/\tau_i} \tag{5.16}$$

is the impulse response function for the uptake of ocean carbon. It is assumed that $\Delta C_a(t) = 0$ for $t < 0$, and thus the lower bound of integration can be set to zero. Equation (5.16) is similar to equation (5.2), except the short term behaviour differs qualitatively and there is no nonlinear dependence on ocean carbon.

5.4 One Box Ocean

The simplest possible ocean box model is a one box model. This will be analysed first to see if it can reproduce the results of the IMOGEN model.

The one box model can be written symbolically through the following set of ODEs

$$\frac{\mathrm{d}C_s}{\mathrm{d}t} = \Pi(C_a) - r_0 C_s \left(\frac{C_a}{C_{a0}}\right)^{\mu} \tag{5.17a}$$

$$\frac{\mathrm{d}C_o}{\mathrm{d}t} = k(C_a - C_{a0}) - \frac{C_o}{\tau} \tag{5.17b}$$

$$C_a = \mathcal{C} - C_s - C_o. \tag{5.17c}$$

Note that unlike the IMOGEN case the dependence on Q_{10} and S is combined into one parameter μ. Again, there is a fixed point at $C_a = C_{a0}$, $C_o = 0$ and $C_s = C_s^{\mathrm{eq}}$. It will be shown that under suitable conditions there is another fixed point.

5.4.1 Stability of Pre-industrial State in the One Box Ocean Model

As shown in section 2.1.1, a fixed point of a system is unstable when the Jacobian, J, of that system evaluated at the fixed point has an eigenvalue, γ, with a positive real part. The Jacobian of equation (5.17) is given by

$$J = \begin{pmatrix} r_0\left(\mu\frac{C_s^{\mathrm{eq}}}{C_{a0}} - 1\right) - \Pi'(C_{a0}) & \mu\frac{C_s^{\mathrm{eq}}}{C_{a0}} - \Pi'(C_{a0}) \\ -k & -k - \frac{1}{\tau} \end{pmatrix} \tag{5.18}$$

where $\Pi'(C_a)$ denotes the derivative of NPP with respect to atmospheric carbon.

To find the eigenvalues of the Jacobian, the characteristic polynomial

$$\det\left(J - \gamma I\right) = 0 \tag{5.19}$$

must be solved for γ.

This equation is quadratic and therefore has two roots. Solving it leads to a solution of the form:

$$\gamma_{\pm} = \frac{B \pm \sqrt{D}}{2\tau C_{a0}} \tag{5.20}$$

where

$$B = -k\tau C_{a0} - \Pi'(C_{a0})\tau C_{a0} - r_0\tau C_{a0} - C_{a0} + \mu\Pi_0\tau \tag{5.21}$$

and

$$D = C_{a0}^2\tau^2\left(\left(k + \Pi' + r_0 + \frac{1}{\tau} - \frac{\mu\Pi_0}{C_{a0}}\right)^2 - \frac{4}{\tau}\left(kr_0\tau + \Pi' + r_0 - \frac{\mu\Pi_0}{C_{a0}}\right)\right) \tag{5.22}$$

is the discriminant and the substitution $\Pi_0 = r_0 C_s^{eq}$ has been made.

The stability of this system is governed by $\mathrm{Re}\,\gamma$. This number is controlled by the sign of D. If $D > 0$, then γ is purely real, but if $D < 0$, then $\mathrm{Re}\,\gamma = B/2\tau C_{a0}$.

5.4.2 Real Eigenvalues

If $\tau < 1/r_0$ then $D > 0$ for all values of μ. As $1/r_0 = C_s^{eq}/\Pi_0 \approx 30$ yr this situation represents a relatively fast ocean response. Under this assumption, it turns out that $\gamma_+ > 0$ when

$$\mu^* = \frac{C_{a0}}{C_s^{eq}} + \frac{C_{a0}}{\Pi_0}\frac{\mathrm{d}\Pi}{\mathrm{d}C_a} + \frac{C_{a0}}{C_s^{eq}} k\tau. \tag{5.23}$$

It is interesting to compare this to the condition given in equation (4.19). If the parameter χ_0 is introduced, as by Cox, Huntingford and Jones 2006, and set to $\chi_0 = k\tau$, then equation (5.23) is identical to equation (4.19). This gives an interpretation to χ_0 as the ratio of the timescale of the ocean carbon flux to the timescale of its response. Previously, χ_0 was interpreted as a fraction. This can be done only if $\tau < 1/k = 5$ yr.

The system equation (5.17) is integrated to equilibrium and the equilibria are plotted as a function of μ in figure 5.5, with $\tau = 3.7$ yr. The dashed line represents the position of the analytically calculated bifurcation point. It can been seen that the agreement is good, and that this is a transcritical bifurcation.

5.4.3 Complex Eigenvalues

In the case where the ocean timescale is larger than $1/r_0$, then $D < 0$. This means if the ocean response is considered to have a long timescale, the stability of the system is given by the sign of B.

The value of B will become positive when μ exceeds the following threshold:

$$\mu^* = \frac{C_{a0}}{C_s^{eq}} + \frac{C_{a0}}{\Pi_0}\frac{\mathrm{d}\Pi}{\mathrm{d}C_a} + \frac{C_{a0}}{C_s^{eq}} k\tau \left(1 + \frac{1}{k\tau}\right) \frac{1}{r_0\tau} \tag{5.24}$$

This is similar to the conditions derived in equations (4.19) and (5.23) except now $\chi_0 = k\tau\left(1 + \frac{1}{k\tau}\right)\frac{1}{r_0\tau} \approx k/r_0$ where the approximation assumes $k \gg r_0$. This means the "fraction absorbed by the oceans" is now controlled by the ratio of the timescale of the ocean flux to the turnover time of the soil. Furthermore because $k > r_0$, then χ_0 will be larger than 1. This means that χ_0 can't be interpreted as a fraction of carbon absorbed any more. In addition, because γ is complex, this bifurcation occurs when the complex conjugate eigenvalue pair crosses the imaginary axis. This means this bifurcation is a Hopf bifurcation rather than a transcritical bifurcation. For the case where $\tau = 300$ yr equation (5.17) was integrated numerically and the equilibrium was found as a function of μ, which is plotted in figure 5.6. Where the equilibrium

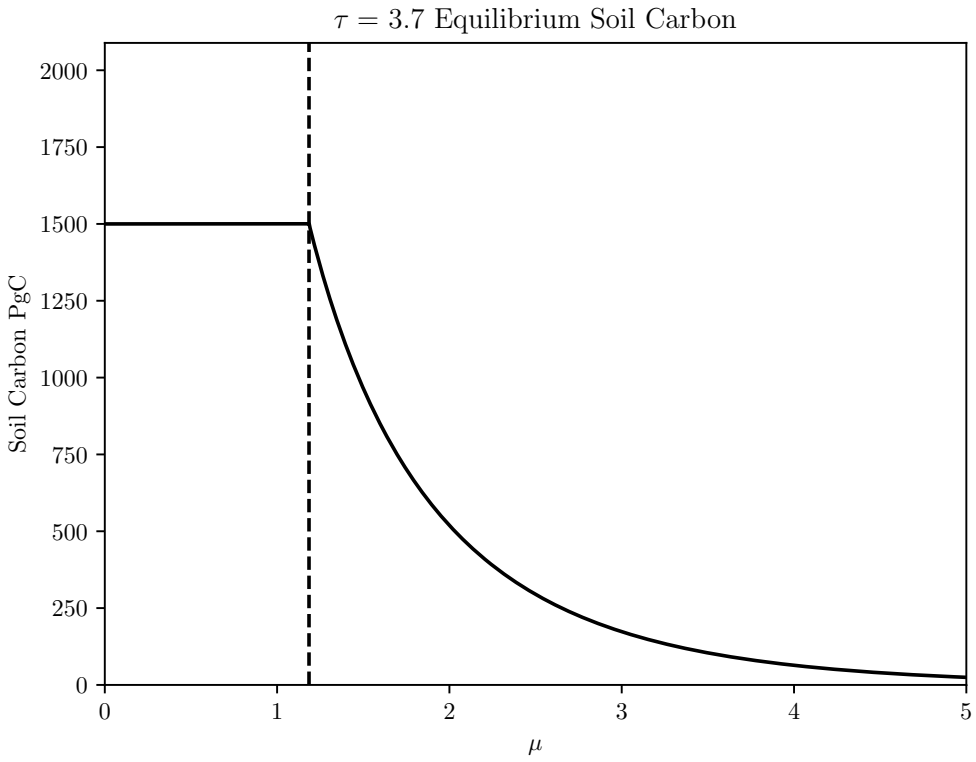

Figure 5.5: Equilibrium levels of soil carbon as a function of μ for the one box ocean model, equation (5.17), calculated numerically. The ocean timescale is 3.7 yr, which is in the fast ocean response regime. The dashed line is the analytically calculated bifurcation point, equation (5.23).

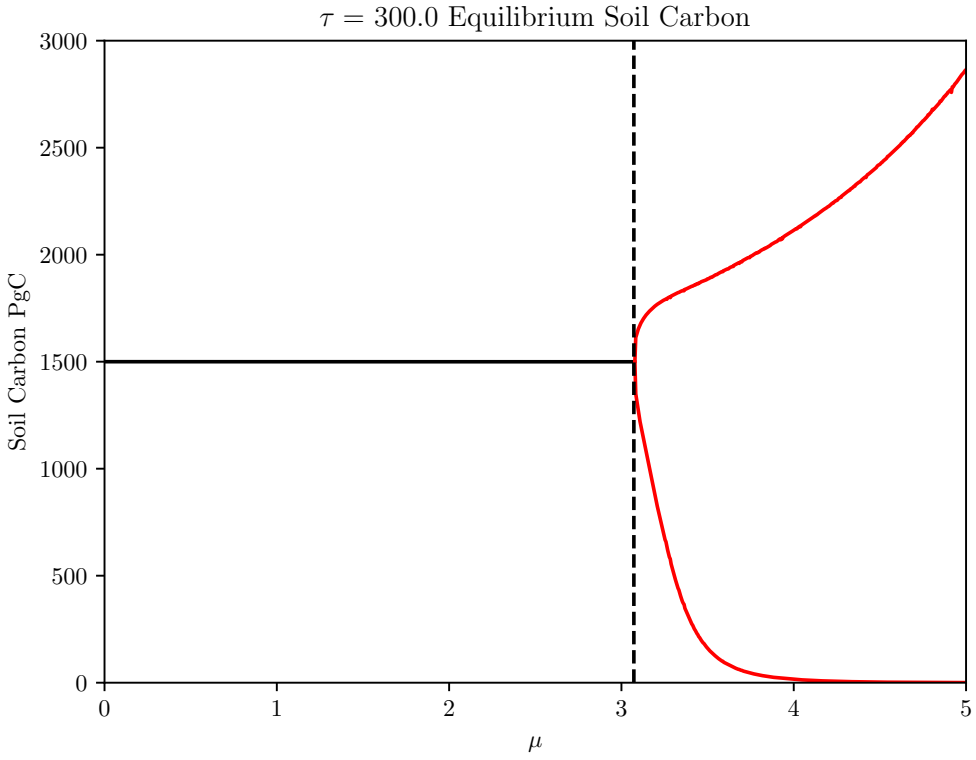

Figure 5.6: Equilibrium levels of soil carbon as a function of μ for the one box ocean model, equation (5.17), calculated numerically. The ocean timescale is 300 yr, which is in the slow ocean response regime. The dashed line is the analytically calculated bifurcation point, equation (5.24). Solid black lines represent a steady state condition, whereas red lines show that maximum and minimum of an oscillatory state. The oscillation period increases almost linearly with μ from around 23 yr to 112 yr.

is an oscillation rather than a steady state the plot shows the maximum and minimum of the oscillation in red. It can be seen that the agreement with the numerics is good.

Based on the conditions derived in equations (5.23) and (5.24) the critical value of μ can be chosen to match the bifurcation point predicted by the IMOGEN model. This involves choosing $\tau = 2.23\,\text{yr}$. This puts the ocean into the fast regime, and therefore a transcritical bifurcation. This is a different sort of bifurcation to the one found in IMOGEN and so motivates increasing the complexity of the ocean model slightly.

5.5 Two Box Model

To improve the realism of the model, the two box ocean case is now considered. In order to do this equation (5.17) must be modified to include two ocean stores of carbon C_1 and C_2. Each box will have their own timescale τ and τ/ε respectively. This notation is suggestive of C_1 responding quickly and C_2 responding slowly to increased atmospheric carbon, although this restriction is not necessary.

This leads to the following system of equations:

$$\frac{\mathrm{d}C_s}{\mathrm{d}t} = \Pi(C_a) - r_0 C_s \left(\frac{C_a}{C_{a0}}\right)^{\mu} \tag{5.25a}$$

$$\frac{\mathrm{d}C_1}{\mathrm{d}t} = fk(C_a - C_{a0}) - \frac{C_1}{\tau} \tag{5.25b}$$

$$\frac{\mathrm{d}C_2}{\mathrm{d}t} = (1-f)k(C_a - C_{a0}) - \varepsilon\frac{C_2}{\tau} \tag{5.25c}$$

$$C_a = \mathcal{C} - C_s - C_1 - C_2. \tag{5.25d}$$

Again note the equilibrium at $C_a = C_{a0}, C_s = C_s^{\text{eq}}$ and $C_1 = C_2 = 0$. To determine the stability of this state the eigenvalues of the Jacobian of equation (5.25) must be computed, which involves finding the roots of a cubic characteristic polynomial. Whilst this is possible in principle it is analytically very challenging.

To avoid this therefore some heuristic arguments are given as to why a Hopf bifurcation occurs at a critical value of μ. A special case of the characteristic polynomial of the Jacobian is solved, which corresponds to assuming the existence of a Hopf bifurcation. Under this assumption critical values of μ are found at which a Hopf bifurcation could occur, which is then verified with a numerical investigation.

5.5.1 A Heuristic Argument

For this section, it will be assumed that C_2 has a slow response to a given atmospheric CO_2 forcing, when compared to C_1. This implies that $\varepsilon \ll 1$. Ignoring equation (5.25b), it has already been shown in section 5.4.3 that a system with a slow ocean response will undergo a Hopf bifurcation at a critical value of μ.

Mechanistically, this happens because the instability leads to the soil releasing its carbon to the atmosphere. The ocean box can then draw down the excess carbon from the atmosphere, which cools the climate and allows carbon to accumulate on land again. Eventually, enough carbon will have accumulated in the soils that the state becomes unstable and it will be released back into the atmosphere, starting the cycle again.

Taking into account equation (5.25b), this will tend to increase the draw down of atmospheric carbon, thus potentially stabilising the system. However it seems reasonable to expect that the above mechanism will not be totally disrupted and therefore a Hopf bifurcation might still be expected.

5.5.2 Computation of Bifurcation Point

If the assumption that there is a Hopf bifurcation can be made, then there is another mode of attack. At the Hopf bifurcation a pair of complex conjugate eigenvalues cross the imaginary axis from the negative real part side to the positive real part side. This means that at the bifurcation, the eigenvalues are purely imaginary. It is comparatively easy to solve a cubic equation under the assumption of imaginary roots.

The characteristic polynomial of the Jacobian of equation (5.25) will be of the form

$$\gamma^3 + a_1\gamma^2 + a_2\gamma + a_3 = 0, \tag{5.26}$$

where γ is an eigenvalue. As has been stated, at the Hopf bifurcation, γ is purely imaginary so the substitution $\gamma = i\lambda$ with $\lambda \in \mathbb{R}$ can be made. Then equation (5.26) becomes

$$-i\lambda^3 - a_1\lambda^2 + ia_2\lambda + a_3 = 0. \tag{5.27}$$

For this equation to be satisfied, both real and imaginary parts of equation (5.27) must be zero. This leads to $\lambda = \pm\sqrt{a_3/a_1}$ and $\lambda = \pm\sqrt{a_2}$. For consistency, these expressions for λ must be equal. This requires that $a_3 = a_1a_2$. Alternatively, both expressions for λ can be satisfied if $\lambda = 0$. However, this leads to $\gamma = 0$ which has no non-zero imaginary part and so cannot lead to oscillatory solutions and thus is not consistent with the assumption that there is a Hopf bifurcation.

The condition $a_1a_2 = a_3$ can now be solved for μ. Doing this gives two solutions.

$$\mu^* = \frac{C_{a0}}{2\Pi_0\tau(1+\varepsilon)}\left(M_1 \pm \sqrt{M_2}\right), \tag{5.28}$$

where

$$\begin{aligned} M_1 = {} & -fk\tau(1-\varepsilon) + r_0\tau(2 + k\tau + 2\varepsilon) + \\ & k\tau(2+\varepsilon) + (1+\varepsilon)(1 + 2\Pi'\tau + \varepsilon) \end{aligned} \tag{5.29}$$

and

$$\begin{aligned} M_2 = {} & f^2k^2\tau^2(1-\varepsilon)^2 - 2fk\tau(1-\varepsilon)\left(r_0\tau(k\tau + 2\varepsilon + 2) - k\tau\varepsilon - (1+\varepsilon)^2\right) \\ & + \left(1 + kr_0\tau^2 - k\tau\varepsilon - \varepsilon^2\right)^2. \end{aligned} \tag{5.30}$$

Equation (5.28) is very unwieldy but in the case of a timescale separation where $\varepsilon \ll 1$, a zeroth order approximation for equation (5.28) can be derived. It is given by

$$\mu^* \sim \frac{C_{a0}}{\Pi_0}\left(\frac{1}{2\tau} + k(1 - \frac{1}{2}f + \frac{1}{2}r_0\tau) + r_0 + \Pi' \pm \frac{1}{2}\sqrt{\frac{1}{\tau^2} + \frac{2kf}{\tau} + k(kf^2 + 2(1-2f)r_0 - 2kr_0\tau f + kr_0^2\tau^2)}\right) \tag{5.31}$$

as $\varepsilon \to 0$. Note that there are 2 values of μ that satisfy the consistency condition and so there could be two Hopf bifurcations. It can be further noted that in the case where $\varepsilon = 0$ and $f = 1$ then equation (5.28) should reduce to the one box condition. Performing this analysis gives

$$\mu^*_\pm = \frac{C_{a0}\left(\pm\left(-kr_0\tau^2 + k\tau + 1\right) + r_0\tau(k\tau + 2) + k\tau + 2\Pi'\tau + 1\right)}{2\Pi_0\tau} \tag{5.32}$$

or

$$\mu^*_+ = \frac{C_{a0}}{C_s^{\mathrm{eq}}} + \frac{C_{a0}}{\Pi_0}\frac{\mathrm{d}\Pi}{\mathrm{d}C_a} + \frac{C_{a0}}{C_s^{\mathrm{eq}}}\left(\frac{k}{r_0} + \frac{\tau^{-1}}{r_0}\right) \tag{5.33}$$

$$\mu^*_- = \frac{C_{a0}}{C_s^{\mathrm{eq}}} + \frac{C_{a0}}{\Pi_0}\frac{\mathrm{d}\Pi}{\mathrm{d}C_a} + \frac{C_{a0}}{C_s^{\mathrm{eq}}}k\tau \tag{5.34}$$

which does indeed correspond to the conditions (equations (5.23) and (5.24)) derived for the one box case.

5.5.3 Numerical Results

To test if the value of μ in equation (5.28) does give rise to a Hopf bifurcation, equation (5.25) was integrated with $f = 0.5$, $\tau = 0.45$ and $\varepsilon = 0.004$. Furthermore the eigenvalues of the Jacobian were numerically computed for a range of values of μ. The eigenvalues of the Jacobian are plotted in figure 5.7, which show the eigenvalues crossing the imaginary axis at the predicted bifurcation point, μ_-. Furthermore, the equilibrium soil carbon state is plotted in figure 5.8. For $\mu \lessapprox 2.1$, the system is in a quiescent state, in which the state variables do not change with time. For larger values of μ, carbon moves between the soil, the atmosphere and the ocean boxes in an oscillatory fashion, with temperature oscillating in phase with atmospheric carbon. It can be seen that the bifurcation corresponds to the theoretical prediction. No bifurcation was found at μ_+. This could be because μ_+ represents a spurious solution. Alternatively there could be other parameters for which μ_+ represents a real bifurcation. In any case as $\mu_+ > \mu_-$, the bifurcation at μ_- will have more relevance to the climate system.

It can be seen therefore that the two box model is complex enough to reproduce the behaviour of the IMOGEN model but simple enough to be analytically tractable.

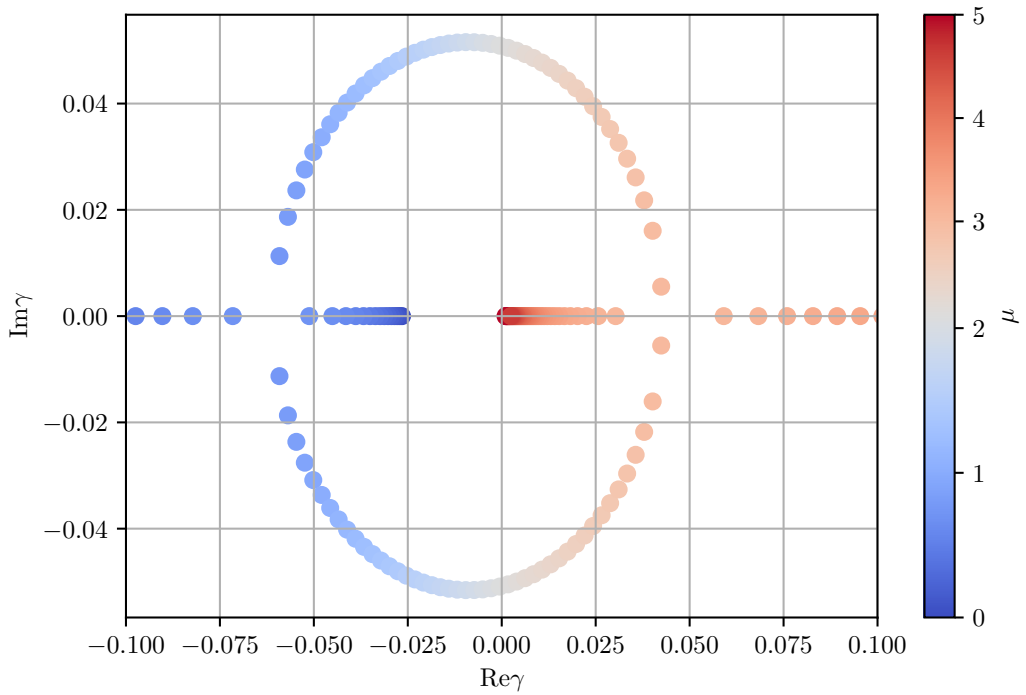

Figure 5.7: The eigenvalues of the Jacobian of the two box model equation (5.25) plotted in the complex plane as a function of μ. The colour of the eigenvalue is given by the value of μ. The colour scheme has been chosen so that the colours transition from blue to red at the bifurcation point μ_- given by equation (5.28). This shows the eigenvalues crossing the imaginary axis at the predicted point, which is where the Hopf Bifurcation happens.

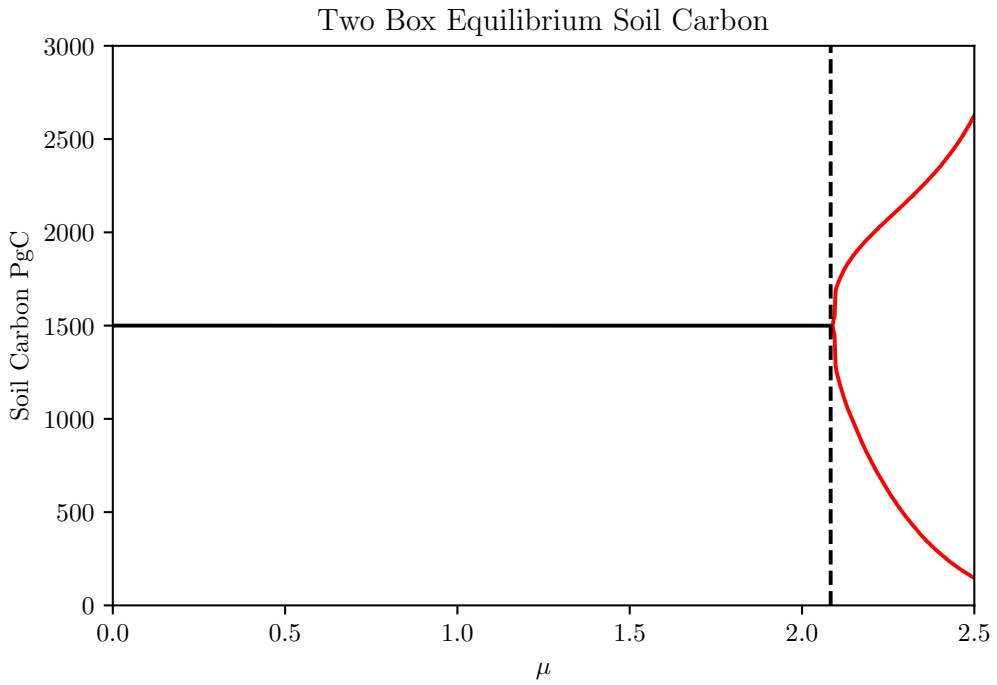

Figure 5.8: Equilibrium levels of soil carbon as a function of μ for the two box ocean model, equation (5.25), calculated numerically. The ocean parameters are $\tau = 0.45$ yr, $\varepsilon = 0.004$ and $f = 0.5$. The dashed line is the analytically calculated bifurcation point, μ_- given by equation (5.28). Solid black lines represent a steady state condition, whereas red lines show the maximum and minimum of an oscillatory state. The oscillation period increases almost linearly with μ from around 23 yr to 64 yr. These periods are comparable, at least near the critical value of μ, with those predicted by the imaginary part of the eigenvalues of the Jacobian, plotted in figure 5.7.

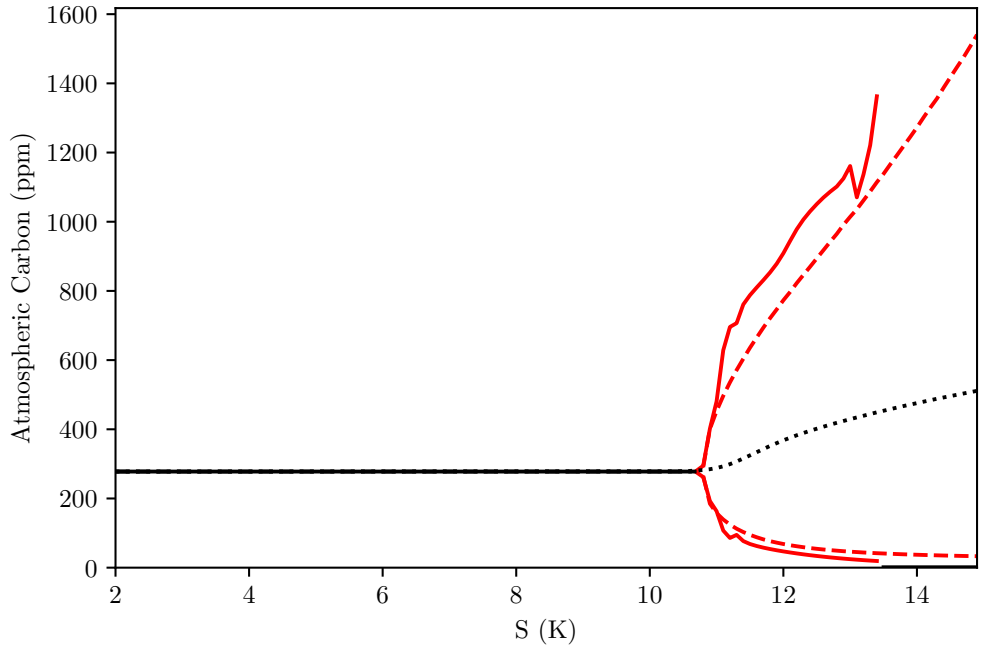

Figure 5.9: A comparison of the bifurcation diagrams of the IMOGEN, one box and two box models. Ocean parameters have been chosen so that the bifurcation happens at the same value of S. Q_{10} has been set to 2. Black lines represent a steady state condition, whereas red lines show that maximum and minimum of an oscillatory state. The solid lines are the values for IMOGEN, the dotted lines are for the one box model and the dashed lines are for the two box model. IMOGEN and the two box model undergo a Hopf bifurcation at $S \approx 10.5$ K, whereas the one box model undergoes a transcritical bifurcation here. The oscillation period for the two box model increases linearly with S from 34 yr to 77 yr. The oscillation period for the IMOGEN model shows little variation with S, having an oscillation period of 1250 yr.

5.6 Model Comparison

In this chapter, the ocean component of the Earth's carbon cycle has been represented in three different ways: by a one-box, a two-box and as a more complex model. Each model suggests the carbon cycle has bifurcations for large enough values of the climate sensitivity. In this next figure, figure 5.9 the equilibria are plotted for each model. The ocean parameters have been chosen so that the bifurcation occurs at the same point. For the one box model, this involved setting $\tau = 2.34$ yr. For the two box model there was more freedom in the parameter choice. The choice $\tau_1 = 0.1$ yr, $f = 0.92$ and $\varepsilon = 1.6 \times 10^{-5}$ was made.

Unlike the other two models, the one box model does not give any oscillatory behaviour. The two box model gives oscillations for all values of S above a threshold, whereas IMOGEN

Parameter	Estimated Quantity	
	One Box	Two Box
τ_1	3.7 yr	0.5 yr
τ_2		124 yr
f_1	1	0.9
f_2	0	0.1

Table 5.2: Parameter Estimates for one and two box ocean models.

shuts the oscillations down at large enough S, and no carbon is found in the atmosphere. However the two box model and IMOGEN give qualitative agreement on the amplitude of the limit cycles beyond the bifurcation point.

5.6.1 Ocean Parameter Estimation

Equation (5.14) can be fitted to observed changes in ocean carbon to estimate the parameters f_i and τ_i in the N-box models. This is done for the one box model, in which only τ_1 needs to be estimated and for the two box model where τ_1,τ_2 and f_1 must be estimated. The quantity f_2 is determined by the requirement that $f_1 + f_2 = 1$.

Using equation (5.14), the ocean carbon uptake for an atmospheric CO_2 time series can be computed for given values of τ_i and f_i. The Global Carbon Budget (Friedlingstein et al. 2022) provide estimates of the ocean carbon uptake as well as the increase atmospheric carbon dioxide, which is ultimately caused by anthropogenic activities, from the year 1781 onwards. Assuming $\Delta C_o = \Delta C_a = 0$ before 1781, a least squares fit of the Global Carbon Budget data can be performed to equation (5.14) to estimate the parameters τ_1 for the one box model, as well as τ_1, τ_2 and f_1 for the two box model. These parameter estimates are shown in table 5.2.

These fits are plotted in figure 5.10. It can be seen that both one and two box models do a reasonable job in capturing the historical record of ocean carbon uptake. However the two box model does better, although this to to be expected given the two extra parameters.

These parameters can also be compared to the ones used to make the bifurcation point in IMOGEN line up with the bifurcation points in the one and two box models. In the one box model case, the single parameter τ_1 is close to that used to match the IMOGEN case. In the two box case, parameters τ_1 and f_1 are similar, however the second timescale obtained from observations is much shorter.

That the second timescale obtained from observations is much shorter than required to make the bifurcation points in the two box and IMOGEN models match may imply that the record is not long enough to allow all the relevant timescales to be resolved. Furthermore, given that the IMOGEN ocean carbon model is able to accurately represent the observed ocean uptake (Joos et al. 1996), this might suggest that the extra factors accounted for by

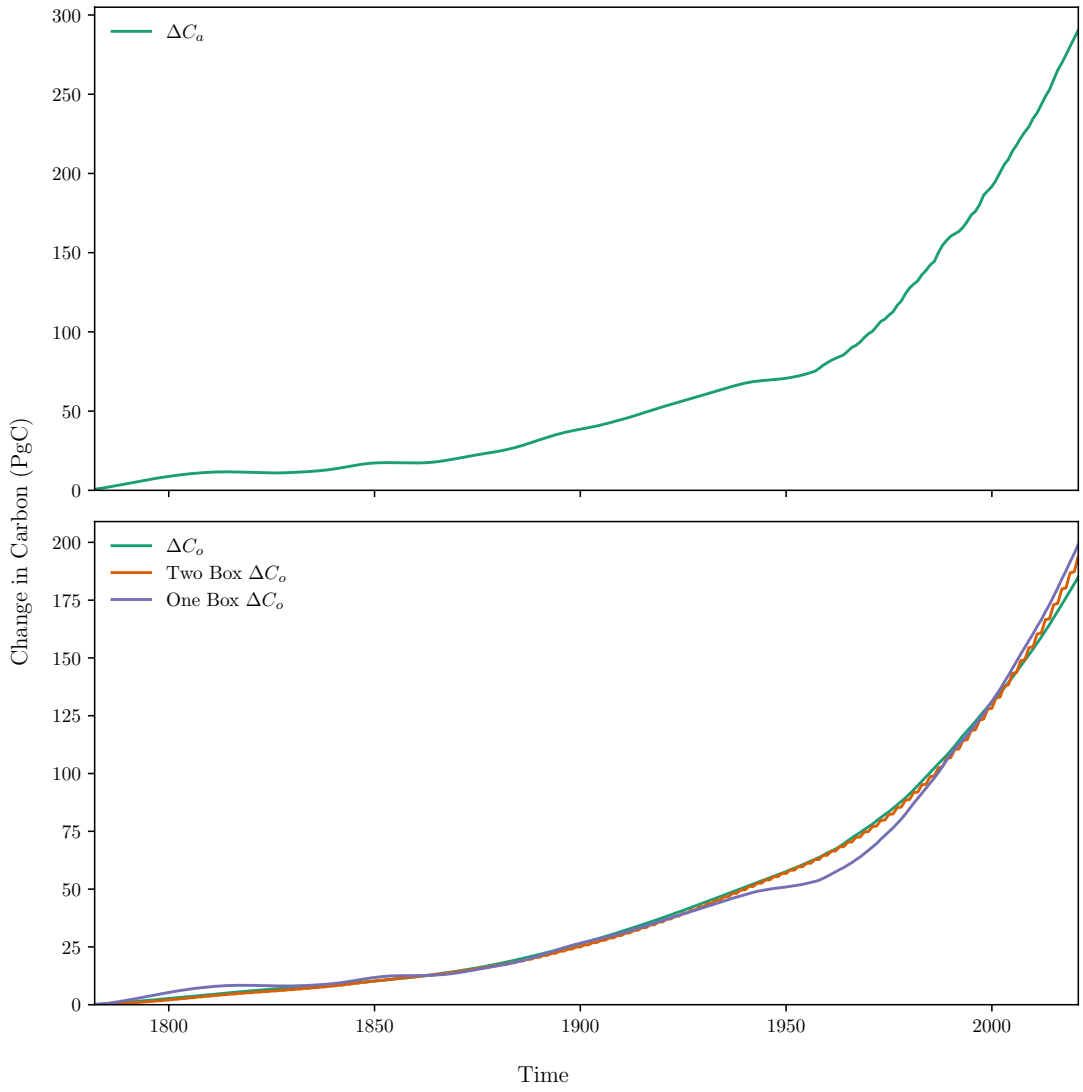

Figure 5.10: The fit of equation (5.14) to the ocean carbon uptake estimated by the Global Carbon Budget using one and two box models. The fitted parameters are given in table 5.2. The driving atmospheric CO_2 is plotted in the top panel, and the ocean uptake in the lower panel. Both one and two boxes give decent fits to the data but the two box model gives a better fit.

IMOGEN (such as the extra time scales and the non-linearities) may be important to get a Hopf bifurcation near to 10.5 K.

5.7 Conclusion

In this chapter I have taken a simple but physically motivated model of the carbon cycle and shown that only certain parameter values are compatible with the qualitative behaviour of the terrestrial carbon cycle during the Holocene. In particular these parameters relate to key sensitivities in the Earth system: the climate sensitivity, the sensitivity of terrestrial carbon to temperature and the sensitivities of net primary production to CO_2. In this model I find that the negative feedbacks on the system (namely changes in net primary production due to increased CO_2) must be sufficiently strong enough to offset the positive feedbacks (the Jenkinson effect).

For realistic parameters of $Q_{10} = 2$ and $C_{1/2} = 280$ ppm, the critical value of S which leads to an instability is 10.7 K. This is similar to, but larger than, the Cox, Huntingford and Jones 2006 critical value of 9 K, a difference which can be attributed to the simplified representation of the ocean in that paper.

Although this model was relatively simple, the ocean component is still too complex to handle analytically. I simplified the ocean model down to a box model of the oceans, which meant I could derive exact results about the bifurcation. I found that a single box could recreate the oscillatory behaviour seen for large enough climate sensitivities, however it did not do this at the correct bifurcation point. On the other hand, a two box model could reproduce the oscillations at the correct bifurcation point.

I could then fit the box models to the observed carbon uptake by the oceans to estimate what parameters best fit the observations. These parameters are similar to those found in the more complex model, although they disagree on the position of the bifurcation.

Chapter 6

Spatial Early Warning Signals

Earlier in this thesis, specific examples of tipping points were examined. There is much interest in creating monitoring systems to determine how close these and other tipping points are to being triggered. One proposed way to do this is with Early Warning Signals. These Early Warning Signals assume the system is forced slowly compared to its timescale. However in the case of many systems of interest, the forcing (climate change) is fast relative to the system's own dynamics. In this chapter I will try to produce Early Warning Signals more appropriate to this case.

6.1 Fast and Slow Tipping Elements

An open question in the theory of Early Warning Signals is how to modify them to be appropriate to the case when the control parameter of a system changes quickly relative to the timescale of the system (Bolt, Nes and Scheffer 2021). To formalise what is meant by a control parameter changing rapidly relative to the system, consider the system

$$\frac{\mathrm{d}y}{\mathrm{d}t} = \frac{f(y, rt)}{T} \tag{6.1}$$

where y is the system state, T is a characteristic timescale of the system and r is the rate the system is linearly forced at. Assume that the partial derivatives of f are of order one. There is an associated frozen system

$$\frac{\mathrm{d}y}{\mathrm{d}t} = \frac{f(y, \mu)}{T} \tag{6.2}$$

where μ is a constant control parameter. Suppose further than there is a bifurcation in the frozen system when $\mu = \mu^*$, which corresponds to a tipping point in equation (6.1) at time $t = t^*$ (i.e. when the forcing reaches a magnitude of $rt^* = \mu^*$). By considering the ratio of the system's timescale T, to forcing timescale, $1/r$, the parameter $\varepsilon = rT$ can be defined. Time can

be rescaled through $t = Ts$ so that equation (6.1) becomes

$$\frac{\mathrm{d}y}{\mathrm{d}s} = f(y, \varepsilon s). \tag{6.3}$$

Alternatively, this can be rewritten autonomously as

$$\frac{\mathrm{d}y}{\mathrm{d}s} = f(y, \mu) \tag{6.4a}$$

$$\frac{\mathrm{d}\mu}{\mathrm{d}s} = \varepsilon. \tag{6.4b}$$

An important limit is the small ε limit. This corresponds to small r, which means the system is forced very slowly, or equivalently to large T — which means the system responds very slowly to forcing. In this limit, equation (6.4) is a fast-slow system (Kuehn 2011) and the usual tools of bifurcation theory can be applied without too much difficulty. In this case, rises in the autocorrelation and variance of fluctuations about the system's quasi-static equilibrium state are to be expected as the tipping point is approached (Scheffer et al. 2009).

In the case of climate change, systems to which this small ε limit applies are known as *fast tipping elements*. An example of a fast tipping element is the Amazon rainforest (Ritchie et al. 2021).

There also exist *slow tipping elements* in which ε is not small. It is difficult to get good early warning signals using the variance and autocorrelation techniques (Bolt, Nes and Scheffer 2021). Unfortunately these systems which respond slowly to forcing, such as the Greenland ice sheet (Ritchie et al. 2021), are common in the Earth system.

The reason slow tipping elements are common in the Earth system is because the rate of global warming is fast, on the order of 1 K per century (Osborn et al. 2021), which is a rate unprecedented in at least the last 2000 years (IPCC 2021). Many important tipping elements have timescales of centuries or longer (Lenton et al. 2008; Armstrong McKay et al. 2022). This implies that, for tipping elements subject to anthropogenic climate change, ε is unlikely to be small, as shown in table 6.1. This motivates the development of Early Warning Signals that are reliable for systems with larger values of ε.

One way to understand the problems with Early Warning Signals for slow tipping elements is to recognise that the equilibrium implied by the changing forcing is changing significantly over the sliding windows used to calculate the Early Warning Indicators. Although it may be possible to make the sliding window shorter, this will increase the uncertainties on any statistical estimate. Furthermore, the sliding window must be large enough to resolve the critical dynamics of the system, which are themselves slowing down, and so will eventually occur on timescales larger than the sliding window. A potential way to avoid this problem is to try to make 'instantaneous' measurements of the variance and autocorrelation of the fluctuations about equilibrium. This could be done by calculating these statistics over space instead of over time.

Tipping Element	System Timescale (years)	Estimated ε
Greenland Ice Sheet	1000–15 000	20–300
West Antarctic Ice Sheet	500–13 000	10–260
Boreal Permafrost	100–300	2–6
AMOC	15–300	0.3–6
Amazon Rainforest	50–200	1–4
Southern Polar Gyre Convection	5–50	0.1–1

Table 6.1: Estimates of ε values for a subset of tipping elements using the estimated timescales in Armstrong McKay et al. 2022. The forcing timescale was chosen to be 50 yr. Assuming a current level of warming of around 1 K, if temperatures increase by 1 K over the forcing timescale then this choice of timescale corresponds to around 3 K of warming by the end of the century. This is about the level of warming expected under current policies (Rogelj et al. 2023).

Spatial early warning signals have been studied before. Donangelo et al. 2010 compared spatial and temporal early warning signals, finding that the spatial variance can give an earlier early warning than the temporal variance. Another study (Kéfi et al. 2014) found rising memory, variability and changes to patchiness were all spatial indicators of an upcoming transition. A range of studies have applied spatial early warnings to ecological problems (Guttal and Jayaprakash 2009; Carpenter and Brock 2010; Dakos et al. 2011). Spatial early warning signals have even been applied to observational data (Kéfi et al. 2007; Eby et al. 2017; Tirabassi and Masoller 2023). It should be noted that recent high profile applications to the Earth system (Boers 2021; Boers and Rypdal 2021; Boulton, Lenton and Boers 2022; Ditlevsen and Ditlevsen 2023) have all involved temporal rather than spatial indicators, even though spatially resolved data was used.

6.2 The System

In order to investigate spatial early warning signals a specific system will be examined. This system will be chosen to be generic enough that broader conclusions can be drawn. The system will be made as simple as possible to aid in the analysis.

As outlined in section 2.1.1 near a B-tipping point many systems are governed by similar one-dimensional dynamics, which motivates the introduction of one dependent variable y. In one dimension there is only one generic type of bifurcation giving rise to catastrophic transitions, the saddle node (Thompson, Stewart and Ueda 1994). The saddle node normal form is $\dot{y} = \mu - y^2$, however y diverges for $\mu < 0$. Therefore to keep y finite and the dynamics simple, the system to be investigated will contain only the lowest order terms which give a saddle node and bounded dynamics, namely $\dot{y} = y - y^3/3 - \mu$, where μ is a control parameter.

To take into account the spatial nature of the problem a coupling in space must be con-

sidered. Attention will be restricted to a 1 dimensional periodic domain of length L. To couple in space the well studied diffusive coupling is used; this acts to smooth out the value of y over the domain. Such a diffusive form has found numerous uses in climate and ecological models. For example, it has been used in energy balance models for the global temperature (Ghil 1976), ecosystem pattern formation (Gowda, Riecke and Silber 2014; Bastiaansen et al. 2018) and in continuum models of the compost bomb (Clarke et al. 2021).

Noise will be introduced into the system and the control parameter, μ, will change linearly with time. These considerations combine to motivate studying

$$\frac{\partial y}{\partial t} = y - \frac{1}{3}y^3 - \mu + D\frac{\partial^2 y}{\partial x^2} + \sigma\zeta \tag{6.5a}$$

$$\frac{\mathrm{d}\mu}{\mathrm{d}t} = \varepsilon \tag{6.5b}$$

where ζ is delta-correlated noise with mean

$$\mathbb{E}\left[\zeta\left(x,t\right)\right] = 0 \tag{6.6}$$

and covariance

$$\mathbb{E}\left[\zeta\left(x,t\right)\zeta(x',t')\right] = \delta(x-x')\delta(t-t') \tag{6.7}$$

The parameter σ^2 is the variance of the noise, and D gives the strength of the spatial coupling. The variable μ linearly increases between $\mu = 0$ and $\mu = 1$ and so the system will undergo a saddle node bifurcation at $\mu = 2/3$.

Whilst the spatially uncoupled system is bistable, travelling waves (Leemput, Nes and Scheffer 2015) generated by noise induced transitions between the two states will destroy the bistability in the spatially coupled system. The timescale of these transitions in the coupled system can be estimated from the Kramers' escape time in the uncoupled system. If $\sigma = 0.1$, then the Kramers' escape time (equation (2.28)) for the uncoupled system is 10^{64} for $\mu = 0$, far longer than any simulation performed in this chapter. This means that although the system is not formally bistable, it is effectively bistable on relevant timescales.

This system, equation (6.5), can be viewed variationally[1]. The deterministic dynamics can be related to the 'energy' of the system, defined as

$$\mathcal{E} = \int_0^L -\frac{1}{2}y^2 + \frac{1}{12}y^4 + \mu y + \frac{1}{2}D\left(\frac{\partial y}{\partial x}\right)^2 \mathrm{d}x. \tag{6.8}$$

This gives further justification for using a diffusive coupling in the following sense. Suppose a general $\mathcal{E}$ was written as a power series

$$\mathcal{E} = \int_0^L -\frac{1}{2}y^2 + \frac{1}{12}y^4 + \mu y + b_1\frac{\partial y}{\partial x} + b_2 y\frac{\partial y}{\partial x} + b_3\left(\frac{\partial y}{\partial x}\right)^2 + \ldots\,\mathrm{d}x. \tag{6.9}$$

[1] A brief review of the concepts of the variational derivative are presented in appendix A.

If the coupling is required to be isotropic in space, then $b_1 = b_2 = 0$, so to lowest order equation (6.9) reduces to equation (6.8).

Given $\mathcal{E}$, equation (6.5a) can be rewritten as

$$\frac{\partial y}{\partial t} = -\frac{\delta \mathcal{E}}{\delta y(x)} + \sigma\zeta, \tag{6.10}$$

which is a Time Dependent Ginzburg Landau equation which describes the mean field dynamics of systems like the Ising model (Goldenfeld 2018).

6.3 Effect of Diffusion on Critical Slowing Down

In chapter 2 it was shown how critical slowing down leads to temporal early warning signals. In this section, I will show that early warning signals are still expected to manifest themselves when viewed spatially. Recognising that equation (6.10) describes the mean field dynamics of the Ising model, I will do this using the results of the Landau theory of phase transitions. To draw connections between this and critical slowing down in non-spatial systems I will begin by calculating the early warning indicators using a Fokker-Planck approach for the uncoupled case.

The uncoupled case corresponds to $D = 0$. Furthermore, assume ε is small enough so that μ can be taken to be a parameter of the system. This is equivalent to calculating the conventional early warning signals over an ensemble of realisations and so should reproduce the well known results about rising variance and autocorrelation (Dakos et al. 2008).

Linearising equation (6.5) about an equilibrium, y^*, gives

$$\frac{\mathrm{d}z}{\mathrm{d}t} = -\lambda z + \sigma\zeta \tag{6.11}$$

where $z = y - y^*$ and $\lambda = (y^*)^2 - 1$. To be precise, z and ζ are both functions of t and x. However, given the periodic boundary conditions and the fact that $D = 0$, the stationary distribution of z will not be a function of x. Hence this distribution can be calculated by looking at a particular x value, say $x = 0$. Therefore, equation (6.11) should be viewed as being evaluated at $x = 0$.

In this case, the Fokker-Planck equation, equation (2.18), can be used to calculate the statistics (Risken 1984). The Fokker-Planck equation associated with equation (6.11) is

$$\frac{\partial p}{\partial t} = \frac{\partial}{\partial z}\left(\lambda z p\right) + \frac{1}{2}\sigma^2 \frac{\partial^2 p}{\partial z^2} \tag{6.12}$$

where p is the pdf for the system. The steady state solution, assuming p and its derivatives vanish as $z \to \pm\infty$ is

$$p(z) = \frac{1}{Z} e^{-\frac{1}{\sigma^2}\lambda z^2}. \tag{6.13}$$

The normalisation factor Z is given by

$$Z = \int_{-\infty}^{\infty} e^{-\frac{1}{\sigma^2}\lambda z^2}\,\mathrm{d}z = \sigma\sqrt{\frac{\pi}{\lambda}}. \tag{6.14}$$

Note that the variance of the stationary distribution of z is

$$\sigma_z^2 = -\sigma^2\frac{\partial \log Z}{\partial \lambda} = \frac{\sigma^2}{2\lambda} \tag{6.15}$$

so that as the system moves towards the bifurcation and thus $\lambda \to 0$, it will be the case that σ_z^2 diverges. It follows from the Fluctuation-Dissipation Theorem (Kubo 1966; Marconi et al. 2008) that the autocorrelation at lag-t is $\alpha(t) = e^{-\lambda t}$ and so $\alpha \to 1$ at the bifurcation. This is the same behaviour as in the non-spatial case, as expected.

If $D \neq 0$, then equation (6.11) becomes

$$\frac{\partial z}{\partial t} = -\lambda z + D\frac{\partial^2 z}{\partial x^2} + \sigma\zeta = -\frac{\delta \mathcal{H}}{\delta z} + \sigma\zeta, \tag{6.16}$$

where

$$\mathcal{H} = \int_0^L \frac{1}{2}\lambda z^2 + \frac{1}{2}D\left(\frac{\partial z}{\partial x}\right)^2 \mathrm{d}x\,. \tag{6.17}$$

Equation (6.16) can be analysed by performing a Fourier series decomposition (Riley, Hobson and Bence 2006), where a function $q(x, t)$ can be split into oscillatory modes in space with amplitude $q_k(t)$ for wavenumber k defined through

$$q(x, t) = \frac{1}{L}\sum_k q_k(t)e^{ikx} \tag{6.18}$$

or

$$q_k(t) = \int_0^L q(x, t)e^{-ikx}\,\mathrm{d}x \tag{6.19}$$

where $q_k = q^*_{-k}$ to ensure that $q(x, t) \in \mathbb{R}$. Performing this decomposition gives an equation for each mode

$$\frac{\mathrm{d}z_k}{\mathrm{d}t} = -\lambda z_k - Dk^2 z_k + \sigma\zeta_k. \tag{6.20}$$

To find the variance of ζ_k, consider the product

$$\zeta_m(t)\zeta_n^*(t') = \int_0^L \zeta(x, t)e^{-imx}\,\mathrm{d}x \int_0^L \zeta(x', t')e^{inx'}\,\mathrm{d}x'\,, \tag{6.21}$$

which can be written

$$\zeta_m(t)\zeta_n^*(t') = \iint \zeta(x, t)\zeta(x', t')e^{-i(mx-nx')}\,\mathrm{d}x\,\mathrm{d}x'\,. \tag{6.22}$$

Taking the expectation of both sides gives the covariance of $\zeta_m(t)$ with $\zeta_n(t')$

$$\mathbb{E}\left(\zeta_m(t)\zeta_n^*(t')\right) = \iint \delta(x-x')\delta(t-t')e^{-i(mx-nx')}\,\mathrm{d}x\,\mathrm{d}x' \tag{6.23}$$

or

$$\mathbb{E}\left(\zeta_m(t)\zeta_n^*(t')\right) = \delta(t-t')\int_0^L e^{-i(m-n)x}\,\mathrm{d}x \tag{6.24}$$

so the covariance structure of the modes of ζ can be written as

$$\mathbb{E}\left(\zeta_m(t)\zeta_n^*(t')\right) = \delta(t-t')\delta_{mn}L, \tag{6.25}$$

where δ_{ij} is the Kronecker delta.

From equation (6.20) it can be seen that each mode with wavenumber k relaxes to equilibrium on a timescale

$$\tau_k = \frac{1}{\lambda + Dk^2}. \tag{6.26}$$

As $\lambda \to 0$, τ_k increases, so critical slowing down is still to be expected. Suppose however that only large k modes were resolved, which corresponds to viewing the system at too small a scale. In this case $\tau_k \sim 1/Dk^2$ so critical slowing down would not be observed, which would hamper early warning signals.

To investigate the effects of critical slowing down on variance and autocorrelation, the probability distribution, $p[z,t]$ which is now a functional of z, of equation (6.16) must be calculated. This system has its own form of the Fokker-Planck equation (Goldenfeld 2018) which describes the evolution of $p[z,t]$,

$$\frac{\partial p}{\partial t} = \int \frac{\delta}{\delta z(x')}\left(\frac{\delta \mathcal{H}}{\delta z(x')}p + \frac{1}{2}\sigma^2\frac{\delta p}{\delta z(x')}\right)\mathrm{d}x'. \tag{6.27}$$

Again, this has an equilibrium solution

$$p[z] = \frac{1}{Z}e^{-\frac{2}{\sigma^2}\mathcal{H}[z]} \tag{6.28}$$

where

$$Z = \int e^{-\frac{2}{\sigma^2}\mathcal{H}[z]}\,\mathcal{D}z. \tag{6.29}$$

In order to find the variance, consider the two-point correlation function

$$G(x_1 - x_2) = \mathbb{E}\left(z(x_1)z(x_2)\right). \tag{6.30}$$

To calculate this function, consider a modified $\mathcal{H}$,

$$\mathcal{H}'[z] = \mathcal{H}[z] - \int_0^L B(x)z(x)\,\mathrm{d}x \tag{6.31}$$

with a modified Z

$$Z' = \int e^{-\frac{2}{\sigma^2}\mathcal{H}'[z]}\,\mathcal{D}z. \tag{6.32}$$

The two point correlation function is equal (Goldenfeld 2018) to

$$G(x_1 - x_2) = \frac{\sigma^4}{4}\frac{\delta}{\delta B(x_1)}\frac{\delta \log Z'}{\delta B(x_2)}\bigg|_{B=0}. \tag{6.33}$$

To see this, note

$$\frac{\delta}{\delta B(x_1)}\frac{\delta \log Z'}{\delta B(x_2)} = -\frac{1}{Z'^2}\left(\frac{\delta Z'}{\delta B(x_1)}\right)^2 + \frac{1}{Z'}\frac{\delta}{\delta B(x_1)}\frac{\delta Z'}{\delta B(x_2)} \tag{6.34}$$

and, from equation (6.32),

$$\frac{1}{Z'}\frac{\delta Z'}{\delta B(x_1)}\bigg|_{B=0} \propto \int z(x_1)\frac{e^{-\frac{2}{\sigma^2}\mathcal{H}[z]}}{Z'}\,\mathcal{D}z = \int z(x_1)p[z]\,\mathcal{D}z = \mathbb{E}(z(x_1)) = 0 \tag{6.35}$$

and similarly

$$\frac{1}{Z'}\frac{\delta}{\delta B(x_1)}\frac{\delta Z'}{\delta B(x_2)}\bigg|_{B=0} \propto \int z(x_1)z(x_2)p[z]\,\mathcal{D}z. \tag{6.36}$$

The integral in equation (6.32) can be evaluated (see appendix B) to give the following form for G

$$G(x) = \frac{1}{4}\sigma^2\frac{\xi}{D}e^{-x/\xi} \tag{6.37}$$

where $x = x_1 - x_2$ and

$$\xi = \sqrt{\frac{D}{\lambda}} \tag{6.38}$$

is the correlation length. The variance is thus $G(0) = \sigma^2/\sqrt{16\lambda D}$, which diverges as the bifurcation is approached.

6.4 Statistics

The autocorrelation and variance of equation (6.5) will be compared when calculated over space and over time. These two different ways of calculating the statistics will now be defined. A summary is given in table 6.2.

6.4.1 Spatial Statistics

The average of a quantity, A, calculated over space is defined to be

$$\langle A \rangle = \frac{1}{L} \int_0^L A(y(x,t),x)\,\mathrm{d}x. \tag{6.39}$$

The spatial variance estimator of y at time t is then

$$\sigma_s(t)^2 = \langle y^2 \rangle - \langle y \rangle^2, \tag{6.40}$$

and the temporal autocorrelation estimator over space is defined as

$$\alpha_s(t,\Delta t) = \frac{\langle y(t,x)y(t+\Delta t,x) - \langle y(t,x)^2 \rangle}{\sigma_s(t)^2}. \tag{6.41}$$

The quantity Δt is the lag of the autocorrelation. However equation (6.5) will ultimately be solved numerically and in everything that follows Δt will be set to the timestep, so that α_s is the lag-1 autocorrelation.

6.4.2 Temporal Statistics

When working over time, the spatio-temporal data will be converted to temporal data by first averaging in space to get $\langle y \rangle$. Averaging in time is defined as follows. Consider the quantity $B(t)$. The temporal average is

$$\overline{B} = \frac{1}{\tau_w} \int_0^{T_w} B(t)\,\mathrm{d}t \tag{6.42}$$

where the average is taken over some suitable window of length T_w.

When computing early warning indicators over time, the time series must first be 'detrended'. The detrended time series of $\langle y \rangle$ is denoted by z. The estimators of variance and autocorrelation, defined over a window of length τ_w are

$$\sigma_t^2 = \overline{z^2} - \overline{z}^2 \tag{6.43}$$

and

$$\alpha_t = \frac{\overline{z(t)z(t+\Delta t)}}{\sigma_t^2}. \tag{6.44}$$

Quantity	Domain	Symbol	Definition
Variance	Space	σ_s^2	$\langle y^2 \rangle - \langle y \rangle$
	Time	σ_t^2	$\overline{z^2} - \bar{z}^2$
Autocorrelation	Space	α_s	$\frac{\langle y(t,x)y(t+\Delta t,x)\rangle - \langle y(t,x)^2 \rangle}{\sigma_s(t)^2}$
	Time	α_t	$\frac{\overline{z(t)z(t+\Delta t)}}{\sigma_t^2}$

Table 6.2: The definition of the early warning indicators used in this chapter, taken from equations (6.40), (6.41), (6.43) and (6.44).

6.5 Numerical Results

6.5.1 Numerical Method

To solve equation (6.5), the domain, of length $L = 2\pi$, was discretized into $N = 100$ grid points and the diffusive term is calculated with finite differences. The value of y at the kth gridpoint is y_k. Integration forward in time was accomplished by using an implicit Euler method, where the resulting nonlinear equation was solved using MINPACK's HYBRD method accessed through SciPy (Virtanen et al. 2020). To avoid excessively long integrations when ε is small, the timestep was set to $\delta t = 0.001/\varepsilon$ and the system was integrated until $t = 1/\varepsilon$. Early warning signals were calculated from $\varepsilon t = 0$ until $\varepsilon t = 2/3$, which is the time of the tipping point. When working over time, the window size was chosen to contain 500 data points (i.e. half the time series), so that the window length is $\tau_w = 1/(2\varepsilon)$. Detrending was accomplished by removing a fitted quadratic polynomial from these windows. To stand a chance of getting good early warning signals in time it is required that $\varepsilon < 1/\tau_w$, which is always satisfied. Systems are initialised in equilibrium and spun up for 1000 time steps.

6.5.2 Two Limits

Before determining the reliability of the early warning signals as a function of ε and D, two important limits will be investigated. They are the uncoupled ($D = 0$) and slowly forced ($\varepsilon \ll 1$) limits.

Uncoupled Limit

First the case when $D = 0$ is investigated, for large and small values of ε. Consider figure 6.1. The left column shows the small ε case. This is the case where temporal early warning signals are expected to work well. For this value of ε the system transitions to its new state near the time of the bifurcation and its variance calculated over space and calculated over time both

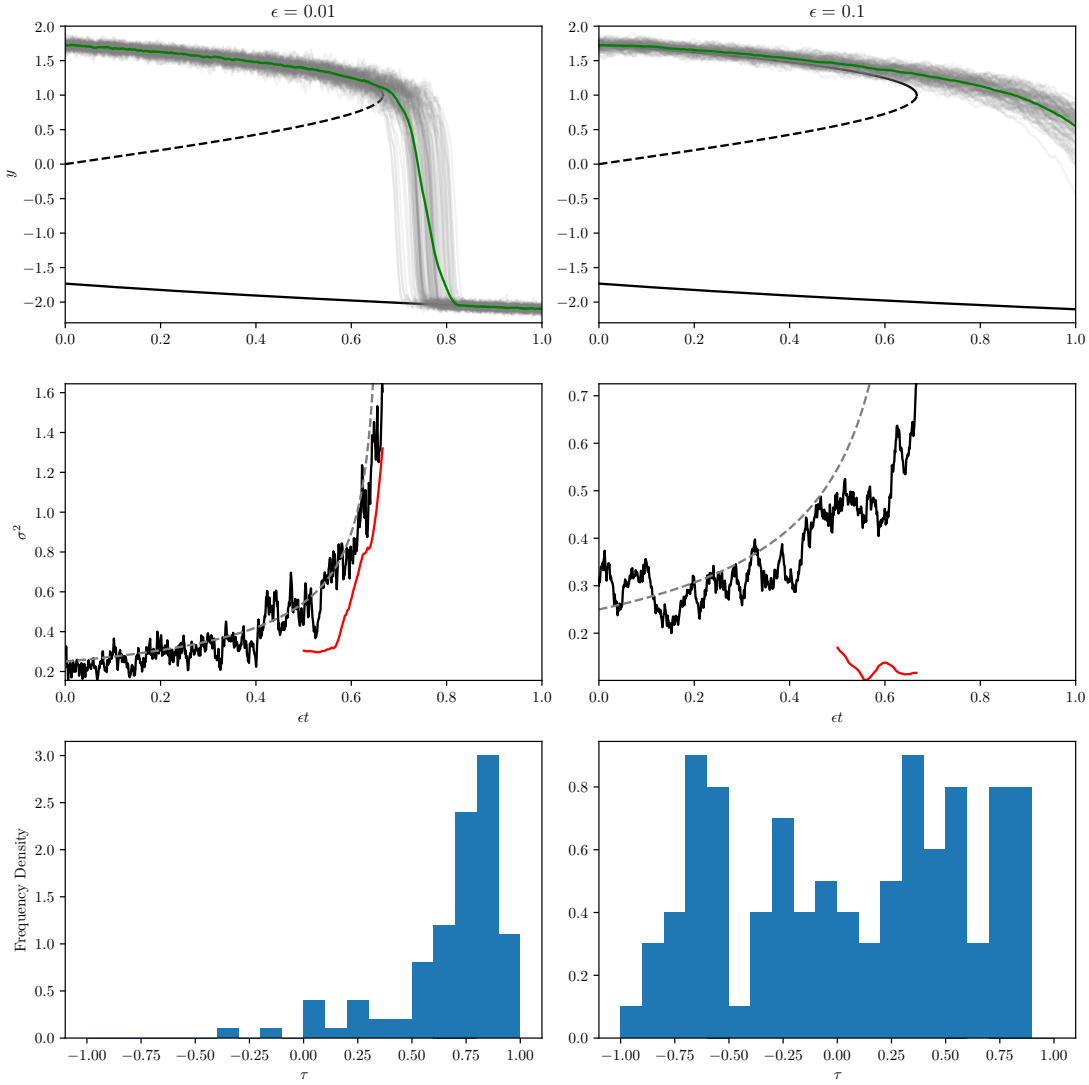

Figure 6.1: Early warning signals when $D = 0$. The left column shows the slow forcing case and the right column shows the fast forcing. The top row shows the individual trajectories with the mean trajectory shown in green. The black curves are the quasi-static equilibria. The second row shows plots of σ_s^2 in black and σ_t^2 in red, normalised by the variance of the driving noise. Note that there is an extra factor of N in the normalisation of the temporal estimate that comes from averaging over trajectories. The grey dashed line shows the analytical variance estimate, which is the same for both spatial and temporal estimates, given by equation (6.15). In the bottom row σ_t^2 is calculated from the individual gridpoints rather than the domain average. The Kendall τ value is calculated for each gridpoint and then a histogram of these τ values is plotted. The mean τ values are 0.69 and 0.06 for the slow and fast case respectively.

clearly increase near the bifurcation point. Furthermore calculating the statistics for each of the individual grid points shows that most grid points experience a rise in variance over time as well.

For the larger ε case the results are different. The system has not yet transitioned to its new state even by the end of the simulation. A clear rise in σ_t^2, given by the red curve, cannot be seen near the bifurcation point. Furthermore looking at the individual grid points in the lower right panel, no coherent warning of the upcoming transition is given. However there is a very clear rise in σ_s^2, the black curve, before the bifurcation, demonstrating that spatial early warning signals are superior in this case.

Slowly Forced Limit

Figure 6.2 is similar to figure 6.1 except it now examines the limit of slow forcing ($\varepsilon = 0.01$) but but with a non-zero coupling in space. D values of $(N/L)^2 D = 1$ and $(N/L)^2 D = 10^5$ were chosen, where N/L is a factor related to the discretisation. For low D and slow forcing early warning signals are expected to work both when calculated spatially or temporally. At higher D the correlations between the grid points will be so great that there will no longer be any variability between different grid points, and so no detection of spatial early warning signals should be possible. This is precisely what is seen in figure 6.2 where for $D = 10^5 (L/N)^2$ the system acts like a single grid point.

6.5.3 Exploring the ε and D parameter space

Now that the two limits have been investigated, the parameter space can be explored more fully. Early warning signals will be investigated in the region of the parameter plane defined by $(\varepsilon, \left(\frac{N}{L}\right)^2 D) \in [10^{-2}, 10^{1}] \times [10^{-7}, 10^{7}]$, where the factor of N/L comes from the discretisation. 50 points are sampled in each direction, geometrically spaced, giving 2500 total points.

It can be determined if an early warning indicator is increasing or decreasing by calculating the Kendall's τ for the data. A positive value implies an increasing trend (Wilks 2019). The reliability of the warning can be assessed by repeating the numerical experiment 100 times (with different realisations of the noise) and calculating a distribution of Kendall's τ. If the signal-to-noise ratio (SNR) of the distribution of τ values, defined as the ratio of the mean to the standard deviation, is smaller than 1 then a reliable early warning cannot be expected.

This signal-to-noise ratio is calculated in figure 6.3 for temporal and spatial early warning statistics. Only for certain regions of the parameter plane are early warning signals of the upcoming tipping point reliable. It can be noted that there is a complementarity between spatial and temporal early warning signals. For rapidly forced systems good early warning signals in space are obtained as long the the coupling in space is not too strong. Conversely, for strongly coupled systems there are good early warning in time as long the forcing is slow enough. It is important to note that the strongly coupled and rapidly forced region does not give good early warning signals with either method.

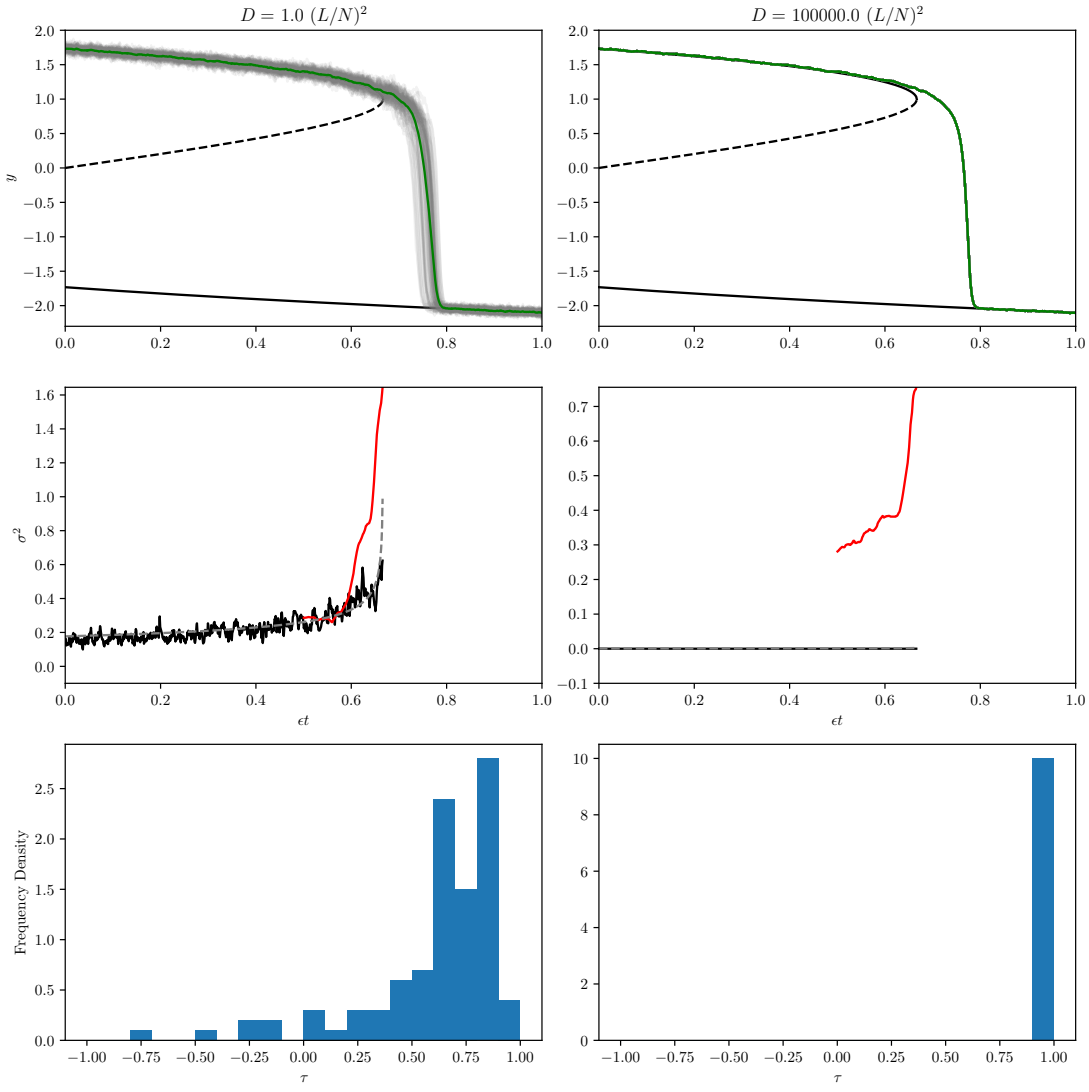

Figure 6.2: Early warning signals when $\varepsilon = 0.01$. The left column shows the weakly coupled case, the right shows what happens in the strongly coupled (large D) case. The top row shows the quasi-static equilibria (black) the individual trajectories of the grid boxes (grey) and the domain average (green). The variance is plotted in the second row, calculated over space (black) and over time (red). The analytical prediction for σ_s^2 is plotted with a dashed grey line. The bottom row shows a histogram of the Kendall τ values calculated over time for each y_k.

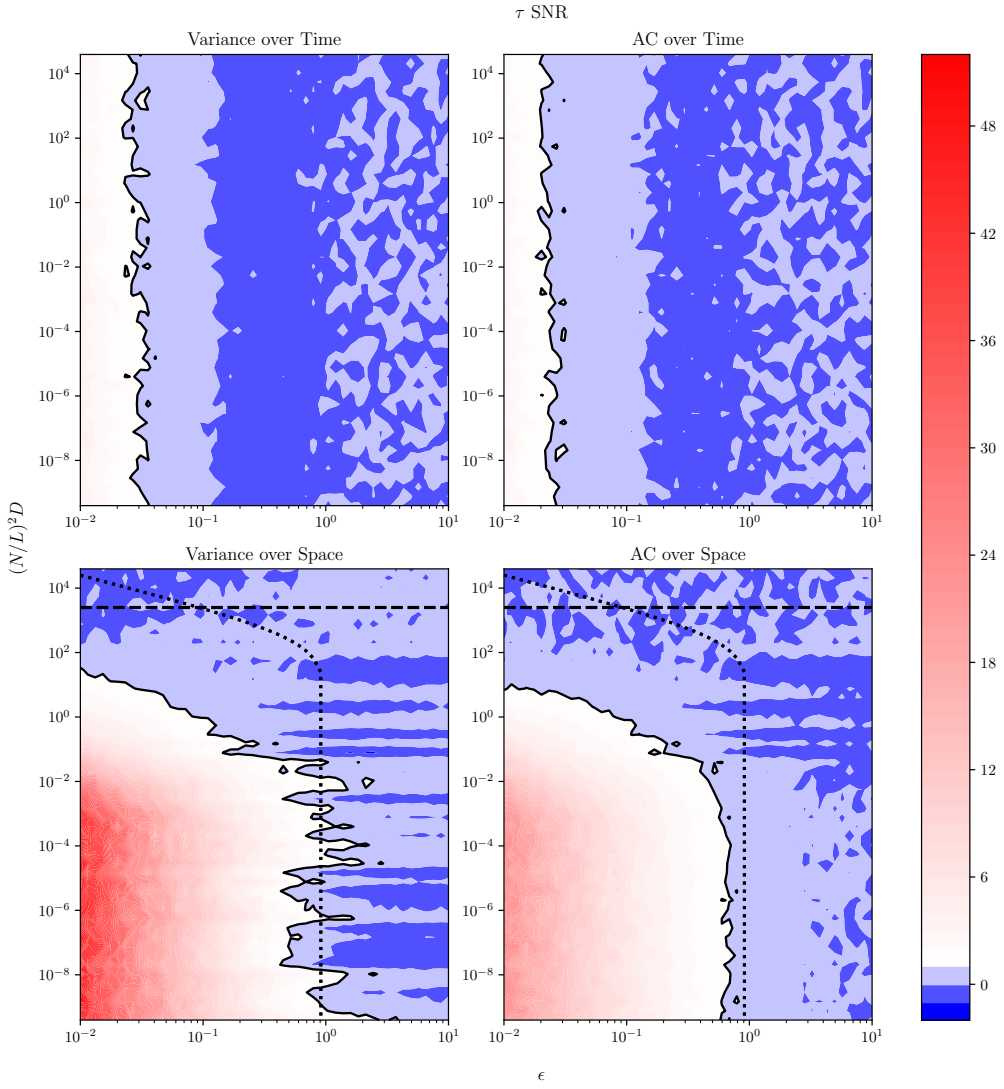

Figure 6.3: Each panel shows the same region of the (ε, D) parameter plane. The left column shows the reliability of the variance as an early warning and the right column the reliability of the autocorrelation. The top row is calculated over time and the bottom row is calculated over space. The colour gives reliability of the early warning. Blue colours correspond to a SNR of less than 1, and thus an unreliable early warning. Red colours correspond to reliable early warnings. The solid line is the SNR = 1 contour. The dashed line is the line given by $\xi = L/2$ and the dotted line is the line $\varepsilon = \tau_k$ for $k = 2\pi/L$.

6.6 Scaling Arguments

In this section an attempt is made to explain why the early warning signals only work in certain regions of the parameter plane plotted in figure 6.3.

6.6.1 Temporal Early Warning Signals

Consider the equilibrium solution to equation (6.10) (i.e. at fixed μ). This will correspond to a minimum of equation (6.8). Noting that equation (6.8) is a strictly increasing function of $\partial y/\partial x$ it must be the case that the equilibrium solution is uniform in x and hence independent of D.

This motivates setting $y = y_{\text{eq}} + z$ where y_{eq} is the spatially uniform equilibrium solution to the deterministic part of equation (6.10). Temporal early warning signals are based on $\langle y \rangle$ so its evolution equation will be determined by averaging equation (6.5) in space. This gives

$$\begin{aligned}\frac{\mathrm{d}\langle y\rangle}{\mathrm{d}t} &= \langle y\rangle - \frac{1}{3}\left\langle y^3\right\rangle - \mu + D\left\langle\frac{\partial^2 y}{\partial x^2}\right\rangle + \sigma\eta \\ &= \langle y\rangle - \frac{1}{3}\left\langle y^3\right\rangle - \mu + \sigma\eta\end{aligned}$$

where $\eta = \langle\zeta\rangle$ is noise delta correlated in time only, with covariance $\mathbb{E}(\eta(t)\eta(t')) = \delta(t-t')/L$. T he diffusive term has vanished due to the periodic boundary conditions. Although there is no explicit dependence on D here, this equation still implicitly depends on D through the nonlinear averaged term $\langle y^3\rangle$.

The evolution equation for $z = y - y_{\text{eq}}$ can be written, to first order in z, as

$$\frac{\mathrm{d}\langle z\rangle}{\mathrm{d}t} = \left(1 - y_{\text{eq}}^2\right)\langle z\rangle + \sigma\eta + \mathcal{O}\left(z^2\right) \tag{6.45}$$

where the fact that y_{eq} is an equilibrium solution of equation (6.5a) has been used and that $\mathcal{O}(z^2)$ is small with high probability. This has no dependence on D and hence it can be expected that the temporal early warning signals are independent of D.

To get good early warning signals it is required that $\langle z\rangle$ is small so that the linearisation in equation (6.45) is valid, but as z is $\mathcal{O}\left(\varepsilon^{1/3}\right)$ (Berglund and Gentz 2006), good temporal early warning signals can only be expected therefore when $\varepsilon^{1/3} \ll 1$.

6.6.2 Spatial Early Warning Signals

It was shown in section 6.3 that by recognising the connection between equation (6.10) and Landau theory for phase transitions, the two point correlation function could be computed and the correlation length $\xi = \sqrt{D/\lambda}$ determined. In order to detect any spatial variability the system must be sampled over scales large compared to the correlation length, which means

$\xi \ll L/2$. Half the domain length has been used because when $\xi = L/2$ all points in the domain are one correlation length or less away from each other.

Applying equation (6.38) and assuming that $\lambda = \mathcal{O}(1)$, which is true at the start of the simulation, the condition for good spatial early warning signals becomes

$$D \ll \frac{L^2}{4}. \tag{6.46}$$

Equation (6.20) shows that the system responds to a fluctuation in mode k of $z_k(0)$ by relaxing to equilibrium like $z_k(t) = \exp(-t/\tau_k)\, z_k(0)$. So for times long compared to τ_k the fluctuation dies away. As it is these fluctuations that will show critical slowing down, they cannot die away too fast or else no early warning signal will be seen. Therefore over a timescale $\mathcal{O}(\varepsilon)$, $\exp(-t/\tau_k) \approx 1$ which requires $\varepsilon \ll \tau_k$. Requiring that this holds for wavenumbers corresponding to the scale of the domain (which is when τ_k is largest) gives the requirement that

$$\varepsilon \ll \frac{1}{1 + \frac{4\pi^2 D}{L}} \tag{6.47}$$

where again it is assumed that $\lambda = \mathcal{O}(1)$ and $k = 2\pi/L$.

6.6.3 Comparison With Numerical Experiments

Figure 6.3 implies the critical ε above which temporal early warning signals fail is $\varepsilon_c \approx 0.04$. Performing the computation $\varepsilon_c^{1/3} = 0.34$ shows that this is indeed compatible with the theory which requires that $\varepsilon^{1/3} \ll 1$. Also plotted in figure 6.3 are the lines $D = L^2/4$ and $\varepsilon = \tau_{2\pi/L}$. It can be seen that they bound the region where good early warning signals can be obtained and also approximate the shape of this region.

The lines do not give the tightest bound possible to the region, but this is to be expected. The reason for this is that the scaling arguments assume a constant value for λ, whereas in reality λ is decreasing towards zero. Furthermore, early warning signals will not suddenly become worse when equations (6.46) and (6.47) are violated. Instead they will become progressively less reliable, and so these scaling arguments should overestimate the reliable region, which indeed they do.

6.7 Discussion

It has been shown that calculating early warning signals over space allows the user to get reliable signals in a previously inaccessible parameter regime (for larger values of ε). As well as having this advantage it is also noted further that calculating early warning signals over space avoids the problems of detrending. These problems are inherent to the method of calculating early warning signals over time.

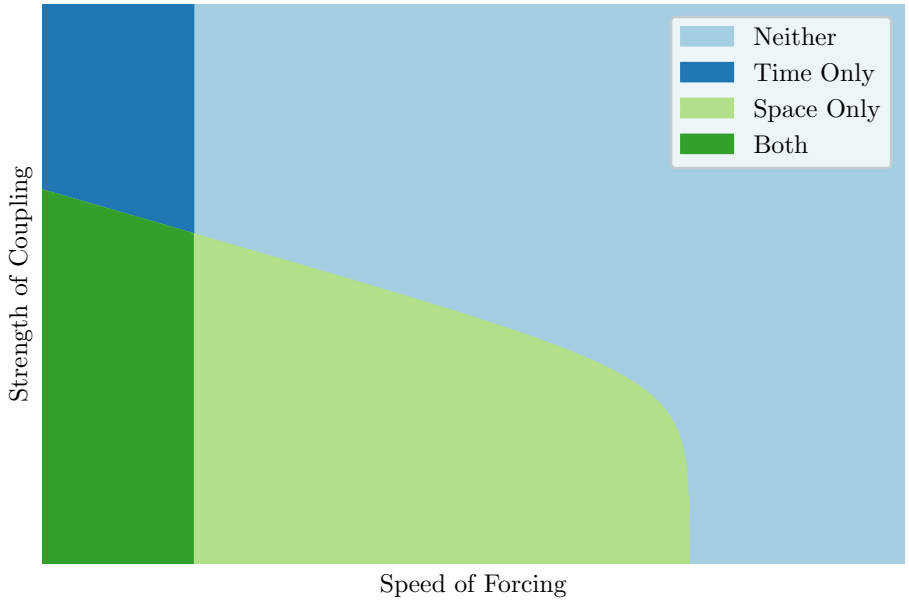

Figure 6.4: A schematic illustrating the complementarity of early warning signals in space and time. The lines are drawn according to the scalings given in section 6.6

There is a interesting complementarity however between early warnings in space and time. For fast forcing and weak coupling in space, early warnings in space are reliable but those in time are not. For slow forcing but strong spatial coupling then early warnings in time are reliable but those in space are not. If the coupling is weak but the forcing is slow both methods are reliable. There is still an inaccessible parameter region, for fast forcing and strong spatial coupling. This is illustrated schematically in figure 6.4.

6.8 Practical Considerations

So far I have applied this method to a simple idealised system. In this section, I will suggest how this method could be applied in practice.

Suppose a candidate tipping element has been identified — which for concreteness I will take to be the Amazon Rainforest. A spatio-temporal dataset which represents the state variable, such as Vegetation Optical Depth (VOD), should be obtained. A value of ε should also be estimated. It is to be hoped that it is small enough. Table 6.1 suggests that the Amazon Rainforest is a marginal case. By calculating a spatial correlation, a correlation length can be determined. If this quantity is small relative to the size of the rainforest, then it is plausible that

the spatial early warning signals investigated in this chapter may give skilful early warnings.

However, other factors should be considered. The Amazon is strongly influenced by ENSO, which may cause the Amazon's variability to change. Other systematic effects, such as a latitudinal climate gradient or human land use, may complicate matters for example by making the parameters D and μ functions of space. This could be avoided by masking out data near human settlement or by working over latitudinal bands.

6.9 Conclusion

Obtaining temporal early warning signals for tipping points are challenging, not least because they are often used in rapidly forced systems. In this chapter the hypothesis has been advanced that spatial early warning signals may be useful in these more rapidly forced systems. It has been found that spatial early warning signals can be used for more rapidly forced systems, as figures 6.1 and 6.3 illustrate.

It has been shown that their usefulness decreases as the spatial interactions increase. In particular there is a dichotomy between temporal early warning signals (which work well in strongly spatially coupled and slowly temporally forced systems) and spatial early warning signals (which work well in weakly spatially coupled and strongly temporally forced systems).

It is noted that there is still an inaccessible parameter region — systems forced strongly in time and strongly coupled in space. There are also further limitations to this approach. Only considered one functional form of coupling has been considered, but others are possible. Secondly, a strong assumption has been made that space is isotropic, but if, for example, D is itself a function of x then this will introduce challenges.

There is no reason for using only one method of calculating early warning signals. It is likely that using spatial early warning signals in conjunction with temporal ones could provide a useful tool to detect approaching tipping points.

Chapter 7

Seeking more robust early warning signals for climate tipping points: the Ratio of Spectra method (ROSA)

Previous chapters were an examination of specific tipping points in the Earth system. These tipping points present challenges for society and ecosystems, yet the global warming thresholds at which these may be triggered remain uncertain. However, a theory of 'critical slowing down' has been developed which could warn of approaching tipping points. Applications of this theory often implicitly assume stationary white-noise forcing, itself requiring a clean separation between forced trends and variability, which is especially difficult under contemporary climate change. This chapter proposes a modified method to derive an early warning signal in a system, such as the climate, which is forced by time correlated processes. The method looks at the *Ratio of Spectra (ROSA)* of a system state variable relative to a forcing variable. I demonstrate the ROSA method on an idealised forced dynamical system, before applying it to a particular challenging example from the Earth system: dieback of the Amazon rainforest. I show that ROSA identifies more examples of abrupt transitions in the Amazon,in state-of-the-art CMIP6 Earth System Models, than conventional early warning signals.

This chapter is based on a published paper, 'Seeking more robust early warning signals for climate tipping points: the ratio of spectra method (ROSA)' (Clarke et al. 2023).

7.1 Introduction

The paleoclimate record contains numerous examples (Brovkin et al. 2021) of major components of the Earth system experiencing rapid change. Such changes can be caused by relatively small changes in external forcing, such as changes in incoming solar radiation or in greenhouse

gas concentrations.

Over the last two hundred years humans have increasingly forced the climate system, primarily through the burning of fossil fuels, which has caused global warming and other related changes to the climate system. As a result there is now major scientific interest and public concern (Steffen et al. 2018; Lenton et al. 2019; Ritchie et al. 2021) that future temperature increases may also cause key Earth system components (so called 'Tipping Elements') to cross critical thresholds known as 'Tipping Points', undergoing rapid irreversible transitions (Lenton et al. 2008).

Tipping points are typically triggered by a small change in a system parameter, such as one describing the forcing or relating to aspects of the internal structure. Crossing some critical threshold associated with this parameter causes the system to be pushed into a qualitatively different state. Mathematically this can be described as a system passing through a bifurcation. Although different types of tipping exist (Ashwin et al. 2012), the analysis here will be concerned with so-called 'Bifurcation-' or 'B-tipping'.

Pioneering work by Stommel suggested that the Atlantic Meridional Overturning Circulation (AMOC) (Stommel 1961) is such a tipping element, although his work predates widespread use of the term. Since then, numerous examples of potential tipping elements have been identified. For example, the Amazon Rainforest can undergo dieback (Cox et al. 2000), the Greenland ice-sheet can melt (Feldmann and Levermann 2015) and permafrost can thaw rapidly (Steffen et al. 2018).

Sophisticated climate model simulations (Rahmstorf 1995) provide evidence that tipping points can occur in the Earth system. For example, multiple instances of abrupt shifts were identified in the Coupled Model Intercomparison Project Phase 5 (CMIP5) (Taylor, Stouffer and Meehl 2012) collection of Earth System Models (ESMs) (Drijfhout et al. 2015) and hysteresis has been found in simulations of the Antarctic Ice Sheet (Garbe et al. 2020).

It is unsurprising that major transitions in important components of the Earth system would have significant impacts. As tipping points are not routinely included in Integrated Assessment Models (IAMs) many of their impacts on society are not yet quantified, yet recent work (Dietz et al. 2021) suggests including tipping points in IAMs substantially increases the Social Cost of Carbon. Impact studies of individual Tipping Points reveal significant challenges for many people. For instance, a collapse of the AMOC is projected to cause widespread cessation of arable farming in Great Britain (Ritchie et al. 2020). High latitude communities face increased fire risks caused by the self-heating of soils (Clarke et al. 2021) and infrastructure damage caused by a rapid increase in permafrost degradation (Teufel and Sushama 2019).

Given the potential for major impacts, it would be useful to know the exact thresholds of these tipping points, however precision remains elusive (Steffen et al. 2018). There is almost no inter-ESM agreement on which tipping points are the most likely to happen, or on the levels of global warming that will trigger their occurrence (Drijfhout et al. 2015). However due to the mathematical theory of Normal Forms (Guckenheimer and Holmes 1983; Strogatz 2015), all

systems approaching a B-tipping point share some common features.

For purposes of this study, the most important of these generic characteristics is *critical slowing down*. Systems generally revert to equilibrium after a small disturbance. The time to return to equilibrium is a characteristic timescale which, importantly, increases as the system approaches a tipping point, at which moment the timescale becomes infinite (Scheffer et al. 2012)—referred to as 'critical slowing down'. For near-equilibrium systems, the variance of a system will increase and its autocorrelation (AC) will tend to unity as the system approaches a bifurcation (Held and Kleinen 2004; Scheffer et al. 2009). These statistical changes lead to the possibility of 'Early Warning Signals' of approaching Tipping Points.

Care is needed when using early warning signals, as both AC and variance are expected to increase as a tipping point is approached (Ditlevsen and Johnsen 2010). Whilst this is only strictly true in the case of near one dimensional systems (an approximation which is often made, such as by using principle component analysis to reduce the dimensionality of the system (Held and Kleinen 2004)), considering one quantity alone increases the chance of a false positive as that quantity may change for other reasons such as an increase in the noise variability. It should be noted that false positives can still occur even when considering both quantities. Additionally, if a transition is noise-induced (rather than bifurcation-induced) then critical speeding up is possible, where a decrease in the variance and AC can be signs of an approaching transition (Titus and Watson 2020).

The technique of observing an increase in the variance and AC has been applied to the paleoclimate record, where it has been shown to give early warnings of tipping points (Boers 2018). It has also been used to suggest that for the present day, due to an increase in global temperatures, there are approaching tipping points in the Greenland Ice Sheet (Boers and Rypdal 2021) and in the AMOC (Boers 2021). However, a key assumption when using the variance and AC as early warning signals is that the system is subject to a statistically stationary white-noise forcing. Unfortunately, for many components of the Earth system, the external drivers do not have variability that exhibits white noise characteristics, and so this assumption is not satisfied. For example, forcing factors in the Earth system are rarely well approximated by stationary white-noise, due to the many quasi-oscillatory modes of variability in the Earth system (Heydt et al. 2021), which add peaks to the power spectrum of the forcing. For example, the Amazon Rainforest, which is of particular interest due to its risk of large-scale vegetation dieback in a potentially hotter and drier climate, experiences forcing which is coherent in space and in time, but is also strongly modulated by the El-Niño Southern Oscillation (ENSO) (Jiménez-Muñoz et al. 2016). White noise forcing is also incompatible with long memory processes (Hurst 1957), such as the effect of sea ice changes on the AMOC (Kuehn, Lux and Neamţu 2022). Recently, it was shown (Kuehn, Lux and Neamţu 2022) that traditional early warning signals can change their characteristics or disappear entirely when these assumptions on the forcing are relaxed. This motivates creating early warning signals that do not assume white noise.

There has been some investigations in using early warning signals with time correlated noise

using generalised least squares (Boers 2021; Boettner and Boers 2022) and a Bayesian method (Heßler and Kamps 2022a,b). Here I examine a different method of estimating the critical slowing down that occurs near a bifurcation that works even in the presence of time-correlated noise is examined.

7.2 Failure of Early Warning Signals

In this section, it will be demonstrated how conventional early warning signals may fail in the presence of autocorrelated noise. Due to the fact that near a saddle node bifurcation all dynamical systems with such a bifurcation behave similarly (Guckenheimer and Holmes 1983), this motivates investigating the simplest bistable system exhibiting a saddle node bifurcation. Hence, the system to be examined is:

$$\varepsilon \frac{\mathrm{d}x}{\mathrm{d}t} = x - \frac{1}{3}x^3 - \mu(t) + \eta(t), \tag{7.1}$$

where ε defines the timescale of the system, μ is a control parameter and η provides the noise. Note that there is a noisy saddle node bifurcation when $\mu = 2/3$, corresponding to a tipping point where x transitions from a positive to a negative state. To ensure x remains in approximate equilibrium, ε is set to be small, take $\varepsilon = 0.01$ throughout.

η is defined by the following Ornstein-Uhlenbeck process (Uhlenbeck and Ornstein 1930):

$$\frac{\mathrm{d}\eta}{\mathrm{d}t} = \frac{r-1}{\delta t}\eta + \sqrt{\frac{1-r^2}{\delta t}}\xi \tag{7.2}$$

where ξ is the derivative of a standard Wiener process. This choice is more transparent when looked at in discrete form, with timestep δt:

$$\eta_{t+1} = r\eta_t + \sqrt{1-r^2}\varepsilon_t \tag{7.3}$$

with $\varepsilon_t \sim \mathcal{N}(0,1)$. When $r = 0$, this is the conventional white noise assumed in most early warning signals studies. However, as r approaches unity the process becomes more and more autocorrelated.

After discretizing with time step $\delta t = 0.0004$, these equations are solved numerically using the Euler-Maruyama method (Jacobs 2010).

7.2.1 False Negatives

As a system approaches a tipping point, the conventional early warning signals suggest that the system should become more autocorrelated. However, if the system is subjected to autocorrelated noise, then this can act to mask the changes in the AC of the system so that such changes are no longer detectable. Furthermore, decreasing variability in the forcing can decrease the

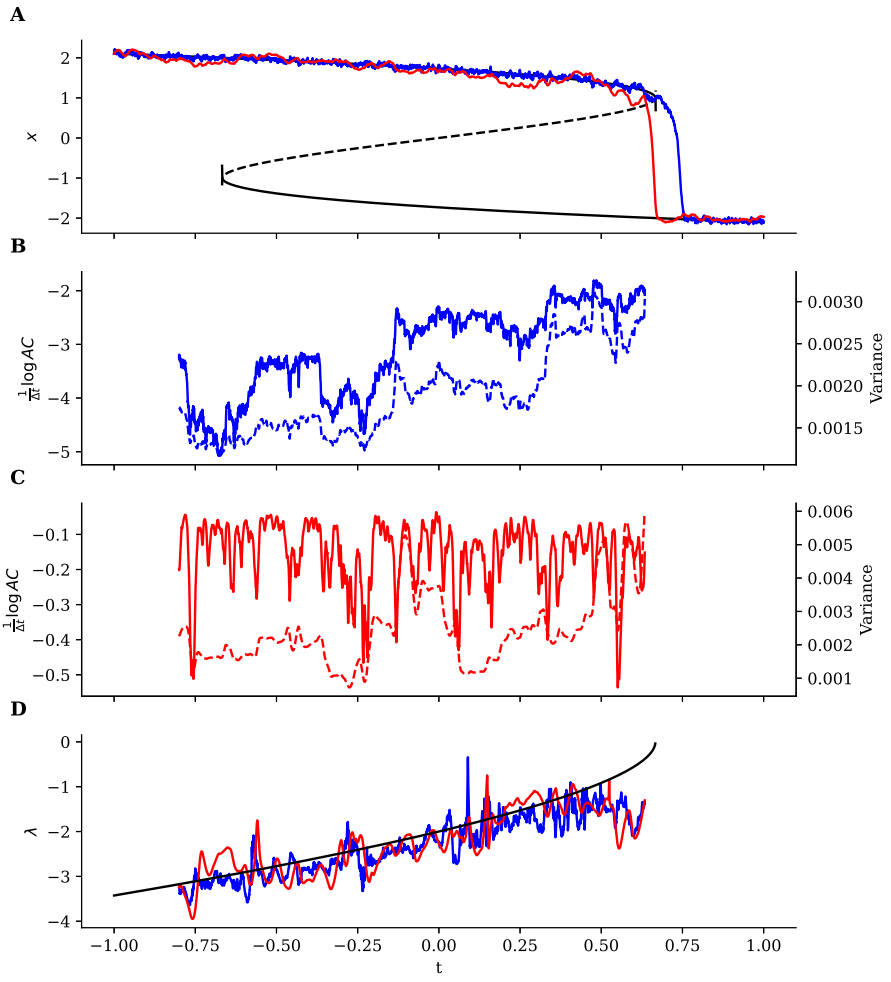

Figure 7.1: Panel A shows two time series of system (equations (7.1) and (7.3)), with $\mu(t) = t$ passing through a saddle node bifurcation at time $t = 2/3$. In the case of the blue curve the system is subject to white noise forcing ($r = 0$), the red curve is subject to red noise forcing ($r = 0.99$). Panels B and C show the classic early warning signals for the case of white and red noise, calculated after a quadratic detrend in a window of width 0.2 (in normalised time units or 500 data points). The AC is plotted with a solid curve and the variance with a dashed curve. The white noise case shows clear early warning signals, but the red noise case gives no indication of the approaching tipping point. Panel D shows λ calculated from ROSA, after a quadratic detrend in windows of length 0.2, in the white (blue curve) and red (red curve) noise case. The solid black line is the true value of λ. In both instances there is a clear Early Warning Signal.

system variance even if the system is approaching a tipping point. This again acts to mask the approaching tipping point, which clearly poses problems for conventional early warning signals as these would present a 'false negative'.

To illustrate this, set $\mu(t) = t$, so that the system described by equation (7.1) has a tipping point at $t = 2/3$ and calculate the conventional Early Warning Signals after detrending with a second order polynomial, plotted in figure 7.1. Panel A of figure 7.1 shows two time series of the state variable of equation (7.1) approaching a tipping point. The series are similar, except that one of them (blue) is subject to white noise ($r = 0$), while the other (red) curve is driven by red noise ($r = 0.99$). To ensure the tipping occurs at a similar time in both cases, the magnitude of the red noise is reduced by half. Despite the qualitative similarity of the time series, the classical early warning signals plotted in Panels B and C, are very different. To assist with comparisons to the method of this chapter, I plot $\frac{1}{\partial t} \log AC$ instead of the AC directly. However, this transformation will have no effect on any trends.

The variance and AC show a clear rise in the white noise case, giving a clear Early Warning Signal. Whereas, for the red noise case there is no trend in the AC. The variance shows both increases and decreases. A positive trend occurs near the tipping point however this would give, if any, very little warning. Figure 7.2 repeats this test for 1000 different noise realisations, showing the challenge of getting early warning signals when the noise is very autocorrelated.

The results of an investigation into subsampling the timeseries plotted in figure 7.1 are plotted in figure 7.3. Subsampling the timeseries will act to reduce the autocorrelation of the timeseries, which may make early warning signals stronger. However, figure 7.1 shows that subsampling does not give better early warning signals in this case, which underscores the need to develop better early warning methods.

7.2.2 False Positives

An additional problem with assuming the system is subject to stationary white noise is that it also implies that the variability and AC of the forcing is constant over time. However in the case of climate change, it is likely that the variability of the forcing, such as temperature, will change (Huntingford et al. 2013). Increasing the variability, such as in Boers 2021, of the forcing will increase the variance of the system even if the system is not approaching a tipping point. This is an example of a false alarm (i.e. a false positive).

An example of this phenomenon is plotted in figure 7.4. Equation (7.1) has been integrated with $\mu = -1$, hence there is no tipping point. The stochastic forcing η, described by equation (7.2), has its r value linearly increasing from $r = 0.2$ at $t = -1$ to $r = 0.7$ at $t = 1$. The state variable is plotted in Panel A. Although there is no tipping point crossed in the system of interest (equation (7.1)), because the forcing is becoming increasingly autocorrelated, the classical early warning indicators (Panel B) falsely suggest a tipping point is approaching.

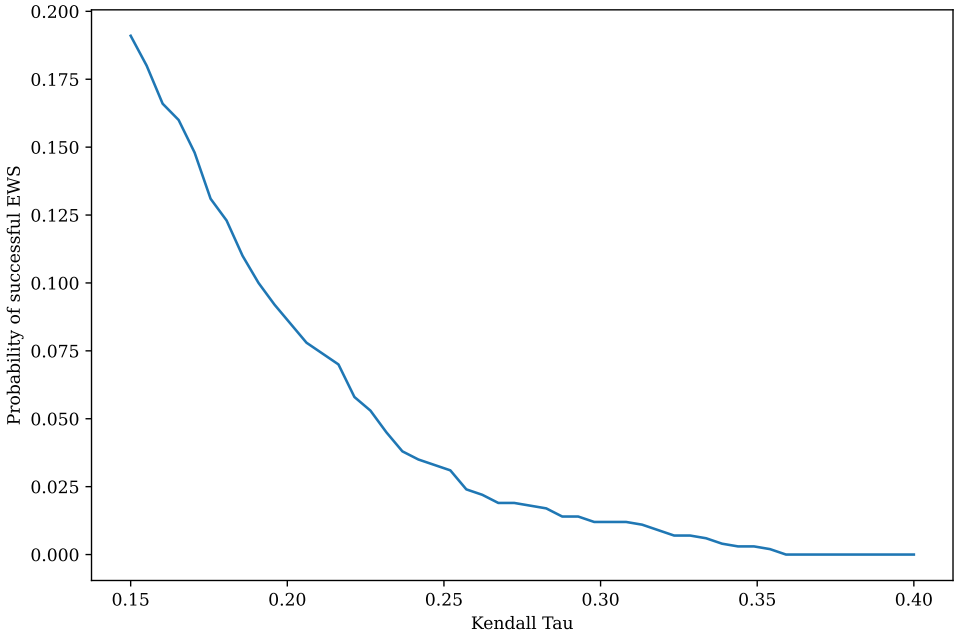

Figure 7.2: This figure shows the results of repeating the red noise experiment illustrated in figure 7.1 1000 times. The conventional early warning indicators are calculated, namely the variance and autocorrelation, up until the tipping time. The increase in these early warning indicators is quantified by Kendall's τ statistic. A successful early warning occurs if the measured τ is greater than or equal to a given threshold. The figure shows the fraction of tipping points that will be identified as a function of that τ threshold. This shows that only at low τ thresholds (i.e. weak enough trends) are there any appreciable chance of successfully detecting the tipping point.

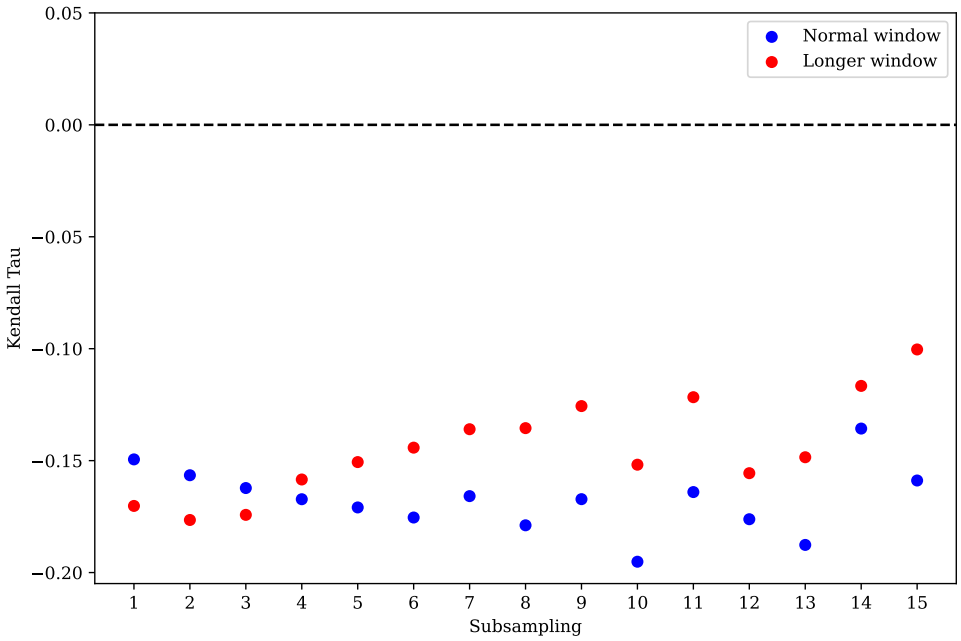

Figure 7.3: By subsampling a time series its level of autocorrelation is reduced. This figure subsamples the time series in figure 7.1 to investigate the effect on the trends in autocorrelation. The value, n of subsampling along the x axis refers to taking every nth timestep. As subsampling reduces the number of point in the window, this was also repeated for a longer window, set at double the length of the original window. Overall, it can be seen that this makes little difference to the trend in the autocorrelation.

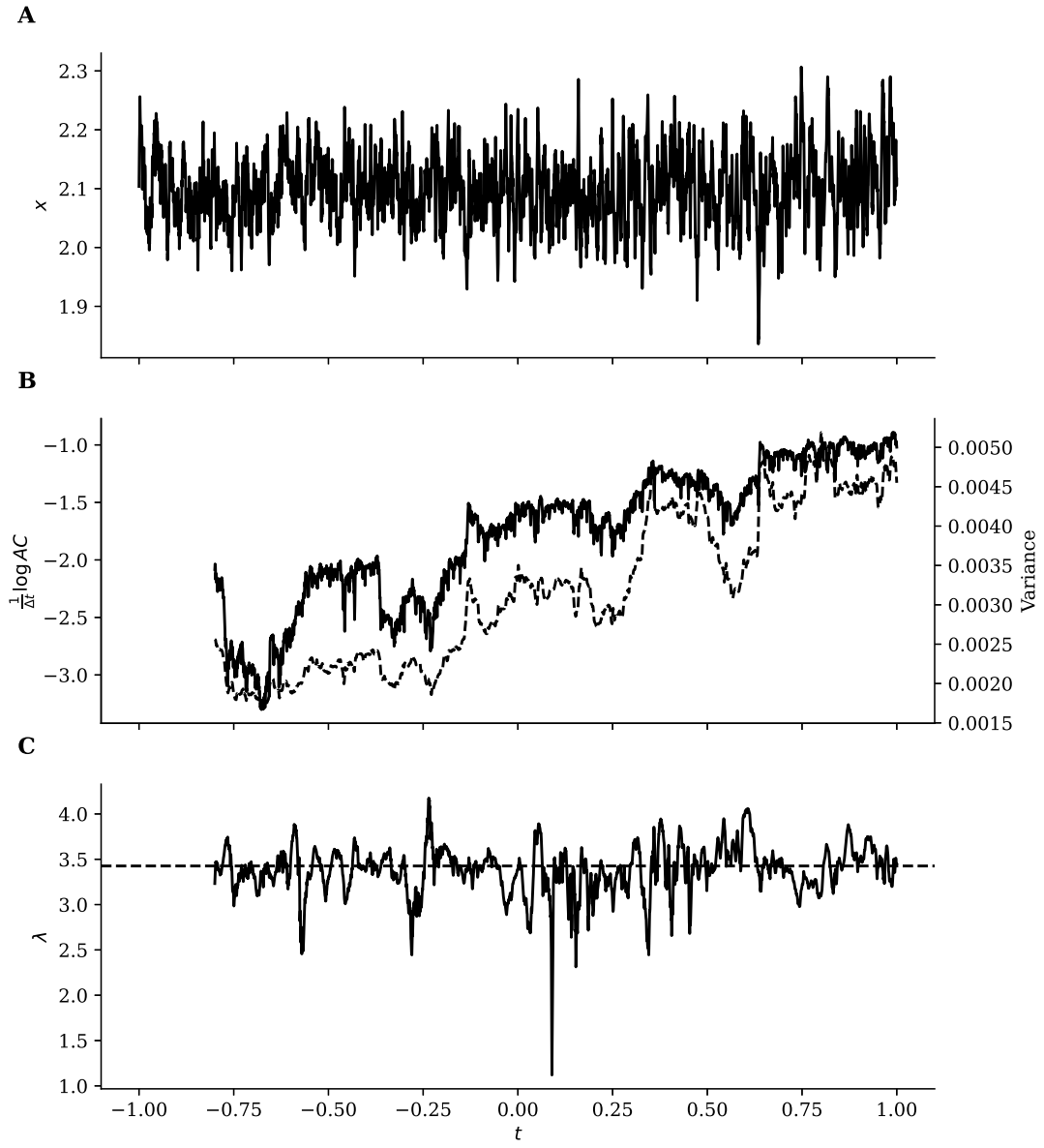

Figure 7.4: Panel A shows a time series obtained by integrating equation (7.1) with $\mu = -1$ when subject to noise described by equation (7.2) where the value of r linearly increases from $r = 0.2$ to $r = 0.7$. Panel B shows the classic Early Warning indicators: AC in the solid line and variance in the dashed line. They falsely indicate a tipping point is approaching. In panel C λ obtained from ROSA is plotted, with the true value plotted in the dashed line. It shows no overall trend hence correctly avoiding the false positive.

7.3 Theory

These issues motivate creating a generic early warning signal, for B-tipping, that is independent of the form of external forcing. Conceptually, the method is to 'divide out the' the noise process. While it is not clear how to do this directly from the time series, it will be shown that this can be achieved by moving to the frequency domain, where it is has been shown to be possible to extract estimates of distances to bifurcation points (Kleinen, Held and Petschel-Held 2003), by taking a Fourier Transform of the data. Under white noise forcing, it is found that the spectrum reddens (Dakos et al. 2012; Kéfi et al. 2014), this study looks at the case where the forcing can mask this reddening.

Begin by modelling a tipping element with a state variable y that evolves in time t, and depends on a slowly evolving parameter μ. The tipping point occurs when $\mu = \mu_c$. This can be written generically as:

$$\frac{\mathrm{d}y}{\mathrm{d}t} = f(y, \mu), \tag{7.4}$$

$$\frac{\mathrm{d}\mu}{\mathrm{d}t} = \varepsilon g(y, \mu). \tag{7.5}$$

for some functions f and g, and $\varepsilon \ll 1$. As $\varepsilon g(y, \mu)$ is small, the theory of fast-slow systems (Kuehn 2011) can be used to reduce to a one dimensional dynamical system depending only on the parameter μ:

$$\frac{\mathrm{d}y}{\mathrm{d}t} = f(y, \mu). \tag{7.6}$$

At this point, an additional time-dependent perturbation $\xi(t)$ is applied, which can have a stochastic component. The system is now:

$$\frac{\mathrm{d}y}{\mathrm{d}t} = f(y, \mu) + \xi(t). \tag{7.7}$$

The classical theory of early warning signals assumes ξ is a white noise process, however no such restriction is made here. It may have both deterministic and stochastic components, it is only required that its Fourier Transform exists.

Linearising about a quasi-equilibrium, x^*, (i.e. that is evolving on the slower timescale), and denoting $y(t) = x^* + x(t)$ to give:

$$\frac{\mathrm{d}x}{\mathrm{d}t} \approx -\lambda x + \xi(t), \tag{7.8}$$

where $\lambda = -f'(x^*, \mu)$ and the prime denotes a derivative with respect to x. Physically, λ represents the rate at which the system returns to equilibrium after a disturbance, and thus characterises the resilience of a system. Held and Kleinen (Held and Kleinen 2004) developed a technique to estimate λ under the assumption that ξ is Gaussian white noise. Here, that

assumption will be relaxed. When $\mu \to \mu_c$, which is to say that the system approaches the tipping point, then it turns out that $\lambda \to 0$ (Guckenheimer and Holmes 1983). This is the phenomenon of critical slowing down. The aim is to therefore identify changes in λ, and in particular discover any evidence of a decrease which would suggest an approaching tipping point, and to do this in a way that is not dependent on ξ being white noise. This can be achieved by moving to the frequency domain.

Denoting the Fourier transform of a function with a tilde, so that when taking the Fourier transform of equation (7.8) it becomes:

$$i\omega\tilde{x}(\omega) = -\lambda\tilde{x}(\omega) + \tilde{\xi}(\omega). \tag{7.9}$$

This can be rearranged equation (7.9), and have its squared modulus taken to get:

$$|\tilde{x}(\omega)|^2 = \frac{|\tilde{\xi}(\omega)|^2}{\omega^2 + \lambda^2}. \tag{7.10}$$

The ratio of spectra (ROSA) can now be defined as: $R(\omega) = |\tilde{x}/\tilde{\xi}|^2$ so that

$$R(\omega) = \frac{1}{\omega^2 + \lambda^2}. \tag{7.11}$$

Note that by construction R takes on a universal form for any forcing process, hence estimates of λ, and thus of the distance to the tipping point, can be made from R regardless of whether the noise is time correlated or not. It also suggests an Early Warning Signal method.

The method is as follows. Take a moving window of length τ_w, smaller than the slow timescale $1/\varepsilon$, but of sufficient length that the power spectrum of x can be calculated, i.e. $|\tilde{x}(\omega)|^2$, and also of ξ, i.e. $|\tilde{\xi}(\omega)|^2$. With the knowledge of these power spectra, a least-squares fit of equation (7.11) can be performed to obtain an estimate for $|\lambda|$. Then consider how $|\lambda|$ varies over longer timescales, i.e. of size $1/\varepsilon$, to see if its value changes. If the estimate for $|\lambda|$ is decreasing towards zero in time this implies that a tipping point is approaching.

7.3.1 Choosing ξ

Unlike most early warning signals, the ROSA method requires knowledge of the driving process that controls the variability of the system. Therefore, using this method requires an understanding of the system. Furthermore the system must be of sufficient temporal resolution such that both x and ξ can be measured. If ξ is not chosen correctly then changes to the calculated λ could be driven by changes to the incorrectly chosen ξ, rather than a tipping point.

It is possible that there is no obvious 'correct' choice as in reality many different quantities may contribute to the forcing, and the output of the system itself may itself influence these quantities.

I argue that these requirements are not too restrictive, at least in the case of early warning signals for transitions caused by contemporary climate change. Many different Earth system quantities are regularly measured and many processes are understood. Furthermore to help guard against choosing the wrong ξ it could first be tested in an Earth System Model (ESM). Note however that ESMs represent tipping elements poorly, with little agreement between models (Drijfhout et al. 2015).

7.4 Test in Simple Models

This ROSA method is examined using the two test cases considered earlier in section section 7.2; namely its ability to avoid false positives and false negatives. The power spectra of x and η is calculated using Welch's method (Welch 1967) after a quadratic detrend in moving windows of length 0.2. A least squares fit to equation (7.11) was performed and λ extracted. The results are plotted in panels D and C of figures 7.1 and 7.4 respectively.

7.4.1 Avoiding False Negatives

In figure 7.1 there is a plot of the case where the system is approaching a tipping point subject to white or red noise. Panel D provides the value of λ estimated from ROSA and shows a clear rise towards zero in both the white and red noise case indicating a successful warning, in contrast to the classical indicators. Furthermore, both the white and red noise estimates lie close to the true value of λ, plotted in the black curve.

7.4.2 Avoiding False Positives

In figure 7.4 the case where the system is not approaching a tipping point is examined, but due to a reddening of the noise process the classic Early Warning Indicators give a false positive. In Panel C there is a plot of λ obtained from ROSA, which stays constant and close to the true value (plotted in the dashed line). ROSA therefore avoids a false positive in this case.

Figure 7.4 shows ROSA avoiding a false positive in one particular case with one particular noise realisation. Figure 7.5 shows the results of repeating this experiment with 1000 different noise realisations. Given a particular Kendall τ threshold, the fraction of realisations that had a τ equal to or greater than that threshold was calculated for each early warning signal. As there was no tipping in this experiment, this fraction represents the probability of a false positive. Figure 7.5 shows that ROSA gives fewer false positives than the variance or autocorrelation do.

7.5 Comparison to alternative methods

Recently, Boers 2021 introduced a new technique, to avoid the problems introduced by noise that isn't white.This was more rigorously analysed by Boettner and Boers 2022. The technique,

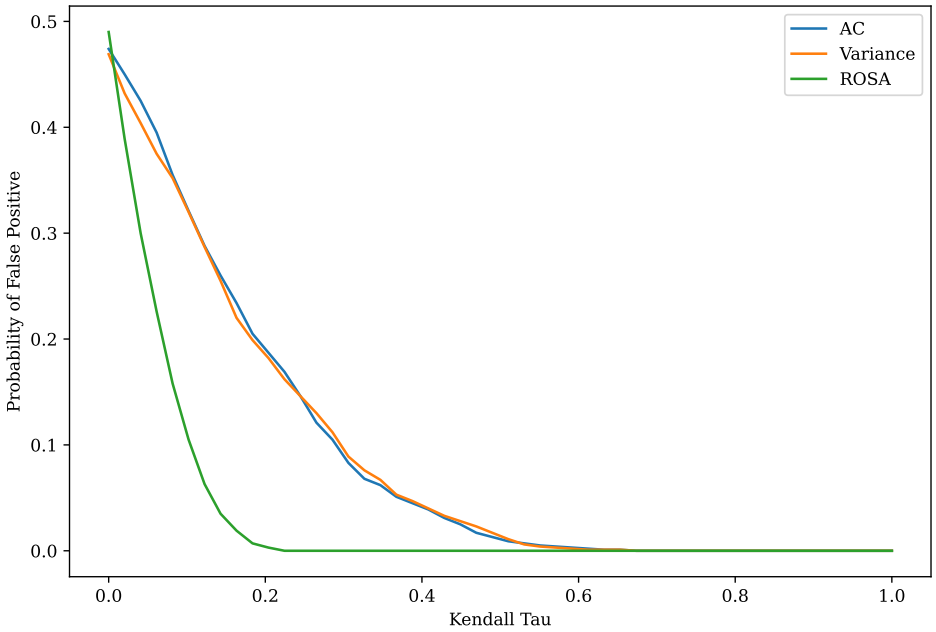

Figure 7.5: The experiment is repeated in figure 7.4 1000 times to calculate the probability of a false detection of a tipping point. A tipping point is 'detected' when Kendall's τ is large enough. A larger τ corresponds to a stronger trend. It can be seen that ROSA is much less likely to falsely detect a tipping point in this case.

which is referred to here as the BB method, is essentially a way of regressing $\dot{x}$ against x, to give an estimate for λ. This requires a model for the noise, for example that it is generated by an Ornstein-Uhlenbeck process. Significantly, the BB method makes a quasi-static assumption about the noise, such that the parameters of the noise model are assumed to be fixed in each window (although can change between windows). On the other hand, ROSA does not have such a restriction because the noise is analysed directly.

The BB method is compared with ROSA for a system defined by equation (7.1). Set $\mu = t$ so that the system reaches a tipping point at $t = 2/3$. Furthermore r is linearly decreased from $r = 0.99$ to $r = 0.0$ between $t = -1$ and $t = 1$. This decreasing AC of the noise can feed through into the system's AC, thus masking the conventional early warning signals. This test therefore combines the challenges of predicting a tipping point with dealing with non-stationary noise.

Both methods give estimates for $-\lambda$, which should rise to zero as the tipping point is approached. To compare the rise a running Kendall τ (Wilks 2019) is computed for all data points up to that time. This quantity, bounded between -1 and 1 gives a measure of whether a sequence is increasing or decreasing. A strongly positive τ suggests a tipping point is approaching, and a strongly negative τ suggests one is not. To give the best early warning τ should become large as long before the tipping point as possible.

This is computed for 10 different noise realisations and the τ values are calculated as a function of time and plotted in figure 7.6. Both indicators show a positive τ near the tipping point. However, ROSA becomes positive substantially earlier than the BB method and there is less variance in the τ values for the ROSA method, as required for a more reliable early warning indicator. This is indicative of an earlier and stronger warning than the BB method.

Nevertheless, the BB method has its advantages. It is flexible and straightforward to modify to different noise models and in many cases gives a good Early Warning Signal ahead of the tipping point. Its principle advantage over ROSA is that an explicit time series of the forcing is not required to use it. As a result, ROSA and BB should be seen as complementary methods: where data is scarce such as in paleoclimate studies, BB is more suitable but for contemporary climate change where the earliness of the warning is important ROSA is more suited.

7.6 Complex Models

The verification of the proposed early warning system with relatively simple conceptual models is important. However, the majority of components of the Earth system are complex, requiring highly detailed numerical models to emulate them. Hence, it is desirable to see if the technique is still successful in the case of a more complex model. The dimensionality of such models can be very high, due to their spatial extent and related heterogeneity, and because the forcing ξ is uncertain and may not be a single dominant forcing, but instead a combination of external fluctuating drivers. These individual components, when combined, make-up 'full-form' Earth System Models (ESMs).

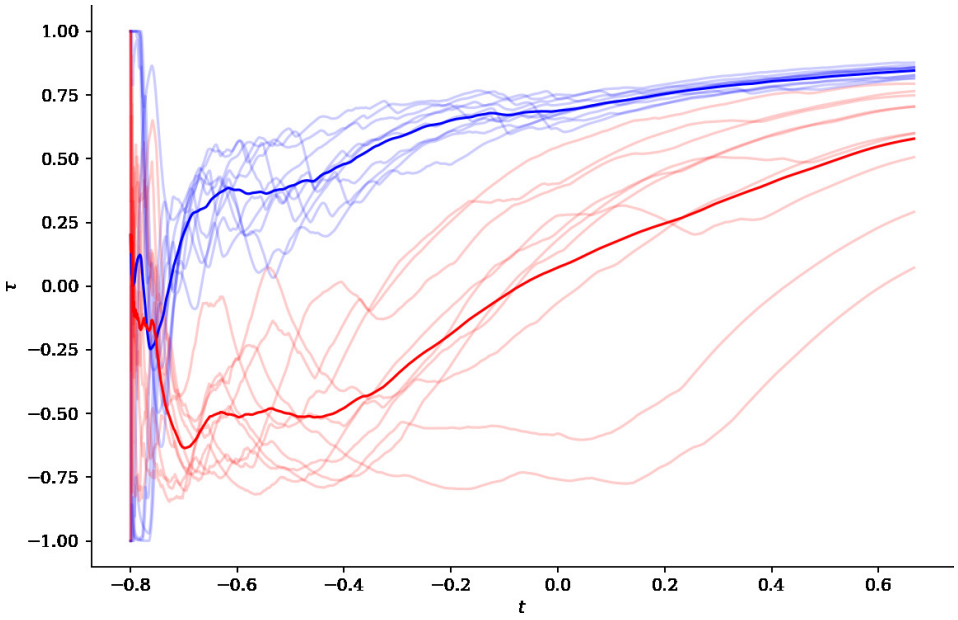

Figure 7.6: A plot of running Kendall τ values as a function of time for the ROSA (blue) and BB (red) methods. Individual realisations are plotted in faint lines and the mean value is plotted in the stronger colour. ROSA gives an earlier and more reliable warning than the BB method.

There are a very large number of ESMs available, and additionally a substantial number of attributes of the Earth system amenable to investigation. Amazon forest dieback is examined here in state-of-the-art ESMs from the Coupled Model Intercomparison Project Phase 6 (CMIP6) (Eyring et al. 2016) database. Recently, five (EC-Earth3-Veg, GFDL-ESM4, NorCPM1, SAMo-UNICON and TaiESM1) of seven models, which possess a Dynamic Global Vegetation Model (DGVM), have been shown to feature abrupt local Amazon dieback shifts (in the IPCC defined North South American region) in an idealised run of increasing CO_2 by 1% per year (Parry, Ritchie and Cox 2022).

The algorithm used in the study (and here) detects an abrupt shift if the following three criteria are satisfied:

1. the abrupt change is fast such that vegetation carbon drops by at least 2 kg C m^{-2} in a 15-year period,
2. the abrupt shift contributes to at least a quarter of the total change in the run, and
3. the mean annual rate of change is more than three times the variability of the rate of changes observed in the unforced control run.

In every grid point identified as containing an abrupt shift, the time series of monthly vegetation carbon had its nonlinear trend and seasonal cycle removed using the seasonal and trend decomposition using LOESS (STL) method (Cleveland et al. 1990). In windows of length 50 years the conventional early warning signals and ROSA were calculated. The 2m air temperature was chosen as the forcing variable, which was detrended similarly to the vegetation carbon.

Although this choice of forcing variable is unlikely to capture all aspects of the forcing, there is a known connection between temperature and Amazon dieback. For example, increases in the temperature seasonal cycle amplitude reveal declines in the evaporative fraction and hence a drying over the Amazon basin (Ritchie et al. 2022). Moreover, high sensitivities of the temperature seasonal cycle to global warming are more likely to incur abrupt forest dieback events (Parry, Ritchie and Cox 2022) in CMIP6. Furthermore there is a link between temperature anomalies and Amazon productivity (Boulton, Good and Lenton 2013). Therefore, the air temperature plays an important role in controlling the resilience of the forest.

Figure 7.7 shows an example of a grid point undergoing an abrupt shift. It also shows λ, calculated by the ROSA method, and the conventional early warning indicators, variance and autocorrelation. The ROSA method shows an increase in λ and thus gives a good early warning of the abrupt shift. There is, however, little change in the autocorrelation and variance, thereby giving no early warning.

Proceeding more systematically, for each of these indicators, the Kendall τ statistic was calculated for the 20 year period prior to the abrupt shift. If that τ is above some threshold, that is counted as a detection. As it is expected that the variance in vegetation carbon to be higher in a high CO_2 world, only increases in variance are taken as a detection if the AC is not decreasing. The results, as a function of threshold value is plotted in figure 7.8.

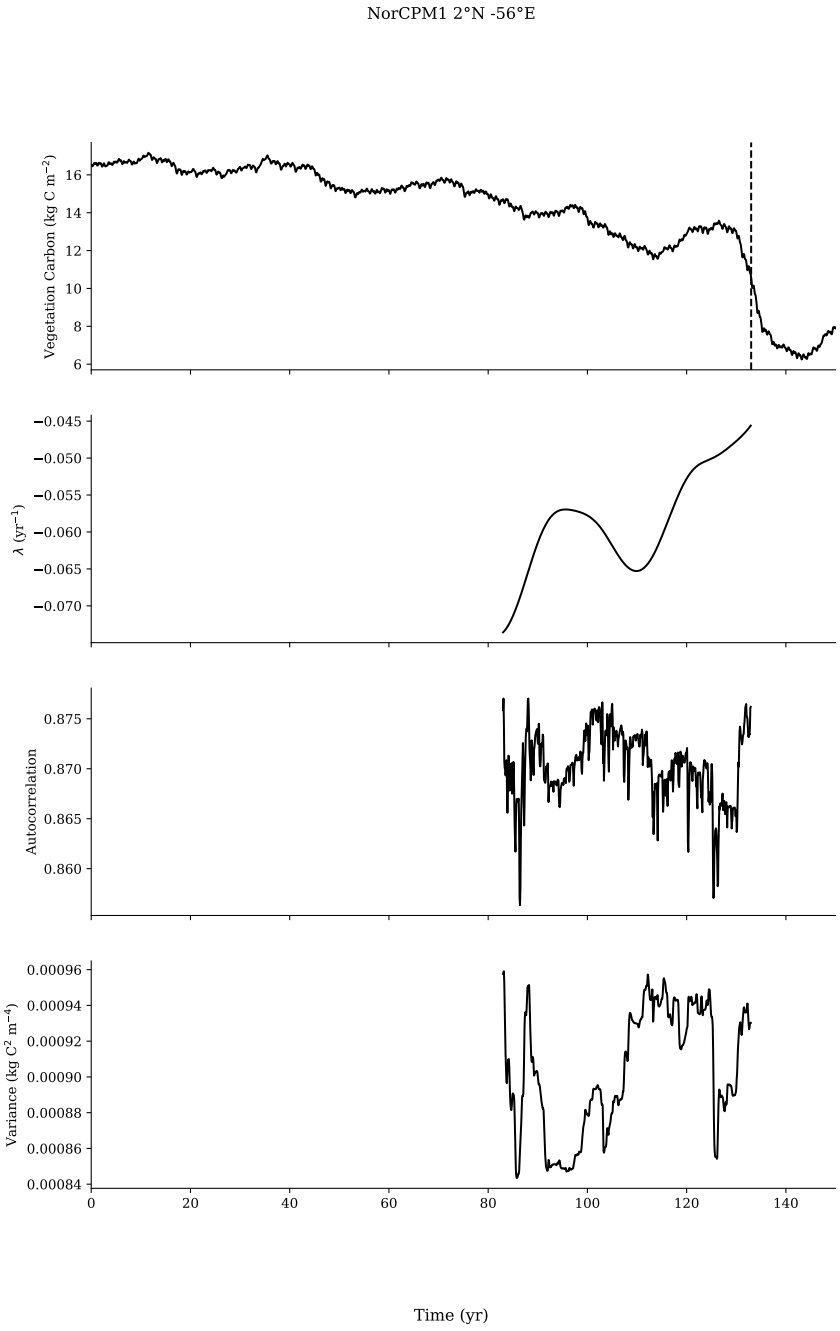

Figure 7.7: An example of an abrupt shift in vegetation carbon happening in a grid cell at 5°N 56°W in the NorCPM1 model. The time of the abrupt shift, calculated by the algorithm detailed in section 7.6 is indicated by a dashed line. Early warning indicators are calculated from 50 years before the early warning signal. Whilst λ, calculated by the ROSA method, shows a clear rise before the abrupt shift, the conventional indicators give little warning.

Note that the algorithm will, in addition to examples of B-tipping, detect examples of N-tipping and rapid change which is not a true tipping point. As a result, no early warning signals will successfully detect all abrupt shifts. This also means that some of the warning signals will be false positives. However this possibility affects all the early warning signals so the comparison remains fair. All three early warning signals are capable of detecting substantial proportions of the identified abrupt shifts. Overall, it can be seen that ROSA outperforms the traditional early warning signals. For individual models, ROSA detects more abrupt shifts than the AC alone and is often better than the variance. Hence, for most of the CMIP6 models considered, ROSA is able to give a more robust early warning for abrupt shifts.

7.7 Discussion and Conclusions

The potential presence of tipping points in the climate system remains of particular concern. Tipping points imply that relatively small changes in forcing could trigger disproportionately large (and possibly irreversible) changes. For these reasons, it is essential to develop statistics that can identify approaching tipping points.

Although there has been much work on early warning signals for Tipping Points, this has tended to focus on the simple case that the system is subject to additive white noise. In this chapter I have shown how early warning signals can be generalised to deal with more general noise characteristics. By normalising by the power spectrum of the forcing, I am able to extract a time-evolving parameter λ, which robustly approaches zero as a tipping point is approached.

Approximating the driving noise as white is reasonable when r is small or when the window length can be chosen to be long relative to the noise's decorrelation time. In these instances, conventional early warning signals will be useful. ROSA is most applicable to the cases where this choice is not possible. This is relevant to anthropogenic climate change given that the changes are fast.

This work relies on a couple of key assumptions:

A. that there is a separation of timescales; and

B. that the power spectrum of the forcing and the system is known.

Item B requires having data for a sufficiently long period of time, which may prove challenging in practise. Item B is notable as other early warning signals, like the BB technique, do not require the forcing to be known. Although item A is typically assumed when dealing with early warning signals, its applicability to the rapidly changing modern climate is still an open question. As a result, future work should investigate early warning signals for systems without this timescale separation. Nevertheless, I believe this approach represents an increase in the flexibility and generality of early warning signals for tipping points in a changing climate.

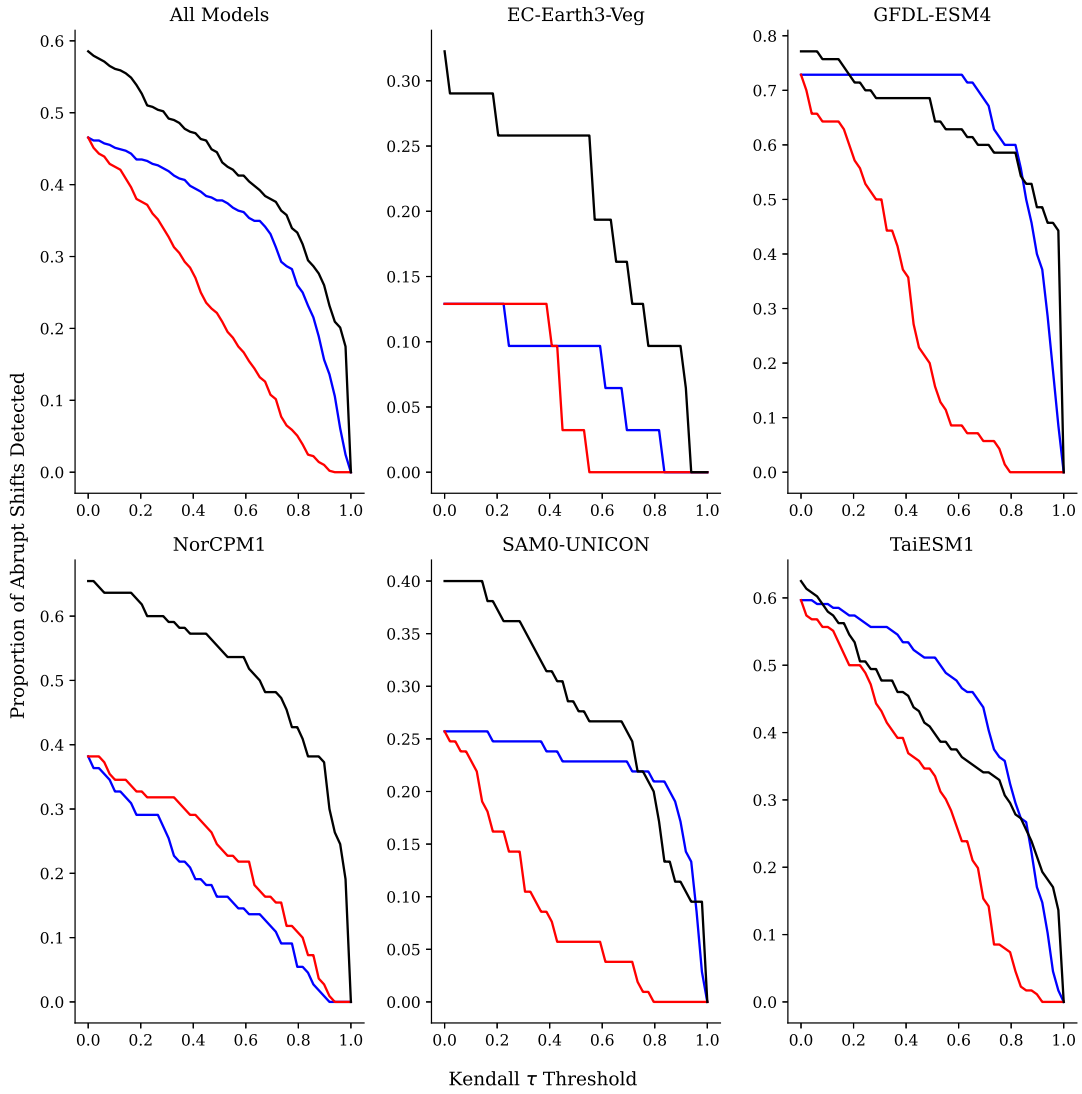

Figure 7.8: The proportion of abrupt shifts in Amazon vegetation carbon detected, as a function of threshold Kendall τ for three early warning signals across 5 ESMs. The blue line is the variance, the red is the AC and the black is ROSA.

Chapter 8

Conclusions

In this thesis I set out to advance understanding of tipping points in the climate-carbon cycle system. Below I summarize the findings of each of the research strands that have been presented in this thesis. I will then discuss potential avenues for further work.

8.1 Research Conclusions

The Compost Bomb Instability in the Continuum Limit

In chapter 3 I investigated the the effect of adding a vertical spatial dimension to a model of the compost bomb instability. The purpose of this was twofold. Firstly, I was interested to see if the instability still existed in a more realistic model. Secondly, I wanted to know if certain wildfires could be caused by biogeochemical heating and in order to do this more realistic physics was desirable.

In order to investigate this, I created a partial differential equation model of soil temperature which included biogeochemical heating. I made the assumption that soil carbon could be viewed as being time invariant, which placed the model into the 'compost bomb limit' of Luke and Cox 2010. This came at the cost of preventing R-tipping so the potential for B-tipping was investigated. Furthermore the effect of a large seasonal cycle in atmospheric temperatures on the soil was investigated.

It was shown that for sufficiently large atmospheric temperatures the model had no steady state. This meant that the soil temperatures had diverged and that a compost bomb had occurred. If, as in the real world, soil carbon was allowed to evolve dynamically then the amount of soil carbon would decrease which would prevent the soil temperatures from diverging; instead they would simply reach a large value.

It was also shown that a sufficiently large seasonal cycle — which could be realised by a summer heat wave — could be enough to trigger a compost bomb. Furthermore, the size of the seasonal cycle was not dissimilar to the seasonal cycles observed in parts of Siberia in

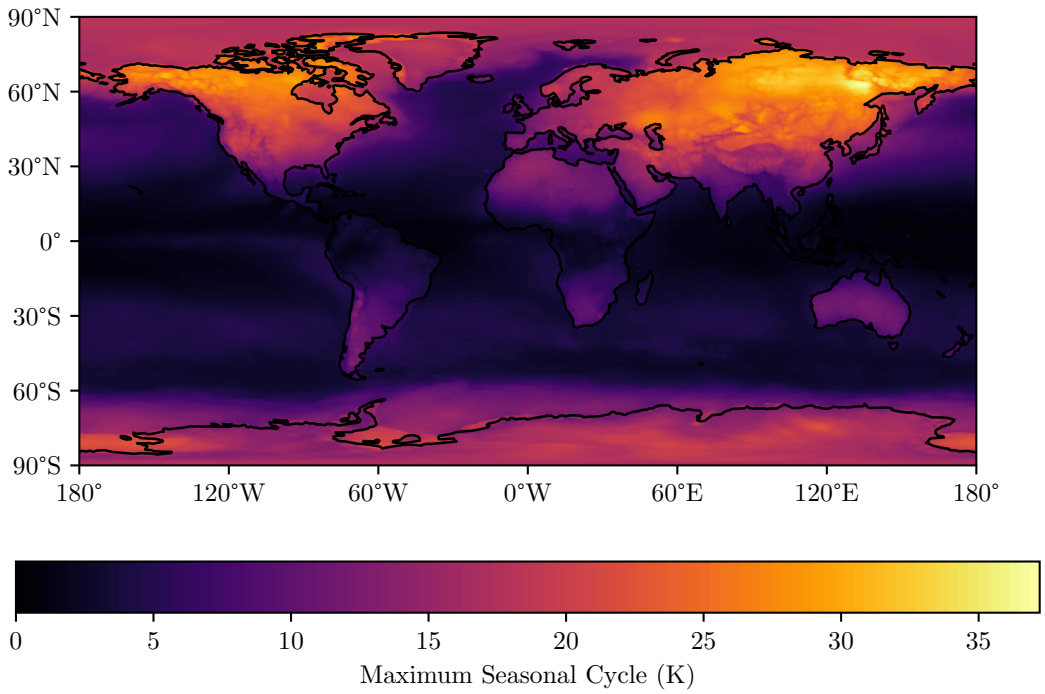

Figure 8.1: The largest observed seasonal cycle in the ERA5 reanalysis (Hersbach et al. 2020) over the period 1940–2022. The magnitude of the seasonal cycle is defined as half the difference between the maximum and minimum monthly averaged 2.0 m air temperatures.

extreme years such as 2010, as shown in figure 8.1. This can be seen as evidence that Siberian wildfires may be caused, in part, by biogeochemical heating.

Due to the approximation that soil carbon was constant in time, the compost bomb instability became an example of B-tipping rather than R-tipping. It does not necessarily follow that the system would experience R-tipping if this approximation was relaxed. However, it is reasonable to assume that the vertical diffusion of heat would not be a barrier to R-tipping, as long as the atmospheric temperatures were raised rapidly compared to the soil carbon timescale, due to the significant timescale separation between the soil thermal and carbon timescales (Luke and Cox 2010).

The approximation that soil carbon is constant is accurate over the timescales of a year, given the multi-decadal turnover time of soil carbon (Varney et al. 2020). It follows therefore, that there can be good confidence in the conclusions drawn about the seasonal cycle. However, the applicability of the results to Siberian wildfires may be more doubtful. This is because it may be better to view a hot summer period as a shorter perturbation to atmospheric temperatures, rather than an amplified sinusoid. This case has since been studied by O'Sullivan, Mulchrone and Wieczorek 2023 for the model of Luke and Cox 2010. They also found for realistic Siberian

summer temperatures compost bombs were possible.

To summarise, in chapter 3 I managed to show that adding in the vertical diffusion of heat does not suppress the compost bomb. This therefore increases the confidence that the effect is real. Furthermore I also showed that a hot summer, as modelled by a large seasonal cycle of temperature, could cause compost bombs, which suggests biogeochemical heating may play a role in Siberian wildfires. A paper based on this chapter has been published as Clarke et al. 2021.

Biogeochemical Heating and the Terrestrial Carbon Cycle

The investigation into the role of biogeochemical heating in the carbon cycle was continued in chapter 4. Instead of looking at the local effect of biogeochemical heating, the effect at the global scale was considered. This was motivated by the fact that the extra carbon released by biogeochemical heating would increase atmospheric temperatures, further increasing respiration and thus biogeochemical heating. This positive feedback therefore increases the chances of a compost bomb occurring, and it is important to quantify.

In order to do this, the model of Luke and Cox 2010 was assumed to hold at the global scale, meaning quantities could be replaced with their globally averaged values. The air temperature was set to scale logarithmically with atmospheric CO_2, which in turn was calculated through carbon conservation. The additional effect of CO_2 fertilisation was considered, by assuming Net Primary Productivity was a saturating function of atmospheric carbon. The role of the ocean was accounted for very simply, by assuming that a fixed fraction of carbon emissions become ocean carbon, which is equivalent to scaling down the flux from the land to the atmosphere by a fixed amount.

First, the stability of this model was investigated. To do this its bifurcation diagram was computed and it was found that there was a bifurcation if the climate sensitivity was large enough or the biogeochemical heating was strong enough. The model was simple enough that the location of the bifurcation point could be computed analytically.

It was found that for realistic amounts of biogeochemical heating, only a small difference to the stability of the system was made. It was however striking, that when there was no CO_2 fertilisation, the system was unstable at comparatively low levels of climate sensitivity. These levels are low enough to be in the range of CMIP models. It is therefore interesting to note that without CO_2 fertilisation the Earth's carbon and thus climate system may not be stable.

This approach to analysing the role of biogeochemical heating has its problems. To begin with, as demonstrated in chapter 3, biogeochemical heating can be important regionally, yet this global modelling approach greatly reduces its influence. For example, for some combination of climate sensitivity and biogeochemical heating it could be the case that a region of the Earth has an unstable carbon cycle whereas the global analysis would give a stable carbon cycle. This is problematic as an instability in one region of the Earth could propagate to give a global instability.

Other modelling assumptions are also suspect. For example, it was assumed that atmo-

spheric temperatures adjust instantaneously to increases in atmospheric CO_2, but in reality this process can take years (Rugenstein et al. 2019). It was also assumed that the ocean could be modelled as absorbing a fixed fraction of carbon, an assumption that is further investigated in chapter 5.

Chapter 4 set out to analyse the effect, at the global scale, of biogeochemical heating. Due to the problems caused by biogeochemical heating being so regionally heterogeneous, firm conclusions cannot be drawn. However, more confidence can be had in the role CO_2 fertilisation and climate-carbon sensitivity play. CO_2 fertilisation acts to destabilise the system with respect to biogeochemical heating, although it still plays a stabilising role overall. The terrestrial carbon system is most unstable at higher values of the climate-carbon sensitivity and lower values of the CO_2 fertilisation strength.

The Stability of Conceptual Models of the Carbon Cycle

In chapter 4, it was noted that the Earth's terrestrial carbon cycle was stable for only some values of the climate-carbon sensitivity and that at low CO_2 fertilisation this critical sensitivity was very low. Chapter 5 took these ideas further to investigate which parameter combinations were compatible with the reconstructed behaviour of atmospheric CO_2 in the the pre-industrial Holocene epoch, which was a time of low CO_2 variability.

In order to constrain the parameters a better ocean model was required than was used in chapter 4. In chapter 5 the ocean carbon cycle from the IMOGEN model was used in addition to simplified box models. Biogeochemical heating was also not accounted for on the grounds that chapter 4 had found the effect weak at the global scale.

Using the IMOGEN ocean carbon cycle model, it was found that there was a critical value of climate sensitivity beyond which the carbon cycle would become unstable. The bifurcation appeared to be a Hopf bifurcation. The oscillations after the bifurcation had a large amplitude and are incompatible with the observed behaviour of the carbon cycle.

Using a two box model, these results could be recreated. Furthermore, it could be confirmed that the bifurcation was a Hopf bifurcation and the bifurcation point could be determined analytically. The two box model could give a Hopf bifurcation at the same point in parameter space as the IMOGEN model.

A one box model was also formulated, which could show a bifurcation of various types depending on the choice of the timescale of the box. For a fast timescale, this was a transcritical bifurcation, similar to the system analysed in chapter 4. Furthermore, because the bifurcation point could be analytically computed, this can be compared to the bifurcation point derived in chapter 4 to give an interpretation to the ocean model in that chapter. It was found that the ocean model in chapter 4 was self-consistent only when the ocean timescale was very short.

If the ocean box timescale was longer, the bifurcation would become a Hopf bifurcation. However the bifurcation point was at a different point in parameter space to that of the bifurcation in IMOGEN.

The critical climate sensitivities found using the IMOGEN model were, for realistic values

of CO_2 fertilisation, around 10 K which could be related to equilibrium climate sensitivities around of 6 K. These values are not substantially larger than those found in a number of CMIP6 (Zelinka et al. 2020). This raises the possibility that when performing coupled climate-carbon simulation some of these models may not be able to simulate a stable pre-industrial period. Furthermore those models which have low enough climate sensitivity to be on the 'correct' side of the bifurcation may still have unrealistic levels of CO_2 variability due to the phenomenon of critical slowing down. As climate models increase the complexity of their carbon cycle representations by including, for example, nutrient limitation, the magnitude of the CO_2 fertilisation effect may decrease (Wiltshire et al. 2021), which would make these models more likely to be unstable.

The analysis in chapter 5 ignored certain effects. It ignored the climate effect on net primary productivity, which is likely to weaken it in the tropics where temperatures exceed the optimum temperatures for photosynthesis and strengthen it in the high latitudes where temperatures are currently below optimum (Sage and Kubien 2007). However, this effect is small relative to the effect of CO_2 fertilisation in most models (Arora et al. 2020). It also made the same assumptions about the instantaneous temperature equilibration to atmospheric CO_2 as was made in chapter 4. Whilst this may effect the behaviour of the carbon cycle beyond the bifurcation point where CO_2 is varying significantly; it is unlikely to effect the position of the bifurcation much as CO_2 levels are constant before the bifurcation and thus the equilibrium assumption is more reasonable.

In summary, chapter 5 showed that certain parameter regimes were not compatible with the behaviour of CO_2 over the Holocene. This behaviour could not be recreated recreated using a one box model, but could be using a two box model. This suggests the importance of two timescales to the bifurcation. Furthermore the critical parameter values identified are close to those in some CMIP6 models suggesting that they would not be able to give a stable pre-industrial control simulation if run in a coupled climate-carbon configuration.

Spatial Early Warning Signals

In the final portion of this thesis I was interested in examining early warning signals for tipping points when the usual assumptions made do not apply. Chapter 6 examined the case where the system is not forced slowly compared to its own timescale. This was of interest because anthropogenic climate change occurs on relatively short timescales compared to the timescales of the Earth system, so there is reason to suspect that early warning signals may be less effective.

The use of spatial early warning signals was investigated. This was motivated by the fact that they give an 'instantaneous' early warning signal and so do not have to be calculated over a non-stationary time series. However, by introducing a spatial dimension into the system, the interaction between different spatial locations need to be considered. This therefore lead to a numerical investigation of the reliability of early warning signals as a function of the rate of forcing and of the strength of the spatial coupling.

To investigate this, a simple system with diffusive coupling was considered which depended

on two parameters: the rate of forcing and the strength of the spatial coupling. This system was identified as a mean field theory of the Ising ferromagnet, which enabled the use of techniques from the theory of phase transitions.

The reliability of both spatial and time series based early warning signals was calculated as a function of the two parameters. It was found that spatial early warning signals were more reliable at larger rates of forcing than time series based early warning signals. However as the spatial coupling strength increased this advantage decreased, until time series based early warning signals became more reliable for very strongly coupled systems. Arguments were given, in terms of the correlation length and the distance from equilibrium in order to explain this dependence.

Although spatial early warning signals are reliable at increased rates of forcing compared to time series based early warning signals, they are still not reliable at rates which exceed the timescale of the system itself. This suggests it may not be applicable to important Earth system tipping elements, such as the ice sheets, which have very slow time scales. Furthermore, the reliability decreases with increasing spatial coupling which could be problematic for some tipping elements which have large-scale coherence. Whilst the coupling considered was the simplest *local* coupling, non-local coupling may be important in the climate system. Non-local couplings could act to increase the correlation length which would decrease the usefulness of spatial early warning signals further.

Overall however, this chapter extends the use of early warning signals to more rapidly forced systems. It also identifies a complementarity; spatial early warning signals are more reliable for rapidly forced systems that are weakly coupled in space but time series based early warning signals are more reliable for slowly forced systems that are strongly coupled in space. Given the vast quantity of remotely sensed spatial data available (Campbell and Wynne 2011) it is hoped that these techniques will be of use to researchers.

Seeking more robust early warning signals for climate tipping points: the Ratio of Spectra method (ROSA)

In chapter 7, I investigated the role of the assumptions made about the noise systems experience and how that affects early warning signals. The typical assumption made is that the noise is white noise — which means it has no temporal correlations. However when a system is forced over short timescales relative to its own time scale, which is of relevance to climate change, temporal correlations become more important. Furthermore, there is no guarantee that these temporal correlations are constant — the stochastic process may not be stationary.

I investigated the effect of temporal correlations in the noise process by comparing early warning signals for a simple system, which could undergo a bifurcation, when subject to white and red noise. It was found that in the presence of red noise the early warning signals were worse than in the case of white noise.

I then showed how, if there was some estimate of the noise, early warning signals could still be obtained for arbitrary noise processes. This could be done by moving to the frequency

domain where the effect of the noise process could be easily removed. I could verify numerically that the early warning signals obtained this way worked well for red and white noise processes. Furthermore, in the case where the noise was not stationary, this method could still give good early warning signals.

I also applied this to the case of local Amazon dieback in CMIP6 models. It was found that the new method could give more early warning signals for abrupt transitions in Amazonia when compared to more conventional early warning signals. The noise process was assumed to be given by the 2 m air temperature; this gives evidence, along with other work (Parry, Ritchie and Cox 2022; Ritchie et al. 2022), of the role air temperature plays in giving early warning signals about Amazon dieback.

The most obvious problem with this method is that it assumes the noise process is known. The correct choice of noise is not in necessarily known for all tipping elements and as such relies on the scientific understanding of the problem. It also requires that the noise has been measured, thus requiring extra data compared to conventional early warning signals. Additionally, it assumes a single noise source, whereas in reality the noise is likely to be a combination of multiple components.

Chapter 7 set out to investigate the role of temporal correlations play in early warning signals. It was able to demonstrate the importance of uncorrelated noise for conventional early warning signals. Furthermore it was able to offer a way to avoid these problems, even in the case where the noise was non-stationary. Whilst in some situations it may not be possible to use the method developed in chapter 7, its usefulness was demonstrated in the case of Amazon dieback where the method did perform well. A paper based on this chapter has been published as Clarke et al. 2023.

8.2 Outlook

One obvious future research direction would be to consider the effect of biogeochemical heating in a complex land surface model, such as JULES. This would enable a more precise quantification of this process, taking into account the effect of spatially heterogeneous soil properties such as soil moisture and changes in conductivity. Conductivity in particular was shown to have a significant control on the magnitude of the effect of biogeochemical heating.

Furthermore, the use of JULES, combined with forcing data sets would enable an investigation into Siberian wildfires. For example, 2020 was a year of unusually widespread Siberian fires (Witze 2020). 'Zombie', or over-winter, fires were identified as a possible cause. This is of interest because fires caused by biogeochemical heating may manifest as zombie fires. Furthermore, using future projections of climate change the changing probability of biogeochemical heating driven fires could be quantified.

It was noted that the investigation in chapter 4 could not capture the regional effects of biogeochemical heating. One way this investigation could be easily extended without resorting

to a complex land surface model is by considering a 'two-region' model of soil carbon:

$$\frac{\mathrm{d}C_1}{\mathrm{d}t} = \Pi_1(C_a) + \Pi_{c1} W\left(-\frac{r_1 C_1}{\Pi_{c1}}\left(\frac{C_a}{C_{a0}}\right)^{\mu_1}\right) \tag{8.1a}$$

$$\frac{\mathrm{d}C_2}{\mathrm{d}t} = \Pi_2(C_a) + \Pi_{c2} W\left(-\frac{r_2 C_2}{\Pi_{c2}}\left(\frac{C_a}{C_{a0}}\right)^{\mu_2}\right) \tag{8.1b}$$

$$\tag{8.1c}$$

where C_i are the soil carbon levels in region i, the parameters Π_{ci} quantify the amount of biogeochemical heating and μ_i the climate-carbon sensitivity in that region. By assuming $\Pi_{c1} \ll \Pi_{c2}$ this then models a region where biogeochemical heating is important, such as high latitude peatlands, coupled to a region where biogeochemical heating is less important, which could represent the rest of the globe.

Another use for JULES could be to determine the bifurcation point which separates stable from unstable carbon cycles. To do this, it could be paired with IMOGEN to emulate both the ocean carbon cycle as well as the effect of changes in atmospheric CO_2 on surface temperatures. It seems likely that this JULES-IMOGEN combination would still experience the sort of bifurcation described in chapter 5. This is because JULES has, at each grid square, essentially the same soil carbon dynamics as in chapter 5 and the ocean carbon cycle as simulated by IMOGEN will be same. However, changing the representation of ocean temperatures in IMOGEN may change the position of the bifurcation.

To extend the investigation into spatial early warning signals, more complex spatial coupling forms could be considered. Furthermore, the investigation was done in 1 dimension, it would be interesting to look at the two and three dimensional case as the behaviour of spatial systems near the bifurcation point is known to be strongly dependent on dimension (Stanley 1999). The ROSA method could also be extended by considering the multidimensional case in terms of both state and noise.

As chapter 6 showed, for very rapidly forced systems early warning signals, even when calculated spatially, are not reliable. It would be useful therefore to establish early warning signals for this regime. Indeed, given the possibility for overshooting tipping points (Ritchie et al. 2021), it would be useful to create warning signals that could indicated when a system has passed the tipping point but not yet transitioned to the new state. As this is a nonautonomous regime, few generic properties can be assumed. It may therefore be most useful to investigate system specific early warning signals in this case.

8.3 Summary

The aim of this thesis was to examine instabilities in the climate-carbon system and adapt early warning signals to more climate relevant cases. It extended the realism of models of biogeochemical heating by adding a spatial dimension, demonstrating its potential relevance to some

types of wildfire. Although this biogeochemical feedback was shown to be small at the global level, that analysis revealed that there are constraints on climate-carbon system parameters. In particular, it showed that only certain values climate sensitivity and CO_2 fertilisation strengths are compatible with the behaviour of CO_2 over the Holocene. Furthermore, these values are close to some values found in CMIP6 models, suggesting some of these models are at risk of being unrealistically unstable.

The theory of early warning signals was advanced, extending them to more realistic cases where the behaviour of the forcing matters — either due to its time correlation structure or because it is rapidly changing. In doing so I have drawn connections to the physics of phase transitions, the theory of which constitutes a rich body of research which I hope will provide many insights in the future.

Appendix A

Variational Calculus

Some of results involving the *functional* or *variational* derivative will be summarised in this section. This section largely follows Lancaster and Blundell 2014 and Goldenfeld 2018. The notation adopted here will be the one used by physicists both for reasons of clarity and also to emphasise the non-rigorous presentation.

A.1 Functionals

A function is a map between numbers. For example the function $f : \mathbb{R} \to \mathbb{R}$

$$f(x) = x^2 \tag{A.1}$$

associates the input number 2 to the output number 4.

However *functionals* associate functions to numbers, they are often denoted with square brackets. For example the definite integral

$$I[f] = \int_{-\infty}^{\infty} f(x)\,\mathrm{d}x \tag{A.2}$$

is a functional of f. It associates the function e^{-x^2} to the number $\sqrt{\pi}$.

An important functional is the action of a system

$$S[q] = \int_0^t L(q(t'), \dot{q}(t'), t')\,\mathrm{d}t'. \tag{A.3}$$

where L is known as the Lagrangian.

A.2 Derivatives

The definition of a derivative is well known:

Definition A.2.1 (Derivative of a Function)**.** Let $f\colon \mathbb{R} \to \mathbb{R}$ be a function. Then the derivative of f is

$$\frac{\mathrm{d}f}{\mathrm{d}x} = \lim_{\varepsilon \to 0} \frac{f(x+\varepsilon) - f(x)}{\varepsilon} \tag{A.4}$$

if the limit exists.

More intuitively, the derivative measures how much a function changes when its input changes by a small quantity.

Similarly, it can be interesting to know what happens to a functional when its input is changed by a small quantity. The functional derivative (also known as a variational derivative) can be defined as follows.

Definition A.2.2 (Functional Derivative)**.** Let J be a functional of f which is in turn a function of $x \in \mathbb{R}$. Then the functional derivative is

$$\frac{\delta J[f(x)]}{\delta f(x')} = \lim_{\varepsilon \to 0} \frac{J[f(x) + \varepsilon\delta(x - x')] - J[f(x)]}{\varepsilon} \tag{A.5}$$

if the limit exists. Here, $\delta(x)$ is the Dirac Delta function.

For example, consider the functional derivative of equation (A.2). From definition A.2.2 we have

$$\frac{\delta I}{\delta f(x)} = \lim_{\varepsilon \to 0} \frac{1}{\varepsilon} \left(\int_{-\infty}^{\infty} f(x) + \varepsilon\delta\left(x - x'\right)\, \mathrm{d}x - \int_{-\infty}^{\infty} f(x)\, \mathrm{d}x \right),$$

which can be simplified to give

$$\frac{\delta I}{\delta f(x)} = \lim_{\varepsilon \to 0} \frac{1}{\varepsilon} \int_{-\infty}^{\infty} \varepsilon\delta(x - x')\, \mathrm{d}x = 1.$$

A.3 Useful Results

Two useful results related to the chain rule will now be proven.

Theorem 2. *Let $f, g\colon \mathbb{R} \to \mathbb{R}$ be suitable functions. Then*

$$\frac{\delta}{\delta f(x)} \int_a^b g\left(f\left(y\right)\right)\, \mathrm{d}y = g'\left(f\left(x\right)\right) \tag{A.6}$$

and

$$\frac{\delta}{\delta f(x)} \int_a^b g\left(f'\left(y\right)\right)\, \mathrm{d}y = -\frac{\mathrm{d}}{\mathrm{d}x}\left(\frac{\mathrm{d}g\left(f'\left(x\right)\right)}{\mathrm{d}f'}\right) \tag{A.7}$$

where conventional derivatives have been denoted with primes.

Proof. Define

$$J[f] = \int_a^b g\left(f\left(y\right)\right)\,\mathrm{d}y$$

Beginning with the first claim using definition A.2.2:

$$\begin{aligned}\frac{\partial J}{\partial f(x)} &= \lim_{\varepsilon\to 0}\frac{1}{\varepsilon}\left(\int_a^b g\left(f(y)+\varepsilon\delta\left(y-x\right)\right)\,\mathrm{d}y - \int_a^b g\left(f\left(y\right)\right)\mathrm{d}y\right)\\ &= \lim_{\varepsilon\to 0}\frac{1}{\varepsilon}\left(\int_a^b g\left(f(y)\right)+\varepsilon\delta\left(y-x\right)g'\left(f\left(y\right)\right)\,\mathrm{d}y - \int_a^b g\left(f\left(y\right)\right)\,\mathrm{d}y\right)\end{aligned}$$

where the function g has been Taylor expanded to first order. The second order terms will vanish in the limit and can therefore be ignored. Taking the limit gives

$$\begin{aligned}\frac{\delta}{\delta f(x)}\int_a^b g\left(f\left(y\right)\right)\,\mathrm{d}y &= \int_a^b \delta(y-x)g'(f(y))\,\mathrm{d}y\\ &= g'(f(x)).\end{aligned}$$

Defining

$$J[f] = \int_a^b g\left(f'\left(y\right)\right)\,\mathrm{d}y,$$

the proof of equation (A.7) proceed similarly for the second claim:

$$\begin{aligned}\frac{\delta J}{\delta f(x)} &= \lim_{\varepsilon\to 0}\frac{1}{\varepsilon}\left(\int_a^b g\left(\frac{\partial}{\partial y}\left(f(y)+\varepsilon\delta(y-x)\right)\right)\,\mathrm{d}y - \int_a^b g\left(f'\left(y\right)\right)\mathrm{d}y\right)\\ &= \lim_{\varepsilon\to 0}\frac{1}{\varepsilon}\left(\int_a^b g(f'(y))+\varepsilon\delta'(y-x)\frac{\mathrm{d}g(f'(y))}{\mathrm{d}f'}\,\mathrm{d}y - \int_a^b g(f'(y))\,\mathrm{d}y\right)\\ &= \int_a^b \delta'(y-x)\frac{\mathrm{d}g(f'(y))}{\mathrm{d}f'}\,\mathrm{d}y\\ &= -\frac{\mathrm{d}}{\mathrm{d}x}\frac{\mathrm{d}g(f'(x))}{\mathrm{d}f'}\end{aligned}$$

after integrating by parts. □

An important special case of theorem 2 is

$$\frac{\partial^2 f}{\partial x^2} = -\frac{\delta}{\delta f(x)}\int_a^b \frac{1}{2}\left(\frac{\partial f}{\partial y}\right)^2\,\mathrm{d}y, \tag{A.8}$$

which explains the sign in equation (6.8).

Appendix B

Correlation Function

Correlation functions play an important role in the analysis of spatially distributed stochastic systems. In this appendix, I will derive the correlation function given by equation (6.37). The correlation function can be derived by taking functional derivatives of a particular functional integral.

The functional integral is given by the partition function of the system described by equation (6.10), where an additional field, B, has been introduced. Symbolically, the partition function is

$$Z = \int \exp\left(-\frac{2}{\sigma^2}\mathcal{H}\right) \mathcal{D}z, \tag{B.1}$$

where

$$\mathcal{H}[z] = \int_0^L \frac{1}{2}\lambda z(x)^2 + \frac{1}{2}D\left(\frac{\partial z}{\partial x}\right)^2 - B(x)z(x)\,\mathrm{d}x\,. \tag{B.2}$$

To attack this integral, the tactic will be to shift to Fourier space, in which the part of the integral that survives differentiation can be factored out. In Fourier space, equation (B.2) becomes

$$\mathcal{H}[\{z_k\}] = \frac{1}{L^2}\sum_{n,m}\left(\frac{1}{2}\left(\lambda - Dnm\right)z_n z_m - B_m z_n\right)\int_0^L e^{i(n+m)x}\,\mathrm{d}x\,. \tag{B.3}$$

The integral over x is non-zero only when $m = -n$, so the sum over m can be eliminated yielding

$$\mathcal{H}[\{z_k\}] = \frac{1}{L}\sum_{n}\left(\frac{1}{2}\left(\lambda + Dn^2\right)z_n z_{-n} - B_{-n}z_n\right). \tag{B.4}$$

Using the fact that $z \in \mathbb{R}$, which means that $z_n = z^*_{-n}$, equation (B.4) can be simplified to

$$\mathcal{H}[\{z_k\}] = \frac{1}{L}\sum_{n}\left(\frac{1}{2}\left(\lambda + Dn^2\right)|z_n|^2 - B_{-n}z_n\right). \tag{B.5}$$

Setting $\phi_k = z_k - \frac{B_k}{Dk^2+\lambda}$ and completing the square means $\mathcal{H}$ is now

$$\mathcal{H}[\{\phi_k\}] = \frac{1}{L}\sum_n \left(\frac{1}{2}\left(\lambda + Dn^2\right)|\phi_n|^2 - \frac{1}{2}\frac{|B_n|^2}{\lambda + Dn^2}\right). \tag{B.6}$$

This can be written as $\mathcal{H}[\{\phi_k\}] = \mathcal{H}_0[\{\phi_k\}] - \frac{1}{2L}\sum_n \frac{|B_n|^2}{\lambda+Dn^2}$, so that equation (B.1) becomes

$$Z = \int \prod_{k>0} \exp\left(-\frac{2}{\sigma^2}\mathcal{H}_0[\{\phi_k\}]\right) \mathrm{d}\phi_k \exp\left(\frac{1}{\sigma^2}\frac{1}{L}\sum_n \frac{|B_n|^2}{\lambda + Dn^2}\right) \tag{B.7}$$

or

$$Z = Z_0 \exp\left(\frac{1}{\sigma^2}\frac{1}{L}\sum_n \frac{|B_n|^2}{\lambda + Dn^2}\right). \tag{B.8}$$

Inverting B_k back into real space gives

$$Z = Z_0 \exp\left(\frac{1}{\sigma^2}\iint B(x_1)g(x_1 - x_2)B(x_2)\,\mathrm{d}x_1\,\mathrm{d}x_2\right). \tag{B.9}$$

where

$$g(x_1 - x_2) = \frac{1}{L}\sum_n \frac{e^{in(x_1-x_2)}}{\lambda + Dn^2}. \tag{B.10}$$

This sum can be evaluated by replacing it with an integral, assuming L is large enough:

$$g(x) = \frac{1}{2\pi}\int_{-\infty}^{\infty} \frac{e^{ikx}}{\lambda + Dk^2}\,\mathrm{d}k = \frac{1}{2}\frac{\xi}{D}e^{-x/\xi}, \tag{B.11}$$

hence using equation (6.33),

$$G(x) = \frac{1}{2}\sigma^2 g(x) = \frac{1}{4}\sigma^2\frac{\xi}{D}e^{-x/\xi}. \tag{B.12}$$

Bibliography

Ainsworth, E. A. and Alistair Rogers (Mar. 2007). "The response of photosynthesis and stomatal conductance to rising [CO2]: mechanisms and environmental interactions". In: *Plant, Cell & Environment* 30.3, pp. 258–270. ISSN: 01407791. DOI: 10.1111/j.1365-3040.2007.01641.x.

Alkhayuon, H., P. Ashwin, L. C. Jackson, C. Quinn and R. A. Wood (May 2019). "Basin bifurcations, oscillatory instability and rate-induced thresholds for Atlantic meridional overturning circulation in a global oceanic box model". In: *Proceedings of the Royal Society A: Mathematical, Physical and Engineering Sciences* 475.2225, p. 20190051. ISSN: 1364-5021. DOI: 10.1098/rspa.2019.0051.

Alkhayuon, H., R. C. Tyson and S. Wieczorek (Oct. 2021). "Phase tipping: how cyclic ecosystems respond to contemporary climate". In: *Proceedings of the Royal Society A: Mathematical, Physical and Engineering Sciences* 477.2254. ISSN: 1364-5021. DOI: 10.1098/rspa.2021.0059. arXiv: 2101.12107.

Alkhayuon, H. M. and P. Ashwin (Mar. 2018). "Rate-induced tipping from periodic attractors: Partial tipping and connecting orbits". In: *Chaos: An Interdisciplinary Journal of Nonlinear Science* 28.3, p. 033608. ISSN: 1054-1500. DOI: 10.1063/1.5000418. arXiv: 1708.04818.

Allee, W. C. and E. S. Bowen (Feb. 1932). "Studies in animal aggregations: Mass protection against colloidal silver among goldfishes". In: *Journal of Experimental Zoology* 61.2, pp. 185–207. ISSN: 0022-104X. DOI: 10.1002/jez.1400610202.

Allen, M. R., D. J. Frame, C. Huntingford, C. D. Jones, J. A. Lowe, M. Meinshausen and N. Meinshausen (Apr. 2009). "Warming caused by cumulative carbon emissions towards the trillionth tonne". In: *Nature* 458.7242, pp. 1163–1166. ISSN: 0028-0836. DOI: 10.1038/nature08019.

Alley, R. B., J. Marotzke, W. D. Nordhaus, J. T. Overpeck, D. M. Peteet, R. A. Pielke, R. T. Pierrehumbert, P. B. Rhines, T. F. Stocker, L. D. Talley and J. M. Wallace (Mar. 2003). "Abrupt Climate Change". In: *Science* 299.5615, pp. 2005–2010. ISSN: 0036-8075. DOI: 10.1126/science.1081056.

Archer, D. (Nov. 2010). *The Global Carbon Cycle*. Vol. 6. August. Princeton University Press, p. 128. ISBN: 9781400837076. DOI: 10.2307/j.ctvcm4hx8.

Arellano-Nava, B., P. R. Halloran, C. A. Boulton, J. Scourse, P. G. Butler, D. J. Reynolds and T. M. Lenton (Aug. 2022). "Destabilisation of the Subpolar North Atlantic prior

to the Little Ice Age". In: *Nature Communications* 13.1, p. 5008. ISSN: 2041-1723. DOI: 10.1038/s41467-022-32653-x.

Armstrong McKay, D. I., A. Staal, J. F. Abrams, R. Winkelmann, B. Sakschewski, S. Loriani, I. Fetzer, S. E. Cornell, J. Rockström and T. M. Lenton (Sept. 2022). "Exceeding 1.5°C global warming could trigger multiple climate tipping points". In: *Science* 377.6611. ISSN: 0036-8075. DOI: 10.1126/science.abn7950.

Arora, V. K., A. Katavouta, R. G. Williams, C. D. Jones, V. Brovkin, P. Friedlingstein, J. Schwinger, L. Bopp, O. Boucher, P. Cadule, M. A. Chamberlain, J. R. Christian, C. Delire, R. A. Fisher, T. Hajima, T. Ilyina, E. Joetzjer, M. Kawamiya, C. D. Koven, J. P. Krasting, R. M. Law, D. M. Lawrence, A. Lenton, K. Lindsay, J. Pongratz, T. Raddatz, R. Séférian, K. Tachiiri, J. F. Tjiputra, A. Wiltshire, T. Wu and T. Ziehn (Aug. 2020). "Carbon–concentration and carbon–climate feedbacks in CMIP6 models and their comparison to CMIP5 models". In: *Biogeosciences* 17.16, pp. 4173–4222. ISSN: 1726-4189. DOI: 10.5194/bg-17-4173-2020.

Ashwin, P. and A. S. von der Heydt (2019). "Extreme Sensitivity and Climate Tipping Points". In: *Journal of Statistical Physics*. ISSN: 15729613. DOI: 10.1007/s10955-019-02425-x. arXiv: 1905.12070.

Ashwin, P., C. Perryman and S. Wieczorek (June 2017). "Parameter shifts for nonautonomous systems in low dimension: bifurcation- and rate-induced tipping". In: *Nonlinearity* 30.6, pp. 2185–2210. ISSN: 0951-7715. DOI: 10.1088/1361-6544/aa675b. arXiv: 1506.07734.

Ashwin, P., S. Wieczorek, R. Vitolo and P. Cox (Mar. 2012). "Tipping points in open systems: bifurcation, noise-induced and rate-dependent examples in the climate system". In: *Philosophical Transactions of the Royal Society A: Mathematical, Physical and Engineering Sciences* 370.1962, pp. 1166–1184. ISSN: 1364-503X. DOI: 10.1098/rsta.2011.0306.

Baker, J. C. A. and D. V. Spracklen (Aug. 2019). "Climate Benefits of Intact Amazon Forests and the Biophysical Consequences of Disturbance". In: *Frontiers in Forests and Global Change* 2.August, pp. 1–13. ISSN: 2624-893X. DOI: 10.3389/ffgc.2019.00047.

Bastiaansen, R., H. A. Dijkstra and A. S. von der Heydt (Apr. 2022). "Fragmented tipping in a spatially heterogeneous world". In: *Environmental Research Letters* 17.4, p. 045006. ISSN: 1748-9326. DOI: 10.1088/1748-9326/ac59a8.

Bastiaansen, R., O. Jaïbi, V. Deblauwe, M. B. Eppinga, K. Siteur, E. Siero, S. Mermoz, A. Bouvet, A. Doelman and M. Rietkerk (Oct. 2018). "Multistability of model and real dryland ecosystems through spatial self-organization". In: *Proceedings of the National Academy of Sciences* 115.44, pp. 11256–11261. ISSN: 0027-8424. DOI: 10.1073/pnas.1804771115.

Batjes, N. (May 2016). "Harmonized soil property values for broad-scale modelling (WISE30sec) with estimates of global soil carbon stocks". In: *Geoderma* 269, pp. 61–68. ISSN: 00167061. DOI: 10.1016/j.geoderma.2016.01.034.

Bauska, T. K., F. Joos, A. C. Mix, R. Roth, J. Ahn and E. J. Brook (May 2015). "Links between atmospheric carbon dioxide, the land carbon reservoir and climate over the past millennium". In: *Nature Geoscience* 8.5, pp. 383–387. ISSN: 1752-0894. DOI: 10.1038/ngeo2422.

Bender, C. M. and S. A. Orszag (1978). *Advanced Mathematical Methods for Scientists and Engineers*. McGraw-Hill, p. 593.

Bereiter, B., S. Eggleston, J. Schmitt, C. Nehrbass-Ahles, T. F. Stocker, H. Fischer, S. Kipfstuhl and J. Chappellaz (2015). "Revision of the EPICA Dome C CO2 record from 800 to 600-kyr before present". In: *Geophysical Research Letters* 42.2, pp. 542–549. ISSN: 19448007. DOI: 10.1002/2014GL061957.

Berglund, N. and B. Gentz (2006). *Noise-Induced Phenomena in Slow-Fast Dynamical Systems*. Vol. 15. Probability and Its Applications 214. London: Springer-Verlag, p. 404. ISBN: 1-84628-038-9. DOI: 10.1007/1-84628-186-5.

Beringer, J., A. H. Lynch, F. S. Chapin, M. Mack and G. B. Bonan (Aug. 2001). "The Representation of Arctic Soils in the Land Surface Model: The Importance of Mosses". In: *Journal of Climate* 14.15, pp. 3324–3335. ISSN: 0894-8755. DOI: 10.1175/1520-0442(2001)014<3324:TROASI>2.0.CO;2.

Best, M. J., M. Pryor, D. B. Clark, G. G. Rooney, R. L. H. Essery, C. B. Ménard, J. M. Edwards, M. A. Hendry, A. Porson, N. Gedney, L. M. Mercado, S. Sitch, E. Blyth, O. Boucher, P. M. Cox, C. S. B. Grimmond and R. J. Harding (Sept. 2011). "The Joint UK Land Environment Simulator (JULES), model description – Part 1: Energy and water fluxes". In: *Geoscientific Model Development* 4.3, pp. 677–699. ISSN: 1991-9603. DOI: 10.5194/gmd-4-677-2011.

Best, M. J., P. M. Cox and D. Warrilow (Jan. 2005). "Determining the optimal soil temperature scheme for atmospheric modelling applications". In: *Boundary-Layer Meteorology* 114.1, pp. 111–142. ISSN: 0006-8314. DOI: 10.1007/s10546-004-5075-3.

Betts, R. A., P. M. Cox, M. Collins, P. P. Harris, C. Huntingford and C. D. Jones (June 2004). "The role of ecosystem-atmosphere interactions in simulated Amazonian precipitation decrease and forest dieback under global climate warming". In: *Theoretical and Applied Climatology* 78.1-3, pp. 157–175. ISSN: 0177-798X. DOI: 10.1007/s00704-004-0050-y.

Bloch-Johnson, J., M. Rugenstein, M. B. Stolpe, T. Rohrschneider, Y. Zheng and J. M. Gregory (Feb. 2021). "Climate Sensitivity Increases Under Higher CO 2 Levels Due to Feedback Temperature Dependence". In: *Geophysical Research Letters* 48.4, pp. 1–12. ISSN: 0094-8276. DOI: 10.1029/2020GL089074.

Boers, N. (July 2018). "Early-warning signals for Dansgaard-Oeschger events in a high-resolution ice core record". In: *Nature Communications* 9.1, p. 2556. ISSN: 2041-1723. DOI: 10.1038/s41467-018-04881-7.

Boers, N. (Aug. 2021). "Observation-based early-warning signals for a collapse of the Atlantic Meridional Overturning Circulation". In: *Nature Climate Change* 11.8, pp. 680–688. ISSN: 1758-678X. DOI: 10.1038/s41558-021-01097-4.

Boers, N., M. Ghil and D.-D. Rousseau (Nov. 2018). "Ocean circulation, ice shelf, and sea ice interactions explain Dansgaard–Oeschger cycles". In: *Proceedings of the National Academy of Sciences* 115.47, E11005–E11014. ISSN: 0027-8424. DOI: 10.1073/pnas.1802573115.

Boers, N., M. Ghil and T. F. Stocker (Sept. 2022). "Theoretical and paleoclimatic evidence for abrupt transitions in the Earth system". In: *Environmental Research Letters* 17.9, p. 093006. ISSN: 1748-9326. DOI: 10.1088/1748-9326/ac8944.

Boers, N., N. Marwan, H. M. J. Barbosa and J. Kurths (Jan. 2017). "A deforestation-induced tipping point for the South American monsoon system". In: *Scientific Reports* 7.1, p. 41489. ISSN: 2045-2322. DOI: 10.1038/srep41489.

Boers, N. and M. Rypdal (2021). "Critical slowing down suggests that the western Greenland Ice Sheet is close to a tipping point". In: *PNAS* 118.21, pp. 1–7. DOI: 10.1073/pnas.2024192118.

Boettner, C. and N. Boers (Mar. 2022). "Critical slowing down in dynamical systems driven by nonstationary correlated noise". In: *Physical Review Research* 4.1, p. 013230. ISSN: 2643-1564. DOI: 10.1103/PhysRevResearch.4.013230.

Bolt, B. van der, E. H. van Nes and M. Scheffer (Mar. 2021). "No warning for slow transitions". In: *Journal of The Royal Society Interface* 18.176, rsif.2020.0935. ISSN: 1742-5662. DOI: 10.1098/rsif.2020.0935.

Boulton, C. A., L. C. Allison and T. M. Lenton (2014). "Early warning signals of atlantic meridional overturning circulation collapse in a fully coupled climate model". In: *Nature Communications* 5.Level 7. ISSN: 20411723. DOI: 10.1038/ncomms6752.

Boulton, C. A., P. Good and T. M. Lenton (Aug. 2013). "Early warning signals of simulated Amazon rainforest dieback". In: *Theoretical Ecology* 6.3, pp. 373–384. ISSN: 18741738. DOI: 10.1007/s12080-013-0191-7.

Boulton, C. A., T. M. Lenton and N. Boers (Mar. 2022). "Pronounced loss of Amazon rainforest resilience since the early 2000s". In: *Nature Climate Change* 12.3, pp. 271–278. ISSN: 1758-678X. DOI: 10.1038/s41558-022-01287-8.

Bozbiyik, A., M. Steinacher, F. Joos, T. F. Stocker and L. Menviel (2011). "Fingerprints of changes in the terrestrial carbon cycle in response to large reorganizations in ocean circulation". In: *Climate of the Past* 7.1, pp. 319–338. ISSN: 18149324. DOI: 10.5194/cp-7-319-2011.

Brienen, R. J. W., O. L. Phillips, T. R. Feldpausch, E. Gloor, T. R. Baker, J. Lloyd, G. Lopez-Gonzalez, A. Monteagudo-Mendoza, Y. Malhi, S. L. Lewis, R. Vásquez Martinez, M. Alexiades, E. Álvarez Dávila, P. Alvarez-Loayza, A. Andrade, L. E. O. C. Aragão, A. Araujo-Murakami, E. J. M. M. Arets, L. Arroyo, G. A. Aymard C., O. S. Bánki, C. Baraloto, J. Barroso, D. Bonal, R. G. A. Boot, J. L. C. Camargo, C. V. Castilho, V. Chama, K. J. Chao, J. Chave, J. A. Comiskey, F. Cornejo Valverde, L. da Costa, E. A. de Oliveira, A. Di Fiore, T. L. Erwin, S. Fauset, M. Forsthofer, D. R. Galbraith, E. S. Grahame, N. Groot, B. Hérault, N. Higuchi, E. N. Honorio Coronado, H. Keeling, T. J. Killeen, W. F. Laurance, S. Laurance, J. Licona, W. E. Magnussen, B. S. Marimon, B. H. Marimon-Junior, C. Mendoza, D. A. Neill, E. M. Nogueira, P. Núñez, N. C. Pallqui Camacho, A. Parada, G. Pardo-Molina, J. Peacock, M. Peña-Claros, G. C. Pickavance, N. C. A. Pitman, L. Poorter, A. Prieto, C. A. Quesada, F. Ramírez, H. Ramírez-Angulo, Z. Restrepo, A. Roopsind, A. Rudas, R. P. Salomão, M. Schwarz, N. Silva, J. E. Silva-Espejo, M. Silveira, J. Stropp, J. Talbot, H. ter Steege, J. Teran-Aguilar, J. Terborgh, R. Thomas-Caesar, M. Toledo, M. Torello-

Raventos, R. K. Umetsu, G. M. F. van der Heijden, P. van der Hout, I. C. Guimarães Vieira, S. A. Vieira, E. Vilanova, V. A. Vos and R. J. Zagt (Mar. 2015). "Long-term decline of the Amazon carbon sink". In: *Nature* 519.7543, pp. 344–348. ISSN: 0028-0836. DOI: 10.1038/nature14283.

Broecker, W. S. (July 1987). "Unpleasant surprises in the greenhouse?" In: *Nature* 328.6126, pp. 123–126. ISSN: 0028-0836. DOI: 10.1038/328123a0.

Brovkin, V., E. Brook, J. W. Williams, S. Bathiany, T. M. Lenton, M. Barton, R. M. DeConto, J. F. Donges, A. Ganopolski, J. McManus, S. Praetorius, A. de Vernal, A. Abe-Ouchi, H. Cheng, M. Claussen, M. Crucifix, G. Gallopín, V. Iglesias, D. S. Kaufman, T. Kleinen, F. Lambert, S. van der Leeuw, H. Liddy, M.-F. Loutre, D. McGee, K. Rehfeld, R. Rhodes, A. W. R. Seddon, M. H. Trauth, L. Vanderveken and Z. Yu (July 2021). "Past abrupt changes, tipping points and cascading impacts in the Earth system". In: *Nature Geoscience*. ISSN: 1752-0894. DOI: 10.1038/s41561-021-00790-5.

Brovkin, V. and M. Claussen (Nov. 2008). "Comment on "Climate-Driven Ecosystem Succession in the Sahara: The Past 6000 Years"". In: *Science* 322.5906, pp. 1326–1326. ISSN: 0036-8075. DOI: 10.1126/science.1163381.

Browne, C. A. (1929). *The spontaneous combustion of hay*. Tech. rep. 141. United States Department of Agriculture, Economic Research Service, pp. 1–39. DOI: 10.22004/ag.econ.157950.

Bryan, F. (Sept. 1986). "High-latitude salinity effects and interhemispheric thermohaline circulations". In: *Nature* 323.6086, pp. 301–304. ISSN: 0028-0836. DOI: 10.1038/323301a0.

Budyko, M. I. (Jan. 1969). "The effect of solar radiation variations on the climate of the Earth". In: *Tellus A: Dynamic Meteorology and Oceanography* 21.5, p. 611. ISSN: 1600-0870. DOI: 10.3402/tellusa.v21i5.10109.

Buizert, C., B. Adrian, J. Ahn, M. Albert, R. B. Alley, D. Baggenstos, T. K. Bauska, R. C. Bay, B. B. Bencivengo, C. R. Bentley, E. J. Brook, N. J. Chellman, G. D. Clow, J. Cole-Dai, H. Conway, E. Cravens, K. M. Cuffey, N. W. Dunbar, J. S. Edwards, J. M. Fegyveresi, D. G. Ferris, J. J. Fitzpatrick, T. J. Fudge, C. J. Gibson, V. Gkinis, J. J. Goetz, S. Gregory, G. M. Hargreaves, N. Iverson, J. A. Johnson, T. R. Jones, M. L. Kalk, M. J. Kippenhan, B. G. Koffman, K. Kreutz, T. W. Kuhl, D. A. Lebar, J. E. Lee, S. A. Marcott, B. R. Markle, O. J. Maselli, J. R. McConnell, K. C. McGwire, L. E. Mitchell, N. B. Mortensen, P. D. Neff, K. Nishiizumi, R. M. Nunn, A. J. Orsi, D. R. Pasteris, J. B. Pedro, E. C. Pettit, P. B. Price, J. C. Priscu, R. H. Rhodes, J. L. Rosen, A. J. Schauer, S. W. Schoenemann, P. J. Sendelbach, J. P. Severinghaus, A. J. Shturmakov, M. Sigl, K. R. Slawny, J. M. Souney, T. A. Sowers, M. K. Spencer, E. J. Steig, K. C. Taylor, M. S. Twickler, B. H. Vaughn, D. E. Voigt, E. D. Waddington, K. C. Welten, A. W. Wendricks, J. W. White, M. Winstrup, G. J. Wong and T. E. Woodruff (Apr. 2015). "Precise interpolar phasing of abrupt climate change during the last ice age". In: *Nature* 520.7549, pp. 661–665. ISSN: 0028-0836. DOI: 10.1038/nature14401.

Burke, E. J., S. E. Chadburn and A. Ekici (Feb. 2017). "A vertical representation of soil carbon in the JULES land surface scheme (vn4.3_permafrost) with a focus on permafrost regions".

In: *Geoscientific Model Development* 10.2, pp. 959–975. ISSN: 1991-9603. DOI: 10.5194/gmd-10-959-2017.

Bury, T. M., R. I. Sujith, I. Pavithran, M. Scheffer, T. M. Lenton, M. Anand and C. T. Bauch (Sept. 2021). "Deep learning for early warning signals of tipping points". In: *Proceedings of the National Academy of Sciences* 118.39. ISSN: 0027-8424. DOI: 10.1073/pnas.2106140118.

Caballero, R. and M. Huber (Aug. 2013). "State-dependent climate sensitivity in past warm climates and its implications for future climate projections". In: *Proceedings of the National Academy of Sciences* 110.35, pp. 14162–14167. ISSN: 0027-8424. DOI: 10.1073/pnas.1303365110.

Caesar, L., G. D. McCarthy, D. J. R. Thornalley, N. Cahill and S. Rahmstorf (Mar. 2021). "Current Atlantic Meridional Overturning Circulation weakest in last millennium". In: *Nature Geoscience* 14.3, pp. 118–120. ISSN: 1752-0894. DOI: 10.1038/s41561-021-00699-z.

Caesar, L., S. Rahmstorf, A. Robinson, G. Feulner and V. Saba (Apr. 2018). "Observed fingerprint of a weakening Atlantic Ocean overturning circulation". In: *Nature* 556.7700, pp. 191–196. ISSN: 0028-0836. DOI: 10.1038/s41586-018-0006-5.

Campbell, J. B. and R. H. Wynne (2011). *Introduction to Remote Sensing, Fifth Edition*. Guilford Publications. ISBN: 9781609181772.

Cardoso, A. W., S. Archibald, W. J. Bond, C. Coetsee, M. Forrest, N. Govender, D. Lehmann, L. Makaga, N. Mpanza, J. E. Ndong, A. F. Koumba Pambo, T. Strydom, D. Tilman, P. D. Wragg and A. C. Staver (June 2022). "Quantifying the environmental limits to fire spread in grassy ecosystems". In: *Proceedings of the National Academy of Sciences* 119.26, pp. 1–7. ISSN: 0027-8424. DOI: 10.1073/pnas.2110364119.

Carpenter, S. R. and W. A. Brock (Nov. 2010). "Early warnings of regime shifts in spatial dynamics using the discrete Fourier transform". In: *Ecosphere* 1.5, art10. ISSN: 2150-8925. DOI: 10.1890/ES10-00016.1.

Charney, J. G. (Apr. 1975). "Dynamics of deserts and drought in the Sahel". In: *Quarterly Journal of the Royal Meteorological Society* 101.428, pp. 193–202. ISSN: 00359009. DOI: 10.1002/qj.49710142802.

Charney, J., A. Arakawa, J. Baker, B. Bolin, R. E. Dickinson, R. M. Goody, C. E. Leith, H. STOMMEL and C. Wunsch (Mar. 1979). *Carbon Dioxide and Climate*. Washington, D.C.: National Academies Press. ISBN: 978-0-309-11910-8. DOI: 10.17226/12181.

Charney, J., P. H. Stone and W. J. Quirk (Feb. 1975). "Drought in the Sahara: A Biogeophysical Feedback Mechanism". In: *Science* 187.4175, pp. 434–435. ISSN: 0036-8075. DOI: 10.1126/science.187.4175.434.

Ciais, P., C. Sabine, G. Bala, L. Bopp, V. Brovkin, J. Canadell, A. Chhabra, R. DeFries, J. Galloway, M. Heimann, C. Jones, C. Le Quéré, R. B. Myneni, S. Piao and P. Thornton (Mar. 2014). "Carbon and Other Biogeochemical Cycles". In: *Climate Change 2013 – The Physical Science Basis*. Ed. by T. F. Stocker, D. Qin, G.-K. Plattner, M. Tignor, S. K. Allen, J. Boschung, A. Nauels, Y. Xia, V. Bex and P. M. Midgley. Cambridge, United Kingdom and New York, NY, USA: Cambridge University Press. Chap. 6, pp. 465–570. ISBN: ISBN 978-1-107-66182-0. DOI: 10.1017/CBO9781107415324.015.

Ciemer, C., N. Boers, M. Hirota, J. Kurths, F. Müller-Hansen, R. S. Oliveira and R. Winkelmann (Mar. 2019). "Higher resilience to climatic disturbances in tropical vegetation exposed to more variable rainfall". In: *Nature Geoscience* 12.3, pp. 174–179. ISSN: 1752-0894. DOI: 10.1038/s41561-019-0312-z.

Clark, D. B., L. M. Mercado, S. Sitch, C. D. Jones, N. Gedney, M. J. Best, M. Pryor, G. G. Rooney, R. L. H. Essery, E. Blyth, O. Boucher, R. J. Harding, C. Huntingford and P. M. Cox (2011). "The Joint UK Land Environment Simulator (JULES), model description – Part 2: Carbon fluxes and vegetation dynamics". In: *Geoscientific Model Development* 4.3, pp. 701–722. ISSN: 1991-9603. DOI: 10.5194/gmd-4-701-2011.

Clarke, J., C. Huntingford, P. Ritchie and P. Cox (Apr. 2021). "The compost bomb instability in the continuum limit". In: *The European Physical Journal Special Topics*. ISSN: 1951-6355. DOI: 10.1140/epjs/s11734-021-00013-3.

Clarke, J. J., C. Huntingford, P. D. L. Ritchie and P. M. Cox (Feb. 2023). "Seeking more robust early warning signals for climate tipping points: the Ratio of Spectra method (ROSA)". In: *Environmental Research Letters*. ISSN: 1748-9326. DOI: 10.1088/1748-9326/acbc8d.

Cleveland, R. B., W. S. Cleveland, J. E. McRae and I. Terpenning (1990). "STL: A seasonal-trend decomposition". In: *Journal of Official Statistics* 6, pp. 3–73.

Cochchrane, M. A. and C. P. Barber (Mar. 2009). "Climate change, human land use and future fires in the Amazon". In: *Global Change Biology* 15.3, pp. 601–612. ISSN: 13541013. DOI: 10.1111/j.1365-2486.2008.01786.x.

Cochrane, M. A. (2002). *Spreading like wildfire: tropical forest fires in Latin America and the Caribbean: prevention, assessment and early warning*. Tech. rep., p. 96.

Corless, R. M., G. H. Gonnet, D. E. G. Hare, D. J. Jeffrey and D. E. Knuth (Dec. 1996). "On the Lambert W function". In: *Advances in Computational Mathematics* 5.1, pp. 329–359. ISSN: 1019-7168. DOI: 10.1007/BF02124750.

Cox, P. M., R. A. Betts, C. B. Bunton, R. L. H. Essery, P. R. Rowntree and J. Smith (Mar. 1999). "The impact of new land surface physics on the GCM simulation of climate and climate sensitivity". In: *Climate Dynamics* 15.3, pp. 183–203. ISSN: 0930-7575. DOI: 10.1007/s003820050276.

Cox, P., C. Huntingford and C. D. Jones (2006). "Conditions for positive feedbacks from the land carbon cycle". In: *Avoiding dangerous climate change*. Ed. by H. J. Schellnhuber, W. Cramer, N. Nakicenovic, T. Wigley and G. Yohe. Cambridge University Press. Chap. 15, pp. 155–162. ISBN: 9780521864718.

Cox, P. M., R. A. Betts, M. Collins, P. P. Harris, C. Huntingford and C. D. Jones (June 2004). "Amazonian forest dieback under climate-carbon cycle projections for the 21st century". In: *Theoretical and Applied Climatology* 78.1-3, pp. 137–156. ISSN: 0177-798X. DOI: 10.1007/s00704-004-0049-4.

Cox, P. M., R. A. Betts, C. D. Jones, S. A. Spall and I. J. Totterdell (Nov. 2000). "Acceleration of global warming due to carbon-cycle feedbacks in a coupled climate model". In: *Nature* 408.6809, pp. 184–187. ISSN: 0028-0836. DOI: 10.1038/35041539.

Cox, P. M., C. Huntingford and M. S. Williamson (Jan. 2018). "Emergent constraint on equilibrium climate sensitivity from global temperature variability". In: *Nature* 553.7688, pp. 319–322. ISSN: 0028-0836. DOI: 10.1038/nature25450.

Crowther, T. W., J. van den Hoogen, J. Wan, M. A. Mayes, A. D. Keiser, L. Mo, C. Averill and D. S. Maynard (Aug. 2019). "The global soil community and its influence on biogeochemistry". In: *Science* 365.6455. ISSN: 0036-8075. DOI: 10.1126/science.aav0550.

Dakos, V., S. R. Carpenter, W. A. Brock, A. M. Ellison, V. Guttal, A. R. Ives, S. Kéfi, V. Livina, D. A. Seekell, E. H. van Nes and M. Scheffer (July 2012). "Methods for Detecting Early Warnings of Critical Transitions in Time Series Illustrated Using Simulated Ecological Data". In: *PLoS ONE* 7.7. Ed. by B. Yener, e41010. ISSN: 1932-6203. DOI: 10.1371/journal.pone.0041010.

Dakos, V., S. Kéfi, M. Rietkerk, E. H. van Nes and M. Scheffer (June 2011). "Slowing Down in Spatially Patterned Ecosystems at the Brink of Collapse". In: *The American Naturalist* 177.6, E153–E166. ISSN: 0003-0147. DOI: 10.1086/659945.

Dakos, V., B. Matthews, A. P. Hendry, J. Levine, N. Loeuille, J. Norberg, P. Nosil, M. Scheffer and L. De Meester (Feb. 2019). "Ecosystem tipping points in an evolving world". In: *Nature Ecology & Evolution* 3.3, pp. 355–362. ISSN: 2397-334X. DOI: 10.1038/s41559-019-0797-2.

Dakos, V., M. Scheffer, E. H. Van Nes, V. Brovkin, V. Petoukhov and H. Held (2008). "Slowing down as an early warning signal for abrupt climate change". In: *Proceedings of the National Academy of Sciences of the United States of America* 105.38, pp. 14308–14312. ISSN: 00278424. DOI: 10.1073/pnas.0802430105.

Dalrymple, G. B. (Jan. 2001). "The age of the Earth in the twentieth century: a problem (mostly) solved". In: *Geological Society, London, Special Publications* 190.1, pp. 205–221. ISSN: 0305-8719. DOI: 10.1144/GSL.SP.2001.190.01.14.

Dansgaard, W., S. J. Johnsen, H. B. Clausen, D. Dahl-Jensen, N. S. Gundestrup, C. U. Hammer, C. S. Hvidberg, J. P. Steffensen, A. E. Sveinbjörnsdottir, J. Jouzel and G. Bond (July 1993). "Evidence for general instability of past climate from a 250-kyr ice-core record". In: *Nature* 364.6434, pp. 218–220. ISSN: 0028-0836. DOI: 10.1038/364218a0.

De Kauwe, M. G., B. E. Medlyn, S. Zaehle, A. P. Walker, M. C. Dietze, T. Hickler, A. K. Jain, Y. Luo, W. J. Parton, I. C. Prentice, B. Smith, P. E. Thornton, S. Wang, Y.-P. Wang, D. Wårlind, E. Weng, K. Y. Crous, D. S. Ellsworth, P. J. Hanson, H. Seok Kim, J. M. Warren, R. Oren and R. J. Norby (June 2013). "Forest water use and water use efficiency at elevated CO 2 : a model-data intercomparison at two contrasting temperate forest FACE sites". In: *Global Change Biology* 19.6, pp. 1759–1779. ISSN: 13541013. DOI: 10.1111/gcb.12164.

DeVries, T. (Oct. 2022). "The Ocean Carbon Cycle". In: *Annual Review of Environment and Resources* 47.1, pp. 317–341. ISSN: 1543-5938. DOI: 10.1146/annurev-environ-120920-111307.

DeVries, T., M. Holzer and F. Primeau (Feb. 2017). "Recent increase in oceanic carbon uptake driven by weaker upper-ocean overturning". In: *Nature* 542.7640, pp. 215–218. ISSN: 0028-0836. DOI: 10.1038/nature21068.

Dharssi, I., P. L. Vidale, A. Verhoef, B. Macpherson, C. Jones and M. Best (2009). *New soil physical properties implemented in the Unified Model at PS18*. Tech. rep. 528. Met Office.

Dickson, A. and F. Millero (Oct. 1987). "A comparison of the equilibrium constants for the dissociation of carbonic acid in seawater media". In: *Deep Sea Research Part A. Oceanographic Research Papers* 34.10, pp. 1733–1743. ISSN: 01980149. DOI: 10.1016/0198-0149(87)90021-5.

Dietz, S., J. Rising, T. Stoerk and G. Wagner (Aug. 2021). "Economic impacts of tipping points in the climate system". In: *Proceedings of the National Academy of Sciences* 118.34, e2103081118. ISSN: 0027-8424. DOI: 10.1073/pnas.2103081118.

Dijkstra, H. A. (2011). *Nonlinear climate dynamics*. 2005. Cambridge: Cambridge University Press, pp. 1–357. ISBN: 9781139034135. DOI: 10.1017/CBO9781139034135.

Ditlevsen, P. and S. Ditlevsen (July 2023). "Warning of a forthcoming collapse of the Atlantic meridional overturning circulation". In: *Nature Communications* 14.1, p. 4254. ISSN: 2041-1723. DOI: 10.1038/s41467-023-39810-w. arXiv: 2304.09160.

Ditlevsen, P. D. (May 1999). "Observation of α-stable noise induced millennial climate changes from an ice-core record". In: *Geophysical Research Letters* 26.10, pp. 1441–1444. ISSN: 00948276. DOI: 10.1029/1999GL900252.

Ditlevsen, P. D. and S. J. Johnsen (Oct. 2010). "Tipping points: Early warning and wishful thinking". In: *Geophysical Research Letters* 37.19. ISSN: 00948276. DOI: 10.1029/2010GL044486.

Donangelo, R., H. Fort, V. Dakos, M. Scheffer and E. H. Van Nes (Feb. 2010). "Early Warnings for Catastrophic Shifts in Ecosystems: Comparison between Spatial and Temporal Indicators". In: *International Journal of Bifurcation and Chaos* 20.02, pp. 315–321. ISSN: 0218-1274. DOI: 10.1142/S0218127410025764.

Doney, S. C., V. J. Fabry, R. A. Feely and J. A. Kleypas (Jan. 2009). "Ocean Acidification: The Other CO2 Problem". In: *Annual Review of Marine Science* 1.1, pp. 169–192. ISSN: 1941-1405. DOI: 10.1146/annurev.marine.010908.163834.

Donovan, G. and C. Brand (June 2022). "Spatial early warning signals for tipping points using dynamic mode decomposition". In: *Physica A: Statistical Mechanics and its Applications* 596, p. 127152. ISSN: 03784371. DOI: 10.1016/j.physa.2022.127152.

Drake, B. G., M. A. Gonzàlez-Meler and S. P. Long (June 1997). "More Efficient Plants: A Consequence of Rising Atmospheric CO2 ?" In: *Annual Review of Plant Physiology and Plant Molecular Biology* 48.1, pp. 609–639. ISSN: 1040-2519. DOI: 10.1146/annurev.arplant.48.1.609.

Drijfhout, S., S. Bathiany, C. Beaulieu, V. Brovkin, M. Claussen, C. Huntingford, M. Scheffer, G. Sgubin and D. Swingedouw (Oct. 2015). "Catalogue of abrupt shifts in Intergovernmental Panel on Climate Change climate models". In: *Proceedings of the National Academy of Sciences* 112.43, E5777–E5786. ISSN: 0027-8424. DOI: 10.1073/pnas.1511451112.

Eby, S., A. Agrawal, S. Majumder, A. P. Dobson and V. Guttal (June 2017). "Alternative stable states and spatial indicators of critical slowing down along a spatial gradient in a savanna ecosystem". In: *Global Ecology and Biogeography* 26.6, pp. 638–649. ISSN: 1466822X. DOI: 10.1111/geb.12570.

Egleston, E. S., C. L. Sabine and F. M. Morel (2010). "Revelle revisited: Buffer factors that quantify the response of ocean chemistry to changes in DIC and alkalinity". In: *Global Biogeochemical Cycles* 24.1, pp. 1–9. ISSN: 08866236. DOI: 10.1029/2008GB003407.

Einstein, A. (1905). "Über die von der molekularkinetischen Theorie der Wärme geforderte Bewegung von in ruhenden Flüssigkeiten suspendierten Teilchen". In: *Annalen der Physik* 322.8, pp. 549–560. ISSN: 00033804. DOI: 10.1002/andp.19053220806.

Eyring, V., S. Bony, G. A. Meehl, C. A. Senior, B. Stevens, R. J. Stouffer and K. E. Taylor (May 2016). "Overview of the Coupled Model Intercomparison Project Phase 6 (CMIP6) experimental design and organization". In: *Geoscientific Model Development* 9.5, pp. 1937–1958. ISSN: 1991-9603. DOI: 10.5194/gmd-9-1937-2016.

Farquhar, G. D., S. von Caemmerer and J. A. Berry (June 1980). "A biochemical model of photosynthetic CO2 assimilation in leaves of C3 species". In: *Planta* 149.1, pp. 78–90. ISSN: 0032-0935. DOI: 10.1007/BF00386231.

Feldmann, J. and A. Levermann (Nov. 2015). "Collapse of the West Antarctic Ice Sheet after local destabilization of the Amundsen Basin". In: *Proceedings of the National Academy of Sciences* 112.46, pp. 14191–14196. ISSN: 0027-8424. DOI: 10.1073/pnas.1512482112.

Fernández-Martínez, M., J. Peñuelas, F. Chevallier, P. Ciais, M. Obersteiner, C. Rödenbeck, J. Sardans, S. Vicca, H. Yang, S. Sitch, P. Friedlingstein, V. K. Arora, D. S. Goll, A. K. Jain, D. L. Lombardozzi, P. C. McGuire and I. A. Janssens (Mar. 2023). "Diagnosing destabilization risk in global land carbon sinks". In: *Nature* 615.7954, pp. 848–853. ISSN: 0028-0836. DOI: 10.1038/s41586-023-05725-1.

Feudel, U. (2023). "Rate-induced tipping in ecosystems and climate : the role of unstable states , basin boundaries and transient dynamics". In: *Nonlinear Processes in Geophysics* March, pp. 1–29. DOI: https://doi.org/10.5194/npg-2023-7.

Fischer, E. M. and R. Knutti (Nov. 2016). "Observed heavy precipitation increase confirms theory and early models". In: *Nature Climate Change* 6.11, pp. 986–991. ISSN: 1758-678X. DOI: 10.1038/nclimate3110.

Flory, P. J. (Nov. 1941). "Molecular Size Distribution in Three Dimensional Polymers. I. Gelation 1". In: *Journal of the American Chemical Society* 63.11, pp. 3083–3090. ISSN: 0002-7863. DOI: 10.1021/ja01856a061.

Fokker, A. D. (1914). "Die mittlere Energie rotierender elektrischer Dipole im Strahlungsfeld". In: *Annalen der Physik* 348.5, pp. 810–820. ISSN: 00033804. DOI: 10.1002/andp.19143480507.

Frank, D. C., B. Poulter, M. Saurer, J. Esper, C. Huntingford, G. Helle, K. Treydte, N. E. Zimmermann, G. H. Schleser, A. Ahlström, P. Ciais, P. Friedlingstein, S. Levis, M. Lomas, S. Sitch, N. Viovy, L. Andreu-Hayles, Z. Bednarz, F. Berninger, T. Boettger, C. M. D'Alessandro, V. Daux, M. Filot, M. Grabner, E. Gutierrez, M. Haupt, E. Hilasvuori, H. Jungner, M. Kalela-Brundin, M. Krapiec, M. Leuenberger, N. J. Loader, H. Marah, V. Masson-Delmotte, A. Pazdur, S. Pawelczyk, M. Pierre, O. Planells, R. Pukiene, C. E. Reynolds-Henne, K. T. Rinne, A. Saracino, E. Sonninen, M. Stievenard, V. R. Switsur, M.

Szczepanek, E. Szychowska-Krapiec, L. Todaro, J. S. Waterhouse and M. Weigl (June 2015). "Water-use efficiency and transpiration across European forests during the Anthropocene". In: *Nature Climate Change* 5.6, pp. 579–583. ISSN: 1758-678X. DOI: 10.1038/nclimate2614.

Frederikse, T., F. Landerer, L. Caron, S. Adhikari, D. Parkes, V. W. Humphrey, S. Dangendorf, P. Hogarth, L. Zanna, L. Cheng and Y.-H. Wu (Aug. 2020). "The causes of sea-level rise since 1900". In: *Nature* 584.7821, pp. 393–397. ISSN: 0028-0836. DOI: 10.1038/s41586-020-2591-3.

Friedlingstein, P., P. Cox, R. Betts, L. Bopp, W. von Bloh, V. Brovkin, P. Cadule, S. Doney, M. Eby, I. Fung, G. Bala, J. John, C. Jones, F. Joos, T. Kato, M. Kawamiya, W. Knorr, K. Lindsay, H. D. Matthews, T. Raddatz, P. Rayner, C. Reick, E. Roeckner, K.-G. Schnitzler, R. Schnur, K. Strassmann, A. J. Weaver, C. Yoshikawa and N. Zeng (July 2006). "Climate–Carbon Cycle Feedback Analysis: Results from the C4MIP Model Intercomparison". In: *Journal of Climate* 19.14, pp. 3337–3353. ISSN: 1520-0442. DOI: 10.1175/JCLI3800.1.

Friedlingstein, P. et al. (Nov. 2022). "Global Carbon Budget 2022". In: *Earth System Science Data* 14.11, pp. 4811–4900. ISSN: 1866-3516. DOI: 10.5194/essd-14-4811-2022.

Frieler, K., M. Meinshausen, A. Golly, M. Mengel, K. Lebek, S. D. Donner and O. Hoegh-Guldberg (2013). "Limiting global warming to 2C is unlikely to save most coral reefs". In: *Nature Climate Change* 3.2, pp. 165–170. ISSN: 1758678X. DOI: 10.1038/nclimate1674.

Garbe, J., T. Albrecht, A. Levermann, J. F. Donges and R. Winkelmann (Sept. 2020). "The hysteresis of the Antarctic Ice Sheet". In: *Nature* 585.7826, pp. 538–544. ISSN: 0028-0836. DOI: 10.1038/s41586-020-2727-5.

Gatti, L. V., L. S. Basso, J. B. Miller, M. Gloor, L. Gatti Domingues, H. L. G. Cassol, G. Tejada, L. E. O. C. Aragão, C. Nobre, W. Peters, L. Marani, E. Arai, A. H. Sanches, S. M. Corrêa, L. Anderson, C. Von Randow, C. S. C. Correia, S. P. Crispim and R. A. L. Neves (July 2021). "Amazonia as a carbon source linked to deforestation and climate change". In: *Nature* 595.7867, pp. 388–393. ISSN: 0028-0836. DOI: 10.1038/s41586-021-03629-6.

Gedney, N. and P. M. Cox (2003). "The sensitivity of global climate model simulations to the representation of soil moisture heterogeneity". In: *Journal of Hydrometeorology* 4.6, pp. 1265–1275. ISSN: 1525755X. DOI: 10.1175/1525-7541(2003)004<1265:TSOGCM>2.0.CO;2.

Ghil, M. (Jan. 1976). "Climate Stability for a Sellers-Type Model". In: *Journal of the Atmospheric Sciences* 33.1, pp. 3–20. ISSN: 0022-4928. DOI: 10.1175/1520-0469(1976)033<0003:CSFAST>2.0.CO;2.

Ghil, M. and V. Lucarini (July 2020). "The physics of climate variability and climate change". In: *Reviews of Modern Physics* 92.3, p. 035002. ISSN: 0034-6861. DOI: 10.1103/RevModPhys.92.035002. arXiv: 1910.00583.

Ginzburg, V. L. and L. D. Landau (1965). "On the Theory of Superconductivity". In: *On Superconductivity and Superfluidity*. Berlin, Heidelberg: Springer Berlin Heidelberg, pp. 113–137. DOI: 10.1007/978-3-540-68008-6_4.

Glendinning, P. (1994). *Stability, Instability and Chaos: An Introduction to the Theory of Nonlinear Differential Equations*. Cambridge Texts in Applied Mathematics. Cambridge University Press. DOI: 10.1017/CBO9780511626296.

Goldenfeld, N. (Mar. 2018). *Lectures on Phase Transitions and the Renormalization Group*. 1st. Boca Raton: CRC Press, p. 420. ISBN: 9780429493492. DOI: 10.1201/9780429493492.

Goode, P. R., E. Pallé, A. Shoumko, S. Shoumko, P. Montañes-Rodriguez and S. E. Koonin (Sept. 2021). "Earth's Albedo 1998–2017 as Measured From Earthshine". In: *Geophysical Research Letters* 48.17, pp. 1–8. ISSN: 0094-8276. DOI: 10.1029/2021GL094888.

Gowda, K., H. Riecke and M. Silber (Feb. 2014). "Transitions between patterned states in vegetation models for semiarid ecosystems". In: *Physical Review E* 89.2, p. 022701. ISSN: 1539-3755. DOI: 10.1103/PhysRevE.89.022701. arXiv: 1310.7210.

Gregory, J. M. (2004). "A new method for diagnosing radiative forcing and climate sensitivity". In: *Geophysical Research Letters* 31.3, p. L03205. ISSN: 0094-8276. DOI: 10.1029/2003GL018747.

Grobman, D. M. (1959). "Homeomorphism of systems of differential equations". In: *Doklady Akademii Nauk SSSR* 128, pp. 880–881.

Guckenheimer, J. and P. Holmes (1983). *Nonlinear Oscillations, Dynamical Systems, and Bifurcations of Vector Fields*. Vol. 42. Applied Mathematical Sciences. New York, NY: Springer New York. ISBN: 978-1-4612-7020-1. DOI: 10.1007/978-1-4612-1140-2.

Guttal, V. and C. Jayaprakash (Mar. 2009). "Spatial variance and spatial skewness: leading indicators of regime shifts in spatial ecological systems". In: *Theoretical Ecology* 2.1, pp. 3–12. ISSN: 1874-1738. DOI: 10.1007/s12080-008-0033-1.

Guttal, V. and C. Jayaprakash (May 2008). "Changing skewness: an early warning signal of regime shifts in ecosystems". In: *Ecology Letters* 11.5, pp. 450–460. ISSN: 1461-023X. DOI: 10.1111/j.1461-0248.2008.01160.x.

Halekotte, L. and U. Feudel (July 2020). "Minimal fatal shocks in multistable complex networks". In: *Scientific Reports* 10.1, p. 11783. ISSN: 2045-2322. DOI: 10.1038/s41598-020-68805-6.

Hargreaves, J. C., J. D. Annan, M. Yoshimori and A. Abe-Ouchi (2012). "Can the Last Glacial Maximum constrain climate sensitivity?" In: *Geophysical Research Letters* 39.24, pp. 1–5. ISSN: 19448007. DOI: 10.1029/2012GL053872.

Hartman, P. (Aug. 1960). "A Lemma in the Theory of Structural Stability of Differential Equations". In: *Proceedings of the American Mathematical Society* 11.4, p. 610. ISSN: 00029939. DOI: 10.2307/2034720.

Hartman, P. (1963). "On the local linearization of differential equations". In: *Proceedings of the American Mathematical Society* 14.4, pp. 568–573. ISSN: 0002-9939. DOI: 10.1090/S0002-9939-1963-0152718-3.

Hasselmann, K. (Dec. 1976). "Stochastic climate models Part I. Theory". In: *Tellus* 28.6, pp. 473–485. ISSN: 00402826. DOI: 10.1111/j.2153-3490.1976.tb00696.x.

Hawkins, E., R. S. Smith, L. C. Allison, J. M. Gregory, T. J. Woollings, H. Pohlmann and B. de Cuevas (May 2011). "Bistability of the Atlantic overturning circulation in a global climate model and links to ocean freshwater transport". In: *Geophysical Research Letters* 38.10, n/a–n/a. ISSN: 00948276. DOI: 10.1029/2011GL047208.

Held, H. and T. Kleinen (Dec. 2004). "Detection of climate system bifurcations by degenerate fingerprinting". In: *Geophysical Research Letters* 31.23, pp. 1–4. ISSN: 00948276. DOI: 10.1029/2004GL020972.

Held, I. M. and M. J. Suarez (Jan. 1974). "Simple albedo feedback models of the icecaps". In: *Tellus A: Dynamic Meteorology and Oceanography* 26.6, p. 613. ISSN: 1600-0870. DOI: 10.3402/tellusa.v26i6.9870.

Hély, C., A.-M. Lézine and A. Contributors (Apr. 2014). "Holocene changes in African vegetation: tradeoff between climate and water availability". In: *Climate of the Past* 10.2, pp. 681–686. ISSN: 1814-9332. DOI: 10.5194/cp-10-681-2014.

Hersbach, H., B. Bell, P. Berrisford, S. Hirahara, A. Horányi, J. Muñoz-Sabater, J. Nicolas, C. Peubey, R. Radu, D. Schepers, A. Simmons, C. Soci, S. Abdalla, X. Abellan, G. Balsamo, P. Bechtold, G. Biavati, J. Bidlot, M. Bonavita, G. Chiara, P. Dahlgren, D. Dee, M. Diamantakis, R. Dragani, J. Flemming, R. Forbes, M. Fuentes, A. Geer, L. Haimberger, S. Healy, R. J. Hogan, E. Hólm, M. Janisková, S. Keeley, P. Laloyaux, P. Lopez, C. Lupu, G. Radnoti, P. Rosnay, I. Rozum, F. Vamborg, S. Villaume and J.-N. Thépaut (July 2020). "The ERA5 global reanalysis". In: *Quarterly Journal of the Royal Meteorological Society* 146.730, pp. 1999–2049. ISSN: 0035-9009. DOI: 10.1002/qj.3803.

Heßler, M. and O. Kamps (June 2022a). "Bayesian on-line anticipation of critical transitions". In: *New Journal of Physics* 24.6, p. 063021. ISSN: 1367-2630. DOI: 10.1088/1367-2630/ac46d4.

Heßler, M. and O. Kamps (Apr. 2022b). "Quantifying resilience and the risk of regime shifts under strong correlated noise". In: arXiv: 2204.03403.

Heydt, A. S. von der, P. Ashwin, C. D. Camp, M. Crucifix, H. A. Dijkstra, P. Ditlevsen and T. M. Lenton (Feb. 2021). "Quantification and interpretation of the climate variability record". In: *Global and Planetary Change* 197.May 2020, p. 103399. ISSN: 09218181. DOI: 10.1016/j.gloplacha.2020.103399.

Hillebrand, H., I. Donohue, W. S. Harpole, D. Hodapp, M. Kucera, A. M. Lewandowska, J. Merder, J. M. Montoya and J. A. Freund (Aug. 2020). "Thresholds for ecological responses to global change do not emerge from empirical data". In: *Nature Ecology & Evolution* 4.11, pp. 1502–1509. DOI: 10.1038/s41559-020-1256-9.

Hirota, M., M. Holmgren, E. H. Van Nes and M. Scheffer (Oct. 2011). "Global Resilience of Tropical Forest and Savanna to Critical Transitions". In: *Science* 334.6053, pp. 232–235. ISSN: 0036-8075. DOI: 10.1126/science.1210657.

Hirsch, M. W., C. C. Pugh and M. Shub (1977). *Invariant Manifolds*. 1st ed. Springer, p. 149. ISBN: 9783540081487.

Hoelzmann, P., D. Jolly, S. P. Harrison, F. Laarif, R. Bonnefille and H.-J. Pachur (Mar. 1998). "Mid-Holocene land-surface conditions in northern Africa and the Arabian Peninsula:

A data set for the analysis of biogeophysical feedbacks in the climate system". In: *Global Biogeochemical Cycles* 12.1, pp. 35–51. ISSN: 08866236. DOI: 10.1029/97GB02733.

Hoffman, P. F. and D. P. Schrag (June 2002). "The snowball Earth hypothesis: testing the limits of global change". In: *Terra Nova* 14.3, pp. 129–155. ISSN: 0954-4879. DOI: 10.1046/j.1365-3121.2002.00408.x.

Holling, C. S. (Nov. 1973). "Resilience and Stability of Ecological Systems". In: *Annual Review of Ecology and Systematics* 4.1, pp. 1–23. ISSN: 0066-4162. DOI: 10.1146/annurev.es.04.110173.000245.

Hopcroft, P. O. and P. J. Valdes (Nov. 2021). "Paleoclimate-conditioning reveals a North Africa land–atmosphere tipping point". In: *Proceedings of the National Academy of Sciences* 118.45, pp. 1–7. ISSN: 0027-8424. DOI: 10.1073/pnas.2108783118.

Hopf, E. (1942). *Abzweigung einer periodischen Lösung von einer stationären Lösung eines Differentialsystems*.

Hugelius, G., J. Strauss, S. Zubrzycki, J. W. Harden, E. A. G. Schuur, C.-L. Ping, L. Schirrmeister, G. Grosse, G. J. Michaelson, C. D. Koven, J. A. O'Donnell, B. Elberling, U. Mishra, P. Camill, Z. Yu, J. Palmtag and P. Kuhry (Dec. 2014). "Estimated stocks of circumpolar permafrost carbon with quantified uncertainty ranges and identified data gaps". In: *Biogeosciences* 11.23, pp. 6573–6593. ISSN: 1726-4189. DOI: 10.5194/bg-11-6573-2014.

Huntingford, C., B. B. B. Booth, S. Sitch, N. Gedney, J. A. Lowe, S. K. Liddicoat, L. M. Mercado, M. J. Best, G. P. Weedon, R. A. Fisher, M. R. Lomas, P. Good, P. Zelazowski, A. C. Everitt, A. C. Spessa and C. D. Jones (Nov. 2010). "IMOGEN: an intermediate complexity model to evaluate terrestrial impacts of a changing climate". In: *Geoscientific Model Development* 3.2, pp. 679–687. ISSN: 1991-9603. DOI: 10.5194/gmd-3-679-2010.

Huntingford, C. and P. M. Cox (Aug. 2000). "An analogue model to derive additional climate change scenarios from existing GCM simulations". In: *Climate Dynamics* 16.8, pp. 575–586. ISSN: 0930-7575. DOI: 10.1007/s003820000067.

Huntingford, C., P. P. Harris, N. Gedney, P. M. Cox, R. A. Betts, J. A. Marengo and J. H. C. Gash (June 2004). "Using a GCM analogue model to investigate the potential for Amazonian forest dieback". In: *Theoretical and Applied Climatology* 78.1-3, pp. 177–185. ISSN: 0177-798X. DOI: 10.1007/s00704-004-0051-x.

Huntingford, C., P. D. Jones, V. N. Livina, T. M. Lenton and P. M. Cox (Aug. 2013). "No increase in global temperature variability despite changing regional patterns". In: *Nature* 500.7462, pp. 327–330. ISSN: 0028-0836. DOI: 10.1038/nature12310.

Hurst, H. E. (Sept. 1957). "A Suggested Statistical Model of some Time Series which occur in Nature". In: *Nature* 180.4584, pp. 494–494. ISSN: 0028-0836. DOI: 10.1038/180494a0.

IPCC (2021). *Climate Change 2021: The Physical Science Basis. Contribution of Working Group I to the Sixth Assessment Report of the Intergovernmental Panel on Climate Change*. Cambridge: Cambridge University Press. DOI: 10.1017/9781009157896.

Ising, E. (Feb. 1925). "Beitrag zur Theorie des Ferromagnetismus". In: *Zeitschrift für Physik* 31.1, pp. 253–258. ISSN: 0044-3328. DOI: 10.1007/BF02980577.

Jackson, L. C., R. Kahana, T. Graham, M. A. Ringer, T. Woollings, J. V. Mecking and R. A. Wood (Dec. 2015). "Global and European climate impacts of a slowdown of the AMOC in a high resolution GCM". In: *Climate Dynamics* 45.11-12, pp. 3299–3316. ISSN: 0930-7575. DOI: 10.1007/s00382-015-2540-2.

Jacobs, K. (Feb. 2010). *Stochastic Processes for Physicists*. Cambridge: Cambridge University Press. DOI: 10.1017/CBO9780511815980.

Jenkinson, D. S., D. E. Adams and A. Wild (1991). "Model estimates of CO2 emissions from soil in response to global warming". In: *Nature* 351.

Jiménez-Muñoz, J. C., C. Mattar, J. Barichivich, A. Santamaría-Artigas, K. Takahashi, Y. Malhi, J. A. Sobrino and G. van der Schrier (Sept. 2016). "Record-breaking warming and extreme drought in the Amazon rainforest during the course of El Niño 2015–2016". In: *Scientific Reports* 6.1, p. 33130. ISSN: 2045-2322. DOI: 10.1038/srep33130.

Johnson, F. S. (Dec. 1954). "The Solar Constant". In: *Journal of Meteorology* 11.6, pp. 431–439. ISSN: 0095-9634. DOI: 10.1175/1520-0469(1954)011<0431:TSC>2.0.CO;2.

Jones, C. (June 2001). "Constraints on the temperature sensitivity of global soil respiration from the observed interannual variability in atmospheric CO2". In: *Atmospheric Science Letters* 2.1-4, pp. 166–172. ISSN: 1530261X. DOI: 10.1006/asle.2001.0041.

Jones, C. D. and P. M. Cox (July 2005). "On the significance of atmospheric CO 2 growth rate anomalies in 2002-2003". In: *Geophysical Research Letters* 32.14, n/a–n/a. ISSN: 00948276. DOI: 10.1029/2005GL023027.

Jones, P. D., M. New, D. E. Parker, S. Martin and I. G. Rigor (May 1999). "Surface air temperature and its changes over the past 150 years". In: *Reviews of Geophysics* 37.2, pp. 173–199. ISSN: 87551209. DOI: 10.1029/1999RG900002.

Joos, F., M. Bruno, R. Fink, U. Siegenthaler, T. F. Stocker, C. Le Quéré and J. L. Sarmiento (Jan. 1996). "An efficient and accurate representation of complex oceanic and biospheric models of anthropogenic carbon uptake". In: *Tellus B: Chemical and Physical Meteorology* 48.3, p. 397. ISSN: 1600-0889. DOI: 10.3402/tellusb.v48i3.15921.

Kéfi, S., V. Guttal, W. A. Brock, S. R. Carpenter, A. M. Ellison, V. N. Livina, D. A. Seekell, M. Scheffer, E. H. van Nes and V. Dakos (Mar. 2014). "Early Warning Signals of Ecological Transitions: Methods for Spatial Patterns". In: *PLoS ONE* 9.3. Ed. by R. V. Solé, e92097. ISSN: 1932-6203. DOI: 10.1371/journal.pone.0092097.

Kéfi, S., M. Rietkerk, C. L. Alados, Y. Pueyo, V. P. Papanastasis, A. ElAich and P. C. de Ruiter (Sept. 2007). "Spatial vegetation patterns and imminent desertification in Mediterranean arid ecosystems". In: *Nature* 449.7159, pp. 213–217. ISSN: 0028-0836. DOI: 10.1038/nature06111.

Khvorostyanov, D. V., P. Ciais, G. Krinner, S. A. Zimov, C. Corradi and G. Guggenberger (Jan. 2008a). "Vulnerability of permafrost carbon to global warming. Part II: sensitivity of permafrost carbon stock to global warming". In: *Tellus B: Chemical and Physical Meteorology* 60.2, p. 265. ISSN: 1600-0889. DOI: 10.1111/j.1600-0889.2007.00336.x.

Khvorostyanov, D. V., G. Krinner, P. Ciais, M. Heimann and S. A. Zimov (2008b). "Vulnerability of permafrost carbon to global warming. Part I: Model description and role of heat generated by organic matter decomposition". In: *Tellus, Series B: Chemical and Physical Meteorology* 60 B.2, pp. 250–264. ISSN: 02806509. DOI: 10.1111/j.1600-0889.2007.00333.x.

Kindler, P., M. Guillevic, M. Baumgartner, J. Schwander, A. Landais and M. Leuenberger (2014). "Temperature reconstruction from 10 to 120 kyr b2k from the NGRIP ice core". In: *Climate of the Past* 10.2, pp. 887–902. ISSN: 18149332. DOI: 10.5194/cp-10-887-2014.

Kirschbaum, M. U. (1995). "The temperature dependence of soil organic matter decomposition, and the effect of global warming on soil organic C storage". In: *Soil Biology and Biochemistry* 27.6, pp. 753–760. ISSN: 00380717. DOI: 10.1016/0038-0717(94)00242-S.

Kirschvink, J. L. (1992). "Late Proterozoic low-latitude global glaciation: the snowball Earth". In: *The Proterozoic Biosphere* 52, pp. 51–52. ISSN: 0521366151.

Kleinen, T., H. Held and G. Petschel-Held (June 2003). "The potential role of spectral properties in detecting thresholds in the Earth system: application to the thermohaline circulation". In: *Ocean Dynamics* 53.2, pp. 53–63. ISSN: 1616-7341. DOI: 10.1007/s10236-002-0023-6.

Klose, A. K., N. Wunderling, R. Winkelmann and J. F. Donges (2021). "What do we mean, 'tipping cascade'?" In: *Environmental Research Letters* 16.12. ISSN: 17489326. DOI: 10.1088/1748-9326/ac3955. arXiv: 2108.09550.

Kolby Smith, W., S. C. Reed, C. C. Cleveland, A. P. Ballantyne, W. R. L. Anderegg, W. R. Wieder, Y. Y. Liu and S. W. Running (Mar. 2016). "Large divergence of satellite and Earth system model estimates of global terrestrial CO_2 fertilization". In: *Nature Climate Change* 6.3, pp. 306–310. ISSN: 1758-678X. DOI: 10.1038/nclimate2879.

Kopp, R. E., R. L. Shwom, G. Wagner and J. Yuan (Aug. 2016). "Tipping elements and climate–economic shocks: Pathways toward integrated assessment". In: *Earth's Future* 4.8, pp. 346–372. ISSN: 2328-4277. DOI: 10.1002/2016EF000362.

Krakovská, H., C. Kuehn and I. P. Longo (June 2023). "Resilience of dynamical systems". In: *European Journal of Applied Mathematics*, pp. 1–46. ISSN: 0956-7925. DOI: 10.1017/S0956792523000141. arXiv: 2105.10592.

Kramers, H. (Apr. 1940). "Brownian motion in a field of force and the diffusion model of chemical reactions". In: *Physica* 7.4, pp. 284–304. ISSN: 00318914. DOI: 10.1016/S0031-8914(40)90098-2.

Kriegler, E., J. W. Hall, H. Held, R. Dawson and H. J. Schellnhuber (Mar. 2009). "Imprecise probability assessment of tipping points in the climate system". In: *Proceedings of the National Academy of Sciences* 106.13, pp. 5041–5046. ISSN: 0027-8424. DOI: 10.1073/pnas.0809117106.

Kröpelin, S., D. Verschuren, A.-M. Lézine, H. Eggermont, C. Cocquyt, P. Francus, J.-P. Cazet, M. Fagot, B. Rumes, J. M. Russell, F. Darius, D. J. Conley, M. Schuster, H. von Suchodoletz and D. R. Engstrom (May 2008). "Climate-Driven Ecosystem Succession in

the Sahara: The Past 6000 Years". In: *Science* 320.5877, pp. 765–768. ISSN: 0036-8075. DOI: 10.1126/science.1154913.

Kubo, R. (Jan. 1966). "The fluctuation-dissipation theorem". In: *Reports on Progress in Physics* 29.1, p. 306. DOI: 10.1088/0034-4885/29/1/306.

Kuehn, C. (June 2011). "A mathematical framework for critical transitions: Bifurcations, fast–slow systems and stochastic dynamics". In: *Physica D: Nonlinear Phenomena* 240.12, pp. 1020–1035. ISSN: 01672789. DOI: 10.1016/j.physd.2011.02.012. arXiv: 1101.2899.

Kuehn, C., K. Lux and A. Neamţu (Mar. 2022). "Warning signs for non-Markovian bifurcations: colour blindness and scaling laws". In: *Proceedings of the Royal Society A: Mathematical, Physical and Engineering Sciences* 478.2259, pp. 1–14. ISSN: 1364-5021. DOI: 10.1098/rspa.2021.0740. arXiv: 2106.08374.

Kuznetsov, Y. A. (2004). *Elements of Applied Bifurcation Theory*. 3rd ed. Vol. 112. Applied Mathematical Sciences. New York, NY: Springer New York. ISBN: 978-1-4419-1951-9. DOI: 10.1007/978-1-4757-3978-7.

Lade, S. J., J. F. Donges, I. Fetzer, J. M. Anderies, C. Beer, S. E. Cornell, T. Gasser, J. Norberg, K. Richardson, J. Rockström and W. Steffen (2018). "Analytically tractable climate- carbon cycle feedbacks under 21st century anthropogenic forcing". In: *Earth System Dynamics* 9.2, pp. 507–523. ISSN: 21904987. DOI: 10.5194/esd-9-507-2018.

Lancaster, T. and S. J. Blundell (Apr. 2014). *Quantum Field Theory for the Gifted Amateur*. Vol. 1. Oxford University Press. ISBN: 9780199699322. DOI: 10.1093/acprof:oso/9780199699322.001.0001.

Langevin, P. (1908). "Sur la theorie du mouvement brownien". In: *Compt. Rendus* 146, pp. 530–533.

Lasslop, G., V. Brovkin, C. H. Reick, S. Bathiany and S. Kloster (June 2016). "Multiple stable states of tree cover in a global land surface model due to a fire-vegetation feedback". In: *Geophysical Research Letters* 43.12, pp. 6324–6331. ISSN: 00948276. DOI: 10.1002/2016GL069365.

Leemput, I. A. van de, E. H. van Nes and M. Scheffer (Feb. 2015). "Resilience of Alternative States in Spatially Extended Ecosystems". In: *PLOS ONE* 10.2. Ed. by E. Paci, e0116859. ISSN: 1932-6203. DOI: 10.1371/journal.pone.0116859.

Leith, C. E. (1975). "Climate Response and Fluctuation Dissipation". In: *Journal of Atmospheric Sciences* 32.10.

Lenton, T. M. (2011). "Early warning of climate tipping points". In: *Nature Climate Change* 1.4, pp. 201–209. ISSN: 1758678X. DOI: 10.1038/nclimate1143.

Lenton, T. M. (Feb. 2012). "Arctic Climate Tipping Points". In: *AMBIO* 41.1, pp. 10–22. ISSN: 0044-7447. DOI: 10.1007/s13280-011-0221-x.

Lenton, T. M., H. Held, E. Kriegler, J. W. Hall, W. Lucht, S. Rahmstorf and H. J. Schellnhuber (2008). "Tipping elements in the Earth's climate system". In: *Proceedings of the National Academy of Sciences of the United States of America* 105.6, pp. 1786–1793. ISSN: 00278424. DOI: 10.1073/pnas.0705414105.

Lenton, T. M., J. Rockström, O. Gaffney, S. Rahmstorf, K. Richardson, W. Steffen and H. J. Schellnhuber (Nov. 2019). "Climate tipping points — too risky to bet against". In: *Nature* 575.7784, pp. 592–595. ISSN: 0028-0836. DOI: 10.1038/d41586-019-03595-0.

Lenton, T. M. and H. T. Williams (July 2013). "On the origin of planetary-scale tipping points". In: *Trends in Ecology & Evolution* 28.7, pp. 380–382. ISSN: 01695347. DOI: 10.1016/j.tree.2013.06.001.

Lever, J. J., E. H. van Nes, M. Scheffer and J. Bascompte (Mar. 2014). "The sudden collapse of pollinator communities". In: *Ecology Letters* 17.3. Ed. by F. Jordan, pp. 350–359. ISSN: 1461023X. DOI: 10.1111/ele.12236.

Levermann, A. and R. Winkelmann (Aug. 2016). "A simple equation for the melt elevation feedback of ice sheets". In: *The Cryosphere* 10.4, pp. 1799–1807. ISSN: 1994-0424. DOI: 10.5194/tc-10-1799-2016.

Lisiecki, L. E. and M. E. Raymo (2005). "A Pliocene-Pleistocene stack of 57 globally distributed benthic δ 18O records". In: *Paleoceanography* 20.1, pp. 1–17. ISSN: 08838305. DOI: 10.1029/2004PA001071.

Livina, V. N. and T. M. Lenton (Feb. 2007). "A modified method for detecting incipient bifurcations in a dynamical system". In: *Geophysical Research Letters* 34.3, p. L03712. ISSN: 0094-8276. DOI: 10.1029/2006GL028672.

Lohmann, J. and P. D. Ditlevsen (2021). "Risk of tipping the overturning circulation due to increasing rates of ice melt". In: pp. 1–6. DOI: 10.1073/pnas.2017989118/-/DCSupplemental.y.

Lorenz, E. N. (Mar. 1963). "Deterministic Nonperiodic Flow". In: *Journal of the Atmospheric Sciences* 20.2, pp. 130–141. ISSN: 0022-4928. DOI: 10.1175/1520-0469(1963)020<0130:DNF>2.0.CO;2.

Lorenz, E. N. (Dec. 1967). "The nature and theory of the general circulation of the atmosphere". In: *World Meteorological Orginisation*.

Lovett, G. M., J. J. Cole and M. L. Pace (Feb. 2006). "Is Net Ecosystem Production Equal to Ecosystem Carbon Accumulation?" In: *Ecosystems* 9.1, pp. 152–155. ISSN: 1432-9840. DOI: 10.1007/s10021-005-0036-3.

Luke, C. M. and P. M. Cox (Feb. 2010). "Soil carbon and climate change: from the Jenkinson effect to the compost-bomb instability". In: *European Journal of Soil Science* 62.1, pp. 5–12. ISSN: 13510754. DOI: 10.1111/j.1365-2389.2010.01312.x.

MacDougall, A. H., T. L. Frölicher, C. D. Jones, J. Rogelj, H. D. Matthews, K. Zickfeld, V. K. Arora, N. J. Barrett, V. Brovkin, F. A. Burger, M. Eby, A. V. Eliseev, T. Hajima, P. B. Holden, A. Jeltsch-Thömmes, C. Koven, N. Mengis, L. Menviel, M. Michou, I. I. Mokhov, A. Oka, J. Schwinger, R. Séférian, G. Shaffer, A. Sokolov, K. Tachiiri, J. Tjiputra, A. Wiltshire and T. Ziehn (June 2020). "Is there warming in the pipeline? A multi-model analysis of the Zero Emissions Commitment from CO2". In: *Biogeosciences* 17.11, pp. 2987–3016. ISSN: 1726-4189. DOI: 10.5194/bg-17-2987-2020.

Malhi, Y., D. Wood, T. R. Baker, J. Wright, O. L. Phillips, T. Cochrane, P. Meir, J. Chave, S. Almeida, L. Arroyo, N. Higuchi, T. J. Killeen, S. G. Laurance, W. F. Laurance, S. L. Lewis, A. Montea and B. Vinceti (July 2006). "The regional variation of aboveground live biomass in old-growth Amazonian forests". In: *Global Change Biology* 12.7, pp. 1107–1138. ISSN: 13541013. DOI: 10.1111/j.1365-2486.2006.01120.x.

Manabe, S. and R. J. Stouffer (Sept. 1988). "Two Stable Equilibria of a Coupled Ocean-Atmosphere Model". In: *Journal of Climate* 1.9, pp. 841–866. ISSN: 0894-8755. DOI: 10.1175/1520-0442(1988)001<0841:TSEOAC>2.0.CO;2.

Manabe, S. and R. T. Wetherald (May 1967). "Thermal Equilibrium of the Atmosphere with a Given Distribution of Relative Humidity". In: *Journal of the Atmospheric Sciences* 24.3, pp. 241–259. ISSN: 0022-4928. DOI: 10.1175/1520-0469(1967)024<0241:TEOTAW>2.0.CO;2.

Mangeon, S., A. Voulgarakis, R. Gilham, A. Harper, S. Sitch and G. Folberth (Aug. 2016). "INFERNO: a fire and emissions scheme for the UK Met Office's Unified Model". In: *Geoscientific Model Development* 9.8, pp. 2685–2700. ISSN: 1991-9603. DOI: 10.5194/gmd-9-2685-2016.

Marconi, U., A. Puglisi, L. Rondoni and A. Vulpiani (June 2008). "Fluctuation-dissipation: Response theory in statistical physics". In: *Physics Reports* 461.4-6, pp. 111–195. ISSN: 03701573. DOI: 10.1016/j.physrep.2008.02.002. arXiv: 0803.0719.

Marcott, S. A., T. K. Bauska, C. Buizert, E. J. Steig, J. L. Rosen, K. M. Cuffey, T. J. Fudge, J. P. Severinghaus, J. Ahn, M. L. Kalk, J. R. McConnell, T. Sowers, K. C. Taylor, J. W. C. White and E. J. Brook (Oct. 2014). "Centennial-scale changes in the global carbon cycle during the last deglaciation". In: *Nature* 514.7524, pp. 616–619. ISSN: 0028-0836. DOI: 10.1038/nature13799.

May, R. M. (June 1976). "Simple mathematical models with very complicated dynamics". In: *Nature* 261.5560, pp. 459–467. ISSN: 0028-0836. DOI: 10.1038/261459a0.

McKean, H. P., Z. W. Birnbaum and E. Lukacs (2014). *Stochastic Integrals*. Probability and mathematical statistics. Elsevier Science. ISBN: 9781483259239.

Michel, S. L. L., D. Swingedouw, P. Ortega, G. Gastineau, J. Mignot, G. McCarthy and M. Khodri (Sept. 2022). "Early warning signal for a tipping point suggested by a millennial Atlantic Multidecadal Variability reconstruction". In: *Nature Communications* 13.1, p. 5176. ISSN: 2041-1723. DOI: 10.1038/s41467-022-32704-3.

Mitchell, J. (Dec. 1976). "An overview of climatic variability and its causal mechanisms". In: *Quaternary Research* 6.4, pp. 481–493. ISSN: 0033-5894. DOI: 10.1016/0033-5894(76)90021-1.

Morice, C. P., J. J. Kennedy, N. A. Rayner, J. P. Winn, E. Hogan, R. E. Killick, R. J. H. Dunn, T. J. Osborn, P. D. Jones and I. R. Simpson (Feb. 2021). "An Updated Assessment of Near-Surface Temperature Change From 1850: The HadCRUT5 Data Set". In: *Journal of Geophysical Research: Atmospheres* 126.3, pp. 1–28. ISSN: 2169-897X. DOI: 10.1029/2019JD032361.

Nelson, M. I., T. R. Marchant, G. C. Wake, E. Balakrishnan and X. D. Chen (2007). "Self-heating in compost piles due to biological effects". In: *Chemical Engineering Science* 62.17, pp. 4612–4619. ISSN: 00092509. DOI: 10.1016/j.ces.2007.05.018.

Noël, B., L. van Kampenhout, J. T. M. Lenaerts, W. J. van de Berg and M. R. van den Broeke (Mar. 2021). "A 21st Century Warming Threshold for Sustained Greenland Ice Sheet Mass Loss". In: *Geophysical Research Letters* 48.5, pp. 1–9. ISSN: 0094-8276. DOI: 10.1029/2020GL090471.

North, G. R., R. F. Cahalan and J. A. Coakley (1981). "Energy balance climate models". In: *Reviews of Geophysics* 19.1, pp. 91–121. ISSN: 19449208. DOI: 10.1029/RG019i001p00091.

North Greenland Ice Core Project members (Sept. 2004). "High-resolution record of Northern Hemisphere climate extending into the last interglacial period". In: *Nature* 431.7005, pp. 147–151. ISSN: 0028-0836. DOI: 10.1038/nature02805.

O'Sullivan, E., K. Mulchrone and S. Wieczorek (July 2023). "Rate-induced tipping to metastable Zombie fires". In: *Proceedings of the Royal Society A: Mathematical, Physical and Engineering Sciences* 479.2275. ISSN: 1364-5021. DOI: 10.1098/rspa.2022.0647. arXiv: 2210.02376.

Oeschger, H., J. Beer, U. Siegenthaler, B. Stauffer, W. Dansgaard and C. Langway (1984). "Late glacial climate history from ice cores". In: *Climate processes and climate sensitivity*. Vol. 29, pp. 299–306. DOI: 10.1029/GM029p0299.

Onsager, L. (Feb. 1944). "Crystal Statistics. I. A Two-Dimensional Model with an Order-Disorder Transition". In: *Physical Review* 65.3-4, pp. 117–149. ISSN: 0031-899X. DOI: 10.1103/PhysRev.65.117.

Osborn, T. J., P. D. Jones, D. H. Lister, C. P. Morice, I. R. Simpson, J. P. Winn, E. Hogan and I. C. Harris (Jan. 2021). "Land Surface Air Temperature Variations Across the Globe Updated to 2019: The CRUTEM5 Data Set". In: *Journal of Geophysical Research: Atmospheres* 126.2. ISSN: 2169-897X. DOI: 10.1029/2019JD032352.

Palmer, T., R. Buizza, F. Doblas-Reyes, T. Jung, Martin Leutbecher, G. Shutts, M. Steinheimer and A. Weisheimer (2009). *Stochastic parametrization and model uncertainty*. Tech. rep. DOI: https://doi.org/10.21957/ps8gbwbdv.

Parry, I., P. Ritchie and P. Cox (2022). "Evidence of Amazon rainforest dieback in CMIP6 models". In: *EGUsphere* 2022, pp. 1–11. DOI: 10.5194/egusphere-2022-82.

Peixoto, J. P. and A. H. Oort (1992). *Physics of climate*. American Institute of Physics. ISBN: 9780883187128.

Pierrehumbert, R. T. (2005). "Climate dynamics of a hard snowball Earth". In: *Journal of Geophysical Research* 110.D1, p. D01111. ISSN: 0148-0227. DOI: 10.1029/2004JD005162.

Pierrehumbert, R., D. Abbot, A. Voigt and D. Koll (May 2011). "Climate of the Neoproterozoic". In: *Annual Review of Earth and Planetary Sciences* 39.1, pp. 417–460. ISSN: 0084-6597. DOI: 10.1146/annurev-earth-040809-152447.

Pierrehumbert, R. T. (Dec. 2010). *Principles of Planetary Climate*. Cambridge: Cambridge University Press. DOI: 10.1017/CBO9780511780783.

Ping, C. L. (July 1987). "Soil Temperature Profiles of Two Alaskan Soils". In: *Soil Science Society of America Journal* 51.4, pp. 1010–1018. ISSN: 0361-5995. DOI: 10.2136/sssaj1987.03615995005100040035x.

Planck, M. (1917). "Über einen Satz der statistischen Dynamik und seine Erweiterung in der Quantentheorie". In: *Sitzungsberichte der Preussischen Akademie der Wissenschaften zu Berlin* 24, pp. 324–341.

Poincaré, H. (1885). "Sur l'équilibre d'une masse fluide animée d'un mouvement de rotation". In: *Acta Mathematica* 7.1, pp. 259–380. ISSN: 0001-5962. DOI: 10.1007/BF02402204.

Rahmstorf, S. (Nov. 1995). "Bifurcations of the Atlantic thermohaline circulation in response to changes in the hydrological cycle". In: *Nature* 378.6553, pp. 145–149. ISSN: 0028-0836. DOI: 10.1038/378145a0.

Rahmstorf, S., J. E. Box, G. Feulner, M. E. Mann, A. Robinson, S. Rutherford and E. J. Schaffernicht (May 2015). "Exceptional twentieth-century slowdown in Atlantic Ocean overturning circulation". In: *Nature Climate Change* 5.5, pp. 475–480. ISSN: 1758-678X. DOI: 10.1038/nclimate2554.

Renssen, H., V. Brovkin, T. Fichefet and H. Goosse (June 2006). "Simulation of the Holocene climate evolution in Northern Africa: The termination of the African Humid Period". In: *Quaternary International* 150.1, pp. 95–102. ISSN: 10406182. DOI: 10.1016/j.quaint.2005.01.001.

Riechers, K., G. Gottwald and N. Boers (Mar. 2023). "Glacial abrupt climate change as a multi-scale phenomenon resulting from monostable excitable dynamics". In: arXiv: 2303.04063.

Rietkerk, M., R. Bastiaansen, S. Banerjee, J. van de Koppel, M. Baudena and A. Doelman (Oct. 2021). "Evasion of tipping in complex systems through spatial pattern formation". In: *Science* 374.6564. ISSN: 0036-8075. DOI: 10.1126/science.abj0359.

Rietkerk, M. and J. van de Koppel (Mar. 2008). "Regular pattern formation in real ecosystems". In: *Trends in Ecology & Evolution* 23.3, pp. 169–175. ISSN: 01695347. DOI: 10.1016/j.tree.2007.10.013.

Riley, K. F., M. P. Hobson and S. J. Bence (2006). *Mathematical Methods for Physics and Engineering: A Comprehensive Guide*. Cambridge University Press. ISBN: 9781139450997.

Risken, H. (1984). *The Fokker-Planck Equation*. Ed. by H. Haken. Vol. 18. Springer Series in Synergetics 11. Berlin, Heidelberg: Springer Berlin Heidelberg, p. 467. ISBN: 978-3-642-96809-9. DOI: 10.1007/978-3-642-96807-5.

Ritchie, P., Ö. Karabacak and J. Sieber (Feb. 2019). "Inverse-square law between time and amplitude for crossing tipping thresholds". In: *Proceedings of the Royal Society A: Mathematical, Physical and Engineering Sciences* 475.2222, p. 20180504. DOI: 10.1098/rspa.2018.0504.

Ritchie, P. and J. Sieber (2016). "Early-warning indicators for rate-induced tipping". In: *Chaos* 26.9. ISSN: 10541500. DOI: 10.1063/1.4963012. arXiv: 1509.01696.

Ritchie, P. D. L., J. J. Clarke, P. M. Cox and C. Huntingford (Apr. 2021). "Overshooting tipping point thresholds in a changing climate". In: *Nature* 592.7855, pp. 517–523. ISSN: 0028-0836. DOI: 10.1038/s41586-021-03263-2.

Ritchie, P. D. L., I. Parry, J. J. Clarke, C. Huntingford and P. M. Cox (Sept. 2022). "Increases in the temperature seasonal cycle indicate long-term drying trends in Amazonia". In: *Communications Earth & Environment* 3.1, p. 199. ISSN: 2662-4435. DOI: 10.1038/s43247-022-00528-0.

Ritchie, P. D. L., G. S. Smith, K. J. Davis, C. Fezzi, S. Halleck-Vega, A. B. Harper, C. A. Boulton, A. R. Binner, B. H. Day, A. V. Gallego-Sala, J. V. Mecking, S. A. Sitch, T. M. Lenton and I. J. Bateman (Jan. 2020). "Shifts in national land use and food production in Great Britain after a climate tipping point". In: *Nature Food* 1.1, pp. 76–83. ISSN: 2662-1355. DOI: 10.1038/s43016-019-0011-3.

Robinson, A., R. Calov and A. Ganopolski (June 2012). "Multistability and critical thresholds of the Greenland ice sheet". In: *Nature Climate Change* 2.6, pp. 429–432. ISSN: 1758-678X. DOI: 10.1038/nclimate1449.

Rocha, J. C., G. Peterson, Ö. Bodin and S. Levin (Dec. 2018). "Cascading regime shifts within and across scales". In: *Science* 362.6421, pp. 1379–1383. ISSN: 0036-8075. DOI: 10.1126/science.aat7850.

Rockström, J., W. Steffen, K. Noone, Å. Persson, F. S. Chapin, E. F. Lambin, T. M. Lenton, M. Scheffer, C. Folke, H. J. Schellnhuber, B. Nykvist, C. A. de Wit, T. Hughes, S. van der Leeuw, H. Rodhe, S. Sörlin, P. K. Snyder, R. Costanza, U. Svedin, M. Falkenmark, L. Karlberg, R. W. Corell, V. J. Fabry, J. Hansen, B. Walker, D. Liverman, K. Richardson, P. Crutzen and J. A. Foley (Sept. 2009). "A safe operating space for humanity". In: *Nature* 461.7263, pp. 472–475. ISSN: 0028-0836. DOI: 10.1038/461472a.

Rogelj, J., P. M. Forster, E. Kriegler, C. J. Smith and R. Séférian (July 2019). "Estimating and tracking the remaining carbon budget for stringent climate targets". In: *Nature* 571.7765, pp. 335–342. ISSN: 0028-0836. DOI: 10.1038/s41586-019-1368-z.

Rogelj, J., T. Fransen, M. G. J. den Elzen, R. D. Lamboll, C. Schumer, T. Kuramochi, F. Hans, S. Mooldijk and J. Portugal-Pereira (June 2023). "Credibility gap in net-zero climate targets leaves world at high risk". In: *Science* 380.6649, pp. 1014–1016. ISSN: 0036-8075. DOI: 10.1126/science.adg6248.

Rothman, D. H. (Sept. 2014). "Earth's carbon cycle: A mathematical perspective". In: *Bulletin of the American Mathematical Society* 52.1, pp. 47–64. ISSN: 0273-0979. DOI: 10.1090/S0273-0979-2014-01471-5.

Rugenstein, M., J. Bloch-Johnson, A. Abe-Ouchi, T. Andrews, U. Beyerle, L. Cao, T. Chadha, G. Danabasoglu, J.-L. Dufresne, L. Duan, M.-A. Foujols, T. Frölicher, O. Geoffroy, J. Gregory, R. Knutti, C. Li, A. Marzocchi, T. Mauritsen, M. Menary, E. Moyer, L. Nazarenko, D. Paynter, D. Saint-Martin, G. A. Schmidt, A. Yamamoto and S. Yang (Dec. 2019). "LongRunMIP: Motivation and Design for a Large Collection of Millennial-Length AO-GCM Simulations". In: *Bulletin of the American Meteorological Society* 100.12, pp. 2551–2570. ISSN: 0003-0007. DOI: 10.1175/BAMS-D-19-0068.1.

Sage, R. F. and D. S. Kubien (Sept. 2007). "The temperature response of C3 and C4 photosynthesis". In: *Plant, Cell & Environment* 30.9, pp. 1086–1106. ISSN: 01407791. DOI: 10.1111/j.1365-3040.2007.01682.x.

Sarmiento, J. L. and J. R. Toggweiler (Apr. 1984). "A new model for the role of the oceans in determining atmospheric PCO2". In: *Nature* 308.5960, pp. 621–624. ISSN: 0028-0836. DOI: 10.1038/308621a0.

Scheffer, M., S. Hosper, M.-L. Meijer, B. Moss and E. Jeppesen (Aug. 1993). "Alternative equilibria in shallow lakes". In: *Trends in Ecology & Evolution* 8.8, pp. 275–279. ISSN: 01695347. DOI: 10.1016/0169-5347(93)90254-M.

Scheffer, M., J. Bascompte, W. A. Brock, V. Brovkin, S. R. Carpenter, V. Dakos, H. Held, E. H. van Nes, M. Rietkerk and G. Sugihara (Sept. 2009). "Early-warning signals for critical transitions". In: *Nature* 461.7260, pp. 53–59. ISSN: 0028-0836. DOI: 10.1038/nature08227.

Scheffer, M., S. R. Carpenter, T. M. Lenton, J. Bascompte, W. Brock, V. Dakos, J. van de Koppel, I. A. van de Leemput, S. A. Levin, E. H. van Nes, M. Pascual and J. Vandermeer (Oct. 2012). "Anticipating Critical Transitions". In: *Science* 338.6105, pp. 344–348. ISSN: 0036-8075. DOI: 10.1126/science.1225244.

Scheffer, M., S. Carpenter, J. A. Foley, C. Folke and B. Walker (Oct. 2001). "Catastrophic shifts in ecosystems". In: *Nature* 413.6856, pp. 591–596. ISSN: 0028-0836. DOI: 10.1038/35098000.

Schertzer, E., A. C. Staver and S. A. Levin (Jan. 2015). "Implications of the spatial dynamics of fire spread for the bistability of savanna and forest". In: *Journal of Mathematical Biology* 70.1-2, pp. 329–341. ISSN: 0303-6812. DOI: 10.1007/s00285-014-0757-z.

Schiesser, W. E. (Jan. 1991). *The Numerical Method of Lines: Integration of Partial Differential Equations.* Elsevier Science. ISBN: 9780126241303.

Schneider, T., C. M. Kaul and K. G. Pressel (Mar. 2019). "Possible climate transitions from breakup of stratocumulus decks under greenhouse warming". In: *Nature Geoscience* 12.3, pp. 163–167. ISSN: 1752-0894. DOI: 10.1038/s41561-019-0310-1.

Schoof, C. (2007). "Ice sheet grounding line dynamics: Steady states, stability, and hysteresis". In: *Journal of Geophysical Research: Earth Surface* 112.3, pp. 1–19. ISSN: 21699011. DOI: 10.1029/2006JF000664.

Schuur, E. A. G., A. D. McGuire, C. Schädel, G. Grosse, J. W. Harden, D. J. Hayes, G. Hugelius, C. D. Koven, P. Kuhry, D. M. Lawrence, S. M. Natali, D. Olefeldt, V. E. Romanovsky, K. Schaefer, M. R. Turetsky, C. C. Treat and J. E. Vonk (Apr. 2015). "Climate change and the permafrost carbon feedback". In: *Nature* 520.7546, pp. 171–179. ISSN: 0028-0836. DOI: 10.1038/nature14338.

Sellers, W. D. (June 1969). "A Global Climatic Model Based on the Energy Balance of the Earth-Atmosphere System". In: *Journal of Applied Meteorology* 8.3, pp. 392–400. ISSN: 0021-8952. DOI: 10.1175/1520-0450(1969)008<0392:AGCMBO>2.0.CO;2.

Serreze, M. C. and R. G. Barry (2011). "Processes and impacts of Arctic amplification: A research synthesis". In: *Global and Planetary Change* 77.1-2, pp. 85–96. ISSN: 09218181. DOI: 10.1016/j.gloplacha.2011.03.004.

Shanahan, T. M., N. P. McKay, K. A. Hughen, J. T. Overpeck, B. Otto-Bliesner, C. W. Heil, J. King, C. A. Scholz and J. Peck (Feb. 2015). "The time-transgressive termination of the African Humid Period". In: *Nature Geoscience* 8.2, pp. 140–144. ISSN: 1752-0894. DOI: 10.1038/ngeo2329.

Sherwood, S. C., M. J. Webb, J. D. Annan, K. C. Armour, P. M. Forster, J. C. Hargreaves, G. Hegerl, S. A. Klein, K. D. Marvel, E. J. Rohling, M. Watanabe, T. Andrews, P. Braconnot, C. S. Bretherton, G. L. Foster, Z. Hausfather, A. S. von der Heydt, R. Knutti, T. Mauritsen, J. R. Norris, C. Proistosescu, M. Rugenstein, G. A. Schmidt, K. B. Tokarska and M. D. Zelinka (Dec. 2020). "An Assessment of Earth's Climate Sensitivity Using Multiple Lines of Evidence". In: *Reviews of Geophysics* 58.4. ISSN: 8755-1209. DOI: 10.1029/2019RG000678.

Sidhu, H. S., M. I. Nelson, T. Luangwilai and X. D. Chen (2007). "Mathematical modelling of the self-heating process in compost piles". In: *Chemical Product and Process Modeling* 2.2. ISSN: 19342659. DOI: 10.2202/1934-2659.1070.

Sinet, S., A. S. von der Heydt and H. A. Dijkstra (Jan. 2023). "AMOC Stabilization Under the Interaction With Tipping Polar Ice Sheets". In: *Geophysical Research Letters* 50.2, pp. 1–9. ISSN: 0094-8276. DOI: 10.1029/2022GL100305.

Singh, J. S. and S. R. Gupta (Oct. 1977). "Plant decomposition and soil respiration in terrestrial ecosystems". In: *The Botanical Review* 43.4, pp. 449–528. ISSN: 0006-8101. DOI: 10.1007/BF02860844.

Skeldon, A. C., D.-J. Dijk and G. Derks (Aug. 2014). "Mathematical Models for Sleep-Wake Dynamics: Comparison of the Two-Process Model and a Mutual Inhibition Neuronal Model". In: *PLoS ONE* 9.8. Ed. by A. Csikász-Nagy, e103877. ISSN: 1932-6203. DOI: 10.1371/journal.pone.0103877. arXiv: 1311.1734.

Spivak, M. (1965). *Calculus On Manifolds: A Modern Approach To Classical Theorems Of Advanced Calculus*. Avalon Publishing, p. 144. ISBN: 9780805390216.

Spracklen, D. V., S. R. Arnold and C. M. Taylor (Sept. 2012). "Observations of increased tropical rainfall preceded by air passage over forests". In: *Nature* 489.7415, pp. 282–285. ISSN: 0028-0836. DOI: 10.1038/nature11390.

Stainforth, D. A., T. Aina, C. Christensen, M. Collins, N. Faull, D. J. Frame, J. A. Kettleborough, S. Knight, A. Martin, J. M. Murphy, C. Piani, D. Sexton, L. A. Smith, R. A. Spicer, A. J. Thorpe and M. R. Allen (Jan. 2005). "Uncertainty in predictions of the climate response to rising levels of greenhouse gases". In: *Nature* 433.7024, pp. 403–406. ISSN: 0028-0836. DOI: 10.1038/nature03301.

Stanley, H. E. (Mar. 1999). "Scaling, universality, and renormalization: Three pillars of modern critical phenomena". In: *Reviews of Modern Physics* 71.2, S358–S366. ISSN: 0034-6861. DOI: 10.1103/RevModPhys.71.S358.

Stauffer, D. and A. Aharony (1994). *Introduction to Percolation Theory*. Revised Se. London: Taylor and Francis, p. 179. ISBN: 0748402535.

Staver, A. C., S. Archibald and S. A. Levin (Oct. 2011). "The Global Extent and Determinants of Savanna and Forest as Alternative Biome States". In: *Science* 334.6053, pp. 230–232. ISSN: 0036-8075. DOI: 10.1126/science.1210465.

Steffen, W., J. Rockström, K. Richardson, T. M. Lenton, C. Folke, D. Liverman, C. P. Summerhayes, A. D. Barnosky, S. E. Cornell, M. Crucifix, J. F. Donges, I. Fetzer, S. J. Lade, M. Scheffer, R. Winkelmann and H. J. Schellnhuber (Aug. 2018). "Trajectories of the Earth System in the Anthropocene". In: *Proceedings of the National Academy of Sciences* 115.33, pp. 8252–8259. ISSN: 0027-8424. DOI: 10.1073/pnas.1810141115.

Stephens, P. A., W. J. Sutherland and R. P. Freckleton (Oct. 1999). "What Is the Allee Effect?" In: *Oikos* 87.1, p. 185. ISSN: 00301299. DOI: 10.2307/3547011.

Stommel, H. (May 1961). "Thermohaline Convection with Two Stable Regimes of Flow". In: *Tellus* 13.2, pp. 224–230. ISSN: 00402826. DOI: 10.1111/j.2153-3490.1961.tb00079.x.

Strogatz, S. H. (May 2015). *Nonlinear Dynamics and Chaos*. 2nd. Boca Raton: CRC Press, p. 532. ISBN: 9780429961113. DOI: 10.1201/9780429492563.

Taubert, F., R. Fischer, J. Groeneveld, S. Lehmann, M. S. Müller, E. Rödig, T. Wiegand and A. Huth (Feb. 2018). "Global patterns of tropical forest fragmentation". In: *Nature* 554.7693, pp. 519–522. ISSN: 0028-0836. DOI: 10.1038/nature25508.

Taylor, K. E., R. J. Stouffer and G. A. Meehl (Apr. 2012). "An Overview of CMIP5 and the Experiment Design". In: *Bulletin of the American Meteorological Society* 93.4, pp. 485–498. ISSN: 1520-0477. DOI: 10.1175/BAMS-D-11-00094.1.

Teufel, B. and L. Sushama (Nov. 2019). "Abrupt changes across the Arctic permafrost region endanger northern development". In: *Nature Climate Change* 9.11, pp. 858–862. ISSN: 1758-678X. DOI: 10.1038/s41558-019-0614-6.

Thompson, J. M. T., H. B. Stewart and Y. Ueda (Feb. 1994). "Safe, explosive, and dangerous bifurcations in dissipative dynamical systems". In: *Physical Review E* 49.2, pp. 1019–1027. ISSN: 1063-651X. DOI: 10.1103/PhysRevE.49.1019.

Thompson, J. M. and J. Sieber (Feb. 2011). "Climate tipping as a noisy bifurcation: A predictive technique". In: *IMA Journal of Applied Mathematics (Institute of Mathematics and Its Applications)*. Vol. 76. 1, pp. 27–46. DOI: 10.1093/imamat/hxq060. arXiv: 1007.1376.

Thornley, J. H. (1971). "Energy, respiration, and growth in plants". In: *Annals of Botany* 35.4, pp. 721–728. ISSN: 03057364. DOI: 10.1093/oxfordjournals.aob.a084519.

Tierney, J. E., C. J. Poulsen, I. P. Montañez, T. Bhattacharya, R. Feng, H. L. Ford, B. Hönisch, G. N. Inglis, S. V. Petersen, N. Sagoo, C. R. Tabor, K. Thirumalai, J. Zhu, N. J. Burls, G. L. Foster, Y. Goddéris, B. T. Huber, L. C. Ivany, S. Kirtland Turner, D. J. Lunt, J. C. McElwain, B. J. W. Mills, B. L. Otto-Bliesner, A. Ridgwell and Y. G. Zhang (Nov. 2020). "Past climates inform our future". In: *Science* 370.6517. ISSN: 0036-8075. DOI: 10.1126/science.aay3701.

Tierney, J. E., F. S. R. Pausata and P. B. DeMenocal (Jan. 2017). "Rainfall regimes of the Green Sahara". In: *Science Advances* 3.1, pp. 1–10. ISSN: 2375-2548. DOI: 10.1126/sciadv.1601503.

Tirabassi, G. and C. Masoller (Jan. 2023). "Entropy-based early detection of critical transitions in spatial vegetation fields". In: *Proceedings of the National Academy of Sciences* 120.1. ISSN: 0027-8424. DOI: 10.1073/pnas.2215667120.

Titus, M. and J. Watson (Dec. 2020). "Critical speeding up as an early warning signal of stochastic regime shifts". In: *Theoretical Ecology* 13.4, pp. 449–457. ISSN: 1874-1738. DOI: 10.1007/s12080-020-00451-0.

Trenberth, K. E., J. T. Fasullo and J. Kiehl (Mar. 2009). "Earth's Global Energy Budget". In: *Bulletin of the American Meteorological Society* 90.3, pp. 311–324. ISSN: 0003-0007. DOI: 10.1175/2008BAMS2634.1.

Turing, A. (Aug. 1952). "The chemical basis of morphogenesis". In: *Philosophical Transactions of the Royal Society of London. Series B, Biological Sciences* 237.641, pp. 37–72. ISSN: 2054-0280. DOI: 10.1098/rstb.1952.0012.

Uhlenbeck, G. E. and L. S. Ornstein (Sept. 1930). "On the Theory of the Brownian Motion". In: *Physical Review* 36.5, pp. 823–841. ISSN: 0031-899X. DOI: 10.1103/PhysRev.36.823.

Van Breedam, J., H. Goelzer and P. Huybrechts (Nov. 2020). "Semi-equilibrated global sea-level change projections for the next 10 000 years". In: *Earth System Dynamics* 11.4, pp. 953–976. ISSN: 2190-4987. DOI: 10.5194/esd-11-953-2020.

Varney, R. M., S. E. Chadburn, E. J. Burke and P. M. Cox (Oct. 2022). "Evaluation of soil carbon simulation in CMIP6 Earth system models". In: *Biogeosciences* 19.19, pp. 4671–4704. ISSN: 1726-4189. DOI: 10.5194/bg-19-4671-2022.

Varney, R. M., S. E. Chadburn, P. Friedlingstein, E. J. Burke, C. D. Koven, G. Hugelius and P. M. Cox (2020). "A spatial emergent constraint on the sensitivity of soil carbon turnover to global warming". In: *Nature Communications* 11.1, pp. 4–11. ISSN: 20411723. DOI: 10.1038/s41467-020-19208-8.

Vettoretti, G., P. Ditlevsen, M. Jochum and S. O. Rasmussen (Apr. 2022). "Atmospheric CO2 control of spontaneous millennial-scale ice age climate oscillations". In: *Nature Geoscience* 15.4, pp. 300–306. ISSN: 1752-0894. DOI: 10.1038/s41561-022-00920-7.

Virtanen, P. et al. (Mar. 2020). "SciPy 1.0: fundamental algorithms for scientific computing in Python". In: *Nature Methods* 17.3, pp. 261–272. ISSN: 1548-7091. DOI: 10.1038/s41592-019-0686-2. arXiv: 1907.10121.

Volk, T. and M. I. Hoffert (Mar. 2013). "Ocean Carbon Pumps: Analysis of Relative Strengths and Efficiencies in Ocean-Driven Atmospheric CO2 Changes". In: *Ocean carbon pumps: analysis of relative strengths and efficiencies in ocean-driven atmospheric CO2 changes*. Vol. 32, pp. 99–110. DOI: 10.1029/GM032p0099.

Wang, R., J. A. Dearing, P. G. Langdon, E. Zhang, X. Yang, V. Dakos and M. Scheffer (Dec. 2012). "Flickering gives early warning signals of a critical transition to a eutrophic lake state". In: *Nature* 492.7429, pp. 419–422. ISSN: 0028-0836. DOI: 10.1038/nature11655.

Wang, S., A. Foster, E. A. Lenz, J. D. Kessler, J. C. Stroeve, L. O. Anderson, M. Turetsky, R. Betts, S. Zou, W. Liu, W. R. Boos and Z. Hausfather (Mar. 2023). "Mechanisms and

Impacts of Earth System Tipping Elements". In: *Reviews of Geophysics* 61.1, pp. 1–81. ISSN: 8755-1209. DOI: 10.1029/2021RG000757.

Wang, S., Y. Zhang, W. Ju, J. M. Chen, P. Ciais, A. Cescatti, J. Sardans, I. A. Janssens, M. Wu, J. A. Berry, E. Campbell, M. Fernández-Martínez, R. Alkama, S. Sitch, P. Friedlingstein, W. K. Smith, W. Yuan, W. He, D. Lombardozzi, M. Kautz, D. Zhu, S. Lienert, E. Kato, B. Poulter, T. G. M. Sanders, I. Krüger, R. Wang, N. Zeng, H. Tian, N. Vuichard, A. K. Jain, A. Wiltshire, V. Haverd, D. S. Goll and J. Peñuelas (Dec. 2020). "Recent global decline of CO2 fertilization effects on vegetation photosynthesis". In: *Science* 370.6522, pp. 1295–1300. ISSN: 0036-8075. DOI: 10.1126/science.abb7772.

Wanninkhof, R. (1992). "Relationship between wind speed and gas exchange over the ocean". In: *Journal of Geophysical Research* 97.C5, p. 7373. ISSN: 0148-0227. DOI: 10.1029/92JC00188.

Weiss, R. (Nov. 1974). "Carbon dioxide in water and seawater: the solubility of a non-ideal gas". In: *Marine Chemistry* 2.3, pp. 203–215. ISSN: 03044203. DOI: 10.1016/0304-4203(74)90015-2.

Weitzman, M. L. (Feb. 2009). "On Modeling and Interpreting the Economics of Catastrophic Climate Change". In: *Review of Economics and Statistics* 91.1, pp. 1–19. ISSN: 0034-6535. DOI: 10.1162/rest.91.1.1.

Welch, P. (June 1967). "The use of fast Fourier transform for the estimation of power spectra: A method based on time averaging over short, modified periodograms". In: *IEEE Transactions on Audio and Electroacoustics* 15.2, pp. 70–73. ISSN: 0018-9278. DOI: 10.1109/TAU.1967.1161901.

Wenzel, S., P. M. Cox, V. Eyring and P. Friedlingstein (Oct. 2016). "Projected land photosynthesis constrained by changes in the seasonal cycle of atmospheric CO2". In: *Nature* 538.7626, pp. 499–501. ISSN: 0028-0836. DOI: 10.1038/nature19772.

Wieczorek, S., P. Ashwin, C. M. Luke and P. M. Cox (2011). "Excitability in ramped systems: The compost-bomb instability". In: *Proceedings of the Royal Society A: Mathematical, Physical and Engineering Sciences* 467.2129, pp. 1243–1269. ISSN: 14712946. DOI: 10.1098/rspa.2010.0485.

Wieczorek, S., C. Xie and P. Ashwin (June 2023). "Rate-induced tipping: thresholds, edge states and connecting orbits". In: *Nonlinearity* 36.6, pp. 3238–3293. ISSN: 0951-7715. DOI: 10.1088/1361-6544/accb37. arXiv: 2111.15497.

Wilks, D. S. (2019). *Statistical Methods in the Atmospheric Sciences*. 4th. Amsterdam: Elsevier. ISBN: 9780128158234. DOI: 10.1016/C2017-0-03921-6.

Williamson, M. S., S. Bathiany and T. M Lenton (Apr. 2016). "Early warning signals of tipping points in periodically forced systems". In: *Earth System Dynamics* 7.2, pp. 313–326. ISSN: 21904987. DOI: 10.5194/esd-7-313-2016.

Williamson, M. S. and T. M. Lenton (Feb. 2015). "Detection of bifurcations in noisy coupled systems from multiple time series". In: *Chaos* 25.3. ISSN: 10541500. DOI: 10.1063/1.4908603.

Wilson, K. G. (July 1983). "The renormalization group and critical phenomena". In: *Reviews of Modern Physics* 55.3, pp. 583–600. ISSN: 0034-6861. DOI: 10.1103/RevModPhys.55.583.

Wiltshire, A. J., E. J. Burke, S. E. Chadburn, C. D. Jones, P. M. Cox, T. Davies-Barnard, P. Friedlingstein, A. B. Harper, S. Liddicoat, S. Sitch and S. Zaehle (Apr. 2021). "JULES-CN: a coupled terrestrial carbon–nitrogen scheme (JULES vn5.1)". In: *Geoscientific Model Development* 14.4, pp. 2161–2186. ISSN: 1991-9603. DOI: 10.5194/gmd-14-2161-2021.

Witze, A. (Sept. 2020). "The Arctic is burning like never before — and that's bad news for climate change". In: *Nature* 585.7825, pp. 336–337. ISSN: 0028-0836. DOI: 10.1038/d41586-020-02568-y.

Wood, R. A., M. Crucifix, T. M. Lenton, K. J. Mach, C. Moore, M. New, S. Sharpe, T. F. Stocker and R. T. Sutton (Apr. 2023). "A Climate Science Toolkit for High Impact-Low Likelihood Climate Risks". In: *Earth's Future* 11.4. ISSN: 2328-4277. DOI: 10.1029/2022EF003369.

Wunderling, N., J. F. Donges, J. Kurths and R. Winkelmann (June 2021). "Interacting tipping elements increase risk of climate domino effects under global warming". In: *Earth System Dynamics* 12.2, pp. 601–619. ISSN: 2190-4987. DOI: 10.5194/esd-12-601-2021.

Wunderling, N., R. Winkelmann, J. Rockström, S. Loriani, D. I. Armstrong McKay, P. D. L. Ritchie, B. Sakschewski and J. F. Donges (Jan. 2023). "Global warming overshoots increase risks of climate tipping cascades in a network model". In: *Nature Climate Change* 13.1, pp. 75–82. ISSN: 1758-678X. DOI: 10.1038/s41558-022-01545-9.

Wuyts, B., A. R. Champneys and J. I. House (May 2017). "Amazonian forest-savanna bistability and human impact". In: *Nature Communications* 8. ISSN: 2041-1723. DOI: 10.1038/ncomms15519.

Wuyts, B. and J. Sieber (July 2022). "Emergent structure and dynamics of tropical forest-grassland landscapes". In: pp. 1–24. arXiv: 2207.14118.

Xie, X.-q., W.-p. He, B. Gu, Y. Mei and S.-s. Zhao (June 2019). "Can kurtosis be an early warning signal for abrupt climate change?" In: *Climate Dynamics* 52.11, pp. 6863–6876. ISSN: 0930-7575. DOI: 10.1007/s00382-018-4549-9.

Zelinka, M. D., T. A. Myers, D. T. McCoy, S. Po-Chedley, P. M. Caldwell, P. Ceppi, S. A. Klein and K. E. Taylor (Jan. 2020). "Causes of Higher Climate Sensitivity in CMIP6 Models". In: *Geophysical Research Letters* 47.1, pp. 1–12. ISSN: 0094-8276. DOI: 10.1029/2019GL085782.

Bibliography

Colophon

This thesis was typeset using LaTeX, developed by Leslie Lamport based on Donald Knuth's TeX. The typesetting owes a debt to Robert Bringhurst's *The Elements of Typographic Style*.

The typeface was EBGaramond-maths, assembled by Clea F. Rees. This extends EB Garamond, designed by Georg Mayr-Duffner and Octavio Pardo, for mathematical use. Calligraphic symbols came from Knuth's computer modern.

The title page, passed onto me by Rebecca Varney, has its origins lost in the mists of time. It was typeset in Helvetica, which was designed by Max Miedinger and Eduard Hoffmann.

I would like to thank those who have contributed to www.tex.stackexchange.com, without whom this document would not compile.